HYBRID INTELLIGENT MACHINE SYSTEMS: DESIGN, MODELING AND CONTROL

A Thesis Submitted to the

College of Graduate Studies and Research

In Partial Fulfillment of the Requirements

For the Degree of Doctor of Philosophy

In the Department of Mechanical Engineering

University of Saskatchewan

Saskatoon, Canada

By

Puren Ouyang

PERMISSION TO USE

In presenting this thesis in partial fulfillment of the requirements for a Postgraduate degree from the University of Saskatchewan, I agree that the Libraries of this University may make it freely available for inspection. I further agree that permission for copying of this thesis in any manner, in whole or in part, for scholarly purposes may be granted by the professor or professors who supervised my thesis work or, in their absence, by the Head of the Department or the Dean of the College in which my thesis work was done. It is understood that any copying or publication or use of this thesis or parts thereof for financial gain shall not be allowed without my written permission. It is also understood that due recognition shall be given to me and to the University of Saskatchewan in any scholarly use which may be made of any material in my thesis.

Requests for permission to copy or to make other use of material in this thesis in whole or part should be addressed to:

Head of the Department of Mechanical Engineering
University of Saskatchewan
Saskatoon, Saskatchewan CANADA S7N 5A9

ABSTRACT

To further improve performances of machine systems, mechatronics offers some opportunities. Traditionally, mechatronics deals with how to integrate mechanics and electronics without a systematic approach. This thesis generalizes the concept of mechatronics into a new concept called hybrid intelligent machine system. A hybrid intelligent machine system is a system where two or more elements combine to play at least one of the roles such as sensor, actuator, or control mechanism, and contribute to the system behaviour. The common feature with the hybrid intelligent machine system is thus the presence of two or more entities responsible for the system behaviour with each having its different strength complementary to the others. The hybrid intelligent machine system is further viewed from the system's structure, behaviour, function, and principle, which has led to the distinction of (1) the hybrid actuation system, (2) the hybrid motion system (mechanism), and (3) the hybrid control system.

This thesis describes a comprehensive study on three hybrid intelligent machine systems. In the case of the hybrid actuation system, the study has developed a control method for the "true" hybrid actuation configuration in which the constant velocity motor is not "mimicked" by the servomotor which is treated in literature. In the case of the hybrid motion system, the study has resulted in a novel mechanism structure based on the compliant mechanism which allows the micro- and macro-motions to be integrated within a common framework. It should be noted that the existing designs in literature all take a serial structure for micro- and macro-motions. In the case of hybrid control system, a novel family of control laws is developed, which is primarily based on the iterative learning of the previous driving torque (as a feedforward part) and various feedback control laws. This new family of control laws is rooted in the computer-torque-control (CTC) law with an off-line learned torque in replacement of an analytically formulated torque in the forward part of the CTC law. This thesis also presents the

verification of these novel developments by both simulation and experiments. Simulation studies are presented for the hybrid actuation system and the hybrid motion system while experimental studies are carried out for the hybrid control system.

ACKNOWLEDGMENTS

I would like to take this opportunity to express my sincere gratitude to my supervisor Professor Chris W.J. Zhang, who provided me with an extraordinary amount of patience, encouragement, and enthusiasm during the development of the study. His invaluable guidance, stimulating discussion, dedication and expertise were immersed into any little progress of this study. His financial support was extremely important for the continuity of my study.

I would like to thank my co-supervisor Professor Madan M. Gupta for his invaluable support, guidance, suggestion and wisdom throughout my Ph.D. study. I would like to extend special thanks to the members of the advisory committee: Professor Aryan Saadat Mehr, Professor Richard Burton, and Professor Daniel X.B. Chen. Their valuable advices and constructive suggestions have greatly improved the present work.

I would like to thank Mr. Ranier C. Tjiptoprodjo and Mr. Reza Moazed for their help to perform some experiments described in Chapter 6.

My research was made possible by the generous support of the Natural Sciences and Engineering Research Council (NSERC) through the PGS-D scholarship and the Department of Mechanical Engineering through the graduate scholarship.

DEDICATED TO

My wife Yanhua
My daughters Lucy and Belle

TABLE OF CONTENTS

LIST OF FIGURES

LIST OF TABLES

ACRONYMS

ANOM	Analysis of means
ANOVA	Analysis of variance
ASL	Adaptive switching learning
ASL-PD	Adaptive switching learning PD
CMA	Complaint mechanical amplifier
CTC	Computer torque control
CV	Constant velocity
DOF	Degree of freedom
FBS	Function-behaviour-structure
FCBS	Function-control-behaviour-structure
FEA	Finite element analysis
FEM	Finite element method
HAS	Hybrid actuation system
HMM	Hybrid motion mechanism
ILC	Iterative learning control
LIGA	Lithographie, galvanoformung und abformung in Germany
MSD	Mean squared deviation
NPD	Nonlinear PD
NPD-LC	Nonlinear PD learning control
OA	Orthogonal array
OLC	Online learning control
PD	Proportional-derivative

PD-OLC	PD type online learning control
PID	Proportional-integral-derivative
PRBM	Pseudo rigid body model
PZT	Piezoelectric transducer
SMA	Shape memory alloy
SMC	Sliding mode control
SNR	Signal to noise ratio

1. INTRODUCTION

1.1 Architecture of Intelligent Machine Systems

An intelligent machine system can be represented by a general architecture as shown in Figure 1.1. In this architecture, the structure is defined as a set of entities connected in a meaningful way. Entities are represented by a set of properties, and these properties are called states. The name of the state is called the state variable. The behaviour is the causal relationship among a set of related state variables. The function is defined as the purpose in the mind of humans and can be realized by the system (structure) due to the provision of certain behaviours generated by the structure. The controlled behaviour is defined as the behaviour resulting from the adjustments on the structure and the state; the adjustments are needed for the reduction of any discrepancy between an actual function and a desired function. The principle governs the behaviour in the sense that the causal relationship is derived from the principle. The principle can be viewed as the constraint that determines a particular behaviour.

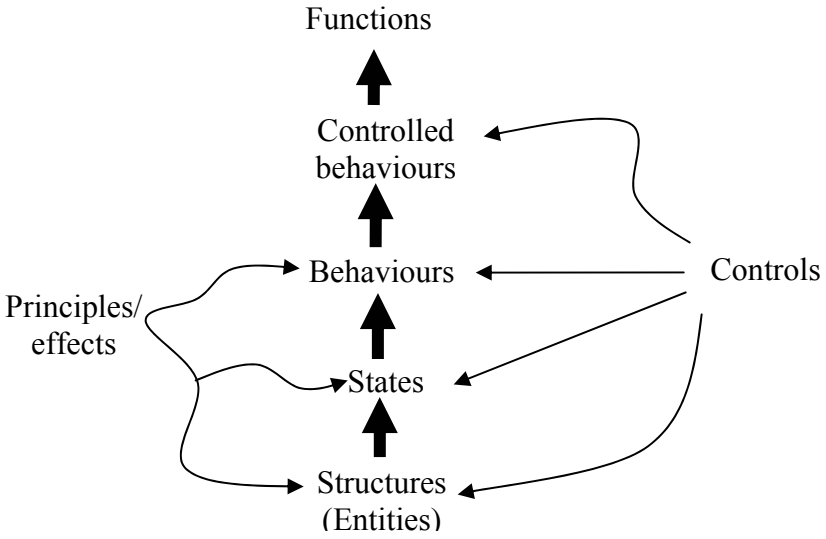

Figure 1.1 Architecture of intelligent machine systems.

The above architecture may be called the function-control–behaviour-structure (FCBS) which is a specialized architecture of a more generalized architecture called the function-behaviour-structure (FBS) (Lin and Zhang, 2003). The behaviour concept in the FBS architecture is further specialized into the sub-behaviour, the controlled behaviour in this case, in the FCBS architecture. Furthermore, the FCBS architecture can be applied to the system decomposition lattice; see Figure 1.2.

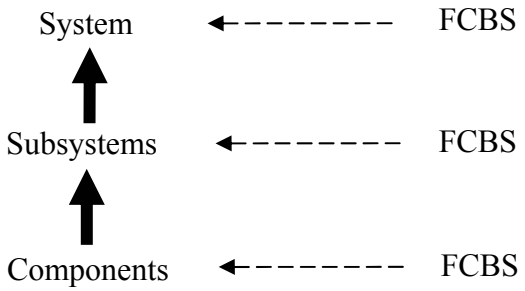

Figure 1.2 FCBS versus the system decomposition.

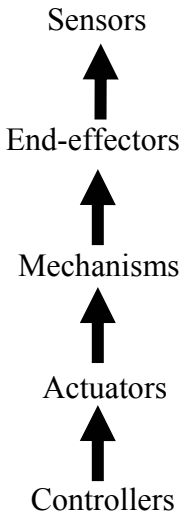

Figure 1.3 Function view of intelligent machine systems.

An intelligent machine system can also be viewed as consisting of (i) sensors, (ii) end-effectors, (iii) mechanisms, (iv) actuators, and (v) controllers; see Figure 1.3. It is noted that the sensor can be placed on the end-effector and/or actuator. The view or architecture of an intelligent machine system, as shown in Figure 1.3, is a generic

function view. For a particular intelligent machine system, this architecture may be extended; for example, the layer of mechanisms in Figure 1.3 may be replaced by a compliant mechanism. It is further noted that the system decomposition illustrated in Figure 1.2 is related to the function architecture; see Figure 1.4.

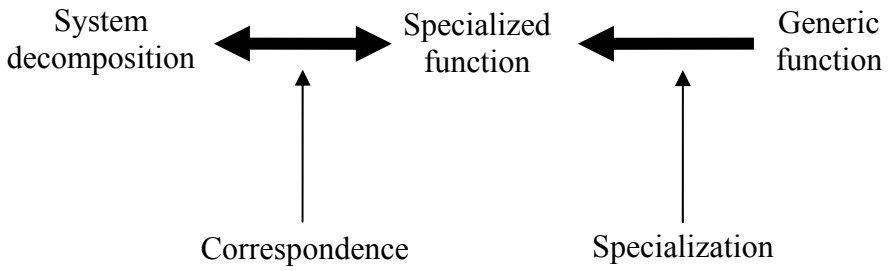

Figure 1.4 Architecture of functions of intelligent machine systems.

Referring to Figure 1.3, actuators may be classified based on how they work or based on principles (or effects) which govern their behaviours (see Figure 1.1 for a general relationship among the structure, state, behaviour, and principle). Mechanisms can also be classified in the same way, so are the controllers.

A note is given to the intelligent machine system. The word “intelligent” mostly refers to the behaviour of a machine system. The intelligent behaviour is called when the system is able to sense, to learn, to reason, to make decisions, and to act with precision and accuracy. The FCBS architecture represents an intelligent machine system because the sensor corresponds to the first intelligent behaviour (i.e., to sense); the controller embodies the second, the third, and the fourth intelligent behaviours; the end-effector, mechanism, and actuator together are responsible for the fifth behaviour. There are many ways to improve the intelligent behaviours of a machine system; for example, various learning and reasoning techniques. This thesis concerns a general method at this point, that is, the hybridization of system components (structural entities).

1.2 Hybrid Intelligent Machine System

The word "hybrid" is often used as a synonym of the word “heterogeneous” in the nature or synthetic realms. In biology, the improvement of capabilities of a plant through some hybridization has been known for years. In material sciences, the notion of composite materials is another example of improvement of material properties. Still another example is the hybrid control system for controlling cell cycles (Antsaklis et al., 2003). The common feature of these hybrid systems is the presence of two entities with each having different characteristics. The combining of these two entities can improve the behaviour of a system with their presence. Further, the improvement of the behaviour can make sense in enhancing or extending or both. In the case of the extending, a unique advantage of the hybrid system is that two contradicting behaviours of a system may exist harmonically; for example the ductility and the strength in material engineering.

In this thesis, the notion of the *hybrid system* is applied to the intelligent machine system; in particular the formation of a hybrid intelligent machine system is based on the system architecture as shown in Figures 1.1 through 1.3. The definition of a hybrid intelligent machine system is thus given below:

> A system is called a *hybrid intelligent machine system* if the system is constructed in such a way that within its scope (components, subsystems) two or more elements are combined to contribute to the system behaviour by playing at least one of the roles: sensor, end-effector, mechanism, actuator, or controller.

For simplicity, the remainder of the thesis will use the term “hybrid system” for the “hybrid intelligent system”.

In the real world, some hybrid systems have been developed; for example the macro-micro manipulator systems (Sharon and Hogan, 1993; Lew, 1996, 1997; Tol et al., 2002), the hybrid machine system (Tokuz and Jones, 1991; Greenough et al.,1995;

Kirecci and Dulger, 2000), etc. The mechatronic system, if properly defined and designed, is also a hybrid system. However, a systematic study on the hybrid system has not appeared yet. The existing literature has merely provided one aspect or another of the total sense of the hybrid system; this situation is largely attributed to the lack of the general architecture of intelligent systems (Figure 1.1), or the lack of the generalization in a system perspective.

This thesis will present a comprehensive study on the hybrid system, in which the previous discussion of the hybrid systems as well as the architecture of the intelligent systems is part of the study. Specifically, this thesis study concerns design, modeling and control of hybrid systems. The types of the hybrid systems considered in this thesis include: (1) a hybrid actuation system, (2) a hybrid motion system or mechanism, and (3) a hybrid control system. These systems can be mixed up with each other. Further, that is to say, a hybrid system may be a combination of a hybrid actuation and a hybrid control, or the combination of a hybrid motion and a hybrid control.

The definitions of the three kinds of hybrid systems are stated as follows.

> A *hybrid actuation system*, in this thesis, is defined as a mechanical system where its drive system integrates two types of motors: the servomotor and the constant velocity (CV) motor to combine the advantages of both of them and to produce inexpensive programmable output. In such a hybrid actuation system, the CV motor is used to provide a main power needed to drive the mechanism, and the servomotor is used either compensate errors produced due to inevitable speed fluctuation in the CV motor, or to produce flexible output trajectories with the end-effector of the system.
>
> A *hybrid motion system* is defined as a mechanical system that combines the macro motion and the micro motion together in one mechanism to achieve a large motion range with a high resolution. In the hybrid motion

system, the macro motion fulfills the large motion; the micro motion does the motion with high resolution but small motion range.

A *hybrid control system* is defined as a control system where different control laws are integrated so that the advantage of each control law can be taken to achieve an improved control performance.

1.3 Challenging Issues in the Design of the Hybrid Systems

As there are two or more entities which come from different domains of ontologies yet potentially fulfill a similar function in a hybrid system, these entities and their interactions can certainly play important roles in the performance of the whole hybrid system. The general goal of designing a hybrid system should be to make these different entities behave complementary to each other; as such an "emergent" behaviour which can certainly not be achieved by each of them alone can be achieved.

The general procedure to achieve this general goal can be: (1) to understand two domains of ontologies involved in the interaction; (2) to identify the strengths and weaknesses of each entity which may further change with respect to time, and (3) to assign function responsibilities for each of them so that they can behave complementary.

Despite its generality with the general procedure, specific design challenges with respect to three types of hybrid systems need to be identified. The challenging issue for the hybrid actuation system is the interaction between the CV motor and the servomotor. For the hybrid motion system the challenging issue is how to minimize the interaction between the macro motion and the micro motion. The main challenging issue in the hybrid control system is how to reduce or eliminate the transient problem caused by the interaction of two or more different control laws.

These issues about the interaction of the hybrid systems are not well studied in the literature, or ad-hoc developments and methodologies are dispersed in the current

literature without a coherent framework. In a specific domain of the hybrid actuation system, the use of a servomotor with a constant velocity profile for the substitution of a constant velocity motor is still very popular in the literature. This is an erroneous practice of mechatronics design because the constant velocity (CV) motor may not perform "constant" velocity (there is usually a velocity fluctuation in the CV motor due to the variation in the operating condition and / or the variation in the workload on the system, or the disturbances) yet the servomotor with the constant velocity profile acts as a (perfect) constant velocity motion generator.

Nevertheless, despite existing studies reported in the literature, such as the hybrid actuation system and the hybrid motion system (Tokuz, 1992; Greenough et al., 1995; Sharon and Hogan, 1993), it would be useful to put these studies in a unified framework and develop specific methodologies to cope with the specific problems in such a unified framework. It is expected that by doing so, these hybrid systems can be designed to achieve better intelligent behaviours.

1.4 Research Objectives

This thesis study was motivated to address the challenging issues identified above with respect to the hybrid systems and aimed to develop new theories and methodologies for designing these hybrid systems. Specifically, the following four objectives were defined, namely:

Objective 1: To develop a hybrid actuation system with the following specific objectives: (i) design of a hybrid actuation system through a 2 degree-of-freedom (DOF) mechanism driven by a CV motor and a servomotor; (ii) modeling of the hybrid actuation system including both the dynamics of the mechanism and the dynamics of the two motors; (iii) design of a hybrid controller which can limit the velocity fluctuation in the CV motor through the servomotor; and (iv) tracking performance improvement through mechanical means.

It is remarked that the existing studies on the hybrid actuation systems did not consider well the interaction problem between the CV motor and the servomotor. This challenge issue should be resolved before the real application of the hybrid actuation system. The general strategy for controlling the hybrid actuation mechanism was proposed to model the propagated speed fluctuation in the CV motor and incorporate it into a controller designed for the servomotor.

Objective 2: To develop a hybrid motion system that integrates two types of motions through one compliant mechanism. In this hybrid motion system, a new interface design paradigm will be explored, in which a macro motion driven by a DC servomotor and a micro motion driven by a PZT actuator are supported by one mechanical frame. Further, three particular issues will be addressed in this study: (i) the design principle and implementation of the hybrid motion system; (ii) the motion analysis of the hybrid motion system; and (iii) the optimization design of the hybrid motion system.

The existing hybrid motion system is called the serial motion system where the macro motion mechanism functions as a base and the micro motion mechanism is mounted on the macro motion one, or vice versa. It is remarked that the existing studies on hybrid motion systems mainly focused on the control algorithm design to minimize the interaction of the macro motion and the micro motion. This thesis will develop a new hybrid motion system that integrates the macro motion and micro motion in one compliant mechanism. This kind of hybrid motion system may also be called the parallel hybrid motion system.

Objective 3: To develop hybrid control systems that can be used in the hybrid actuation system and the hybrid motion system. Two types of hybrid control systems will be proposed. One is the hybrid control system designed for the control of the hybrid actuation system, and the other is the PD type adaptive learning control system designed for the control of the hybrid motion system and the general robotic systems as well. The stability and convergence analysis of these hybrid control systems will be performed.

It is remarked that the hybrid control systems discussed in the literature are limited on the switching control systems that are characterized by the interaction of continuous parts, governed by differential or difference equations, and by discrete parts, described by finite state machines. In such a hybrid control system, the switching processes occur in the time domain. The switching technique will be extended to the iteration domain in this study to avoid some inherent problems with the switching in the time domain. Another care should be taken that the term "hybrid control system" is used in literature, referring to the control system for a mixed event-driven discrete and time-driven continuous dynamic system (Antsaklis et al, 1998).

Objective 4: To conduct simulation and experiment studies for the three developed hybrid systems. Specifically, for the hybrid actuation system, the performance of trajectory tracking will be examined; for the hybrid motion system, the feasibility of the new design paradigm (i.e., one mechanical frame for two types of actuators) will be examined; finally for the hybrid control system, the performance of trajectory tracking for some general robot manipulators will be examined.

1.5 Organization of the Thesis

To provide the background of the research conducted in this thesis, Chapter 2 presents a literature review that includes details about hybrid actuation system, hybrid motion system, hybrid control systems, compliant mechanism and general control algorithms. The literature review should also serve for the purpose of justifying the proposed objectives in Chapter 1. Chapter 3 discusses the integrated design, modeling and control of the hybrid actuation system. A new control method is proposed to compensate the speed fluctuation in the CV motor. Chapter 4 presents the design, modeling and optimization of the hybrid motion system. A new topology for motion amplification implemented by the compliant mechanism is proposed. The motion amplification mechanism is designed as a part of the hybrid motion system. The optimization of the hybrid motion system is performed using the finite element method and the Taguchi

method. Chapter 5 focuses on the hybrid control system design and analysis. Chapter 6 presents the simulation and experiment results for the hybrid systems. Finally, Chapter 7 outlines the contribution of the thesis as well as future research work.

2. LITERATURE REVIEW

2.1 Introduction

In this chapter, the state of the art on the development of three types of hybrid systems mentioned in the previous chapter is reviewed to provide justification regarding the significance of the research conducted in this thesis. This review also provides a common basis for the subsequent discussions. Section 2.2 summarizes the design of hybrid actuation systems where different actuation methods are involved. Section 2.3 discusses the hybrid motion system where macro motion and micro motion are formed by individual mechanical systems. In Section 2.4, the compliant mechanism is reviewed, as it is an important concept as well as building block for the hybrid motion system developed in this thesis. Section 2.5 addresses the commonly used algorithms in the control area that are the basis of the hybrid control systems developed in this thesis. Section 2.6 discusses several important hybrid control systems in different control domains. Section 2.7 gives some concluding remarks.

2.2 Hybrid Actuation Systems

A hybrid actuation offers the promise of becoming a viable alternative to the major conventional forms of actuation. This technology was created in an effort to produce a form of actuation combining the most desirable features of the CV motor and the servomotor, while remaining economically feasible to compete with them.

The demands for greater machine productivity with improved quality, diversity of product, and industrial automation have accelerated the needs of hybrid actuation

systems to generate programmable output motions with a high payload capability. The metal forming press machine, printing machine, injection moulding machine, and stamping press are some of industrial examples where a hybrid actuation system has been used with different configurations (Du and Guo, 2003). For example, ARBURG (http://www.manufacturingtalk.com/news/abg/abg103.html) developed the hybrid actuation machines that feature servo-controlled plastication and a variable-speed main pump motor for energy savings combined with hydraulic clamping and hydraulic servo-controlled injection for achieving high accuracy and good repeatability.

Tokuz and Jones (1991) and Tokuz (1992) proposed the hybrid actuation machine system concept and described the modeling of an experimental hybrid machine, which is shown in Figure 2.1. In their hybrid machine, a 2 DOF epicyclical differential gearbox, driven by a CV motor and a servomotor, generates an output motion that further drives a slider-crank mechanism. Their study showed that, for some predefined slider motion, a required servomotor power turned out to be smaller in the hybrid machine than the "single servo configuration". However, it should be noted that the CV motor was physically substituted by a servomotor in their studies.

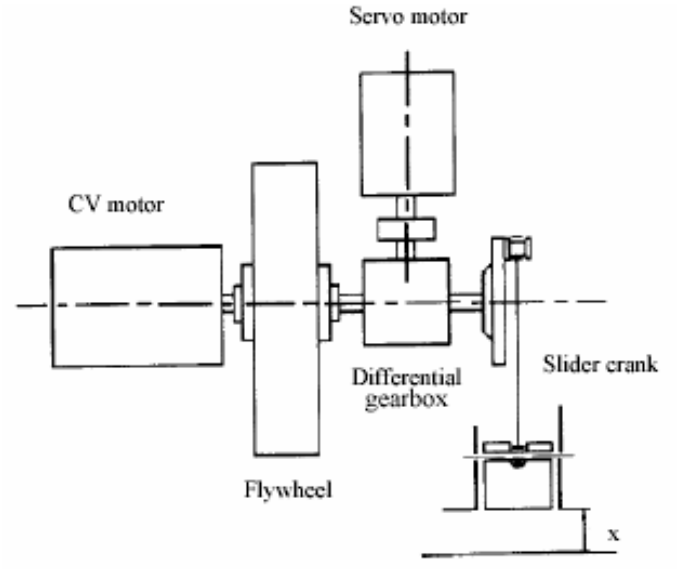

Figure 2.1 Schematic of a hybrid actuation machine (Tokuz, 1992).

Greenough et al. (1995) defined a hybrid actuation machine as a servomotor with a CV motor that are coupled through a 2 DOF mechanism and drive a single output. The servomotor and the CV motor drive two independent shafts of the mechanism. A flywheel is attached to the shaft of the CV motor. The CV motor provides the majority of the power to the system via the 2 DOF mechanism, whilst the servomotor acts as a low torque-modulating device. It was shown that the reduction of the power in the servomotor could be up to 70% of the power if two servomotors were used. But their work did not consider the trajectory tracking; therefore, the torque (thus the power) was not calculated from the dynamic model and the control law. Furthermore, due to the introduction of a flywheel on the CV motor, they assumed the speed of the CV motor be constant and ignored the speed fluctuation in the CV motor.

Straete and Schutter (1996) presented a hybrid cam mechanism with a similar configuration shown in Figure 2.1. The hybrid cam mechanism consists of a hybrid drive, which combined a servomotor and a CV motor, and a cam follower mechanism. They assumed that the CV motor has a large inertia to ensure its constant velocity. Through simulation, they showed that after judicious selection of the cam profile it is possible to reduce the peak torque and the power in the servomotor up to 50%. But the assumption of constant velocity for the CV motor during the real application may not be true if the dynamics of the mechanism and the output load are considered in the hybrid cam mechanism.

Kirecci and Dulger (2000) discussed a hybrid actuation mechanism where a seven-link mechanism with 2 DOF was used as an example to test the hybrid actuation idea that is shown in Figure 2.2. But in the implementation of their study, the servomotor was used to “mimic” the CV motor by prescribing a constant velocity trajectory profile. It is obvious that this departs away from the real situation where a CV motor is in place. Following the same setup, Dulger et al. (2003) developed the dynamic model of the same hybrid mechanism and performed a simulation study where PID controller was applied to the control of two servomotors used in the hybrid actuation system.

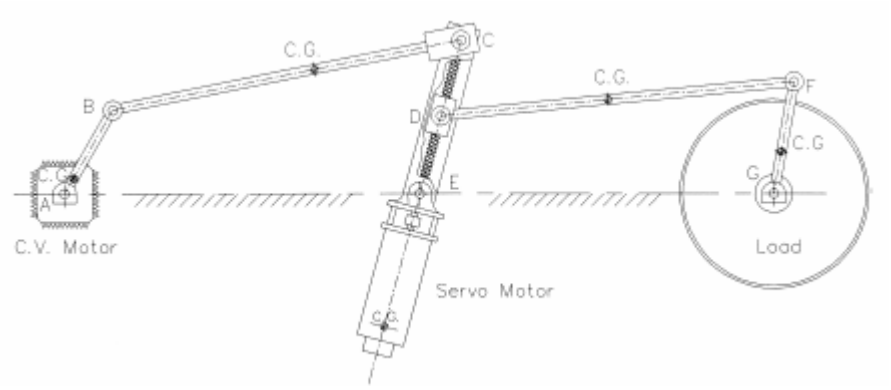

Figure 2.2 A seven link mechanism with hybrid actuation (Kirecci and Dulger, 2000).

Du and Guo (2003) designed a controllable mechanism for the metal forming press application where a 2 DOF seven bar linkage mechanism, driven by a CV motor and a servomotor, was used to form the output stroke. The design optimization was carried out using the Genetic Algorithm. It should be noted that their design only considered the kinematic optimization; no dynamics were included in the design process. Furthermore, the maximum required torque for the optimized design case was about 4000 Nm that is beyond the capacity of the commercial servomotor.

Arai et al. (2002) proposed a hybrid drive parallel arm which was driven by cables and cylinders in order to design a compact handling arm with a large workspace for the application of assembly. The main idea in their design is to enlarge the limited workspace of the cable drive mechanism by replacing some cables with cylinders since the cylinder is capable of generating tension and compression.

There are some other types of hybrid actuators developed and applied in many applications. Although those actuation systems are not involved in my thesis work, for the sake of completeness, some of them are reviewed as well in this section.

Morrell and Salisbury (1998) developed an actuator system called parallel-coupled micro-macro actuator that consists of a micro-actuator and a macro-actuator coupled in parallel via a compliant transmission that is shown in Figure 2.3. In that actuator system, the micro-actuator is capable of high-bandwidth force control owing to its low mass and

direct-drive connection to the output shaft. The compliant transmission of the macro-actuator reduces the impedance (stiffness) at the output shaft and increases the dynamic range of force.

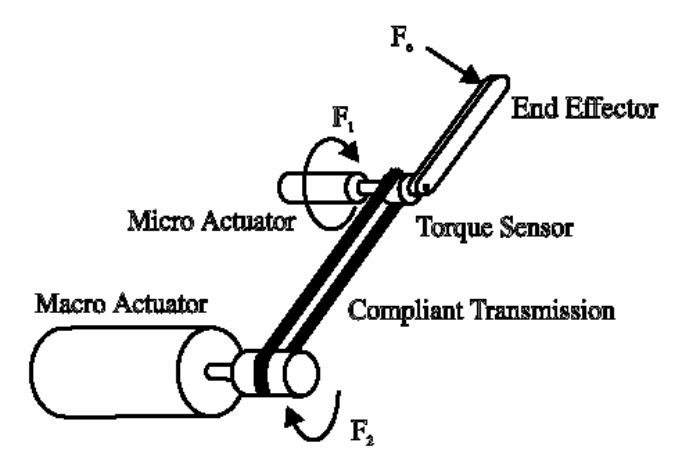

Figure 2.3 The parallel coupled micro-macro actuator concept (Morrell and Salisbury, 1998).

Ferrara et al. (2001) discussed the vibration suppression of a large space structure by switching between different actuators in order to optimize control performance and reduce energy consumption. The variable structure control technique was applied for the jet thrusters actuators and the PZT rods actuators.

The combination of smart material (such as PZT) driving a hydraulic fluid system is called a hydraulic-hybrid actuator or piezohydraulic actuator. In the hydraulic-hybrid concept, an active smart material, most commonly piezoelectric, is driven at a high frequency to pressurize fluid in a pumping chamber. The flow of the pressurized fluid is then rectified by a set of one-way valves, creating pulsing flow in a specified direction. The one directional flow is then utilized to transfer power from the active material to a hydraulic output cylinder. Through this stepwise actuation process, the high frequency, small stroke of the active material is converted into a larger, lower frequency displacement of the output cylinder. There are extensive researches about the design, modeling and control of piezohydraulic actuators, see the review conducted by Niezrecki (2001).

Nakamura et al. (2002) developed a hybrid actuator used in an active micro-vibration control system. The hybrid actuator combines a giant-magnetostrictive actuator and an air actuator arranged in parallel, see Figure 2.4. This structural feature enables the hybrid actuator to make up for both of the single actuators' demerits. The hybrid actuator has a frequency range of about 100 Hz and a maximum displacement of more than 1 mm.

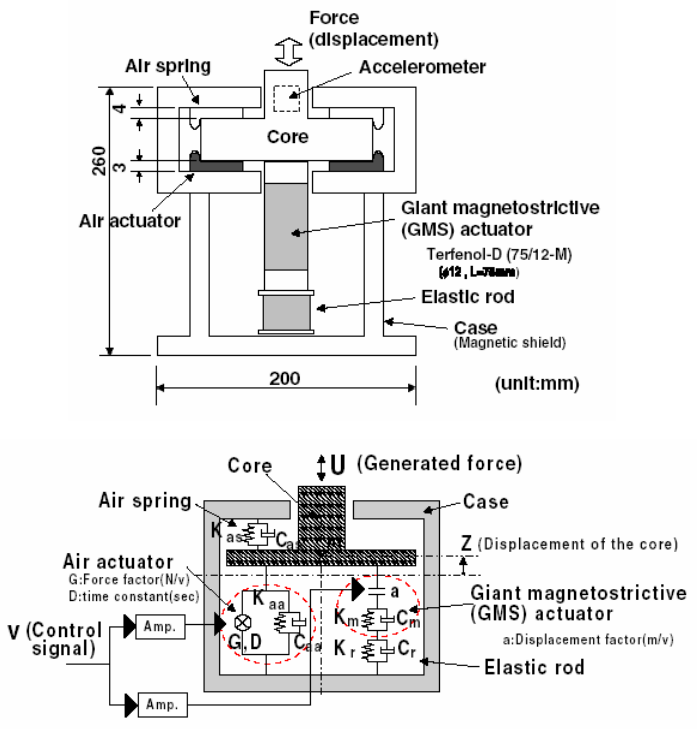

Figure 2.4 Schematic of a hybrid actuator and its mathematical modeling (Nakamura et al., 2002).

2.3 Hybrid Motion Systems

Many applications require robotic manipulators have a large workspace and are capable of fast, precise motion throughout the workspace such as that offered by a macro-micro manipulator system. The long reach, or macro, manipulator is characterized by a "slow" response due to its size. In contrast, the short reach, or micro, manipulator is characterized by a small work volume with fast, precise manipulation capability over that work volume. Combining the two manipulators offers an approach that can satisfy the requirement of fast, precise manipulation over a large workspace. The concept of a

macro-micro manipulator was first introduced by Sharon and Hogan (1993). A typical macro-micro manipulator is shown in Figure 2.5. Obviously, the macro-micro manipulator system is a hybrid motion system.

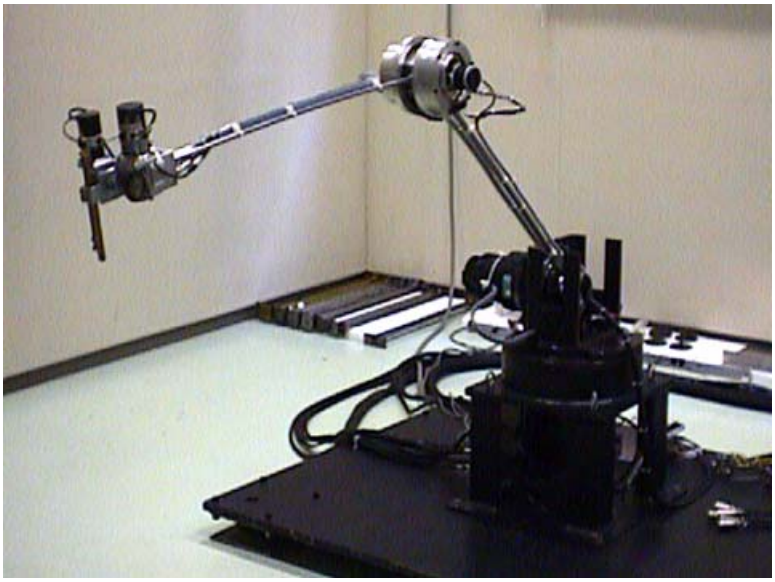

Figure 2.5 An example of a macro-micro manipulator (Yoshikawa et al., 1996).

The macro-micro manipulators provide advantages of a large workspace and accurate end-effector positioning for space and industrial applications. Therefore, recently there has been an increasing research interest in this area. Most macro-micro manipulator systems studied in the literature have flexible macro mechanisms (M-part), and rigid micro mechanisms (m-part) that are attached on the tip of the M-part. The flexible mechanism has long arms and can move in a large workspace, but it cannot be controlled precisely at high speed due to the structural deformation of links. The rigid micro mechanism can achieve fast and precise motion. So the principle for macro-micro systems is to combine a relatively rigid structure with a relative flexible structure. The main focuses on the macro-micro manipulators are the position/ force control, vibration reduction, and performance improvement.

Yoshikawa et al. (1996) described a hybrid position/force control of flexible manipulators by a macro-micro manipulator system. In that macro-micro manipulator

system, the macro manipulator was controlled to roughly realize the desired position and force by a simple PD feedback, and the micro manipulator compensated the position and force errors caused in the macro part.

Lew (1996, 1997) discussed the contact control of a flexible macro-micro manipulator. The controller combined the force damping controller and the inertial force active damping controller. In his studies, using a force sensor at the wrist and a strain measurement at the flexible link, the micro manipulator regulated the contact force to a desired value without causing contact instability.

In Jiang and Goldenberg's (1998) research, an ideal manifold was used to prescribe the desired performance of a flexible macro-micro manipulator in terms of end-effector trajectory tracking and link vibration damping. The control scheme was divided into two parts: one was to compensate the nonlinear forces due to the micro arm motion, and join motion of the macro arm directly; the other was to compensate the nonlinear forces due to the link flexural motion of the macro arm in such a way that the stability of the system would be maintained.

Vliet et al. (1998) described the development of a macro-micro manipulator test-bed. The facility includes a 2 DOF macro manipulator with two flexible links, to which is attached a 3 DOF small robot. The manipulators rest on a planar glass-top table that makes them ideal for studies relevant to space applications. That paper presented the design of the complete system, focusing on the micromanipulator and its integration with the existing hardware, the dynamics model and the frequency domain validation results.

Hodac et al. (1999) pointed out that mounting a fine manipulator on a coarse manipulator would produce a dynamic interaction that might degrade the performance of the whole system. A micromanipulator composed of a flexible suspension and of an electrodynamic actuator placed between the endpoint and ground was proposed and it could reduce the dynamic coupling between the two systems.

Angles et al. (2000) studied the design of the mechanical structure of an 11-axis robot to accomplish accurate positioning and velocity-controlled tasks in the presence of a flexible substructure. The manipulator is designed as a cascade of three modules, the proximal one being termed the macromanipulator which is responsible for a long reach and a high flexibility. The other two modules, comprising the seven-axis micromanipulator, are responsible for the accurate positioning and orientation of the tool attached to the end-effector.

Kwon et al. (2001) discussed the control issue for a coarse/fine dual-stage manipulator that is shown in Figure 2.6. The coarse stage works as a base that offers a large workspace, while the fine stage mounted on the coarse stage enables high resolution of motion and fast response. In their controller design, the single input single output control archtecture for the coarse motion control and the fine motion control was adopted seperately without considering the cross coupling effect between the two stages.

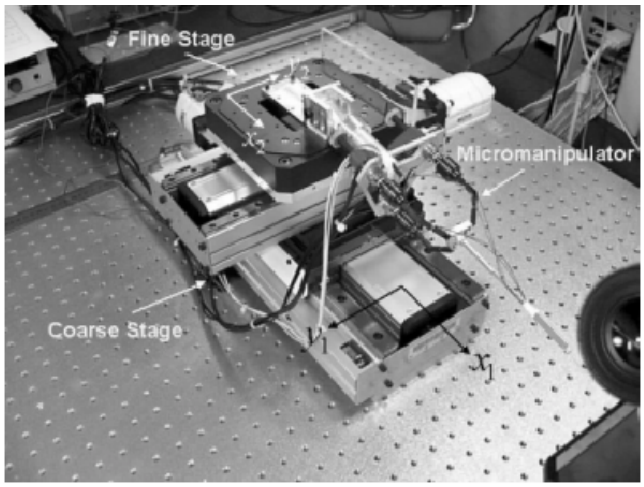

Figure 2.6 A coarse/fine dual-stage manipulator (Kwon et al., 2001).

Xu et al. (2000) studied the macro-micro manipulator system intended to enhance the tracking/positioning performance of flexible manipulators. Additional actuation of the micro rigid manipulator was employed to compensate for the deflections due mainly to the link flexibility involved. In their study, a PD feedback controller was employed incorporating a fuzzy adaptive tuner for the macro manipulator, and a control scheme

was proposed for the micro manipulator, where the sensed flexible states were used as feedforward signals and added to the control command for the rigid motion control of the micro manipulator.

Tol et al. (2002) described the concept of macro-micro system integration using a pallel kinematic mechanism and a 2 DOF micro manipulator for the application of deburring and finishing operations. In their system, seperate control laws were applied to the macro mechanism and the micro mechanism, respectively. The interaction between the micro and macro mechanisms was not taken into consideration.

Gilsinn et al. (2002) discussed a macro-micro motion system that was used to locate the nano-structures, see Figure 2.7. In their design, an XY stage using linear piezo actuators performed the macro motion by moving the sample to where the scanning tunneling microscope (STM) tip could scan a particular region of the die to make an analysis, while the STM tip functioned as the micro motion device.

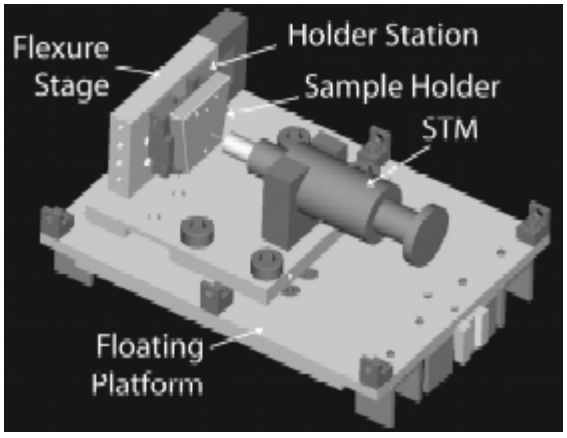

Figure 2.7 A macro-micro motion system (Gilsinn et al., 2002).

From the literature reviews conducted above one can see that all the architectures of the macro-micro manipulator systems are connected in series. It means that the micro manipulator is mounted on the macro manipulator. Such an architecture can be called a serial hybrid motion system. The majority of the hybrid motion system researches were focused on the attenuation of the vibration of the macro manipulator caused by the fast

action of the micro manipulator. The very similar architecture, among the studies reviewed, for macro-micro manipulators may have implied the absence of the general concept of hybrid systems discussed before, specifically, hybrid mechanisms. There may be the architecture of hybrid motion systems, such as serial macro (rigid) – micro (compliant) and complete parallel compliant mechanisms.

2.4 Compliant Mechanisms

A mechanism is a mechanical device used to transfer or transform motion, force, or energy. Traditional rigid-body mechanisms consist of rigid links connected at movable joints. A compliant mechanism also transfers or transforms motion, force, or energy. Unlike rigid-link mechanisms, however, compliant mechanisms gain at least some of their mobility from the deflection of flexible members rather than from movable joints only. An example of the compliant mechanism for crimping is shown in Figure 2.8 (Zhang et al., 2002).

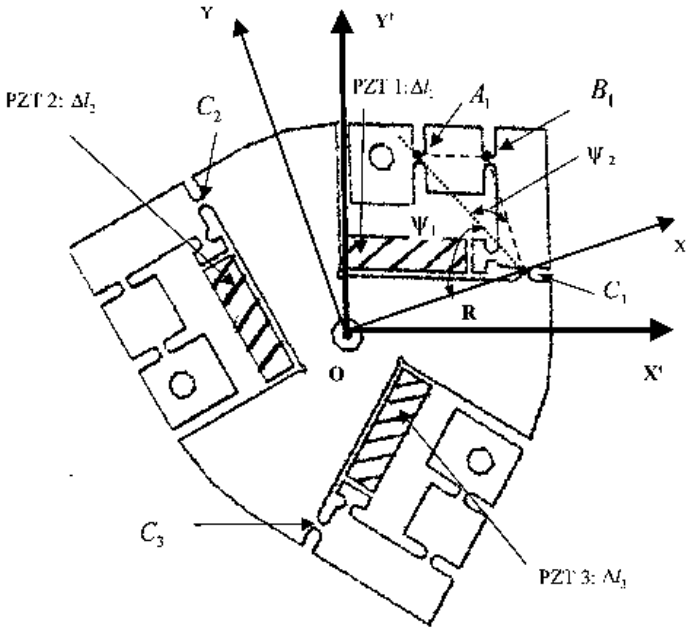

Figure 2.8 A 3 DOF compliant mechanism (Zhang et al., 2002).

A compliant mechanism is a piece of material on which there are notches and holes. The distribution of the notches and holes can result in a structure with a set of flexural hinges. Clearly, when a compliant material receives forces, it behaves such that significant deformations occur around the flexural hinges. A fully compliant mechanism is the one that has no “rigid” kinematic pairs. The benefit of the compliant mechanism includes: (i) reduced or eliminated backlash and no friction; (ii) smooth and continuous displacement; (iii) small resolution, and (iv) lubrication free.

Within modern manufacturing there is a growing need for micropositioning units with very fine resolution, high accuracy, high precision, and repeatability. All of these constraints on system performance are increasingly coupled with the requirement that the system also be durable and of low cost.

In many applications such as assembly in the semiconductor industry, cell manipulation in biotechnology, and surgery automation in medicine, there is a need for devices to perform very small motion (about or less than one millimeter) with very high positioning accuracy (in the micron range) and complex trajectories. This range of motion is known as the micro motion.

A straightforward approach to developing micro motion systems is based on conventional servomotors, such as DC-servo or stepper motors and ball screws or other types of rigid linkages. But, these systems have inherent problems, such as backlash, friction and assembly errors, which significantly hinder the development of both cost-effective and functional micro motion systems. Another approach to developing such systems is based on the compliant mechanism concept. Since the compliant mechanisms do not entail any sliding or rolling, they are free of backlash and Coulomb friction, and thus have perfectly smooth mechanics. The absence of hard nonlinearities in compliant mechanism behaviour places no fundamental physical limitations on the resolution of position or force control. Additionally, the absence of conventional joints or other bearing surfaces produces a clean device that is free of lubricants or other contaminants,

and thus is extremely conducive to clean environments. Complaint mechanisms can be designed for any desired input/output force/displacement characteristics, including specified volume/weight, stiffness, and natural frequency constraints. As flexure is permitted in these mechanisms, they can be readily integrated with unconventional actuation schemes, including thermal, electrostatic, piezoelectric, and shape memory alloy (SMA) actuators.

Compliance in design leads to jointless, no-assembly, monolithic mechanical devices. Since it is often not very practical to fabricate jointed micromechanisms, due to difficulties in microassembly, compliant mechanisms offer an alternative to obtain micromechanical movements without requiring mechanical assembly. Although simple deformable structures, such as beams and diaphragms, have performed adequately in many micro devices, more sophisticated micromechanical function can be realized by fully exploiting the preferred uses of elastic deformation. Figure 2.9 (Kota et al., 1999) shows two examples of micro compliant mechanisms.

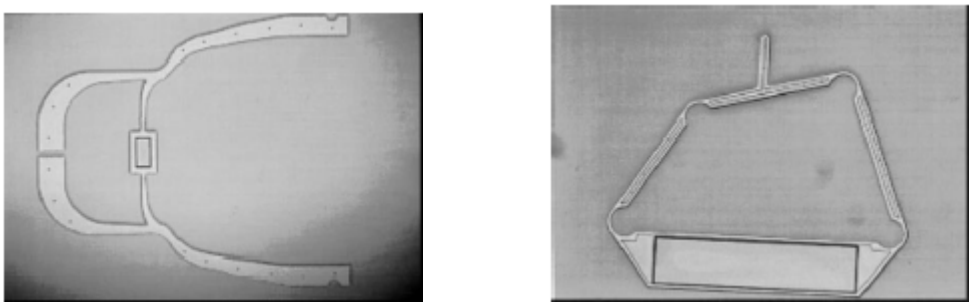

(a) Compliant gripper. (b) Micro compliant four-bar mechanism.

Figure 2.9 Two examples of micro compliant mechanisms (Kota et al., 1999).

A micro motion system based on the compliant mechanism concept can be constructed as a closed-loop configuration or a parallel manipulator, see Figure 2.9(b). The closed-loop mechanism configuration can provide better stiffness and accuracy, which should be one of the important design goals for micro motion systems. Moreover, such a configuration allows the actuators be mounted on the ground, which thus minimizes the inertia of moving parts.

Since the 1970s, compliant micro-positioning stages, which consist of piezoelectric actuators and flexure hinges (Paros and Weisbord, 1965), have been developed. Scire and Teague (1978) designed a compliant single-axis stage that combined a PZT actuator and a flexure pivoted level operating as a displacement amplifier. Furukawa and Mizuno (1992) designed a flexure-hinged translation stage, which combined a linkage as a mechanical amplifier and a guidance system for rectilinear movement. It is noted that these types of compliant mechanism were only able to generate one-axis translation motions and hence, their applications are limited.

In the 1980s, micro-positioning stages that can produce more complex motions than just linear translations have been developed. Lee and Arjunan (1991) designed a spatial 3 DOF compliant micro-positioning in-parallel stage. The kinematic analysis of this mechanism, based on the pseudo-rigid-body model (PRBM) approach, was studied, and a dynamic model of the piezoelectric actuated link was determined experimentally. Ryu et al (1997) designed a flexure hinge based XY-theta stage and discussed the optimal design of the stage. The objective defined in their optimization problem was to achieve a maximum yaw angle. Their work was based on static analysis only.

The PRBM approach mentioned above is a method widely used to design and analyze compliant mechanisms. By its nature, the PRBM is an equivalent rigid body description of compliant mechanisms. It is further noted that the stiffness of the flexure hinge in a compliant mechanism will be equivalently represented by a torsional spring on the joint of the PRBM. The relationship or mapping between a compliant mechanism and its PRBM has been extensively studied, which has resulted in some useful mapping formulae (Paros and Weisbord, 1965; Her and Chang, 1994; Jensen et al., 1997; Derderian et al., 1996; Howell and Midha, 1994). Finite element analysis and experiments were performed and their results were compared with the results predicted by the PRBM approach (Jensen et al., 1997; Millar et al., 1996), and a good agreement of the results obtained by these approaches was achieved.

Micro motion compliant mechanisms, which use parallel manipulators as their PRBM, have been studied with substantial research interests. In the literature, the micro motion compliant mechanism designed with its PRBM as a parallel manipulator was also called a parallel micromanipulator (Hara and Sugimoto, 1989). In parallel micromanipulators, because the motion is very small, the relationship between the input displacements and output displacements can be approximated by a Taylor series expansion, which resulted in a constant matrix obtained from the original position of its PRBM (Hara and Sugimoto, 1989). An approximate analysis of the motion of the compliant mechanism was presented by Zong et al. (1997). Their work led to a constant relationship between the elongation of the PZT actuators and the end-effector motion. Further improvement was achieved by Zhang et al. (2002).

Another important application of the compliant mechanism is in the area of mechanical amplification. There are extensive researches on the mechanical amplifier based on the compliant mechanism that is a special type of compliant mechanism with a proper design of the topology and geometry. The design goal of a mechanical amplifier is to achieve a large amplification ratio which can, however, compromise the generating force and the natural frequency of the amplification mechanism.

Gao et al. (1999) developed an x-y micro-positioning stage utilizing flexure hinges based on a single lever arm topology where the lateral effect was ignored because of the limited motion range of the designed stage. Tenzer and Mrad (2004) discussed the mechanical amplification in inchworm linear motors where a double lever amplifier was included in the motor frame. Su and Yang (2001) analyzed the force amplification ratio of single- and multiply-stage flexure-based micro-level systems. Varma and Dixon (2002) designed a meco-scale mobile robot where a double lever compliant amplification device was developed to realize the lift and pull movement of the legs.

Pokines and Garica (1998) designed a micro-amplifier with an amplification ratio of 5.48 based on a four-bar topology that was fabricated using LIGA (Lithographie, galvanoformung und abformung in Germany). Bharti and Frecher (2004) discussed the

optimal design of a compliant mechanism amplifier in the application of an inertially stabilized rifle. Lobontiu and Garica (2003) formulated an analytical method for displacement and stiffness calculation of planar compliant mechanisms with single-axis flexure hinges.

2.5 Control Algorithms

As the control system is the core part of the mechanisms where the desired trajectory needed to achieve. There are many types of control algorithms being used in the research areas and industrial applications. In this section, some common control algorithms are reviewed as a fundamental of the hybrid control systems discussed in this thesis.

2.5.1 PID/PD Control

The popular widely used feedback controller is the proportional-integral-derivative (PID) controller that has the following form:

$$T(t) = K_P e(t) + K_I \int_0^t e(\tau) d\tau + K_D \dot{e}(t) \tag{2.1}$$

where K_P , K_I , and K_D are constant proportional, integral, and derivative gains, respectively, and $T(t)$ is the torque. Such a simple and effective controller has been extensively studied for different types of systems and widely used in many industrial processes, especially in robot control. If the control gain K_I is set to zero, the PID control turns to be the PD control.

It is well known that when position and velocity measurements are available, a PD control is the simplest control law and can be implemented using commercial control modules. In Craig (1986, 1988) and Kelly (1997), the PD control with desired gravity compensation was shown to guarantee global and asymptotic stability for a point-set

tracking problem. More works on the global stability of trajectory tracking with the manipulators under PD control were given by Qu (1995), and Chen et al. (2001). To improve the trajectory tracking performance of robot manipulators, significant effort has been made to seek advanced control strategies. Achievements were made in developing adaptive control and robust control approaches that ensure the globally asymptotical convergence of the tracking errors. However, since these approaches are all based on centralized control structures that require rather tedious computation, their practical applications are not very promising. In fact, in spite of the theoretical results obtained, the majority of the industrial robots are still controlled by the decentralized (independent joint) PD law in favor of its simple computation and low-cost set-up. This is because the PD controllers, despite their simple structures, assure acceptable performances for a wide range of industrial plants. Furthermore, their usages are well known among industrial operators. Hence, the PD controllers provide a cost effective mean in industrial environments.

2.5.2 Nonlinear PD Control

Trajectory tracking with PD/PID control may not lead to a high-accuracy tracking performance, especially at high speeds, because PD control is only a linear control. One of the refinements for a PD controller is the Nonlinear PD (NPD) controller (Rugh, 1987; Shahruz and Schwartz, 1994; Xu et al., 1995; Seraji, 1998; Armstrong and Wade, 2000).

Generally speaking, the NPD control is a control where the control gains are functions of the tracking errors. Rugh (1987) designed a Nonlinear PID control by the extended linearization technique in which the three gains of the controller are functions of the error state. Xu et al. (1995) proposed a NPD control for the force control tasks, and also pointed out that the method is also applicable to position control. Seraji (1998) introduced a new class of simple NPD controllers and provided a formal treatment of their stability analysis based on the Popov criterion. It should be noted that many previous studies on NPD control were applied to the point-set control of linear systems.

There are only few papers describing the NPD control for trajectory tracking of nonlinear systems such as parallel manipulators. In this thesis, the NPD control will be extended to form a NPD learning control for the repetitive tasks of the mechanisms.

2.5.3 Adaptive Control

Adaptive control (Craig, 1988) can be viewed as being composed of two parts: (1) an identification portion, which identifies parameters of the plant itself, or parameters that appear in the controller for the plant; (2) a control law portion, which implements a control law that is in some way a function of the parameters identified. Adaptive control provides adaptation mechanisms that adjust a controller online for a system with parametric, structural, and environmental uncertainties to achieve the desired system performance. Typical adaptive control applications reported in literature include temperature control, chemical reactor control, automobile control, robot control, and ship steering control. The important issue in adaptive control is the design of an adaptive law that updates the controller parameters online to achieve some desired system performance.

2.5.4 Learning Control

A learning control is such a control that has the ability to improve its performance in the future, based on experimental information it has gained in the past, through interactions with the plant and its environment. Learning control has the autonomous capability, has memory, and it is dynamic since it may vary over time. The learning control operates in the context of an objective function and it receives performance feedback that characterizes the appropriateness of its current behaviour in that context. The advantages of learning control include: (1) it is not necessary to have a parametric model of the system; (2) the unstructured uncertainty can be compensated for to the extent that it is repeatable from one trial to the next.

White and Sofge (1992) discussed the difference between the adaptive control and the learning control. They pointed out that a control system that treats every distinct operating situation as a novel one is limited to adaptive operation, whereas a system that correlates past experiences with past situations, and that can recall and exploit those past experience, is capable of learning.

The purpose of using adaptive and learning control is to simplify the implementation process, to improve the system's reliability and thus achieve a good performance of the system.

2.6 Hybrid Control Systems

In this section, the switching control and sliding mode control associated with the thesis, which can be viewed as hybrid control systems, are reviewed in detail. Also, the iterative learning control that can be used as part of the hybrid control system is also reviewed.

2.6.1 Switching Control

In the control area, the switching control systems, also called as hybrid control systems in the control research area, mean the complex control systems which have discrete event dynamics as well as continuous time dynamics. This broad class of systems includes continuous systems with phased operation (bouncing ball, walking robots, biological cell growth and division), continuous systems controlled by discrete logic (aircraft autopilot modes, thermostats, chemical plants with valves and pumps, automobile automatic transmissions), and coordinating processes (air and ground transportation systems, swarms of air vehicles). Figure 2.10 shows a scheme of a switching control system.

From Figure 2.10, one can see that the switching control systems are characterized by the interaction of the continuous parts, governed by differential or difference equations,

and the discrete parts, described by finite state machines, if-then-else rules, propositional and temporal logic. Such systems switch between many operating modes where each mode is governed by its own characteristic dynamical laws. Mode transitions are triggered by variables crossing specific thresholds (state events), by the elapse of certain time periods (time events), or by external inputs (input events). Typical switching control systems are embedded systems, constituted by dynamical components governed by logical/discrete decision components. Application areas of switching control systems include automotive, manufacturing, communication networks, aerospace, robotics, traffic control, and chemical processes.

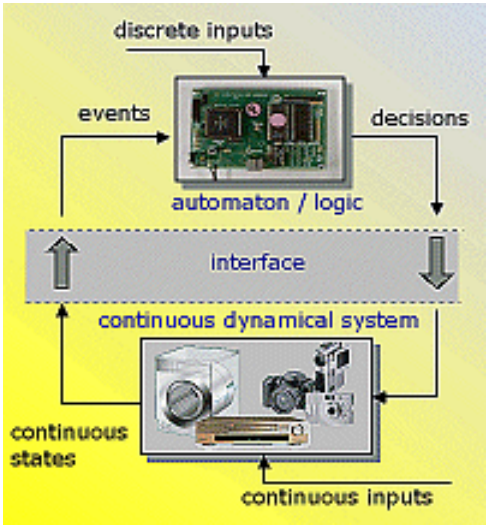

Figure 2.10 A switching control system and the interaction.
(http://www.ieeecss.org/TAB/Technical/hybrid/)

Excellent reviews of switching control systems were given by Antsaklis and Nerode (1998) and Antsaklis et al. (1998). Schaft and Schemacher (1998) developed a framework for the modeling of certain classes of mixed continuous/discrete dynamic systems. Branicky et al. (1998) proposed a general framework that systematizes the notion of a switching control system, combing differential equations and automata, governed by a hybrid controller that issues continuous-variable commands and makes logic decisions.

Switching control systems produce switches between a finite, or at least countable, number of fixed controllers until stability is detected. Such controllers are very attractive from a theoretical viewpoint, in providing stabilisation and asymptotic performance for a broad class of plants. However, such controllers are also known to have very poor transient properties, due to the long time required to search for a stabilizing feedback. This transient problem may be so serious that it casts doubt on the practical value of the switching control.

2.6.2 Sliding Mode Control

The sliding mode control (SMC) or variable structure control evolved from the pioneering working in Russia of Emel'yanov and Barbashin in the early 1960s (Edwards and Spurgeon, 1998) and has been studied extensively to deal with problems of the nonlinear dynamic control systems with modeling uncertainties, time varying parameter fluctuation, and external disturbances (Utkin, 1977; Slotine and Li, 1991). The sliding mode control has been utilized in the design of robust regulators, model-reference systems, adaptive schemes, tracking systems, and state observers. The SMC was successfully applied to problems such as automatic flight control, control of electric motors, chemical processes, space systems and robots.

One of the most intriguing aspects of the SMC is the discontinuous nature of the control action whose primary function of each of the feedback channels is to switch between two distinctively different system structures such that a new type of system action, called sliding mode, exists in a manifold. This means that the control law is deliberately changed during the control process according to some defined rules which depend on the state of the system. In this sense, the SMC can also be viewed as a kind of switching control. In the SMC, the sliding region is defined as a manifold or a hyperplane (Utkin, 1992). In the case of two dimensional systems, the sliding region will be a line. The control action of the SMC is a maximum on one side of the manifold and a minimum on the other side of the manifold. Theoretically, it is assumed that the controller can switch from one extreme to another extreme infinitely fast. A system trajectory then can stay on

the sliding manifold as soon as it reaches the manifold. However, due to the limited sampling rate in practice, system trajectories will chatter instead of sliding along the switching manifold. The control action alternatively changes its sign along the switching manifold.

The chattering phenomenon is generally perceived as motion which oscillates about the sliding manifold. The main reasons for such a phenomenon are the switching delay of the switching devices and the high-frequency switching between the two different control structures. In many situations the chattering phenomenon would not be considered acceptable. A natural solution is to attempt to smooth the discontinuity of the control signal. The most commonly used approach to reduce the effects of chattering was the so called piecewise linear or smooth approximation of the switching element in a boundary layer of the sliding manifold (Young et al., 1977; Slotine and Sastry, 1983; Slotine and Li, 1991). Within the boundary layer, the control command is a linear function of the distance between the actual system state and the sliding manifold.

Besides the general SMC, many progresses were achieved where advanced control strategies were used for different purposes. Some of the developments in the sliding model control area are summarized in Table 2.1.

Table 2.1 Some advancements of the sliding mode control methods in literature.

Source	**Control strategy**	**Objective**	**Application**
Moinv et al., 1995	Genetic algorithm	Optimize control gains	Linear/nonlinear systems
Li et al., 1996	Genetic algorithm	Optimize control gains	Linear/nonlinear systems
Chang, 2002	Genetic algorithm	Disturbance rejection	Linear system
Chou et al., 2003	Genetic algorithm	Gain on-line tuning	Servomotor control

Lee et al., 2001	GA +Fuzzy	Gain on-line tuning	Trajectory tracking of robot
Hwang, 2002	Fuzzy	Fuzzy switching control	biped robot system
Allamehzadeh and Cheung, 2002	Fuzzy	Chattering free control	an inverted pendulum
Xu et al., 2001	Robust adaptive	Controller design	Nonlinear system
Wai et al., 2004	Adaptive fuzzy	Fuzzy rule adjust	Rotor control of a servomotor
Chen and Moskwa, 1997	Nonlinear observer	Gain tuning	Pressure reconstruction
Man and Palaniswami, 1994	Feedback + sliding mode control	Controller design	Robotic manipulator
Kachroo, 1999	Boundary layer	Chattering-free control	Nonlinear system
Chen et al., 2002	Boundary layer	Chattering-free control	Linear system

2.6.3 Iterative Learning Control

The majority of manipulators used in industry today repeat their motions over and over in cycles. Such repeated movements can be used to reveal the properties of unknown dynamics during the completion of a specific task. The idea of using an iterative method to compensate for a repetitive error is not new. When letting a machine do the same task repeatedly, it is, at least from an engineering point of view, very sound to use knowledge from previous iterations of the same task to try to reduce the error the next time the task is performed. Arimoto et al. (1984) defined iterative learning control (ILC) as a class of control algorithms that achieve asymptotic zero tracking error by an iterative process. In such a process, a single tracking task is repeatedly performed by the system, starting always from the same initial condition. Emulating human learning, ILC uses knowledge

obtained from the previous trial to adjust the control input for the current trial so that a better performance can be achieved.

ILC is one kind of control methodology effectively dealing with repeated tracking control problems or periodic disturbance rejection problems, see Arimoto et al. (1984), Moore (1993), Owens et al. (1995). A typical ILC, in the time domain, is under a simple closed-loop or even open-loop control. Therefore, two types of ILC can be classified: one is off-line ILC, the other is on-line ILC which are shown in Figure 2.11 (a) and (b), respectively.

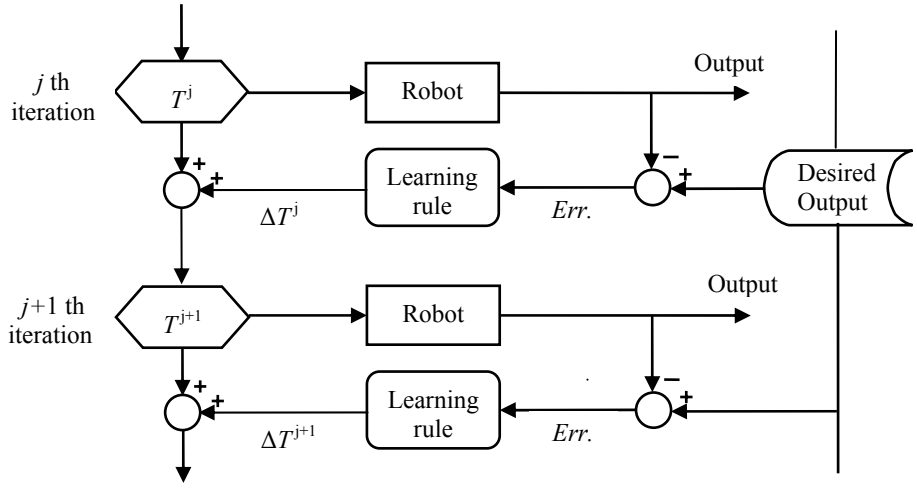

(a) Off-line iterative learning control

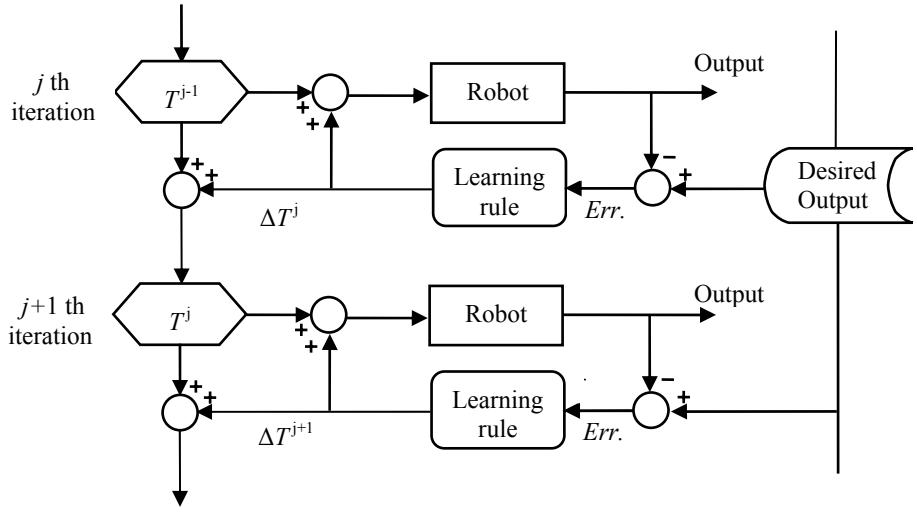

(b) On-line iterative learning control

Figure 2.11 Two types of iterative learning control.

Following the direction of ILC, there are many researches focused on the adaptive ILC. ILC can be classified into P-type, D-type, and PID type. Yan et al. (2001) proposed a D-type learning control algorithm that can be applied to the offline learning and the online learning. The proposed controller is robust in the sense that exact knowledge about nonlinear dynamics is not required except for the bounding functions on their magnitudes.

Qu (1993) proposed a controller that consists of two parts, a standard PID control and a linear iterative term that is D-type learning with small learning gains. But in practice, it is difficult to satisfy the required conditions discussed in his paper. Kuc (1992) developed an iterative learning control scheme that is a kind of P-type online learning. Kuc and Han (2000) proposed an adaptive PID learning control for the control of robot manipulators where the control gains are not only the functions of the previous iteration but also the complex functions of the errors of the current one. Park et al. (1996) discussed the adaptive learning control of uncertain robotic systems that included a linear feedback, a feedforward error compensator and a learning strategy where the dynamic model was a priori. Hatonen et al. (2004) discussed the discrete-time iterative learning control systems where an adaptive P-type learning algorithm was proposed. Sun and Wang (2002) proposed a PID-type on-line learning control for nonlinear systems where the high order time derivatives of the errors were included in the feedback control law. Note that it is difficult to get the high order derivative of the errors from the application point of view. Ahn et al. (1993) discussed the classical iterative learning control using the relative degree of a system. Norrlof and Gunnarsson (2002) proposed an adaptive iterative learning control algorithm based on an estimation procedure using a Kalman filter. It was noted that in that controller, there are many parameters involved in the design process and real-time computation. Jang et al. (1995) proposed a learning law based on the high order time derivatives of the errors of the previous trial in the PD feedback configuration. Chen et al. (1997) developed a high-order P-type iterative learning controller where the previous and current iteration tracking errors were included in the update law. Choi and Li (2000) discussed the adaptive iterative learning control

with the consideration of the computed torque based on the adaptation for the parameter estimation.

2.7 Concluding Remarks

This chapter presented the state of the art on the developments in three types of hybrid systems. Based on the literature review in the previous sections, it is clear, with reference to the research objectives defined in this thesis, that none of these objectives has been fully achieved. This is the starting point of this research.

With respect to the hybrid actuation system, the existing research on this topic usually either uses a servomotor to mimic the CV motor by prescribing a constant velocity trajectory profile, or assumes the speed of a CV motor be constant. Such a replacement or presumption is far away from the real application of the hybrid actuation system. This thesis will consider the real use of the CV motor in the hybrid actuation system. Detailed information will be provided in Chapter 3. It should be noted that the main challenge in the hybrid actuation system is that the CV motor will bring the speed fluctuation which can not be attenuated by the CV motor itself due to the lack of control capacity, yet be propagated to the servomotor, and further to the end-effector of the mechanism. Also in Chapter 3, to control the hybrid actuation system, a new hybrid controller will be developed that integrates the sliding mode control, model based control, and the compensating control for the reduction of the speed fluctuation in the CV motor.

With respect to the hybrid motion system, traditionally, the design of a macro-micro mechanism is divided into two separate motion stages. One is for the macro motion as a base with a large motion range; the other is for the micro motion with high accuracy which is mounted on the macro motion stage. Such a design is easy to realize, but the assemble error and the backlash force will affect the accuracy of the end-effector. Also, the full device is much complex. Further, mounting a micro manipulator at the tip of a macro manipulator results in a dynamically coupled system. The purpose for studying the hybrid motion system in this thesis is to develop a new design strategy for the spatial

compliant mechanism with the parallel actuation that has the potential of macro and micro motions. The main idea behind the design is that two types of actuators, i.e., DC servomotor for the macro motion and the PZT actuator for the micro motion, are integrated to form the actuation system. In such a design, only one compliant mechanism is needed to complete coarse and fine positioning performance. Chapter 4 will discuss the design, modeling and optimization of the hybrid motion system.

With respect to the hybrid control systems, the existing researches focused on the time domain for the development of the control algorithms. In this thesis, four hybrid control systems will be developed. They are: (1) PD type online learning control, (2) adaptive NPD learning control, (3) adaptive switching learning PD control, and (4) Sliding mode plus model based control. The PD type online learning control can be viewed as a hybrid control in the iteration domain that has the ability of learning. The adaptive NPD learning control can be viewed as a hybrid control in the error domain. The adaptive switching learning PD control is also a hybrid control that combines the iterative learning control and the switching control method. The unique feature of the PD type learning control systems is that the switching acts not in the time domain but in the iteration domain and the error domain. This is the main difference between the adaptive switching control method and the traditional switching control method, where switching occurs in the time domain. Therefore, the transient process of the switched system, which must be carefully treated in the case of the traditional switching control method, does not occur in the new control method. Chapter 5 will focus on the development of the hybrid control systems.

3. HYBRID ACTUATION SYSTEM

3.1 Introduction

For most manufacturing automation applications in high volume production industries, expensive multi-axis robots are employed for simple repetitive operations that require only a limited flexibility, and their inherent flexibility is often underutilized. In order to provide a middle ground between conventional inflexible machines and overly flexible robots and to take the advantages of both the traditional mechanism (which refer to a closed chain mechanism) and the servo driving mechanism, the association of a servomotor to a conventional mechanism has been studied. This chapter discusses the design, modeling and control of a hybrid actuation system (HAS) where a 2 DOF parallel mechanism is used as an example. The parallel mechanism in this case is a five bar linkage where one input is provided by a CV motor and the other by a servomotor.

As implied in the discussion presented in Chapter 2, the control of a HAS is still a challenge. This is mainly because of: (1) the uncontrollability of the CV motor and the speed fluctuation in it during the operation of the system, and (2) the coupling of the dynamics between the two input links associated with the CV motor and the servomotor, respectively. A preliminary study demonstrated that traditional PD/PID control and Computer torque control (CTC) methods do not work for the HAS. The present study aimed to develop an understanding of the dynamic behavior of the hybrid actuation that consists of the CV motor (not any substituted one by the servomotor) and the servomotor. A new controller integrating the SMC technique (Emelyanvo, 1967; Utkin, 1977; Slotine and Li, 1991) and the compensation technique is developed to implement a general control strategy, i.e., designing the controller for servomotor to compensate the disturbance propagated from the CV motor due to its speed fluctuation. The main task

for the simulation study was to verify the developed controller. The speed fluctuation in the CV motor was examined, and its impact to the dynamic performance in the servomotor was observed. Furthermore, the effect of the mechanical flywheel on the dynamic performance in the servomotor was studied, which is interesting because an optimal integration of mechanical design (meant for design of a flywheel) and control system design can be observed -- known as a mechatronic design approach (Zhang et al., 1999, Li et al., 2001).

The reminder of this chapter is organized as follows. Section 3.2 discusses the design of the HAS, including the mobility and workspace analysis. Section 3.3 derives the dynamic model of the HAS, including the dynamics of the motors. Section 3.4 develops a new control algorithm and presents a stability analysis for this algorithm for the trajectory tracking task. Section 3.5 presents the simulation study for the hybrid actuation system. Section 3.6 is a conclusion.

3.2 Design of the Hybrid Actuation System

3.2.1 Mobility of the Hybrid Actuation System

Mobility of the HAS is defined such that two input links operate as an independent driving unit and are capable of revolving around their rotating shafts, respectively. These links are called driving links hereafter. In addition, the linkage must be ensured that there is no singularity in the whole domain of the two input variables. In the following, the condition for the driving link to have a full rotation capability is derived.

Figure 3.1 shows the scheme of a five-bar linkage HAS. The angle between any two adjacent links of the linkage is defined as a revolvable angle if it can revolve relatively to each other about the joint axis between them; otherwise the angle is a non-revolvable one. Except for the angle between two coupler links (end effector point P lies on the

joint point of the two coupler links), all the other angles with respect to their corresponding joints must be revolvable.

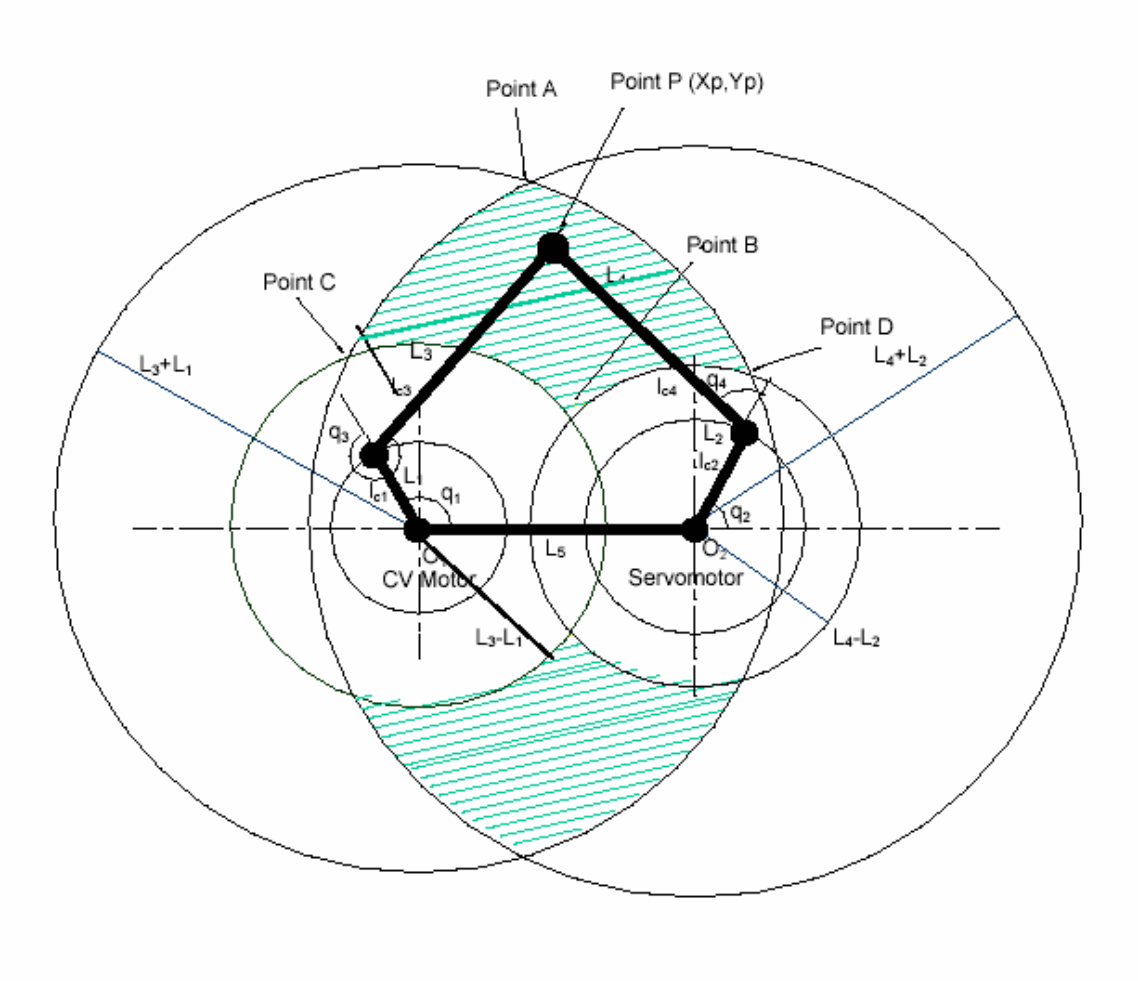

Figure 3.1 Scheme of the hybrid actuation system and its workspace.

A theorem for the full rotatability of the closed loop linkage was given by Ting and Liu (1991) and Ting (1991). For the five-bar linkage HAS, the theorem can be described as follows:

Conditions:

(1) The inequality equation:

$$L_{\max} + L_{\min 2} + L_{\min 1} \leq L_m + L_n \tag{3.1}$$

where $L_{\max}$, $L_{\min 1}$ and $L_{\min 2}$ are the lengths of the longest link and the two shortest links in the five-bar linkage, L_m and L_n are the lengths of the other two links, and further $L_{\max} \geq L_m \geq L_n \geq L_{\min 2} \geq L_{\min 1}$.

(2) One of two coupler links must be among $(L_{\max}, L_m, L_n)$.

Concluding remarks:

The links with $L_{\min 1}$ and $L_{\min 2}$ can revolve relatively to any of their neighbouring link; while any angle between two of the remaining three other links $(L_{\max}, L_m, L_n)$ is a non-revolvable one. Alternatively, the conclusion can be stated as: each driving link and its adjacent links must be either $L_{\min 1}$ or $L_{\min 2}$.

The above theorem is for the five-bar linkage in which two driving links can be any two of the four moving links (notice: one link is the ground link). For the five-bar linkage in which two driving links are not adjacent, more specific conditions for the five-bar linkage were derived by Lin and Lee (2003); i.e.,

$$\begin{cases} L_1 + L_2 + L_5 \leq L_3 + L_4 \\ L_1 - L_2 - L_5 \geq \left| L_3 - L_4 \right| \end{cases} \text{ or } \begin{cases} L_1 + L_2 + L_5 \leq L_3 + L_4 \\ L_2 - L_1 - L_5 \geq \left| L_3 - L_4 \right| \end{cases} \text{ or } \begin{cases} L_1 + L_2 + L_5 \leq L_3 + L_4 \\ L_5 - L_1 - L_2 \geq \left| L_3 - L_4 \right| \end{cases}$$

Based on the above discussion, one of the ways to have a five-bar HAS with two full rotatable driving links is to define a common link associated with the two driving links, and to define it as the ground link; further define $L_{\min 1}$ and $L_{\min 2}$ to be the two driving links, respectively.

3.2.2 The Workspace Analysis of the Hybrid Actuation System

The detailed geometric and kinematic properties of the manipulator kinematic structure play an important role in the range of manipulation tasks which can be performed by the manipulator. For this reason, the kinematic structure has been investigated for five bar manipulators that have symmetric configurations (Gosselin and Guillot, 1991; Feng et al., 1996; Cervantes-Sanchez and Rendon-Sanchen 1999). The workspace analysis has two objectives: (1) to determine the valid space for the end-effector to reach given the structure of the HAS, and (2) to determine the geometry of the HAS (e.g., the length of links) such that a desired trajectory is within the workspace. These two objectives can be achieved if the relationship between the workspace and the geometry of the mechanism is known. In the following the workspace is derived.

In the HAS, the end-effector point *P* is assumed on the joint point of link 3 and link 4; see Figure 3.1. As the two driving links have full rotation property, respectively, the linkage is composed of two dyads (dyad 1: links 1 and 3; dyad 2: links 2 and 4). Therefore, the workspace of the five-bar linkage is the common space of the workspaces for the two dyads, i.e., the shadow region in Figure 3.1. The boundary of the workspace can be found in the following way.

Define the limit configuration of the dyad (dyad 1 and dyad 2) as the configuration where the angle between two links (for dyad 1: link 1 and link 3; for dyad 2: link 2 and link 4) is either 0 or π. Hence for each dyad, there are two limit configurations. Geometrically, the limit configurations of a dyad can be drawn as two concentric circles; see Figure 3.1 where the circle (L1+L3) and the circle |L3-L1| are two limit configurations of dyad 1, and the circle (L2+L4) and the circle |L4-L2| are two limit configurations of dyad 1. The limit configurations for two dyads create four intersection points (A, B, C, D); see Figure 3.1, and these points are the boundary points of the workspace. At the limit configurations, the end-effector *P* reaches these boundary points, respectively.

3.2.3 Parameters of the Hybrid Actuation System

A schematic diagram of the HAS is illustrated in Figure 3.2. The HAS consists of a five-bar linkage, an servomotor and a servo amplifier with a gear transmission, a CV motor and a frequency controller, a flywheel, a belt, and a shaft encoder. In this arrangement, the CV motor with a belt of 3:1 and the servomotor generate the expected output trajectories of the end-effector through a five-bar linkage. Different combinations of motion profiles of the two inputs driven, respectively, by the CV motor and the servomotor can be implemented to obtain various types of output trajectories of the end-effector.

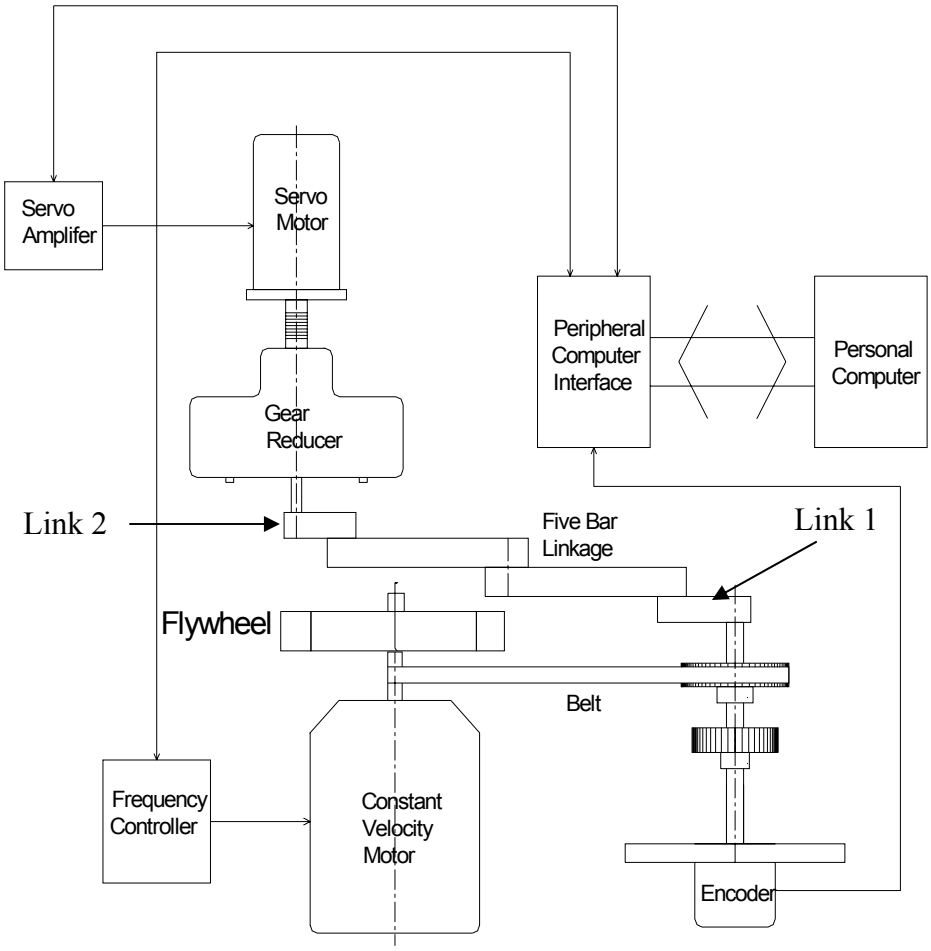

Figure 3.2 Schematic diagram of the hybrid actuation system.

To satisfy the requirement of full rotatability of the HAS, the parameters of the parallel mechanism are selected carefully according to Eq. (3.1) and are listed in Table 3.1.

Table 3.1 Parameters of the parallel mechanism.

Link i	m_i (kg)	L_i (m)	l_{ci} (m)	I_i ($\times 10^{-2}$ $kg.m^2$)
1	0.91	0.080	0.0061538	0.84718
2	0.28	0.100	0.02860	0.63001
3	0.38	0.250	0.125	4.00195
4	0.38	0.250	0.125	4.00195
5	--	0.250	--	--

3.3 Dynamic Modeling of the Hybrid Actuation System

Modelling of the dynamics of a plant is a key to the effective control of the plant. The HAS prototype has 2 DOFs, but only one is controllable. Therefore, it is necessary to build a complete dynamic model in such a way that the speed fluctuation in the CV motor can be compensated by a controller governing the servomotor. In this section, both the dynamic model of the mecahnical system and that of the motors are established and then integrated into a single one.

3.3.1 The Dynamic Model of the Parallel Mechanism

To derive the dynamic model of the parallel mechanism, the method called the reduced model method for the closed chain mechanism in (Ghorbel 1995; Ghorbel and Gunnawardana, 1997) is employed in this thesis. As defined in Figure 3.1, m_i, l_{ci}, L_i are, respectively, the mass, the distance to the center of mass from the joint of link i, and the

length of link *i,* and I_i is the inertia of link *i*. For the more general application, one can assume that the center of mass of each link is off-line with an angle δ_i (Figure 3.1). Following the similar procedures in references (Ghorbel 1995, Ghorbel and Gunnawardana, 1997), the dynamic model of the closed chain linkage can be expressed as follows.

$$\begin{cases} D(q')\ddot{q} + C(q', \dot{q}')\dot{q} + g(q') = \tau \\ \dot{q}' = \rho(q')\dot{q} \\ q' = \sigma(q) \end{cases} \tag{3.2}$$

where $q = [q_1 \quad q_2]^T$, $q' = [q_1 \quad q_2 \quad q_3 \quad q_4]^T$

$\dot{q} = [\dot{q}_1 \quad \dot{q}_2]^T$, $\dot{q}' = [\dot{q}_1 \quad \dot{q}_2 \quad \dot{q}_3 \quad \dot{q}_4]^T$

$\tau = [\tau_1 \quad \tau_2]^T$

and

$$D(q') = \rho(q')^T D'(q')\rho(q') \tag{3.3}$$

$$C(q', \dot{q}') = \rho(q')^T C'(q', \dot{q}')\rho(q') + \rho(q')^T D'(q')\dot{\rho}(q', \dot{q}') \tag{3.4}$$

$$g(q') = \rho(q')^T g'(q') \tag{3.5}$$

$D'(q')$, $C'(q', \dot{q}')$, $g'(q')$, $\dot{\rho}(q', \dot{q}')$, $\rho(q')$, and $\sigma(q)$ are determined as follows.

By means of the Lagrangian method one can obtain:

$$D'(q') = \begin{bmatrix} d_{1,1} & 0 & d_{1,3} & 0 \\ 0 & d_{2,2} & 0 & d_{2,4} \\ d_{3,1} & 0 & d_{3,3} & 0 \\ 0 & d_{4,2} & 0 & d_{4,4} \end{bmatrix} \tag{3.6}$$

where $d_{1,1} = m_1 l_{c1}^2 + m_3(L_1^2 + l_{c3}^2 + 2L_1 l_{c3}\cos(q_3 + \delta_3)) + I_1 + I_3$,

$d_{1,3} = m_3(l_{c3}^2 + L_1 l_{c3}\cos(q_3 + \delta_3)) + I_3$, $d_{3,1} = d_{1,3}$,

$$d_{2,2} = m_2 l_{c2}^2 + m_4 (L_2^2 + l_{c4}^2 + 2L_2 l_{c4} \cos(q_4 + \delta_4)) + I_2 + I_4 ,$$

$$d_{2,4} = m_4 (l_{c4}^2 + L_2 l_{c4} \cos(q_4 + \delta_4)) + I_4 ,$$

$$d_{3,3} = m_3 l_{c3}^2 + I_3 , \; d_{4,2} = d_{2,4} , \; d_{4,4} = m_4 l_{c4}^2 + I_4$$

$$C'(q', \dot{q}') = \begin{bmatrix} h_1 \dot{q}_3 & 0 & h_1(\dot{q}_1 + \dot{q}_3) & 0 \\ 0 & h_2 \dot{q}_4 & 0 & h_2(\dot{q}_2 + \dot{q}_4) \\ -h_1 \dot{q}_1 & 0 & 0 & 0 \\ 0 & -h_2 \dot{q}_2 & 0 & 0 \end{bmatrix} \tag{3.7}$$

where $h_1 = -m_3 L_1 l_{c3} \sin(q_3)$, and $h_2 = -m_4 L_2 l_{c4} \sin(q_4)$,

$$g'(q') = g \begin{bmatrix} (m_1 l_{c1} + m_3 L_1) \cos(q_1 + \delta_1) + m_3 l_{c3} \cos(q_1 + q_3 + \delta_3) \\ (m_2 l_{c2} + m_4 L_2) \cos(q_2 + \delta_2) + m_4 l_{c4} \cos(q_2 + q_4 + \delta_4) \\ m_3 l_{c3} \cos(q_1 + q_3 + \delta_3) \\ m_4 l_{c4} \cos(q_2 + q_4 + \delta_4) \end{bmatrix} \tag{3.8}$$

where g is the gravitational acceleration constant. The items, $\dot{\rho}(q', \dot{q}')$, $\rho(q')$, and $\sigma(q)$, are further determined as follows.

From Figure 3.1, one can see that the five-bar linkage is configured from two open-chain serial links by means of the introduction of two independent constraint equations, i.e.,

$$\phi(q') = \begin{bmatrix} \phi(1) \\ \phi(2) \end{bmatrix} = 0 \tag{3.9}$$

where

$$\phi(1) = L_1 \cos(q_1) + L_3 \cos(q_1 + q_3) - L_5 - L_2 \cos(q_2) - L_4 \cos(q_2 + q_4)$$

$$\phi(2) = L_1 \sin(q_1) + L_3 \sin(q_1 + q_3) - L_2 \sin(q_2) - L_4 \sin(q_2 + q_4)$$

The parameterization $\alpha(q') = q$ presents a transformation from $q' = [q_1 \quad q_2 \quad q_3 \quad q_4]^T$ to $q = [q_1 \quad q_2]^T$ and is given by

$$\alpha(q') = \begin{bmatrix} 1 & 0 & 0 & 0 \\ 0 & 1 & 0 & 0 \end{bmatrix} q' = q \tag{3.10}$$

Define $\psi(q') \stackrel{\Delta}{=} \begin{bmatrix} \phi(q') \\ \alpha(q') \end{bmatrix}$, $\psi_{q'}(q') \stackrel{\Delta}{=} \dfrac{\partial \psi}{\partial q'}$.

Differentiating Eq. (3.9) with respect to q' and noticing Eq. (3.10) one can obtain

$$\psi_{q'}(q') = \begin{bmatrix} \psi_{q'}(1,1) & \psi_{q'}(1,2) & \psi_{q'}(1,3) & \psi_{q'}(1,4) \\ \psi_{q'}(2,1) & \psi_{q'}(2,2) & \psi_{q'}(2,3) & \psi_{q'}(2,4) \\ 1 & 0 & 0 & 0 \\ 0 & 1 & 0 & 0 \end{bmatrix} \tag{3.11}$$

where

$\psi_{q'}(1, 1) = -L_1 \sin(q_1) - L_3 \sin(q_1 + q_3)$, $\psi_{q'}(1, 2) = L_2 \sin(q_2) + L_4 \sin(q_2 + q_4)$,

$\psi_{q'}(1, 3) = -L_3 \sin(q_1 + q_3)$, $\psi_{q'}(1, 4) = L_4 \sin(q_2 + q_4)$,

$\psi_{q'}(2, 1) = L_1 \cos(q_1) + L_3 \cos(q_1 + q_3)$, $\psi_{q'}(2, 2) = -L_2 \cos(q_2) - L_4 \cos(q_2 + q_4)$,

$\psi_{q'}(2, 3) = L_3 \cos(q_1 + q_3)$, and $\psi_{q'}(2, 4) = -L_4 \cos(q_2 + q_4)$

According to Eq. (3.2) and Eqs. (3.9 – 3.11), $\rho(q')$ can be expressed as follows:

$$\rho(q') = \psi_{q'}^{-1}(q') \begin{bmatrix} 0 & 0 \\ 0 & 0 \\ 1 & 0 \\ 0 & 1 \end{bmatrix} \tag{3.12}$$

$\det[\psi_{q'}(q')] \neq 0$, i.e. $\psi_{q'}^{-1}(q')$ exists if $q' = [q_1 \quad q_2 \quad q_3 \quad q_4]^T$ is in the workspace region where the geometrical contraints are satisfied and the linkage is not in a singular configuration (Ghorbel 1995; Ghorbel and Gunnawardana, 1997).

Since $\rho(q')$ is related to an inverse matrix, it is not easy to take the time derivative. But, the following expression for $\dot{\rho}(q', \dot{q}')$ can be obtained by pre-multiplying Eq. (3.11) with $\psi_{q'}(q')$ and taking the time derivative:

$$\dot{\rho}(q', \dot{q}') = -\psi_{q'}^{-1}(q')\dot{\psi}_{q'}(q', \dot{q}')\rho(q') \tag{3.13}$$

where $\dot{\psi}_{q'}(q', \dot{q}')$ can be obtained by differentiating Eq. (3.11) with respect to time.

In general, it is difficult to derive an analytical expression for the parameterisation $q' = \sigma(q)$, and it must be computed by means of numerical methods. For the closed- chain five-bar linkage, however, it is possible to do so. The following equations can be obtained for the two independent variables q_3 and q_4.

$$q_4 = 2\tan^{-1}\left[\frac{\pm\sqrt{A(q_1, q_2)^2 + B(q_1, q_2)^2 - C(q_1, q_2)^2}}{C(q_1, q_2)}\right] + \tan^{-1}\left[\frac{B(q_1, q_2)}{A(q_1, q_2)}\right] - q_2 \tag{3.14}$$

$$q_3 = \tan^{-1}\left[\frac{\mu(q_1, q_2) + L_4 \sin(q_2 + q_4)}{\lambda(q_1, q_2) + L_4 \cos(q_2 + q_4)}\right] - q_1 \tag{3.15}$$

where $A(q_1, q_2) = 2L_4\lambda(q_1, q_2)$, $B(q_1, q_2) = 2L_4\mu(q_1, q_2)$,

$$C(q_1, q_2) = L_3^2 - L_4^2 - \lambda(q_1, q_2)^2 - \mu(q_1, q_2)^2,$$

$$\lambda(q_1, q_2) = L_2\cos(q_2) - L_1\cos(q_1) + L_5,\ \mu(q_1, q_2) = L_2\sin(q_2) - L_1\sin(q_1)$$

3.3.2 The Dynamic Model of the Motors

According to the schematic diagram shown in Figure 3.2, the torque applied on link 1 is produced by the CV motor through a belt. The torque applied on link 2 is produced by the servomotor directly. Using the Newtonian kinematics law, the torque equation for the motor dynamics can be expressed as (Nasar and Unnrwehr, 1979; Pillay and Krishnam, 1989):

$$\tau_e = \tau_L + B_m\omega_r + J_m\dot{\omega}_r \tag{3.16}$$

where τ_e is the magnetic motor torque, B_m the viscous damping coefficient representing the torque loss, J_m the moment of inertia of the motor, τ_L the load torque, and ω_r the motor speed. Also, the motor torque can be expressed by

$$\tau_e = k_\tau i_q \tag{3.17}$$

Rearranging Eq. (3.16) leads to:

$$\tau_e - \tau_L = B_m\omega_r + J_m\dot{\omega}_r \tag{3.18}$$

For the CV motor, the motor start-up is possible only if the electromagnetic torque τ_e is larger than the load torque τ_L. At the start-up, since the speed is zero and the left-hand side of Eq. (3.18) is greater than its right-hand side, the electric machine gets accelerated. As long as such a situation holds, the motor will continue to accelerate. The steady (work) state is reached when $\tau_e - \tau_L = B_m\omega_r$; at this point of time, the acceleration is zero and the motor operates at a constant speed.

Since the CV motor is not programmable, its electromagnetic torque is constant (so is its armature current) at its work state. If the load torque τ_L is constant, the CV motor will operate at a constant speed at all times. Unfortunately, in the process of the non-uniform

periodical machine motion such as the hybrid actuation, the load torque τ_L varies periodically, so the speed fluctuation in the CV motor will be present, even if the mechanism is driven by the "constant" speed motor. It should be noted that in the HAS, there is a belt between the CV motor and the link 1 of the five-bar linkage. So Eq. (3.16) should be modified when the motor dynamics and the mechanical dynamics are integrated into a complete model, see the discussion in the next section.

3.3.3 The Integrated Model of the Hybrid Actuation System

According to the arrangement of the HAS shown in Figure 3.1, the CV motor drives the actuated joint 1 through a belt with a ratio $\eta = 3$, while the servomotor directly drives the actuated joint 2. Therefore, one can get $\omega_{r1} = \eta \dot{q}_1$ and $\omega_{r2} = \dot{q}_2$. Integration of the motor dynamic Eq. (3.18) and the five bar mechanism dynamic Eq. (3.2) to form a dynamic model of the full system results in the following equation:

$$\begin{cases} \bar{D}(q')\ddot{q} + C(q', \dot{q}')\dot{q} + B\dot{q} + g(q') = \tau \\ \dot{q}' = \rho(q')\dot{q} \\ q' = \sigma(q) \end{cases} \tag{3.19}$$

where $\bar{D}(q') = (D(q') + J)$, $J = diag[\eta J_{m1} \quad J_{m2}]$, $B = diag[\eta B_{m1} \quad B_{m2}]$. J_{mi} and $B_{mi}(i = 1, 2)$ are the moment of the inertia and the viscous damping coefficient of the *i*-th motor, respectively.

3.4 Control System of the Hybrid Actuation System

3.4.1 Proposed Control System

First of all, for the HAS governed by the dyanmic model expressed in Eq. (3.19), the following properties and assumptions are held.

1) The inertia matrix $\bar{D}(q')$ is symmetric and positive definite.

2) $\dot{\bar{D}}(q') - 2C(q', \dot{q}')$ is a skew symmetric matrix.

3) $\dot{\bar{D}}(q')$, $C(q', \dot{q}')$ and $g(q')$ are bounded.

4) The dynamics of the HCA plant system has some uncertainty. That is to say, items, $\dot{\bar{D}}(q')$, $C(q', \dot{q}')$, and $g(q')$, are only partially known.

Properties 1 and 2 can be proved as follows.

The matrix $\boldsymbol{D}(\boldsymbol{q}')$ is symmetric and positive definite (Ghorbel 1995, Ghorbel and Gunnawardana, 1997), and so is $\boldsymbol{J}$. Therefore, the matrix $\bar{\boldsymbol{D}}(\boldsymbol{q}') = \boldsymbol{D}(\boldsymbol{q}') + \boldsymbol{J}$ is symmetric and positive definite. Because the matrix $\boldsymbol{J}$ is constant, then the term $\dot{\bar{D}}(q') - 2C(q', \dot{q}') = \dot{D}(q') - 2C(q', \dot{q}')$ is skew (Ghorbel, 1995; Ghorbel and Gunnawardana, 1997).

The control objective is to drive the joint positon q to the desired position q_d as close as possible with the presence of the fluctuation of $\dot{q}_1$ in the CV motor.

Define the tracking error as

$$\begin{cases} e = q - q_d \\ \dot{e} = \dot{q} - \dot{q}_d \end{cases} \tag{3.20}$$

where $q_d = \begin{bmatrix} q_{1d} & q_{2d} \end{bmatrix}^T$ and $\dot{q}_d = \begin{bmatrix} \dot{q}_{1d} & \dot{q}_{2d} \end{bmatrix}^T$. As link 1 is connected with a CV motor, for simplicity, assume $\dot{q}_{1d} = \omega_d$, and $q_{1d} = \omega_d t$.

As mentioned in Chapter 2, the SMC is a powerful control technique for nonlinear systems with uncertainties. The basic idea of the SMC is to constrain the state of a controlled plant to reach a given manifold in the state-space and then to slide towards an equilibrium state along this manifold.

Following the SMC method, a sliding manifold is defined as

$$s = \dot{e} + \lambda e \tag{3.21}$$

where $\lambda = \text{diag}[\lambda_1, \lambda_2]$ in which λ_1 and λ_2 are positive constants.

Define the reference state as

$$\begin{cases} \dot{q}_r = \dot{q} - s = \dot{q}_d - \lambda e \\ \ddot{q}_r = \ddot{q} - \dot{s} = \ddot{q}_d - \lambda \dot{e} \end{cases} \tag{3.22}$$

Also let $\hat{\bar{D}}(q')$, $\hat{C}(q', \dot{q}')$, and $\hat{g}(q')$ be the estimates of $\bar{D}(q')$, $C(q', \dot{q}')$, and $g(q')$, respectively. Let $\Delta\bar{D}(q') = \hat{\bar{D}}(q') - \bar{D}(q')$, $\Delta C(q', \dot{q}') = \hat{C}(q', \dot{q}') - C(q', \dot{q}')$, and $\Delta g(q') = \hat{g}(q') - g(q')$. Submitting Eqs. (3.20-3.22) into Eq. (3.19), one can obtain the dynamic model of the hybrid mechanism in terms of the sliding manifold vector s

$$\bar{D}(q')\dot{s} + C(q', \dot{q}')s + Bs = \begin{bmatrix} \tau_1 - f_1 + \Delta f_1 - B_{m1}\dot{q}_1 + B_{m1}s_1 \\ \tau_2 - f_2 + \Delta f_2 - B_{m2}\dot{q}_2 + B_{m2}s_2 \end{bmatrix} \tag{3.23}$$

where

$$f_1 = \hat{\bar{d}}_{11}(q')\ddot{q}_{r1} + \hat{\bar{d}}_{12}(q')\ddot{q}_{r2} + \hat{c}_{11}(q', \dot{q}')\dot{q}_{r1} + \hat{c}_{12}(q', \dot{q}')\dot{q}_{r2} + \hat{g}_1(q') \tag{3.24}$$

$$f_2 = \hat{\bar{d}}_{21}(q')\ddot{q}_{r1} + \hat{\bar{d}}_{22}(q')\ddot{q}_{r2} + \hat{c}_{21}(q', \dot{q}')\dot{q}_{r1} + \hat{c}_{22}(q', \dot{q}')\dot{q}_{r2} + \hat{g}_2(q') \tag{3.25}$$

$$\Delta f = [\Delta f_1 \quad \Delta f_2]^T = \Delta \bar{D}(q')\ddot{q}_r + \Delta C(q', \dot{q}')\dot{q}_r + \Delta g(q') \tag{3.26}$$

Assume that the torque in the CV motor is constant. When the CV motor is running at its operating speed, we assume that $\lambda_1 = 0$, and the constant torque in the CV motor is set to:

$$\tau_1 = B_{m1}\omega_d \tag{3.27}$$

Further, the controlled torque τ_2 for the servomotor is defined as

$$\tau_2 = B_{m2}\dot{q}_{2r} + f_2 - k\,\mathrm{sgn}(s_2) - as_2 + \tau_c \tag{3.28}$$

where k and a are design parameters that are positive constant, τ_c is the compensation torque of the servomotor used to reduce the speed fluctuations in the CV motor. Assume $|\Delta f_i| < \Delta f_{bi}$ (i=1,2), where Δf_{bi} is a positive constant that represents the boundary of Δf_i. Choose k such that

$$k \geq \Delta f_{b2} \tag{3.29}$$

Define the compensation torque τ_c as

$$\tau_c = \begin{cases} -|s_1|\left(|f_1| + \Delta f_{b1}\right)/s_2, & \text{if } s_2 \neq 0 \\ 0, & \text{if } s_2 = 0 \end{cases} \tag{3.30}$$

So far, the controlled torque τ_2 for the servomotor was defined by Eqs. (3.28 - 3.30).

The control system can also be represented by a block diagram shown in Figure 3.3, in which the controller consists of three parts: (1) an estimated model control ($B_{m2}\dot{q}_{2r} + f_2$);

(2) a compensation of the speed fluctuation in the CV motor (τ_c); and (3) a sliding mode control law ($k\,\mathrm{sgn}(s_2) + as_2$).

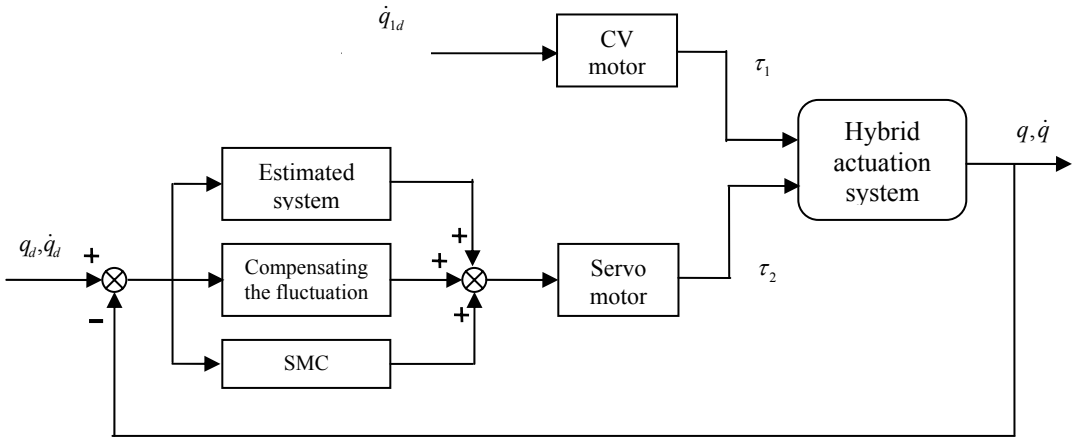

Figure 3.3 The control block diagram for the hybrid actuation system.

From Figure 3.3, one can see that the proposed control system can be viewed as a hybrid control system where three control laws are put together to form one control system. The stability of the control system will be studied in the next section.

3.4.2 Stability Analysis of the Control System

Theorem 3.1: For the HAS with uncertainty in the dynamic model expressed in Eq. (3.19), if the torque for the CV motor is given by Eq. (3.27), the controlled torque for the servomotor is given by Eq. (3.28), and the compensation torque for the servomotor is defined as Eq. (3.30), then, the trajectory tracking errors $\dot{e}_1(t)$, $e_2(t)$, and $\dot{e}_2(t)$ will converge to zero when time t tends to infinite large, and $e_1(t)$ is bounded for any time $t \geq 0$.

The proof of this theorem will be provided as follows.

Proof: Submitting Eqs. (3.27) and (3.28) into Eq. (3.23) yields

$$\bar{D}(q')\dot{s} + C(q', \dot{q}')s + \bar{B}s = \begin{bmatrix} -f_1 + \Delta f_1 \\ \tau_c + \Delta f_2 - k\,\mathrm{sgn}(s_2) \end{bmatrix} \tag{3.31}$$

where the matrix $\bar{B} = \mathrm{diag}\begin{bmatrix} B_{m1} & B_{m2} + a \end{bmatrix}$. One can see that the matrix $\bar{B}$ is symmetric and positive definite.

Consider the Lypunove function to be

$$V = \frac{1}{2} s^T \bar{D}(q')s \tag{3.32}$$

Since $\bar{D}(q')$ is symmetric and positive definite according to property 1, for $s \neq 0$, one can see that

$$V > 0 \tag{3.33}$$

Using property 2, the following can be found.

$$\begin{aligned} \dot{V} &= s^T \bar{D}(q')\dot{s} + \frac{1}{2} s^T \dot{\bar{D}}(q')s \\ &= s^T \left(\tfrac{1}{2} \dot{\bar{D}}(q') - C(q', \dot{q}') - \bar{B} \right) s + s^T \begin{bmatrix} -f_1 + \Delta f_1 \\ \tau_r + \Delta f_2 - k\,\mathrm{sgn}(s_2) \end{bmatrix} \\ &= -s^T \bar{B}s - s_1(f_1 + \Delta f_1) + s_2\tau_c + s_2\left(\Delta f_2 - k\,\mathrm{sgn}(s_2)\right) \end{aligned} \tag{3.34}$$

From Eq. (3.29), the following inequality should hold.

$$s_2\left(\Delta f_2 - k\,\mathrm{sgn}(s_2)\right) \le 0 \tag{3.35}$$

Using Eq. (3.30), it can easily be verified that

$$\begin{aligned} &-s_1(f_1 + \Delta f_1) + s_2\tau_c \\ &= -s_1(f_1 + \Delta f_1) - |s_1|\left(|f_1| + \Delta f_{b1}\right) \le 0 \end{aligned} \tag{3.36}$$

As the matrix $\overline{B}$ is symmetric and positive definite, one can get

$$-s^T \overline{B} s \le 0 \tag{3.37}$$

From Eqs. (3.35-3.37), one can verify

$$\dot{V} \le 0 \tag{3.38}$$

Equation (3.32) can be viewed as an indicator of the energy of *s*. Therefore, equation (3.38) guarantees the decay of the energy of *s* as long as $s \neq 0$. According to the Lyapunov's stability theorem, $s(t)$ will exponentially tends to zero when *t* tends to infinite large. From the standard stable filter theory, this implies that errors $\dot{e}_1(t)$, $e_2(t)$, and $\dot{e}_2(t)$ will exponentially converge to zero when time *t* tends to infinite large. Furthermore, since $\dot{e}_1(t)$ exponentially converges to zero, $e_1(t)$ will be normally bounded.

End-of-Proof.

Several remarks regarding the theorem are given further.

Remark 1: From Eq. (3.28), one can see that the controlled torque in the servomotor is discontinuous. In order to eliminate the chattering of the servomotor, the smoothing technique (Slotine and Li, 1991) can be applied. Specifically, modify the controlled torque τ_2 as follows:

$$\tau_2 = B_{m2}\dot{q}_{2r} + f_2 - k\, sat(s_2 / \Phi) - as_2 + \tau_c \tag{3.39}$$

where Φ is called the boundary layer and $\Phi > 0$.

Remark 2: As the sliding manifold s is also discontinuous, so does the compensation torque τ_c in Eq. (3.30). To avoid the chattering of the designed torque, equation (3.30) can be changed into

$$\tau_c = -\frac{|s_1|\left(|f_1| + \Delta f_{b1}\right)s_2}{\delta + s_2^2} \tag{3.40}$$

where δ is called the boundary layer thickness, and δ>0.

Remark 3: After the smoothing technique is used in Eqs. (3.39) and (3.40) for the servomotor control, one can see that the trajectory tracking error is globally uniformly ultimately bounded, and the boundary can be controlled by carefully selecting Φ and s.

3.5 Simulation Study of the Hybrid Actuation System

In this section, a simulation study is presented for the trajectory tracking of the HAS to examine the effectiveness of the proposed hybrid control algorithm. Also, the feasbility of attaching a flywheel to improve the tracking performance is studied. It should be

noted that the uncertainty of the dynamic model is included in the simulation study to demonstrate the robustness of the proposed hybrid control system.

The physical paramters of the HAS used in the simulation are shown in Table 3.1, while the parameters of the two motors (CV motor and servomotor) are listed in Table 3.2.

Table 3.2 Parameters of the CV motor and the servomotor

Motor type	$J(\text{kg}\bullet\text{m}^2)$	$B_m(\text{N}\bullet\text{m}\bullet\text{s})$
CV motor	0.5	0.5
Servomotor	0.05	0.05

3.5.1 Trajectory Planning for the Two Input Links

The desired trajectories for the two input links are expressed as a constant velocity rotation for the CV motor connecting with link 1 through a belt and the Hermite polynomial of the fifth degree in t with continuous bounded conditions for position, velocity and acceleration for the servomotor driving link 2, i.e.,

$$q_1^d(t) = \omega_d t \tag{3.41}$$

$$q_2^d(t,t_f) = q_{20}^d + (6\frac{t^5}{t_f^{\ 5}} - 15\frac{t^4}{t_f^{\ 4}} + 10\frac{t^3}{t_f^{\ 3}})(q_{2f}^d - q_{20}^d) \tag{3.42}$$

where $q_1^d(t)$ and $q_2^d(t,t_f)$ are the desired angular displacements for the two input links, q_{20}^d and q_{2f}^d are the desired initial and final positions of the input link 2 driven by the servomotor, and t_f represents the time at which the desired trajectory for the end-

effector reaches the desired final position. In the simulation, it is assumed that $q_{20}^{d} = 0$, $q_{2f}^{d} = 2\pi$, and $q_1(0) = 0, q_2(0) = 0$ for simplification. Two cases with different operating speeds are studied. Case 1: the speed is $\omega_d = 0.5\pi\ (rad/s)$ for the CV motor and $t_f = 4s$ for the servomotor. Case 2: the speed is double the speed of case 1, i.e., $\omega_d = \pi\ (rad/s)$ and $t_f = 2s$. Furthermore, the uncertainty of the dynamic model is estimated by applying factors to the corresponding parameters matrices as follows:

$$\hat{\bar{D}}(q') = 0.95\,\bar{D}(q')\,,\ \hat{C}(q',\dot{q}') = 0.9\,C(q',\dot{q}')\,,\text{ and }\ \hat{g}(q') = 1.05\,g(q')$$

The controlled torque for the servomotor is selected as described in Eq. (3.39), where the control parameters are chosen as $a = 10$, $\lambda_2 = 15$, and $k = 30$.

3.5.2 Trajectory Tracking Results of the Hybrid Actuation System

Simulation results are shown in Figures 3.4 and 3.5 for case 1 and case 2, respectively. From Figure 3.4, one can see that the maximum speed fluctuation in link 1 is about 0.1 rad/s that is about 6.4% of the desired speed, while the maximum position error is less than 0.06 rad. It is noted that a manual measurement of the velocity fluctuation on the CV motor through a tachometer confirmed the speed fluctuation. The high tracking performance (position error less than 10^{-4} rad, and velocity error less than 10^{-3} rad/s, respectively) for the servomotor was obtained. Furthermore, the controlled torque for the servomotor is smooth, which can avoid the chattering of the servomotor while the required torque for the CV motor is maintained at a constant level. The simulation result is promising.

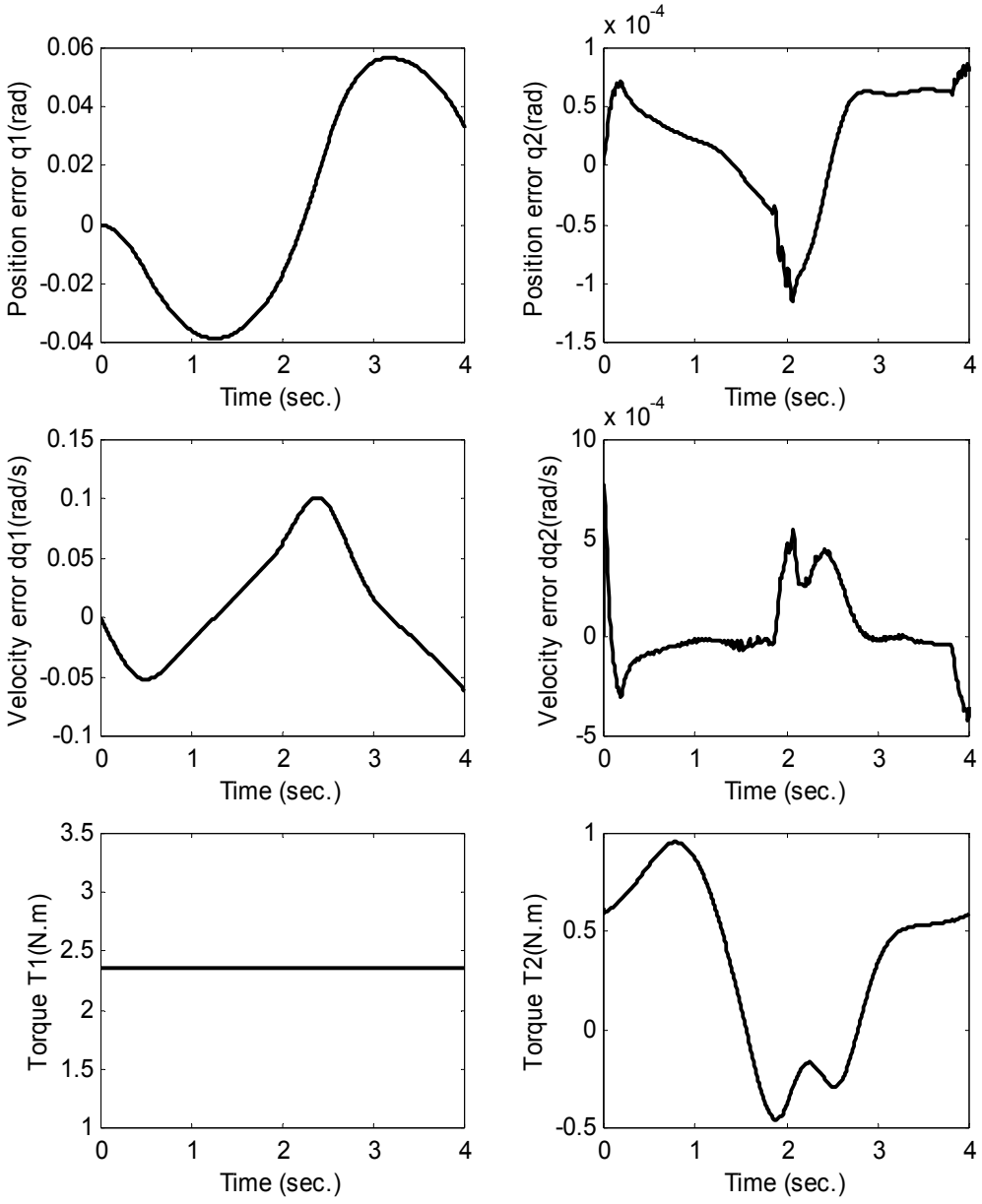

Figure 3.4 Tracking performances for the HAS without flywheel – case 1.

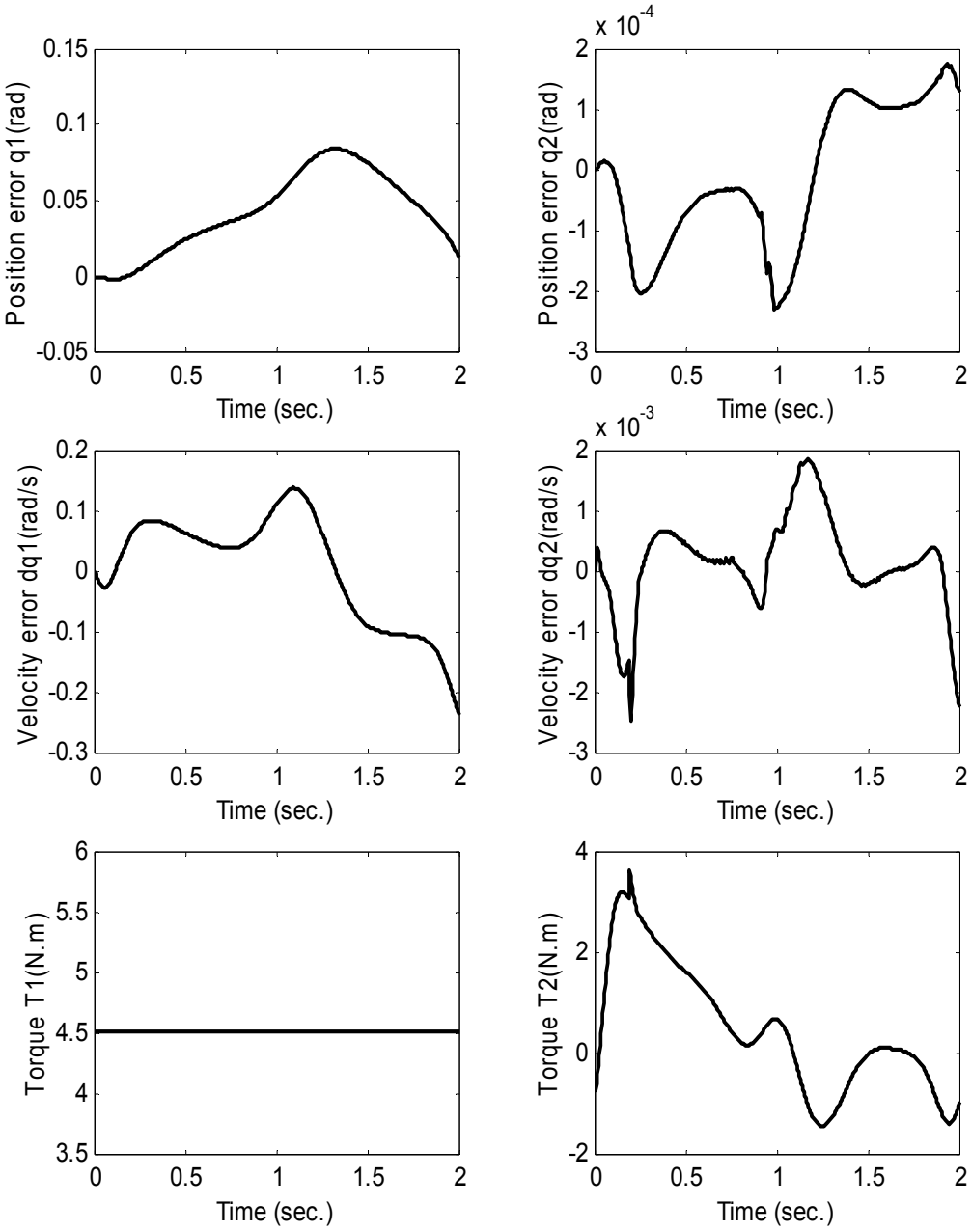

Figure 3.5 Tracking performances for the HAS without flywheel – case 2.

From Figure 3.5, one can see that a similar result is obtained for a relatively high speed operation using the same control gains. The developed hybrid control law can still maintain the fluctuation of the speed of the CV motor in a reasonable range. As the

average speed for the servomotor was doubled in case 2, the positioning accuracy of the servomotor reduced very little (the position error is about 2.5×10^{-4} rad and the velocity error is about 2.6×10^{-3} rad/s, respectively).

3.5.3 Tracking Performance Improvement with the Adding of a Flywheel

In mechanical design, it is common knowledge that adding a flywheel on the shaft of a CV motor can reduce the velocity fluctuation. To examine such an effect in the HAS, the flywheel inertia is included in the dynamic model. In the simulation, the same control parameters are chosen as before. Two flywheels with different inertias (5 kg.m^2 and 10 kg.m^2, respectively) were used to examine their effects on the tracking performance and the required torque for the servomotor. Figures 3.6 and 3.7 show the tracking performances after attaching a flywheel with different inertias on the shaft of the CV motor for case 1, while Figures 3.8 and 3.9 show the tracking performances for case 2.

It is observed that, by adding the flywheel, the overall performance of the whole system was improved significantly, especially for link 1 associated with the CV motor. For case 1, the velocity fluctuation in the CV motor was reduced from 0.1 rad/s (no flywheel) to 0.012 rad/s (a small flywheel), and further to 0.006 rad/s (a big flywheel). Again, the reduction of the speed fluctuation in the CV motor was confirmed by the manual measurement using a tachometer. The maximum position error for link 1 was decreased from 0.06 rad to 0.01 rad , and to 0.004 rad, respectively. Also one can see that the tracking performance of the servomotor is still maintained at an excellent level, and the controlled torque barely changed for these three operating situations.

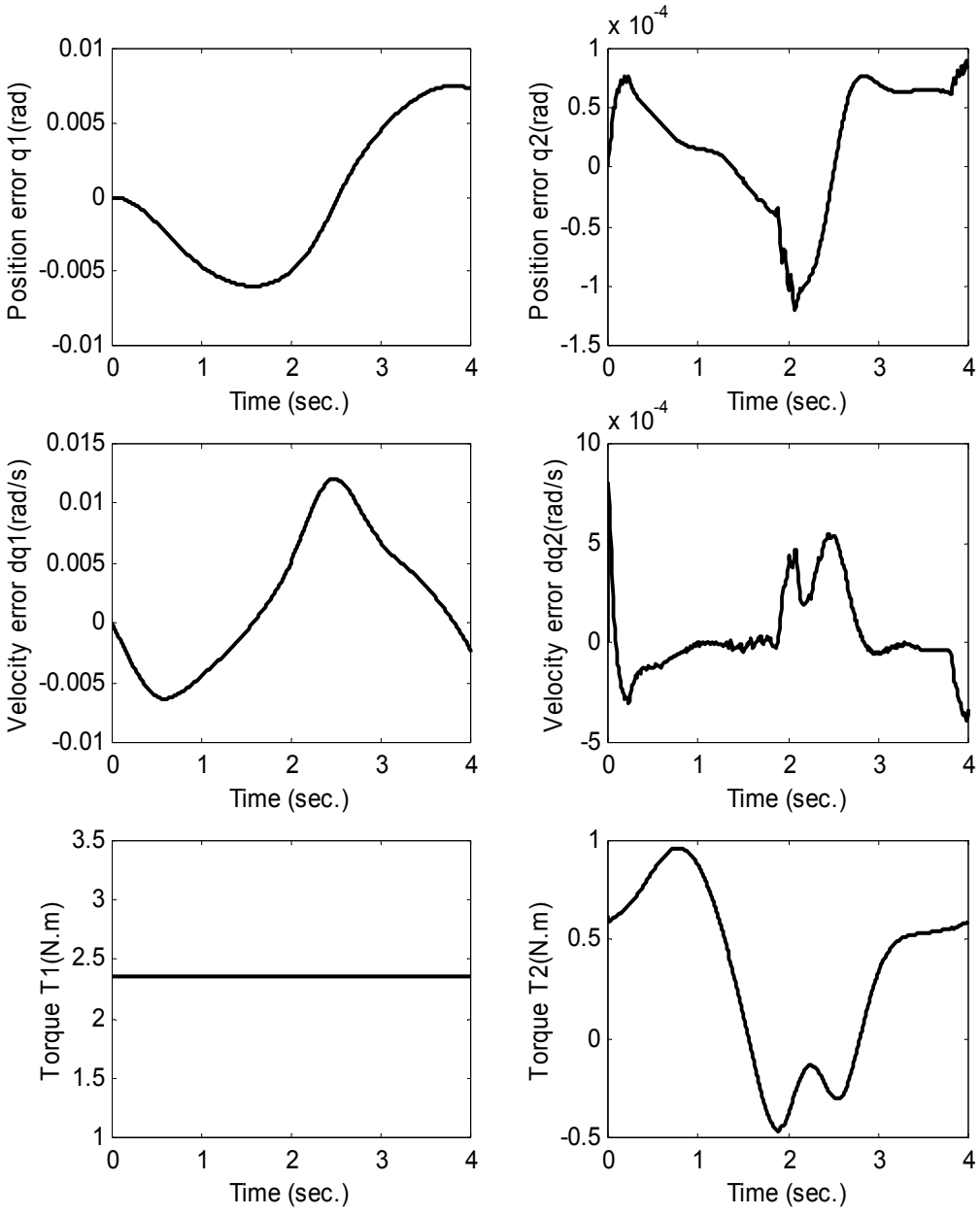

Figure 3.6 Tracking performances for the HAS attaching a flywheel with $J_f = 5.0\ \text{kg}\bullet\text{m}^2$ - case 1.

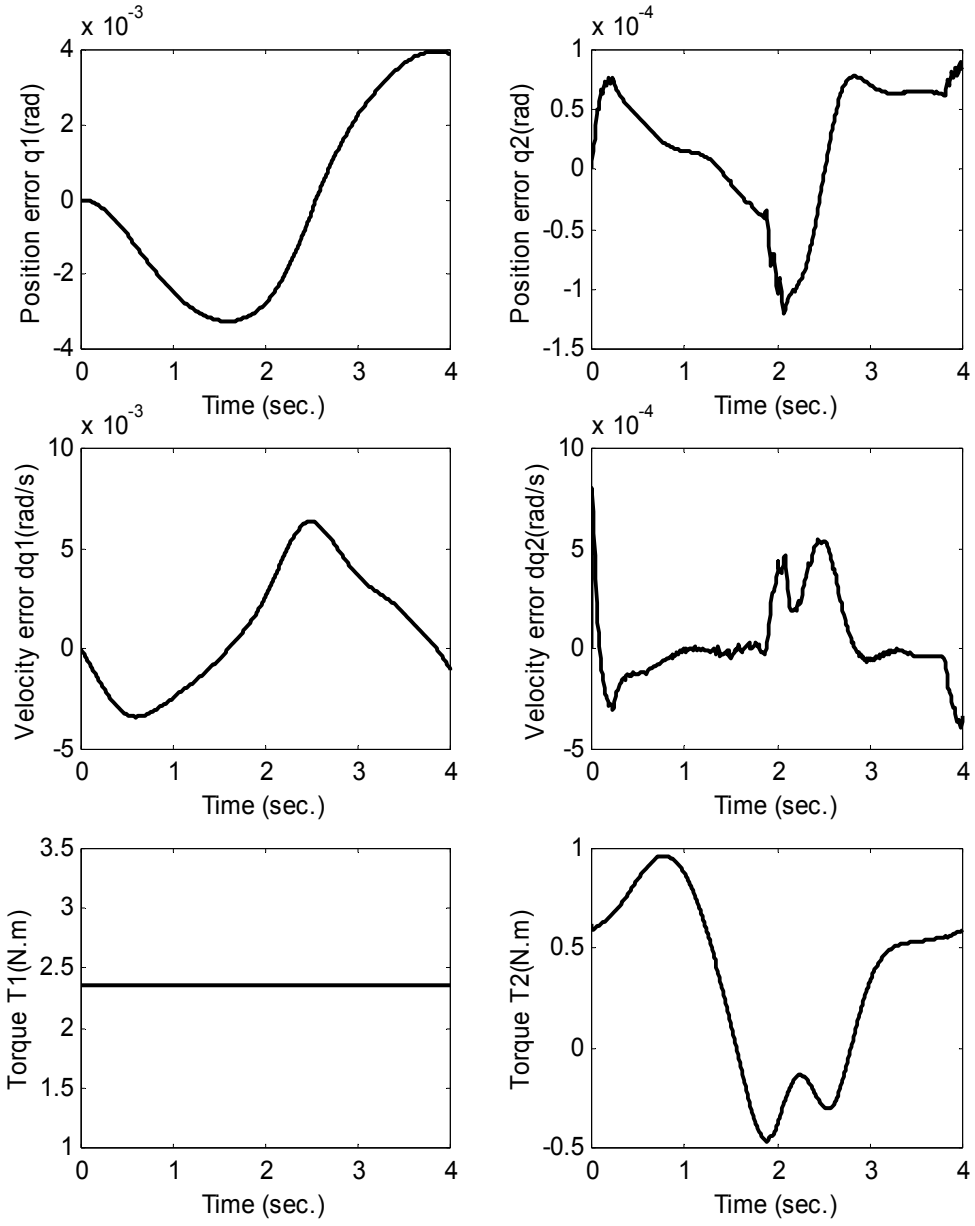

Figure 3.7 Tracking performances for the HAS attaching a flywheel with $J_f = 10.0\ \text{kg}\bullet\text{m}^2$ - case 1.

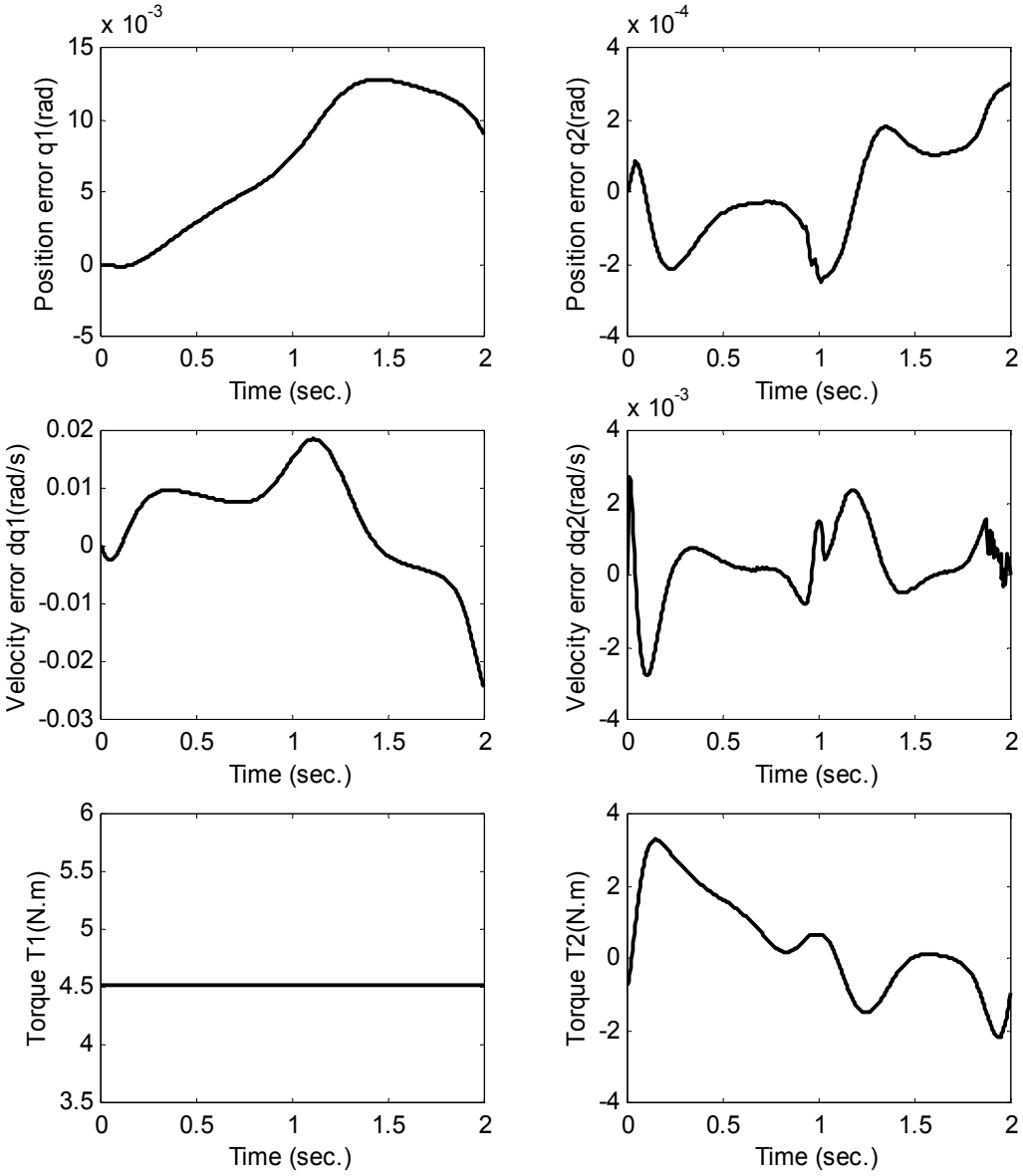

Figure 3.8 Tracking performances for the HAS attaching a flywheel with $J_f = 5.0\ \text{kg}\bullet\text{m}^2$ - case 2.

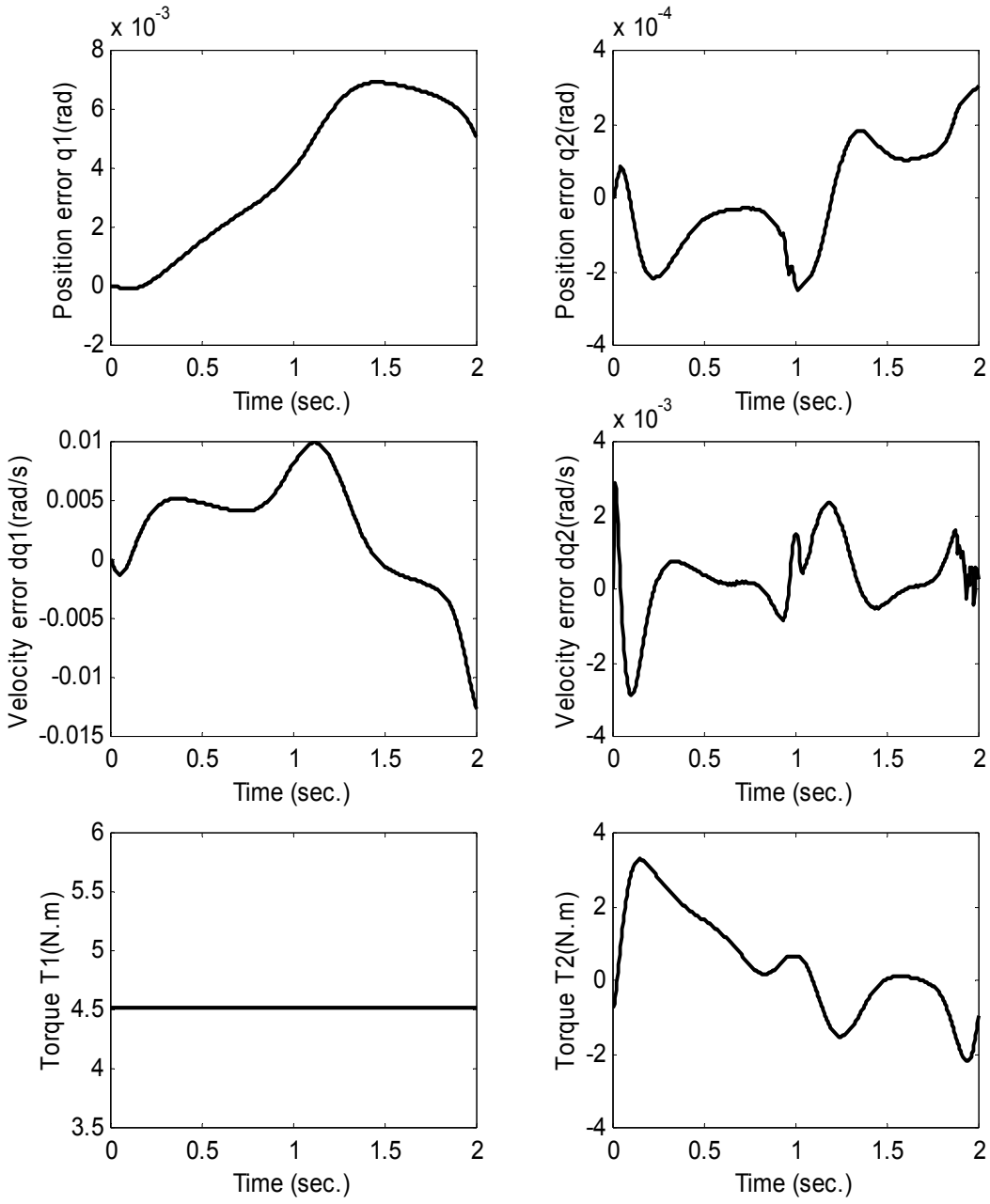

Figure 3.9 Tracking performances for the HAS attaching a flywheel with $J_f = 10.0\ \text{kg}\bullet\text{m}^2$ - case 2.

It is also observed that no matter what a flywheel is, the speed fluctuation in the CV motor for case 2 (high speed) is larger than that for case 1. This is quite natural, as the

increase in motor speed will increase the fluctuation of the inertia of a total system which further leads to the increase of the speed fluctuation in the CV motor. The increase of the speed fluctuation in the CV motor will bring more "disturbances" to the servomotor. As a result, the tracking error in the servomotor will increase if the same control system is used. The above results demonstrate the effectiveness and robustness of the control algorithm. When a big flywheel is added to the shaft of the CV motor, the fluctuation of the speed of the CV motor decreases dramatically, while the tracking performances of the servomotor are very good.

From Figures 3.6 – 3.9, one can see that with the adding of a flywheel to the CV motor, the performance (the speed fluctuation) is improved considerably for the CV motor but not for the servomotor. This phenomenon is due to the special feature of the sliding mode control, i.e., the robustness of the SMC for the uncertainty of the dynamic model. The introduction of the flywheel can be viewed as "adding" some uncertainty in the dynamics of the HAS. As the control parameters for the servomotor remained the same for all three operation conditions, the uncertain dynamics due to the flywheel did not change the performance of the controlled HAS.

3.6 Concluding Remarks

In this chapter, the design of the HAS was presented; the modeling of the full system including both the mechanical system and the driving system was developed. A new control algorithm for the servomotor was proposed that can be used to compensate the speed fluctuation in the CV motor, and its stability was analyzed. It is shown that the proposed control algorithm can achieve the asymptotical stability. The general strategy behind the developed control algorithm for the HAS is the incorporation of the speed fluctuation in the CV motor into the control algorithm designed for the servomotor.

4. HYBRID MOTION MECHANISM

4.1 Introduction

Applications such as semiconductor test, cell manipulation, and space manipulation need a large movement with high accuracy. A concept called macro-micro manipulator was proposed by Sharon and Hardt (1984) to meet these applications. A macro-micro motion system is a hybrid system where two different motions are combined together to achieve different goals. The combination of a macro manipulator and a micro manipulator enables fast, precision manipulation through a large workspace. The macro manipulator is characterized by its large workspace and slow response, while the micro manipulator is characterized by its small workspace, high accuracy and high acceleration. In the macro-micro manipulator, a small manipulator that provides micro motion is mounted on the end of a larger one that produces macro motion, and the former is controlled to compensate the inaccuracy due to the latter. As mentioned in Chapter 2, such a design is easy to realize, but the assembly error and the backlash force will affect the accuracy of the end-effector. Also, the full device is relatively complex. Furthermore, mounting a micro manipulator at the tip of a macro manipulator results in a dynamically coupled system. The interaction between the macro motion system and the micro motion one is a challenge issue in such a design, and little progress on addressing this issue has been made.

In this chapter, a new design strategy for the spatial compliant mechanism that can fulfill the hybrid motion is proposed. The main idea behind this design is that two types of actuators, i.e., DC servomotor for the macro motion and the PZT actuator for the micro motion, are integrated to form one actuating motion that can be called the hybrid motion. The mechanism using the hybrid motion device is called the hybrid motion mechanism

(HMM). In this new design, only one compliant mechanism is used to complete both coarse and fine positioning function. Therefore, such a HMM is capable of minimizing the backlash force and free of friction and thus has an improved smooth and accurate movement.

This chapter will focus on the design, modeling and optimization of the HMM and is organized as follows. In Section 4.2, the topology of the mechanical amplifier is discussed and a new topology based on the symmetric five bar structure is proposed which is used to design a new compliant mechanical amplifier (CMA). Section 4.3 discusses the design of the CMA using the finite element analysis (FEA) method, the design parameters are fine-tuned in terms of the amplification ratio and the natural frequencies. Based on the CMA, a spatial compliant mechanism with 3 DOF is designed to form a HMM in Section 4.4. Specifically, the kinematics analysis of this HMM is performed. Then the static and dynamic analyses are presented for different configurations of the HMMs using the finite element method (FEM). Section 4.5 discusses the design optimization of the HMM using the Taguchi method and orthogonal array (OA) experiments based on several objective functions. Section 4.6 concludes this chapter.

4.2 Topology Synthesis of Mechanical Amplifiers

Topology refers to the connectivity among materials without involving the geometry of the materials. Topology of mechanical amplifiers thus contains the fundamental features that are responsible for the behaviours and performances of mechanical amplifiers. In this section, first, three known topologies of mechanical amplifiers are presented, and their drawbacks are discussed. Then, a new topology is proposed.

4.2.1 Topology I: Buckling Beam Structure

A long slender beam subjected to an axial compressive force will buckle when the force exceeds a critical value (Timoshenko and Gere, 1961). As shown in Figure 4.1, if the

slender beam has an axial compressed deformation δ, a transverse deformation D can be produced. Based on such a buckling effect, a displacement amplifier can be made. Saif and Macdonald (1998) used the buckling beam as a mechanical amplifier to measure the forces and spring constant of micro-instruments. Jiang and Mockensturm (2003) designed a motion amplifier for obtaining large rotations from small linear displacements based on the concept of buckling beam. One drawback with buckling beam topology is that the amplifier has a large dimension size compared with others. Another drawback with this topology is that the driving force must be larger than a critical value to meet the condition for buckling to occur. Furthermore, the amplifier based on this topology has relatively low natural frequencies which will limit its applications.

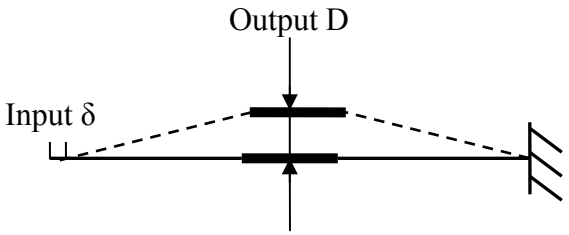

Figure 4.1 Buckling beam topology for the displacement amplification.

4.2.2 Topology II: Lever Structure

The simplest and direct way to increase the displacement of a PZT actuator is the use of a mechanical lever arm; see Figure 4.2. The mechanism increases the displacement output but decreases the force output at the same time. Also, from Figure 4.2 one can see that there is a lateral displacement at the end of the lever arm, and the system stiffness is decreased. Such a lateral displacement is undesirable in many applications. Based on the lever topology, the doubled lever arm structures and multiple lever arm amplification devices were developed and extensively used in applications; see King and Xu (1996), Xu and King (1996), Yang et al. (1996), Scire and Teague (1978), Gao et al. (1999), Tenzer and Mrad (2004), Su and Yang (2001), Jouaneh and Yang (2004), and Varma and Dixon (2002). Scire and Teague (1978) developed a micropositioning stage by applying a two-stage lever structure in a volume of 100 x 100 x 20 mm^3 which amplified

the linear travel a PZT actuator from 3 μm (in 1000V voltage) to a 50 μm travel range with a subnanometer resolution. The resonant frequency of the micropositioning stage was about 110 Hz. Gao et al. (1999) developed an x-y micro-positioning stage utilizing flexure hinges based on the single lever arm topology where the lateral effect was ignored because of the limited motion range of the designed stage. King and Xu (1996) studied the design and characteristics of two piezomotors where the lever type flexure-hinged displacement amplification mechanisms were used. Tenzer and Mrad (2004) discussed the mechanical amplification in inchworm linear motors where a double lever amplifier was included in the motor frame. Su and Yang (2001) analyzed the force amplification ratio of single- and multiply-stage flexure-based micro-level systems. Jouaneh and Yang (2003) developed the design equations for the flexure-hinge type multiple lever mechanism based on the static analysis of a general configuration. Varma and Dixon (2002) designed a meco-scale mobile robot where a double lever compliant amplification device was developed to realize the lift and pull movement of the legs.

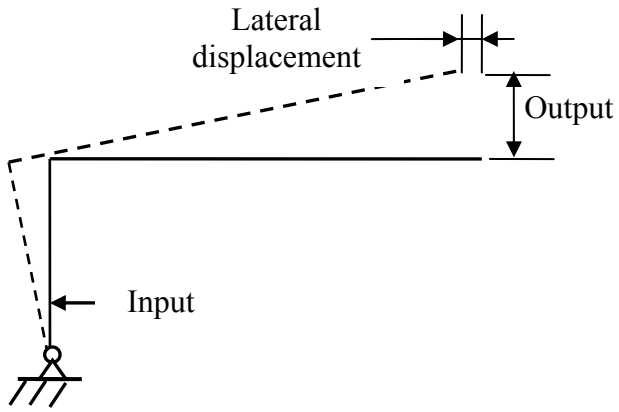

Figure 4.2 Lever arm topology for the displacement amplification.

4.2.3 Topology III: Parallel and Symmetric Four Bar Structure

To increase the stiffness of the mechanical amplifiers, the topology based on a parallel four bar structure can be used; see Figure 4.3. Although the system stiffness with this topology increases compared with the lever arm topology, the lateral displacement

problem still exists as shown in Figure 4.3. Ryu and Gweon (1997) studied the motion errors induced by manufacturing errors using a parallel four-bar structure.

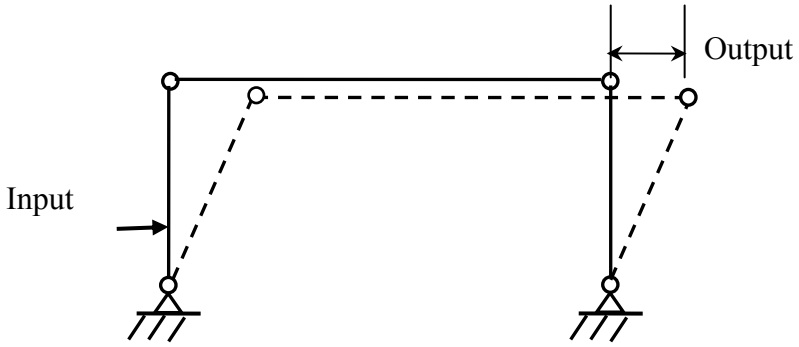

Figure 4.3 Parallel four bar topology for the displacement amplification.

To eliminate the lateral displacement, the double symmetric four-bar structures were developed in Pokines and Garicia (1998), and Lobontiu and Garicia (2003). Figure 4.4 shows two double symmetric four-bar topologies in which Figure 4.4(a) is used in the case of compression in an actuator, while Figure 4.4(b) is used for the extension in an actuator. Figure 4.4(b) is more compact and geared with the PZT actuator characteristics (i.e., the extension deformation). It should be noted that the bridge displacement amplifier discussed in Xu and King (1996) can be viewed as an application of this topology. Pokines and Garica (1998) designed a micro-amplifier with an amplification ratio of 5.48 based on this topology which was fabricated using LIGA (Lithographie, galvanoformung und abformung in Germany). Bharti and Frecher (2004) discussed the optimal design of a compliant mechanism amplifier in the application of an inertially stabilized rifle. Lobontiu and Garica (2003) formulated an analytical method for the displacement and stiffness calculation of planar compliant mechanisms with single-axis flexure hinges. It should be noticed that the compliant mechanism based on the double symmetric four bar topology suffers from a low natural frequency that can limit the frequency band of the control system. Another drawback with the double symmetric four bar topology is the relatively low stiffness of its structure.

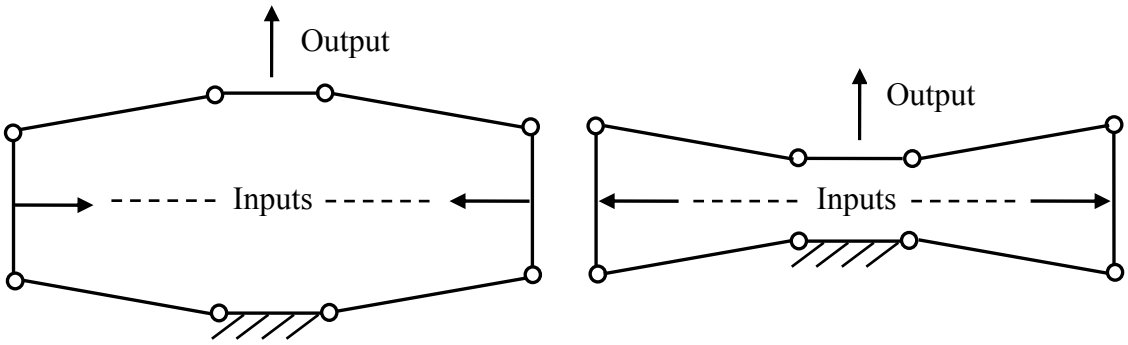

(a) For compression of actuator (b) For extension of actuator

Figure 4.4 Double symmetric four bar topologies for the displacement amplification.

4.2.4 The Proposed Topology: Symmetric Five Bar Structure

Motivated from the double symmetric four bar topology, a new topology for the displacement amplification is proposed which is based on a symmetric five bar structure. Generally speaking, a five bar linkage is a 2 DOF mechanism that can provide the x-y plane motion. However, if the five bar linkage is designed to be symmetrical, and the two driving links rotate simultaneously in the opposite directions driven by one actuator, the output of the mechanism can be in one direction only. This is the basic principle underlying the new topology for the displacement amplification. Figure 4.5 shows the schematic of the symmetric five bar topology where Figure 4.5(a) is used in the case of the compression in an actuator while Figure 4.5(b) is used for the extension in an actuator. The same as the symmetric four bar topology case, Figure 4.5(b) suits the PZT actuator.

The symmetric five bar topology can also be viewed as a combination of the symmetric four bar topology and lever arm topology. Therefore, it has the advantages of the both. The main advantage with this new topology, compared with the double symmetric four bar topology, is the high natural frequency and high amplification ratio in a compact size. Also, there is no lateral displacement because of the symmetric structure. In the next section, the design of CMAs based on this new topology will be discussed.

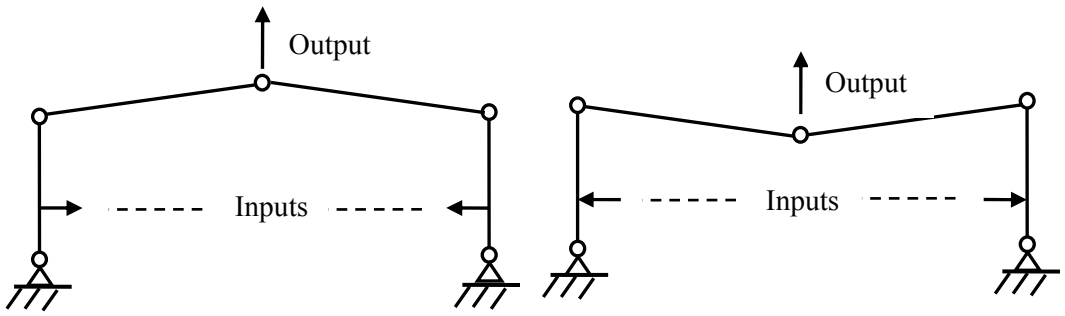

(a) For compression of actuator (b) For extension of actuator

Figure 4.5 Symmetric five bar topologies for the displacement amplification.

4.3 Design and Modeling of the Compliant Mechanical Amplifier (CMA)

4.3.1 Design and Analysis of the CMA

Figure 4.6 shows the schematic of a CMA based on the new topology with double-beam corner filleted hinges where Figure 4.6(a) is its FEA model and Figure 4.6(b) is its PRBM model. In Figure 4.6(b), δ represents the displacement of the PZT actuator while y represents the output displacement. Figure 4.7 is a corresponding CMA based on the double symmetric four bar topology for comparison.

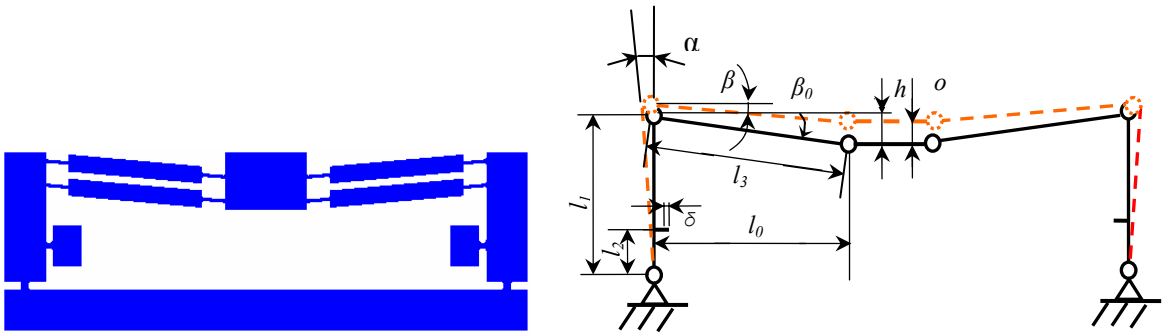

(a) The FEA model (b) The PRBM model

Figure 4.6 Compliant mechanical amplifier (CMA) based on the symmetric five bar topology.

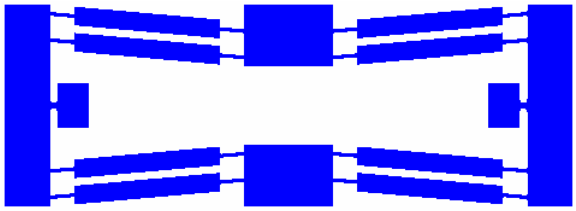

Figure 4.7 CMA based on double symmetric four bar topology.

Assume that the mechanism gets to a new configuration shown in the dashed lines in Figure 4.6(b) when the input links have a relative rotation α due to the extension δ of the PZT actuator. According to Figure 4.6(b), the following equations can be obtained:

$$\sin\alpha = \frac{\delta}{l_2} \tag{4.1}$$

$$o = h - l_3 \sin\beta \tag{4.2}$$

$$\cos\beta = \frac{l_1 \sin\alpha + l_0}{l_3} \tag{4.3}$$

Note that $h^2 + l_0^2 = l_3^2$. Let k represent the input amplification of the PZT actuator by the lever arm where $k = {l_1}/{l_2}$. From Eq. (4.2) and Eq. (4.3), the following equation can be obtained.

$$o^2 - 2ho + \left(k\delta + 2l_0\right)k\delta = 0 \tag{4.4}$$

From Eq. (4.4), the output displacement can be written as follows:

$$o = h \mp \sqrt{h^2 - \left(k\delta + 2l_0\right)k\delta} \tag{4.5}$$

From Eq. (4.5), the following conclusions can be derived. First, the displacement amplification ratio will increase with the decrease of initial height h. Second, a large displacement amplification ratio can be obtained by using a large input amplification k or a large value of l_0.

Likewise, for the double symmetric four bar mechanical amplifier shown in Figure 4.7, the output displacement can be derived as shown below:

$$o' = 2\left(h - \sqrt{h^2 - \left(\delta + 2l_0\right)\delta}\right) \tag{4.6}$$

Considering the small value of δ, compared with l_0 and h, from Eq. (4.5) and Eq. (4.6) one can show that $o > o'$ if $k > 2$. This means that the amplifier based on the five bar topology has a lager displacement amplification than the amplifier based on the double symmetric four bar topology under the same overall structural parameters.

As discussed in Section 4.2, the flexure hinges are used in the CMA to achieve a high positioning accuracy. To construct the CMA discussed in this section, four profiles of flexure hinges are considered. They are (a) single beam circular hinge profile, (b) single beam corner-filleted hinge profile, (c) double beam un-symmetric hinge profile, and (d) double beam symmetric hinge profile. All these profiles are shown in Figure 4.8.

(a) Single beam circular hinge five bar (b) Single beam corner-filleted five bar

(c) Double beam un-symmetric five bar (d) Double beam symmetric five bar

Figure 4.8 Different profiles of the designed CMA.

Also, different flexure hinges can be used for the connection between the driving links and the base. Here, three types of flexure hinges are considered in the design. They are

(1) right circular hinge, (2) single corner-filleted hinge, and (3) double corner-filleted hinge. All the profiles shown in Figure 4.8 use the right circular hinges connecting to the bases. Figure 4.9(a) is the single corner-filleted hinge case, while Figure 4.9(b) is the double corner-filleted hinge case.

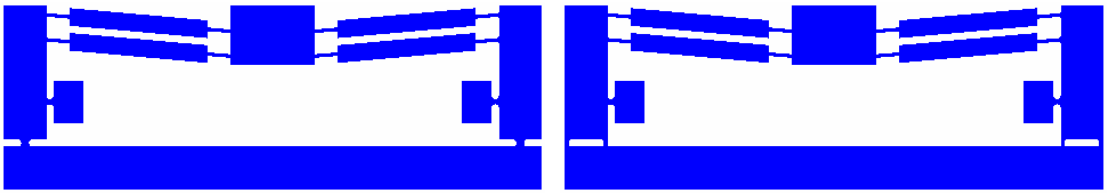

(a) Single corner-filleted hinge on the base (b) Double corner-filleted hinge on the base

Figure 4.9 CMA profiles using different flexure hinges connecting the driving links to the base.

In the next section, the performances with different types of the CMAs are compared so that a best profile can be chosen.

4.3.2 Finite Element Analysis of the CMA

The over dimension of the structures shown in Figures 4.6 – 4.9 are all 65 mm x 22 mm x 10 mm. Other parameters associated with the structures and the flexure hinges are indicated in Figure 4.10.

The stiffness of the flexure hinge mainly determines the displacement amplification of the CMAs and can be calculated via the equations given by Paros and Weisbord (1965) and Lobontiu and Paine (2001) as follows.

For right circular hinge:

$$K = \frac{2Ebt^{5/2}}{9\pi R^{1/2}} \tag{4.7}$$

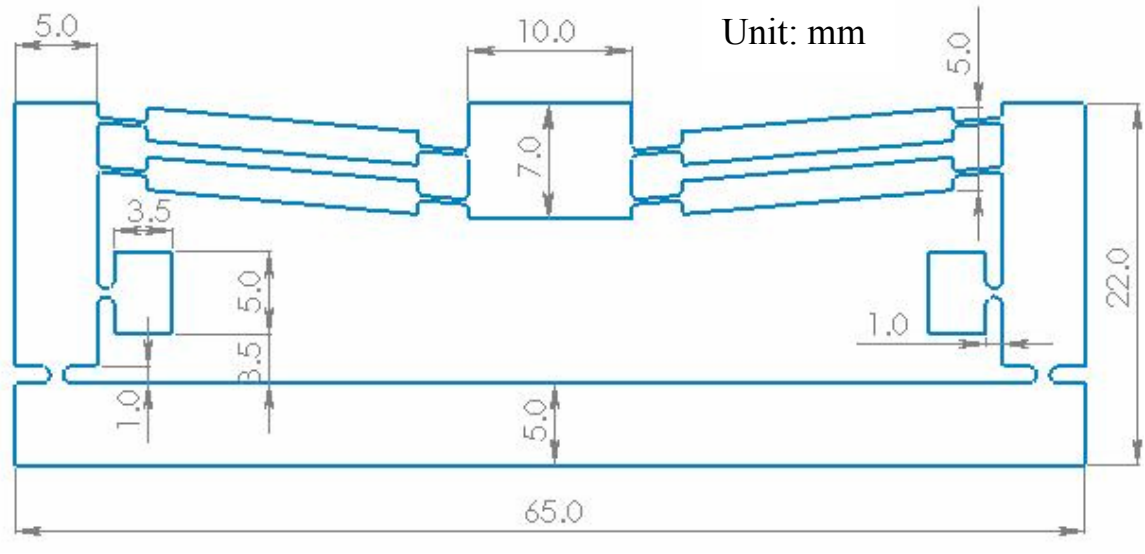

(a) Dimension of the double beam five bar CMA

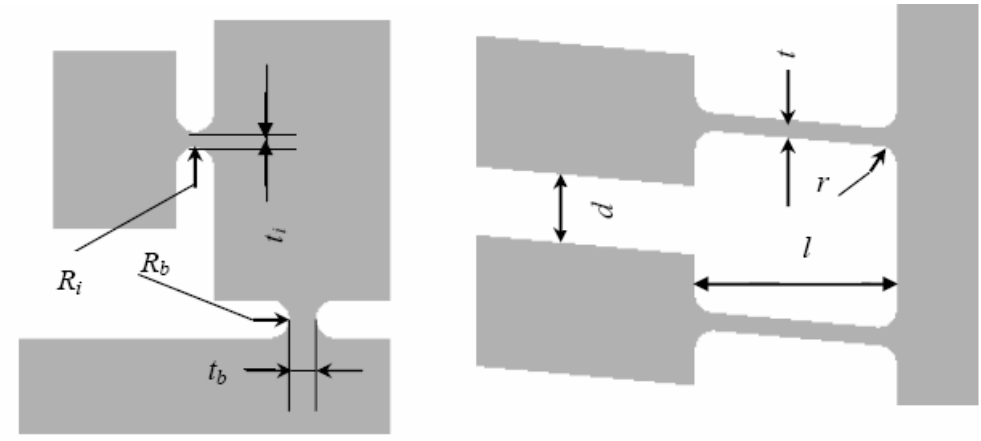

(b) Circular hinge parameters (c) Corner-filleted hinge parameters

Figure 4.10 Dimension of the flexure hinge parameters in CMA.

For corner filleted hinge:

$$K = \frac{Ebt^3}{12\left(l - 2r + 2rf(s)\right)} \tag{4.8}$$

where $s = 2r/t$ and $f(s) = \dfrac{(2s+1)\left(3s^2+2s+1\right) + 3s(s+1)^2\sqrt{2s+1}\tan^{-1}\left(\sqrt{2s+1}\right)}{(s+1)(2s+1)^3}$.

From Eqs. (4.7) and (4.8) one can see that the most significant parameter that affects the stiffness of the flexure hinge is the thickness *t* of the hinge. Also, the length of the corner filleted hinge has some influence on the stiffness.

In the first stage, different structures shown in Figure 4.6 and Figure 4.8, where the same right circular hinges are used to connect the driving links and the base, are analyzed using the ANSYS software with element 82 (a 2D eight-node plane element). The FEA was used to analyze the amplification ratio and natural frequencies. In the finite element analysis, the modulus of the elasticity E is set to $1.17\times10^{11}\ N/m^2$ and the Poisson ratio $\mu = 0.3$. Here only two cases are studied for the purpose of comparison, and their parameters are listed as follows.

Case 1:

$t_i = 0.5mm$, $t_b = 0.5mm$, $h = 3.0mm$, $l\ or\ 2R = 3.0mm$, $t = 0.5mm$, $d = 0.5mm$.

Case 2:

$t_i = 0.5mm$, $t_b = 0.8mm$, $h = 2.0mm$, $l\ or\ 2R = 3.0mm$, $t = 0.3mm$, $d = 0.5mm$.

Figure 4.11 plots the results of the comparison where no payload is included. From this figure, one can see that the symmetric five bar structure with double-beam is better than the symmetric double four bar structure with double-beam in terms of the displacement amplification. According to the FEA calculation, the displacement amplification ratios of the symmetric double-beam five bar structure are the biggest and as high as 15.02 in case 1 and 24.44 in case 2, respectively. The displacement amplification ratios of the single beam circular hinge structure are the smallest, with 7.82 in case 1 and 14.2 in case 2, respectively. Also, different structure and flexure hinge parameters produce different displacement amplification ratios even for the same type of structure. Further, a different stiffness of the compliant mechanism can provide different displacement amplification. Through this analysis, one can see that the symmetric double-beam five bar structure is the best structure and the single beam with the right circular hinge is the worst one in terms of the displacement amplification.

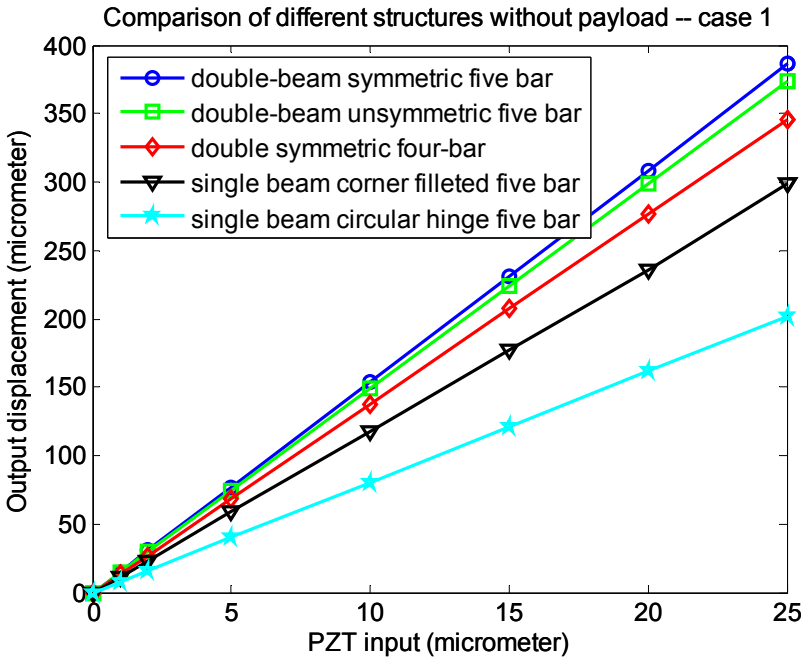

(a) Displacement amplification comparison for case 1

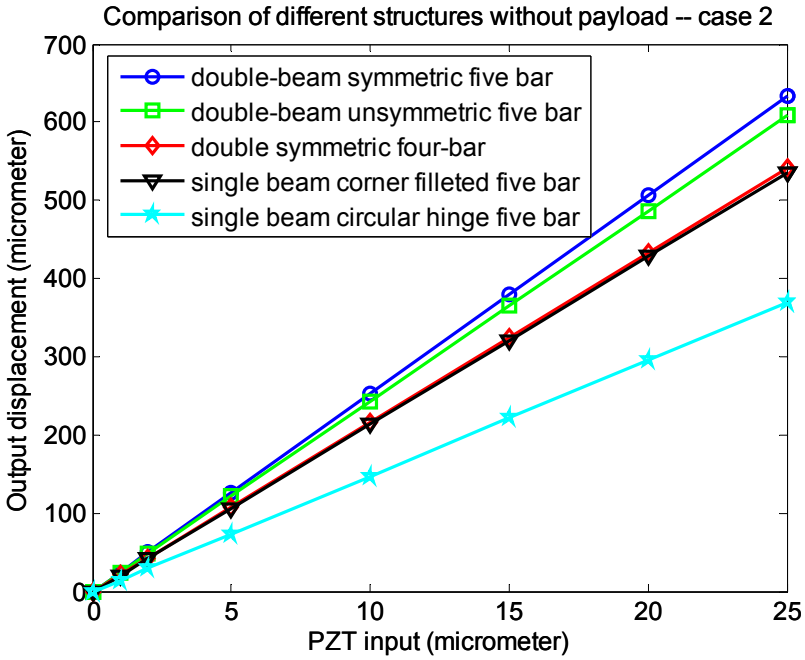

(b) Displacement amplification comparison for case 2

Figure 4.11 Comparison of different structures for the displacement amplification without payload.

The above results can be explained as follows. From a practical point of view, all bending occurs in the center of the circular hinge or at the end of the corner filleted hinge. Therefore, the value of l_0 of the PRBM in Eq. (4.5) for the circular hinge is smaller than that for the corner filleted hinge. According to Eq. (4.5), the displacement amplification ratio of the circular hinge structure that has the smallest value of l_0 is the smallest in all five structures. From Eq. (4.8), for all the corner filleted hinge structures, the structure with a large thickness of the hinge has large stiffness that makes the bending more difficult. That is the reason why the single beam structure with the corner filleted hinge obtains smaller displacement amplification than the double beams structures.

Besides the free payload situation considered before, the CMAs are applied by some payloads to examine the displacement amplification. Here two types of payloads with stiffness of 20 N/mm and 100 N/mm are acted on the output plate, respectively. The result is shown in Figure 4.12. From this figure, one can see that the symmetric double-beam five bar structure still obtained the best displacement amplification. Comparing Figure 4.12 with Figure 4.11, one can see that the displacement amplification of the double symmetric four bar structure decreases significantly under the payload conditions. This means that the double symmetric four bar structure has very low stiffness compared with other structures.

The dynamic behaviour of the CMA is one of the most important characteristics of the system. As the precision mechanisms such as the CMAs are greatly influenced by the vibration effects in their applications, the natural frequencies of the CMA should be examined. Table 4.1 lists the first three modes of the natural frequencies obtained from the FEA dynamic modal analysis. The first natural frequency of the symmetric double-beam five bar structure is about 573 Hz that is much larger than that of the symmetric four bar structure which is only about 150 Hz.

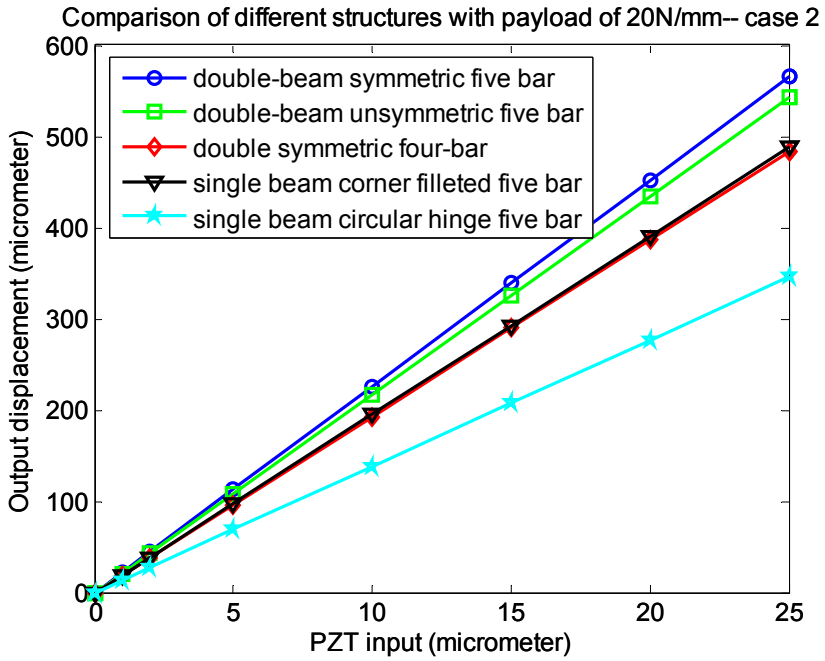

(a) Comparison of displacement amplification comparison under payload of 20 N/mm

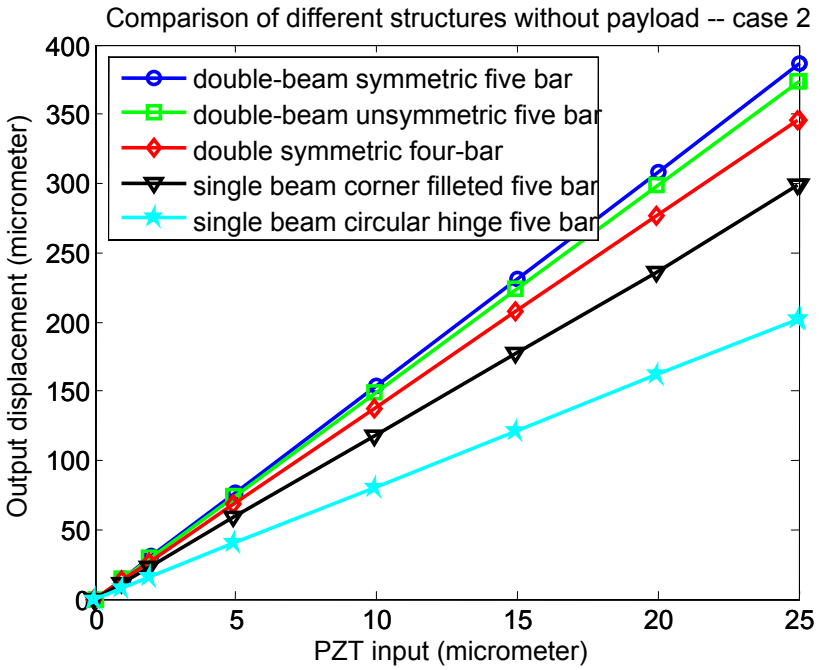

(b) Comparison of displacement amplification under payload of 100 N/mm

Figure 4.12 Comparison of different structures for the displacement amplification with payload.

From table 4.1 one can see that the new CMA based on the symmetric double-beam five bar structure has the best dynamic behaviour among all the structures. Comparing the two cases, case 1 can be viewed as a rigid situation, and case 2 as a flexible situation because of the different stiffnesses of the flexure hinges in the structures. It is shown that when the stiffness of the flexure hinge increases the natural frequencies of the system will increases as shown in Table 4.1. Also, one can see that the natural frequency of the first mode of the new CMA is about 2.8 times that of the symmetric four bar CMA in case 1 and even about 3.8 times in case 2. From these comparisons, one can see that the new CMA has the advantages both in the displacement amplification and the dynamic behaviour.

Table 4.1 Calculated natural frequencies of different CMAs

Frequency	**Case 1**			**Case 2**		
	Symmetric double-beam five bar	Un-symmetric double-beam five bar	Double symmetric four bar	Symmetric double-beam five bar	Un-symmetric double-beam five bar	Double symmetric four bar
f_1	824.86	810.89	290.06	573.13	559.15	150.59
f_2	881.13	865.95	379.32	957.51	945.46	220.07
f_3	4380.2	3901.9	1008.3	3221.1	2950.4	725.21

From the above figures, it can be seen that different parameters result in different displacement amplifications even for the same structure. Therefore, it is necessary to fine-tune the parameters based on the displacement amplification, and such an issue will be addressed in the next section.

4.3.3 Fine-tuned Parameters Based on the Displacement Amplification

In this section, the FEA method is used to analyze the parameter effect on the displacement amplification for the new CMA. It should be noticed that in this study, only one parameter is varied meanwhile the other parameters were fixed as the following values:

$$h = 2.0\ mm,\ l = 3.0\ mm, t_i = 0.5\ mm,\ t = 0.3\ mm,$$

$$t_b = 0.8\ mm,\ R_i = R_b = 0.5\ mm,\ \ d = 0.5\ mm.$$

4.3.3.1 Displacement amplification using different types of flexure hinges on the base

First of all, different types of flexure hinges on the base for the new CMA are examined to determine the best flexure hinge. The flexure hinge parameters listed above are used in the FEA, and the displacement amplification results using three types of flexure hinges on the base are shown in Figure 4.13.

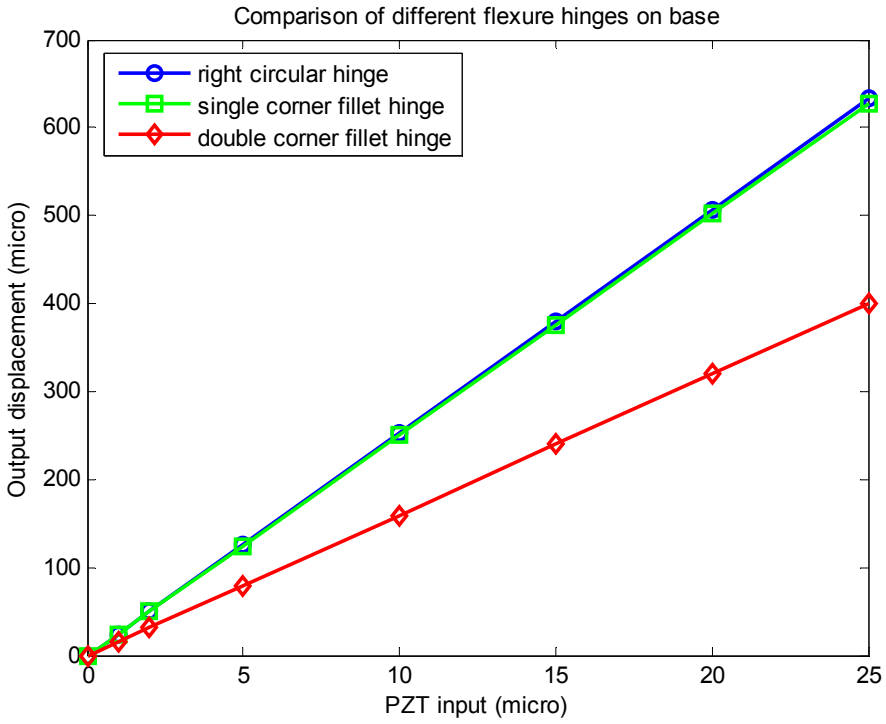

Figure 4.13 Displacement amplification using different types of flexure hinges on the base.

From this figure, one can see that the structure using the circular hinge gets the best displacement amplification, although there is no significant difference in the displacement amplification between the circular hinge and the corner filleted hinge. Such a result can be explained as follows: the two flexure hinges have different bending centers when the PZT force is acted on the driving beam, which means that the circular hinge has a smaller l_1 than the corner filleted hinge. Therefore, a larger input amplification ratio k in Eq. (4.5) exists for the circular hinge. This results in a large displacement amplification.

The structure using double corner filleted hinges on the base is the worst structure in terms of the displacement amplification. The reason for this result can be explained as follows. The double corner filleted hinge on the base can be viewed as a parallel four bar linkage. There is only translation of the driving beam associated with the hinge on the base. Therefore, the input displacement of the PZT actuator can not be amplified by the double corner filleted hinge because the input point is out of the parallel four bar linkage. As such, the structure with double corner filleted hinges on the base belongs to the topology of a parallel four bar structure.

4.3.3.2 Insignificant parameters

As mentioned before, the circular hinge on the base for the symmetric double-beam five bar CMA can obtain the best displacement amplification. Therefore, the following analyses only focus on that type of structure.

First of all, the effect of the thickness t_i of the flexure hinge used to transfer the linear movement of the PZT actuator to the rotation of the lever arm is examined. The FEA results show that the variation of t_i has little influence on the displacement amplification as listed in Table 4.2. A similar conclusion is obtained for the variation of the thickness t_b of the flexure hinge on the base, and the result is shown in Table 4.3.

Table 4.2 System behaviour of the CMA in terms of the thickness on the input side

PZT input (μm)	Output displacement (μm)				block force (N)			
	t_i=0.4 (mm)	t_i=0.5 (mm)	t_i=0.6 (mm)	t_i=0.8 (mm)	t_i=0.4 (mm)	t_i=0.5 (mm)	t_i=0.6 (mm)	t_i=0.8 (mm)
1	24.37	24.44	24.47	24.42	3.99	4.10	4.19	4.33
2	49.66	49.79	49.84	49.72	8.14	8.36	8.54	8.82
5	125.56	125.86	125.93	125.59	20.57	21.13	21.58	22.29
10	252.06	252.63	252.78	252.04	41.30	42.41	43.32	44.73
15	378.56	379.41	379.61	378.5	62.03	63.69	65.05	67.18
20	505.07	506.19	506.45	504.95	82.76	84.98	86.79	89.62
25	631.57	632.96	633.28	631.41	103.49	106.26	108.52	112.07

Table 4.3 System behaviour of the CMA in terms of the thickness on the base

PZT input (μm)	Output displacement (μm)			block force (N)		
	t_b=0.6 (mm)	t_b=0.8 (mm)	t_b=1.0 (mm)	t_b=0.6 (mm)	t_b=0.8 (mm)	t_b=1.0 (mm)
1	24.35	24.44	24.35	3.91	4.10	4.22
2	49.65	49.79	49.6	7.97	8.36	8.59
5	125.59	125.86	125.32	20.16	21.13	21.73
10	252.13	252.63	251.54	40.48	42.41	43.60
15	378.68	379.41	377.76	60.80	63.69	65.48
20	505.23	506.19	503.97	81.12	84.98	87.36
25	631.77	632.96	630.18	101.43	106.26	109.24

From Tables 4.2 and 4.3, one can see that as the thickness of the flexure hinge either on the PZT actuator or on the base side increases, the block forces increase slightly. This is because using a large thickness will increase the stiffness of the flexure hinge, and hence a potential to sustain a large force.

Also, the variation of d , the gap between the two beams on the output side, has insignificant influence on the system behaviour, i.e., the displacement amplification and the block force. The result is shown in Table 4.4.

It should be noted that the value d must be greater than zero even though it has little influence on the displacement amplification. If d sets to zero, the two beams will combine to form a single beam. FEA demonstrates that the displacement amplification ratio will decrease dramatically in such a situation.

Table 4.4 System behaviour of the CMA in terms of the gap of the two beams

PZT input (μm)	**Output displacement (μm)**			**block force (N)**		
	d=0.4 (mm)	*d*=0.5 (mm)	*d*=0.6 (mm)	*d*=0.4 (mm)	*d*=0.5 (mm)	*d*=0.6 (mm)
1	24.53	24.44	24.36	4.0981	4.10	4.11
2	49.99	49.79	49.61	8.3537	8.36	8.37
5	126.41	125.86	125.35	21.121	21.13	21.14
10	253.76	252.63	251.59	42.399	42.41	42.43
15	381.12	379.41	377.83	63.677	63.69	63.72
20	508.47	506.19	504.08	84.955	84.98	85.01
25	635.82	632.96	629.96	106.23	106.26	106.31

4.3.3.3 Significant parameters

In the design process, three parameters were identified that have significant effect on the displacement amplification. They are the height h of the initial position, the thickness t of the corner filleted hinge, and the length l of the corner filleted hinge. Figure 4.14 shows the results under different heights h of the initial position. From Figure 4.14, one can see that the displacement amplification increases significantly while the block force decreases dramatically with the decrease of the height h. Such a conclusion can also be obtained from Eq. (4.5). A similar conclusion was obtained for the double symmetric four bar CMA as shown in Conway and Kim (2004).

Table 4.5 list the first three natural frequencies under different values of the height h. From this table, one can see that the first natural frequency of the CMA increases with the increase of the height h. But the second and the third natural frequencies slightly decrease with the increase of the height h.

Table 4.5 Natural frequencies vs. the height of the initial position

Natural frequencies	**Height of initial position (*mm*)**			
	h=1.5	h=2.0	h=2.5	h=3.0
f_1 (Hz)	460.61	573.13	681.85	785.61
f_2 (Hz)	977.77	957.51	936.68	915.39
f_3 (Hz)	3227.7	3221.1	3211.2	3198.2

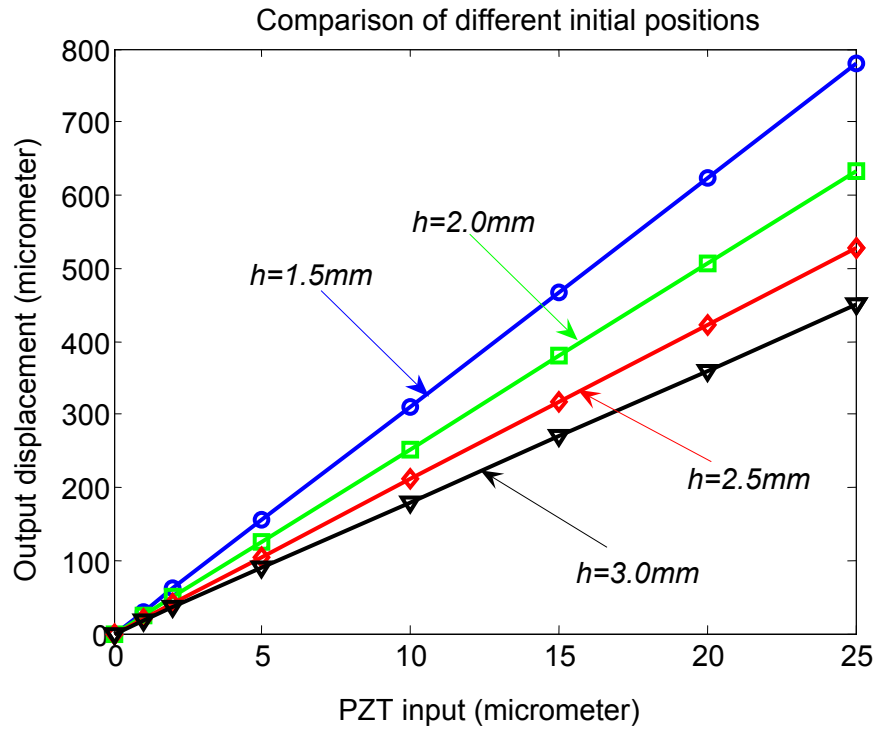

(a) Displacement amplification for various the initial positions

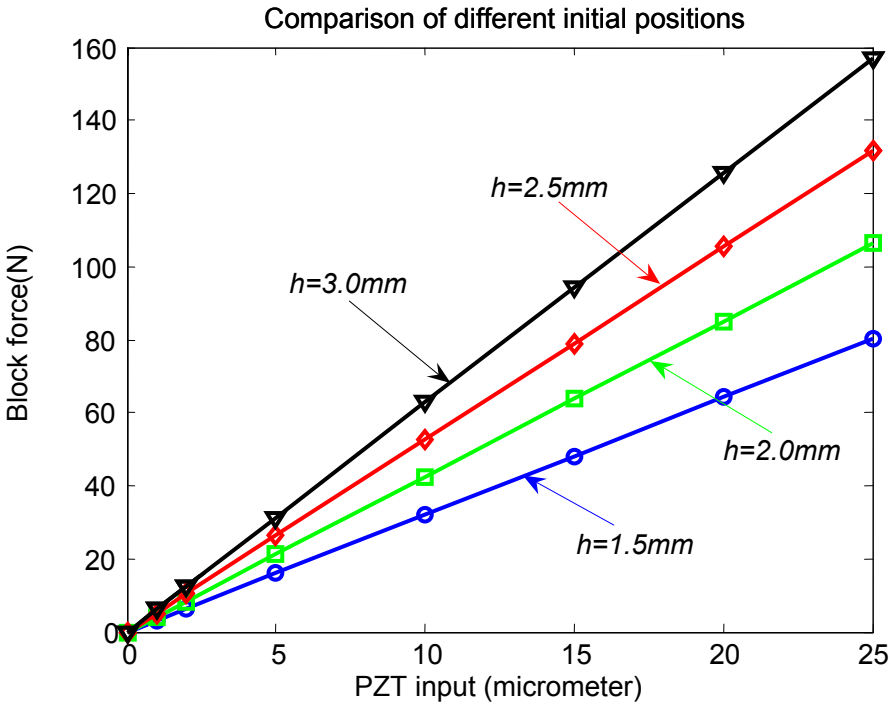

(b) Block force for various the initial positions

Figure 4.14 System behaviour of the CMA under different heights of the initial position.

The thickness t and length l of the corner filleted hinge also have influence on the displacement amplification as both of them affect the stiffness of the flexure hinge according to Eq. (4.8), but the effect of the thickness t is more significant than that of the length l as shown in Figure 4.15. Therefore a smaller thickness of the flexure hinge will provide large displacement amplification. This also means that the thickness t of the hinge has much more contribution to the displacement amplification than the length l of the flexural hinge.

Table 4.6 lists the first three natural frequencies under different thicknesses t of the corner filleted hinge. From this table one can see that the natural frequencies increases with the increase of the thickness t of the corner filleted hinge. This means the larger the stiffness of the flexure hinge the higher the natural frequency. It should be pointed out that there are slight changes in the natural frequencies with the variation of the length l of the corner filleted hinge.

Table 4.6 Natural frequencies vs. thicknesses of the corner filleted hinge

Natural frequencies	**Thickness of the corner filleted hinge (*mm*)**			
	t=0.2	t=0.3	t=0.4	t=0.5
f_1 (Hz)	537.1	573.13	613.55	663.61
f_2 (Hz)	919.51	957.51	1023.4	1117.1
f_3 (Hz)	2150.3	3221.1	3964.3	4462.4

In summary, through the FEA simulation, it is found that three parameters, the height h of the initial position, the thickness t and the length l of corner filleted hinge, have significant influences on the displacement amplification. Two parameters, the height h of the initial position and the thickness t of the corner filleted hinge, have significant influences on the natural frequency. Other parameters, such as the thickness of the circular hinges and the gap of the two beams, have insignificant influences on the displacement amplification and the natural frequency.

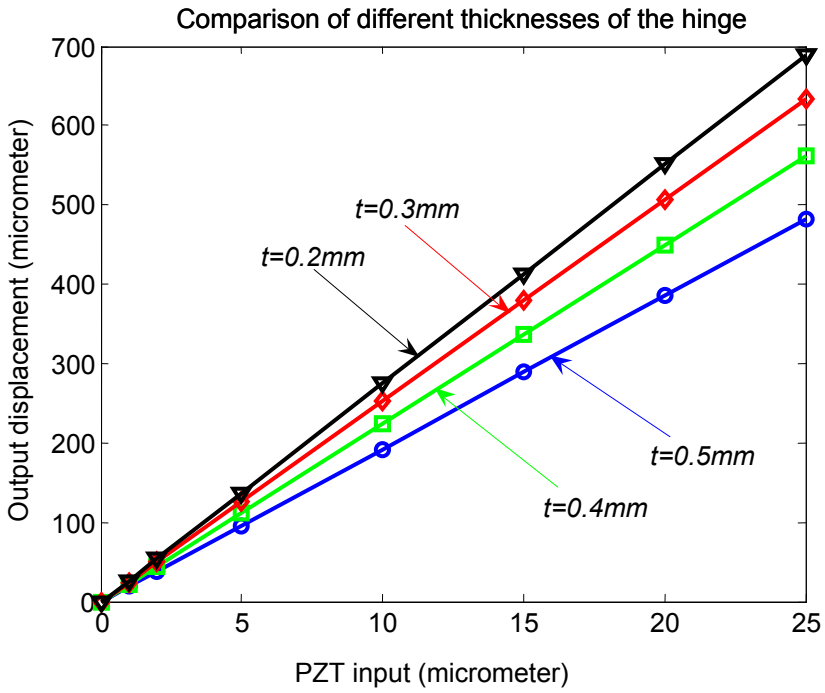

(a) Displacement amplification for various thicknesses of hinge

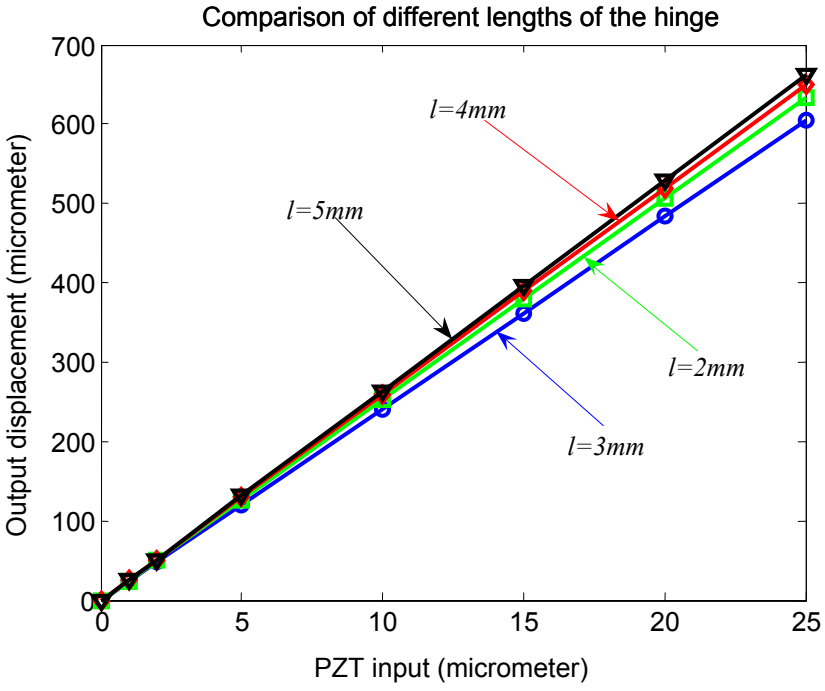

(b) Displacement amplification for various lengths of hinge

Figure 4.15 Displacement amplification of the CMA in terms of the corner filleted hinge parameters.

4.4 Design and Modeling of the Spatial Hybrid Motion Mechanism

In the previous section, a CMA was designed, and an optimal structure using the double-beam flexural hinge was obtained after examining different structures. In this section, based on the developed CMA, a spatial HMM is developed which can be used to perform the macro-micro motion.

4.4.1 Two Design Principles for the Macro-micro Mechanism

Traditionally, the design of a macro-micro mechanism is divided into two separate motion mechanisms. One is for the macro motion that functions as a base with a large motion range, while the other is for the micro motion with high accuracy which is mounted on the macro motion mechanism. Such a macro-micro mechanism can be viewed as a serial configuration and its topology can be expressed in Figure 4.16(a).

To overcome the problems associated with the traditional macro-micro mechanism, a new design strategy is proposed which can be viewed as a parallel configuration and the topology is shown in Figure 4.16(b). In the parallel configuration, the macro motion and micro motion are carried out by the same mechanism. Only one mechanism is needed to complete the coarse and fine positioning performance. Such a characteristic can be realized using the compliant mechanism based on the flexural hinge. The unique feature of the parallel configuration is the reduction or elimination of the interaction between the macro motion and the micro motion. In the next section, the details of the design and analysis of such a hybrid motion mechanism (HMM) are discussed.

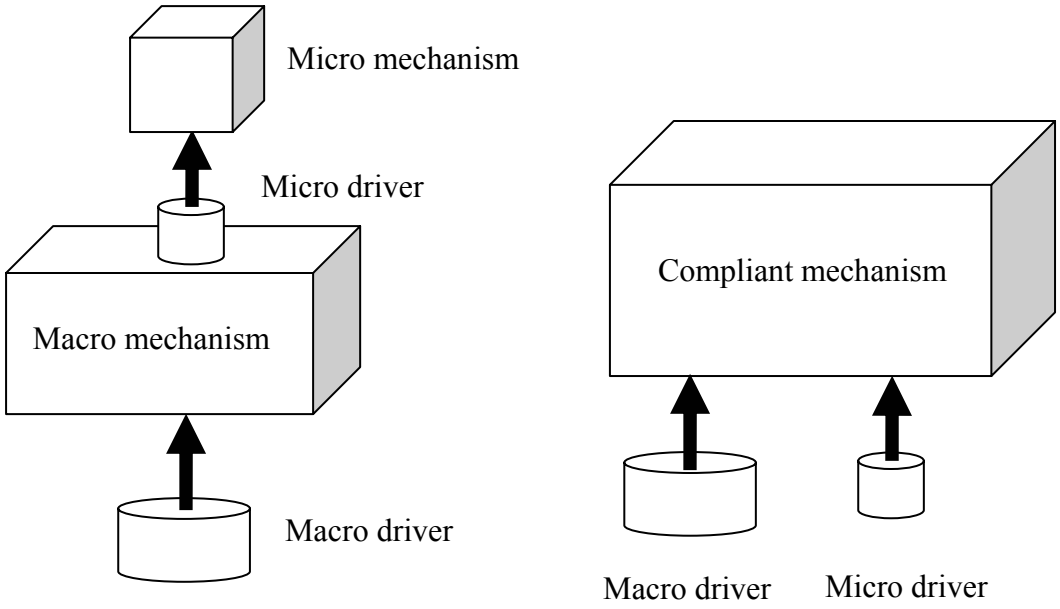

(a) Serial configuration (b) Parallel configuration

Figure 4.16 Two design principles of the macro-micro mechanism.

4.4.2 Design and Analysis of the Spatial Hybrid Motion Mechanism

4.4.2.1 Design of the spatial HMM

The proposed spatial HMM is a parallel type compliant mechanism with three serial chains or legs. Each leg consists of a one-axis flexural hinge as revolute joint and a three-axis flexural hinge as a spherical joint. Figure 4.17 describes the model and coordinate systems of one leg in the HMM and Figure 4.18 shows the schematic of this HMM, while Figure 4.19 is a 3D model of the HMM.

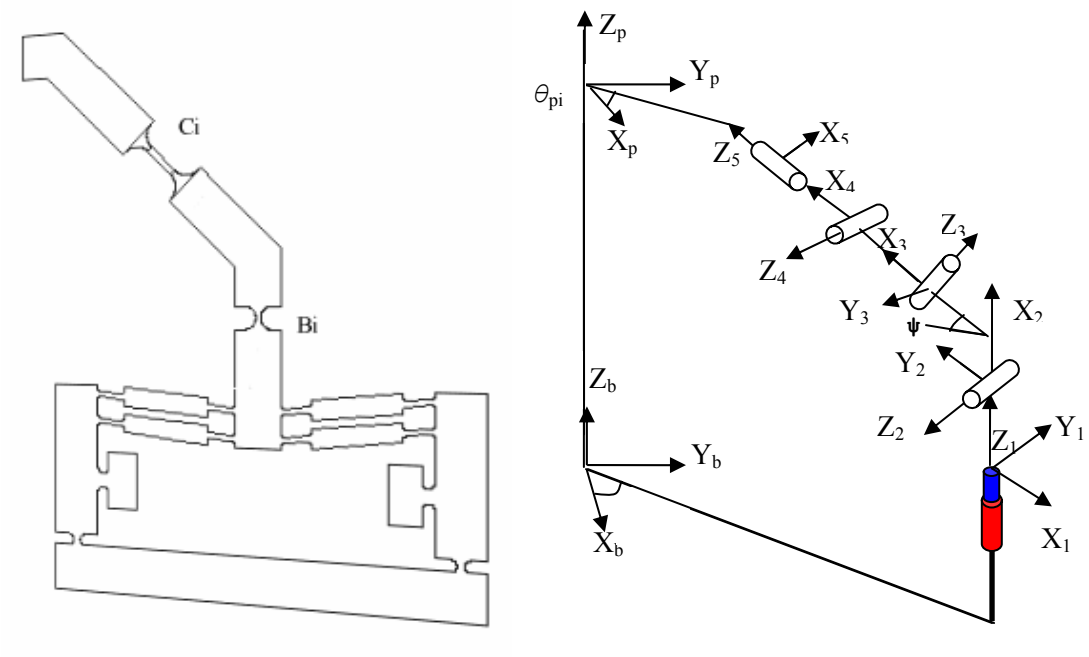

Figure 4.17 The model and coordinate systems of the *i-th* leg.

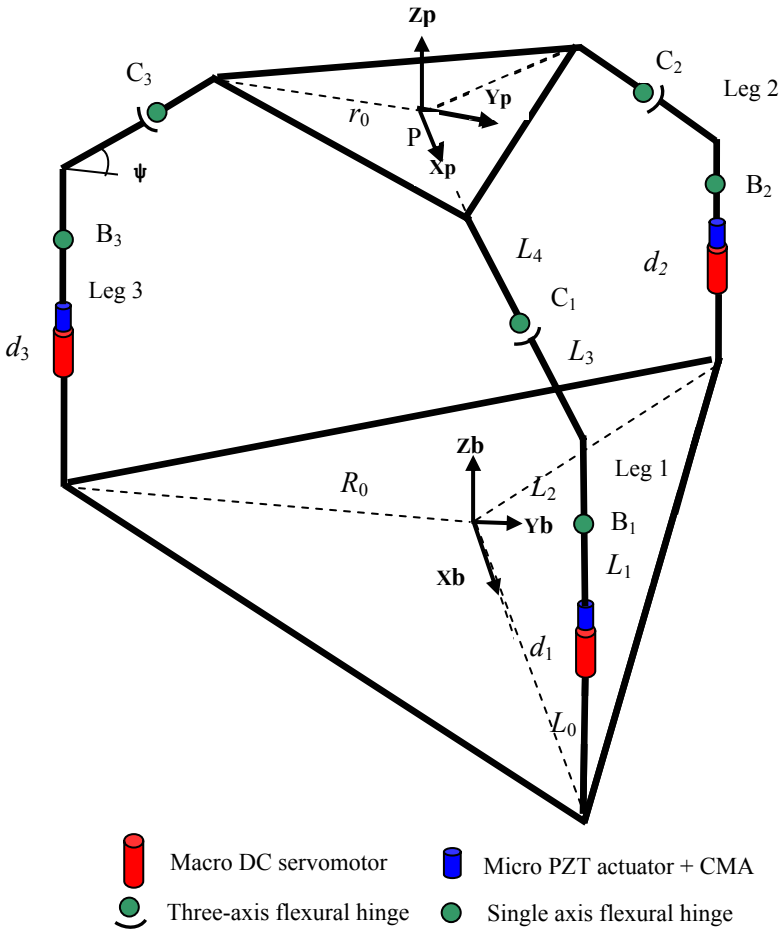

Figure 4.18 Schematic of the spatial HMM.

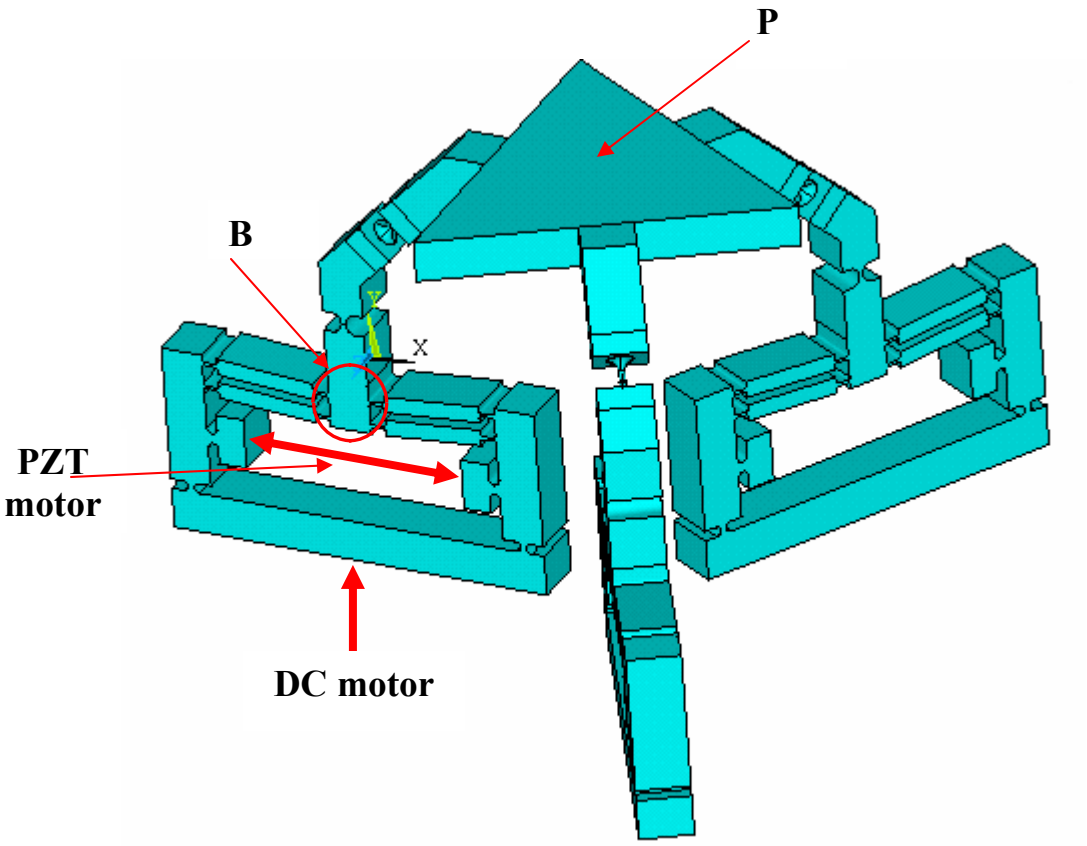

(a) The 3D model of the spatial HMM.

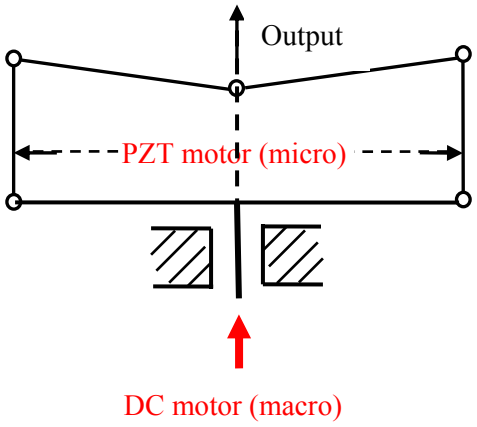

(b) PRBM of one leg.

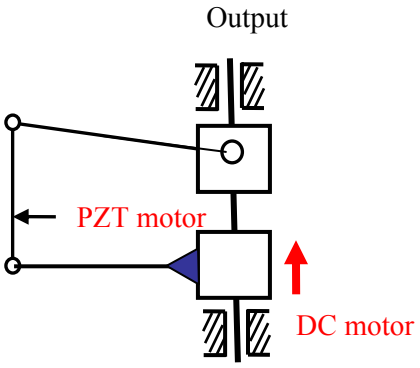

(c) Half PRBM of one leg.

Figure 4.19 Spatial hybrid motion mechanism and its PRBM.

In the designed HMM, the CMA discussed in the previous section was applied to fulfill the micro motion, and the macro motion can be realized by the use of the DC motors attaching to the bottom of each leg; see Figure 4.19. Such an arrangement can implement the parallel macro-micro HMM, which is explained as follows. First, from the viewpoint of the end-effector point P, the structure is apparently parallel, especially with respect to the same three legs. The motion generated and transferred to the end-effector is a mixed macro and micro motion. Second, from the viewpoint of point B which is an output portal of the CMA mechanism, its motion is a mixed macro and micro motion synchronously contributed by the PZT motor and the DC motor. According to the PRBM of the compliant mechanisms (Howell, 2000), this situation can be schematically described, as shown in Figure 4.19(b). Due to the structural symmetric property with the system, the diagram can be further described as shown in Figure 4.19(c). The degree of freedom of the mechanism of Figure 4.19(c) is two, which implies that for the mechanism (in Figure 4.19(c)) to have a definite motion, two motors are needed; one PZT (micro) motor and one DC (macro) motor in this case.

The designed HMM has the following characteristics.

(1) The compliant mechanism is symmetric with three same legs.
(2) The moving plate and the base plate are designed to be the equilateral triangles, respectively.
(3) The CMA structure discussed in Section 4.3 is applied to amplify the stroke of the PZT motor of the micro motion.
(4) The DC servomotors are used to directly drive the base of the CMA to fulfill the macro motion.
(5) The reaction force acted on the DC servomotor caused by the PZT motor is eliminated by the inverse arrangement of the PZT motor and the symmetric structure of the CMA.
(6) The designed spatial compliant mechanism can be used as a micro motion mechanism if only the PZT motors are used to drive the three legs.

4.4.2.2 Transformation matrix

A transformation matrix is defined as a matrix which represents a movement of a frame relative to a fixed reference frame. To get the transformation matrix of the local coordinate attached to the end plate with respect to the global coordinate, the X-Y-Z reference system with Euler angles (α, β, γ) (Niku, 2001) is used. In this way, the matrix representing the change in orientation of Euler angles can be expressed as:

$$Euler(\alpha,\beta,\gamma) = R_x(\alpha)R_y(\beta)R_z(\gamma)$$

$$= \begin{vmatrix} 1 & 0 & 0 \\ 0 & \cos\alpha & -\sin\alpha \\ 0 & \sin\alpha & \cos\alpha \end{vmatrix} \begin{vmatrix} \cos\beta & 0 & \sin\beta \\ 0 & 1 & 0 \\ -\sin\beta & 0 & \cos\beta \end{vmatrix} \begin{vmatrix} \cos\gamma & -\sin\gamma & 0 \\ \sin\gamma & \cos\gamma & 0 \\ 0 & 0 & 1 \end{vmatrix} \tag{4.9}$$

$$= \begin{vmatrix} n_x & o_x & a_x \\ n_y & o_y & a_y \\ n_z & o_z & a_z \end{vmatrix}$$

where

$$\begin{cases} n_x = \cos\beta\cos\gamma \\ n_y = \sin\alpha\sin\beta\cos\gamma + \cos\alpha\sin\gamma \\ n_z = -\cos\alpha\sin\beta\cos\gamma + \sin\alpha\sin\gamma \end{cases} \tag{4.10}$$

$$\begin{cases} o_x = -\cos\beta\sin\gamma \\ o_y = -\sin\alpha\sin\beta\sin\gamma + \cos\alpha\cos\gamma \\ o_z = -\cos\alpha\sin\beta\sin\gamma + \sin\alpha\cos\gamma \end{cases} \tag{4.11}$$

$$\begin{cases} a_x = \sin\beta \\ a_y = -\sin\alpha\cos\beta \\ a_z = \cos\alpha\cos\beta \end{cases} \tag{4.12}$$

Therefore, the transformation matrix can be described as

$$T_p^b = \begin{vmatrix} n_x & o_x & a_x & x_p \\ n_y & o_y & a_y & y_p \\ n_z & o_z & a_z & z_p \\ 0 & 0 & 0 & 1 \end{vmatrix} \tag{4.13}$$

where the end-effector P is described by parameters x_p, y_p, z_p, α, β, and γ.

As there are only three active drives, the HMM has 3 DOFs. Assume that three independent parameters are α, β, and z_p, respectively, then the other three parameters (x_p, y_p, and γ) are the dependent ones.

4.4.2.3 Solution of the dependent parameters

To obtain the explicit expression of the transformation matrix, the three dependent variables should be represented by functions of the three independent variables. Due to the symmetric design of the HMM, the position vector c_i of the point C_i (i=1, 2, 3) with respect to the local coordinate system $X_pY_pZ_p$ can be described as

$$c_1 = \begin{bmatrix} c_x \\ 0 \\ -c_z \end{bmatrix}, \quad c_2 = \begin{bmatrix} -\frac{1}{2}c_x \\ \frac{\sqrt{3}}{2}c_x \\ -c_z \end{bmatrix}, \quad c_3 = \begin{bmatrix} -\frac{1}{2}c_x \\ -\frac{\sqrt{3}}{2}c_x \\ -c_z \end{bmatrix} \tag{4.14}$$

where $c_x = r_0 + L_4 \cos\psi$ and $c_z = L_4 \sin\psi$.

Using the transformation Eq. (4.13), the position vector c_i can be described with respect to the global coordinate system $X_bY_bZ_b$ as follows.

$$\begin{vmatrix} C_i \\ 1 \end{vmatrix} = T_p^b \begin{vmatrix} c_i \\ 1 \end{vmatrix} \quad \text{for } i = 1,\ 2,\ 3 \tag{4.15}$$

As the links B_1C_1, B_2C_2, and B_3C_3 are constrained into three specific planes. According to Figure 4.18, the following equations can be derived.

$$\begin{cases} C_{1y} = 0 \\ C_{2y} = -\sqrt{3}C_{2x} \\ C_{3y} = -\sqrt{3}C_{3x} \end{cases} \tag{4.16}$$

Applying Eq (4.16) to Eq. (4.15), one can get

$$n_y = o_x \tag{4.17}$$

$$x_p = -\frac{1}{2}\left(o_y c_x - n_x c_x - 2a_x c_z\right) \tag{4.18}$$

$$y_p = a_y c_z - n_y c_x \tag{4.19}$$

Submitting Eqs. (4.10) and (4.11) into (4.18), the Euler angle γ is obtained as

$$\gamma = \arctan\left(\frac{-\sin\alpha \sin\beta}{\cos\alpha + \cos\beta}\right) \tag{4.20}$$

So far, the three dependent variables were derived using Eqs. (4.18 – 4.20).

4.4.2.4 Inverse kinematics of the hybrid motion mechanism

The problem of inverse kinematics is to determine the values of the actuated drivers from the desired position and orientation (α, β, and z_p) of the end-effector P attached to the moving platform in the HMM. The procedure can be summarized as follows.

(1) Obtaining the Euler angle γ from Eq. (4.20);

(2) Getting position vector (x_p, y_p) using Eqs. (4.18) and (4.19);

(3) Obtaining the C_{ix}, C_{iy}, C_{iz} (i=1,2,3) using Eq. (4.15);

(4) Calculating the B_{ix}, B_{iy} (i=1,2,3) according to the global coordinate system in Figures 4.17 and 4.18;

(5) Using the following equation to obtain the required displacement d_i (i=1,2,3) for the macro-micro motion.

$$d_i = C_{iz} - L_0 - L_1 - \sqrt{L_{BC}^2 - \left(C_{ix} - B_{ix}\right)^2 - \left(C_{iy} - B_{iy}\right)^2} \tag{4.21}$$

where L_{BC} is the distance between joint B and joint C.

4.4.3 Motion Prediction and Dynamic Analysis

4.4.3.1 Selection of the design parameters

According to the schematic of the spatial HMM described in Figure 4.18, two types of spatial HMMs are designed which use different flexural hinges as the spherical joints. One is called the square type HMM where the three-axis flexural hinge with a square section is used; the other is called the cylinder type HMM where the three-axis flexural hinge with a circular section is used. They are shown in Figure 4.20. These two types of flexural hinges can be viewed as the ball or spherical joints with the ability of three rotations around the x, y, and z axes. These joints enable very smooth movements with extremely high accuracy compared with the traditional spherical joints.

In this section, the 3D finite element model using the ANSYS software is built to predict the static and dynamic performances of the two HMMs. A 3D FEA model of the mechanism is shown in Figure 4.21. A mixed meshing process (the auto meshing and manual meshing methods) is used in the finite element model so that the number of the total nodes will be not beyond the limitation of the software and the analysis time can be reduced. From this figure, one can see that the meshing of the rigid body is rough and the meshing of the flexural hinge is fine so that a more accurate analysis result can be obtained.

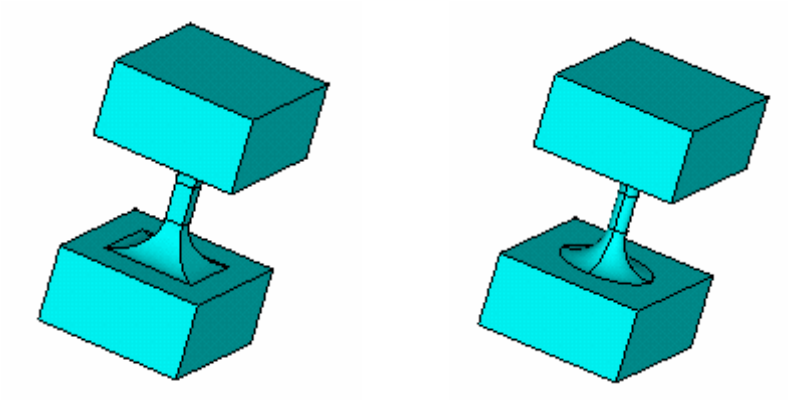

(a) Square section (b) Circular section

Figure 4.20 Two spherical flexural hinges

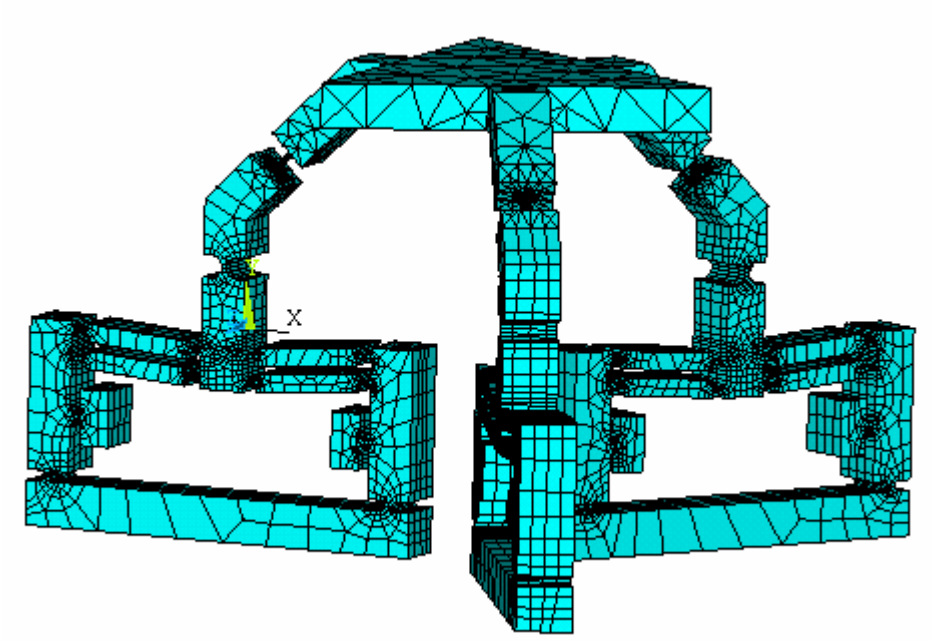

Figure 4.21 FEM model of the designed HMM.

To compare the performances of these two types of the HMMs, two different configurations with different design parameters are used to predict the orientation of the moving plate of mechanisms. Design parameters that significantly affect the performances of mechanisms are identified according to the complaint mechanism theory and the kinematic analysis. The design parameters of the CMA are shown in Figure 4.10, while the parameters of the legs in the HMM are shown in Figure 4.22. In the design process, eleven design parameters are chosen and listed in Table 4.7.

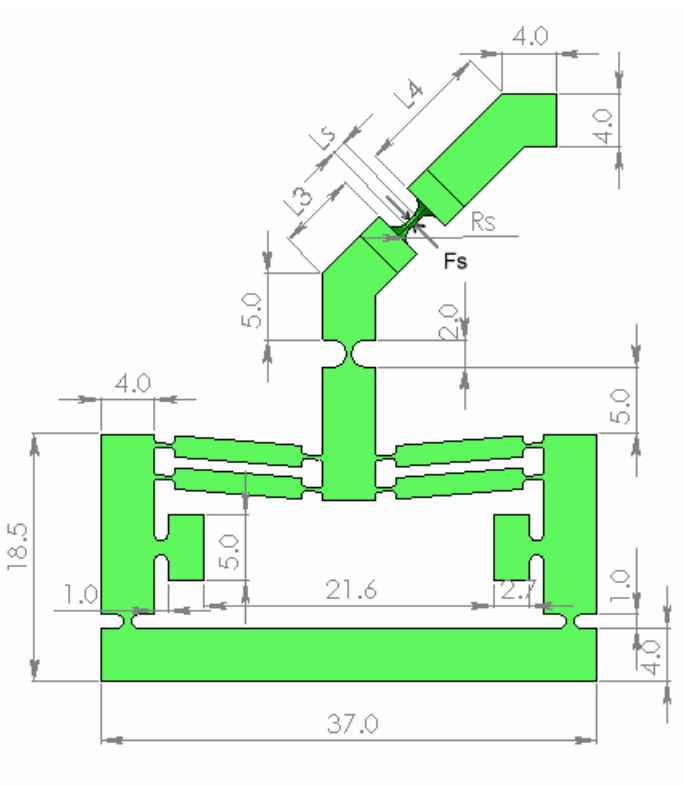

Figure 4.22 Some design parameters about the leg of the HMM.

Table 4.7 Design parameters of the HMMs (unit: mm).

Parameters	h	l	t	d	R_b	R_i	L_3	L_4	L_s	F_s	R_s
Case 1	1.0	1.5	0.3	0.4	0.3	0.5	6.0	10.0	1.0	0. 5	1.0
Case 2	1.0	2.0	0.4	0.5	0.4	0.6	10.0	14.0	3.0	0. 5	1.0

In the following, the static and dynamic analyses of two HMMs are presented to get the primary knowledge about the HMM. These analyses also serve as the basis for the optimal design of the HMM which will be discussed in Section 4.5.

4.4.3.2 Orientation prediction of the HMM

According to the arrangement of the actuation in the HMM, one can see that the translation along the Z direction can be easily achieved by simultaneously moving the three legs using 3 DC motors to achieve the macro motion or by actuating the 3 PZT actuators to achieve the micro motion. Therefore, only the orientation of the HMM is performed for the static analysis in this section.

In the FEA, the 3D element Solid185 is selected to model the structure of the HMM. The modulus of the elasticity E of the material is set to $7.5\times10^{10}\,N/m^2$ and the Poisson ratio $\mu = 0.33$. In the following, the HMM with the square section in the spatial flexural hinge is called the square type HMM, while the HMM with the circular section in the spatial flexural hinge is called the cylinder type HMM. These two types of HMMs with two different configurations are analyzed under the micro motion, macro motion, and macro-micro motion conditions. Figure 4.23 shows the micro movement of the HMM driven by two PZT actuators, and Figure 4.24 shows the stress profile of the HMM.

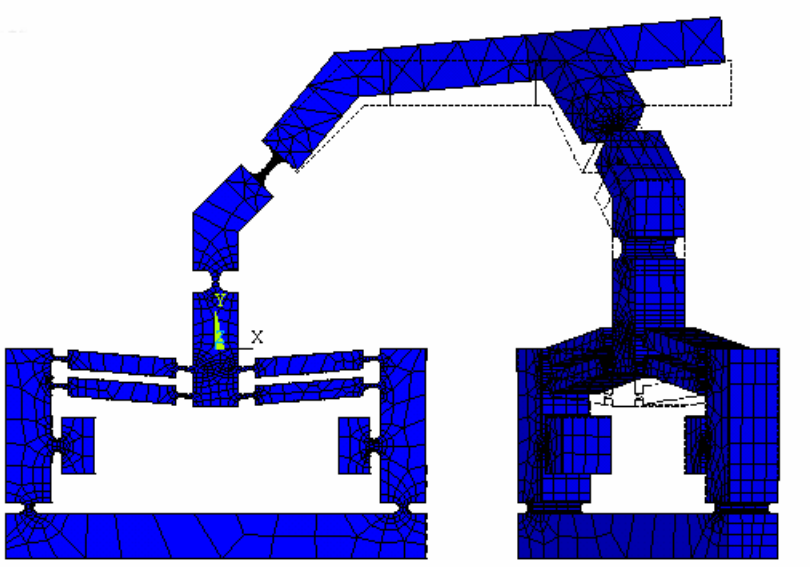

Figure 4.23 Micro movement of the HMM driven by two PZT actuators.

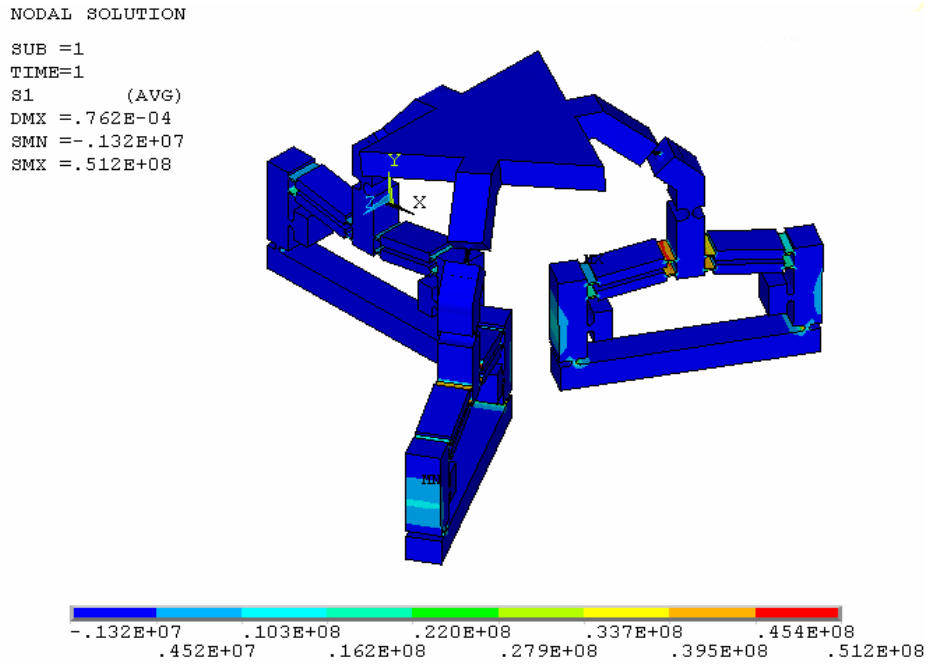

Figure 4.24 Stress profile for the micro motion driven by two PZT actuators.

From Figure 4.24 one can see that the maximum stress of the HMM occurs at the flexural hinges of the CMA. Figure 4.25 shows the macro motion of the HMM driven by one DC motor, and Figure 4.26 depicts the stress profile of the HMM under the macro motion. From Figure 4.26 one can see that the maximum stress of the HMM occurs at the spatial flexural hinge of the driving leg. A more clear stress distribution on the spatial flexural hinge is shown in Figure 4.27.

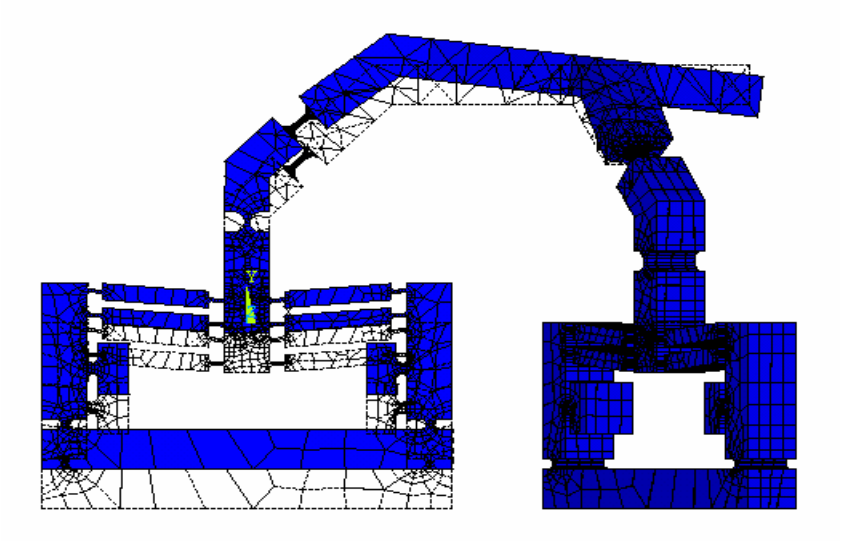

Figure 4.25 Macro movement of the HMM driven by one DC motor.

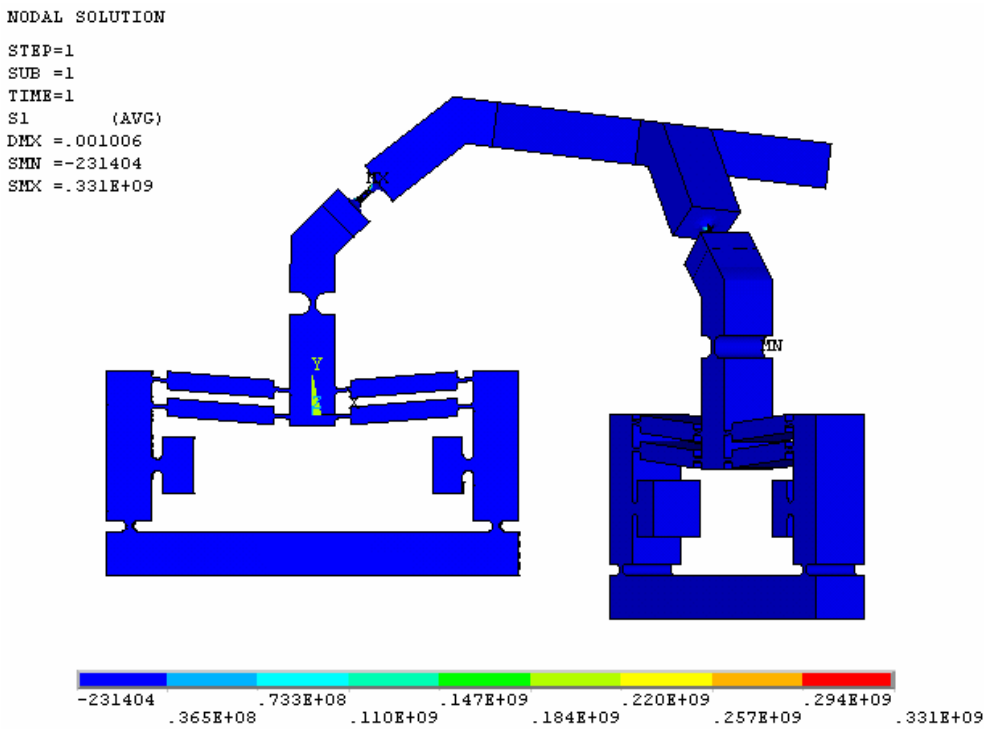

Figure 4.26 Profile of the stress of the HMM under deformation.

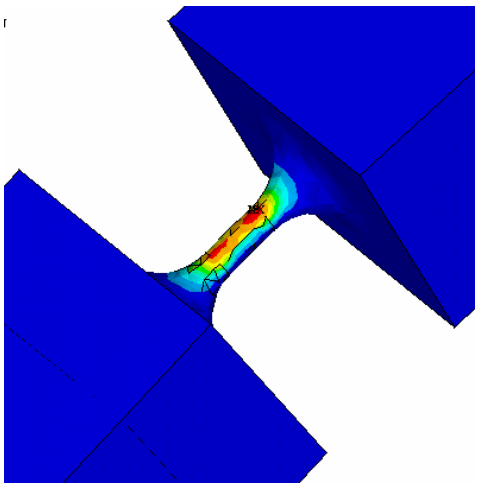

Figure 4.27 Zoom of the stress profile on the spatial flexural hinge.

In the design process, the predicted orientation (rotation around the Y axis), the force performance and the maximum stress of the HMMs are obtained for two cases under the micro motion, macro motion, and macro-micro motion situations, respectively. Table 4.8

shows the micro orientation results driven by one PZT and two PZTs, respectively. Table 4.9 and Table 4.10 show the macro and macro-micro orientation results, respectively. From these three tables, one can obtain the following conclusions. First, the orientation angle of the HMMs driven by one leg is the same but in the other direction as that driven by two legs. This is due to the symmetric design of the three legs in the HMMs. Second, the cylinder type HMM has the potential of a larger orientation movement than the square type HMM has. This is because the spatial flexural hinge with the circular section has a larger compliance than the one with the square section.

Table 4.8 Micro orientation results of the HMMs (deg.).

PZT input (μm)	Case 1				Case 2			
	One PZT		Two PZTs		One PZT		Two PZTs	
	square type	cylinder type	square type	cylinder type	square type	cylinder type	square type	cylinder type
1	-0.018	-0.018	0.018	0.018	-0.012	-0.013	0.012	0.013
2.5	-0.045	-0.046	0.045	0.046	-0.030	-0.031	0.031	0.032
5	-0.089	-0.091	0.090	0.091	-0.061	-0.063	0.061	0.064
7.5	-0.134	-0.137	0.135	0.137	-0.091	-0.094	0.092	0.097
10	-0.179	-0.182	0.180	0.183	-0.122	-0.125	0.122	0.129

Table 4.9 Macro orientation results of the HMMs (deg.).

DC input (mm)	Case 1				Case 2			
	One PZT		Two PZTs		One PZT		Two PZTs	
	square type	cylinder type	square type	cylinder type	square type	cylinder type	square type	cylinder type
0.5	-0.51	-0.52	0.51	0.52	-0.59	-0.61	0.59	0.61
1	-1.02	-1.04	1.02	1.04	-1.18	-1.21	1.18	1.21
1.5	-1.53	-1.56	1.53	1.56	-1.78	-1.82	1.78	1.82
2	-2.03	-2.08	2.03	2.08	-2.37	-2.42	2.37	2.42
2.5	-2.54	-2.60	2.54	2.60	-2.96	-3.03	2.96	3.03

Table 4.10 Macro-micro orientation results of the HMMs (deg.).

Hybrid inputs (mm)	Case 1				Case 2			
	One leg		Two legs		One leg		Two legs	
	square type	cylinder type	square type	cylinder type	square type	cylinder type	square type	cylinder type
0.501	-0.61	-0.62	0.61	0.62	-0.52	-0.53	0.52	0.53
1.0025	-1.23	-1.26	1.23	1.26	-1.05	-1.07	1.05	1.07
1.5005	-1.87	-1.91	1.87	1.91	-1.59	-1.63	1.59	1.63
2.0075	-2.50	-2.56	2.50	2.56	-2.13	-2.18	2.13	2.18
2.5010	-3.14	-3.21	3.14	3.22	-2.66	-2.73	2.67	2.73

Focusing on the macro-micro orientation, the required driven force for the PZT actuators and the DC motors are depicted in Figure 4.28 and Figure 4.29, respectively. From these two figures, one can see that, for these two cases, the required forces for the square type HMMs are larger than that of the cylinder type HMMs. Also, one can see that the DC driven forces are relatively small for two cases, especially for case 2. This indicates that the DC driven force is not the main concern in the optimization of the structure design of the HMM. Figure 4.30 and Figure 4.31 show the maximum stresses of the HMMs for the macro motion and macro-micro motion, respectively. As mentioned before, the maximum stress occurs on the surface of the spatial flexural hinge and is larger about a factor of ten than the maximum stress under the micro motion situation.

From Figures 4.30 and 4.31, one can see that the cylinder type HMM has a smaller stress than the square type HMM under the same driving condition. The big difference can be found for case 2, especially. Also, the maximum stress sustained by the spatial flexural hinge is the main constraint in the macro and macro-micro orientation motions for the HMMs.

In summary, comparing the square type HMM with the cylinder type HMM, it is seen that the cylinder type HMM has the characteristics of such as large output performance, low required driving force, and small maximum stress in the flexural hinge. Those features will be considered in the following optimal design of the HMM.

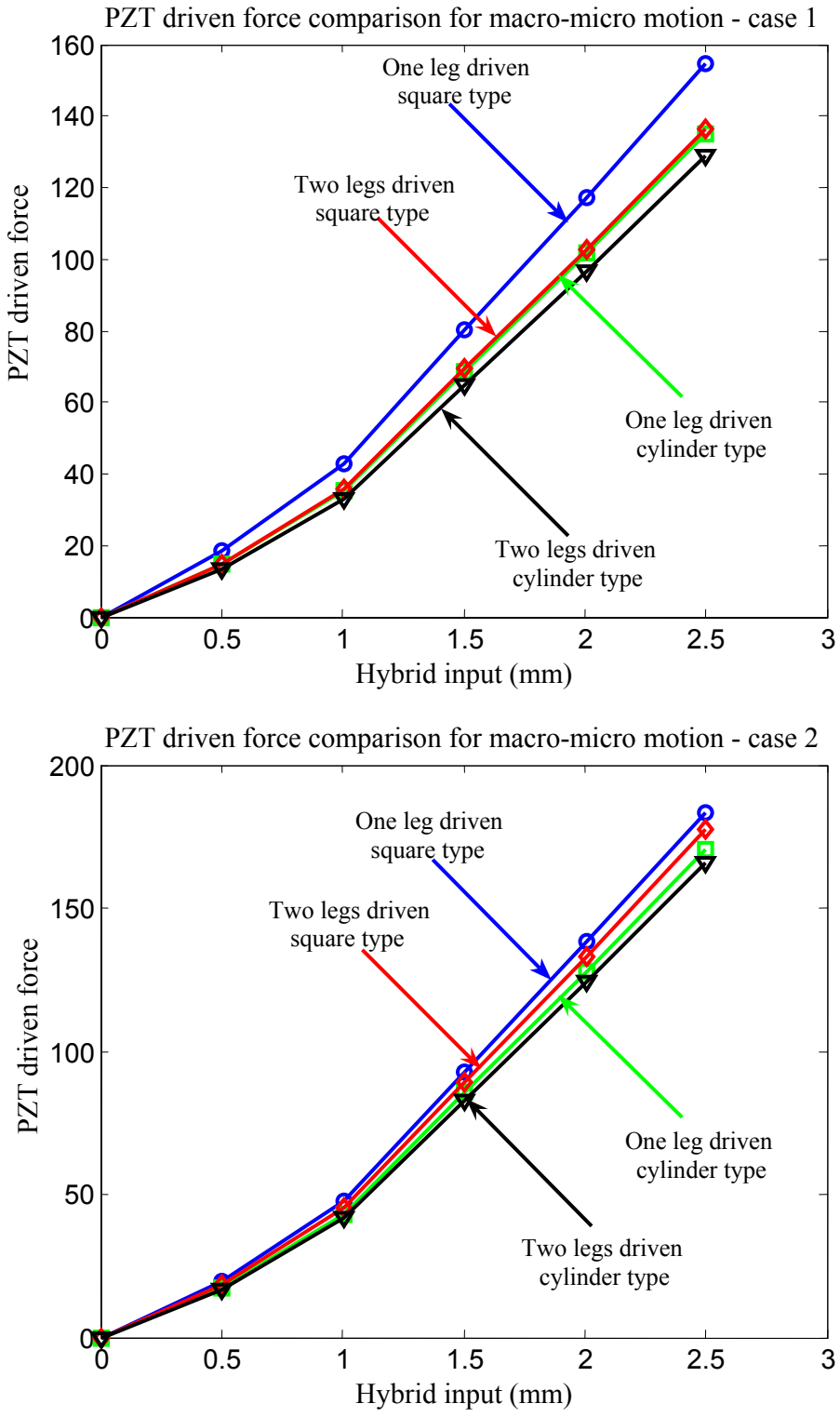

Figure 4.28 PZT driven forces for the macro-micro motion.

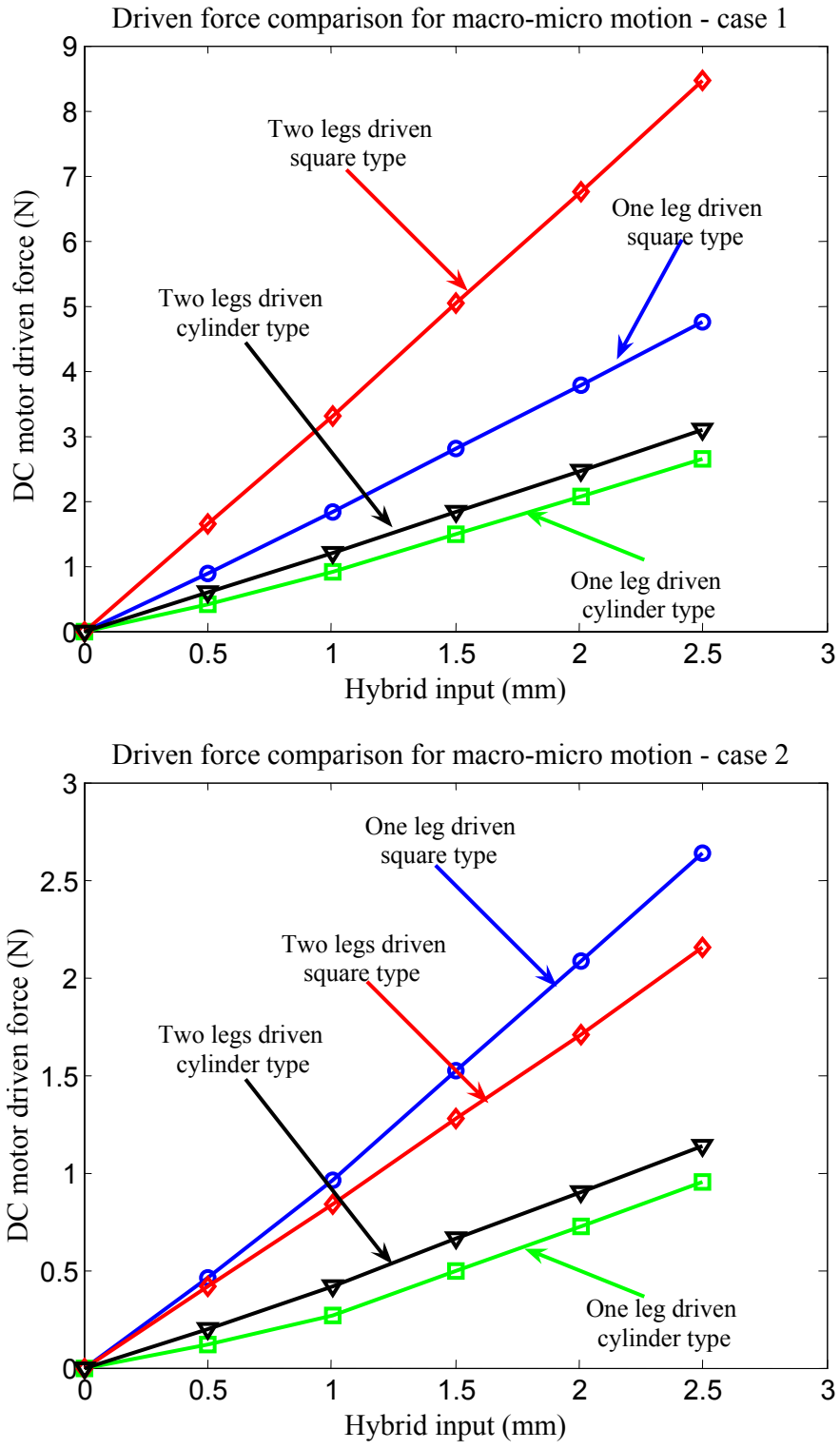

Figure 4.29 DC motor driven forces for the macro-micro motion.

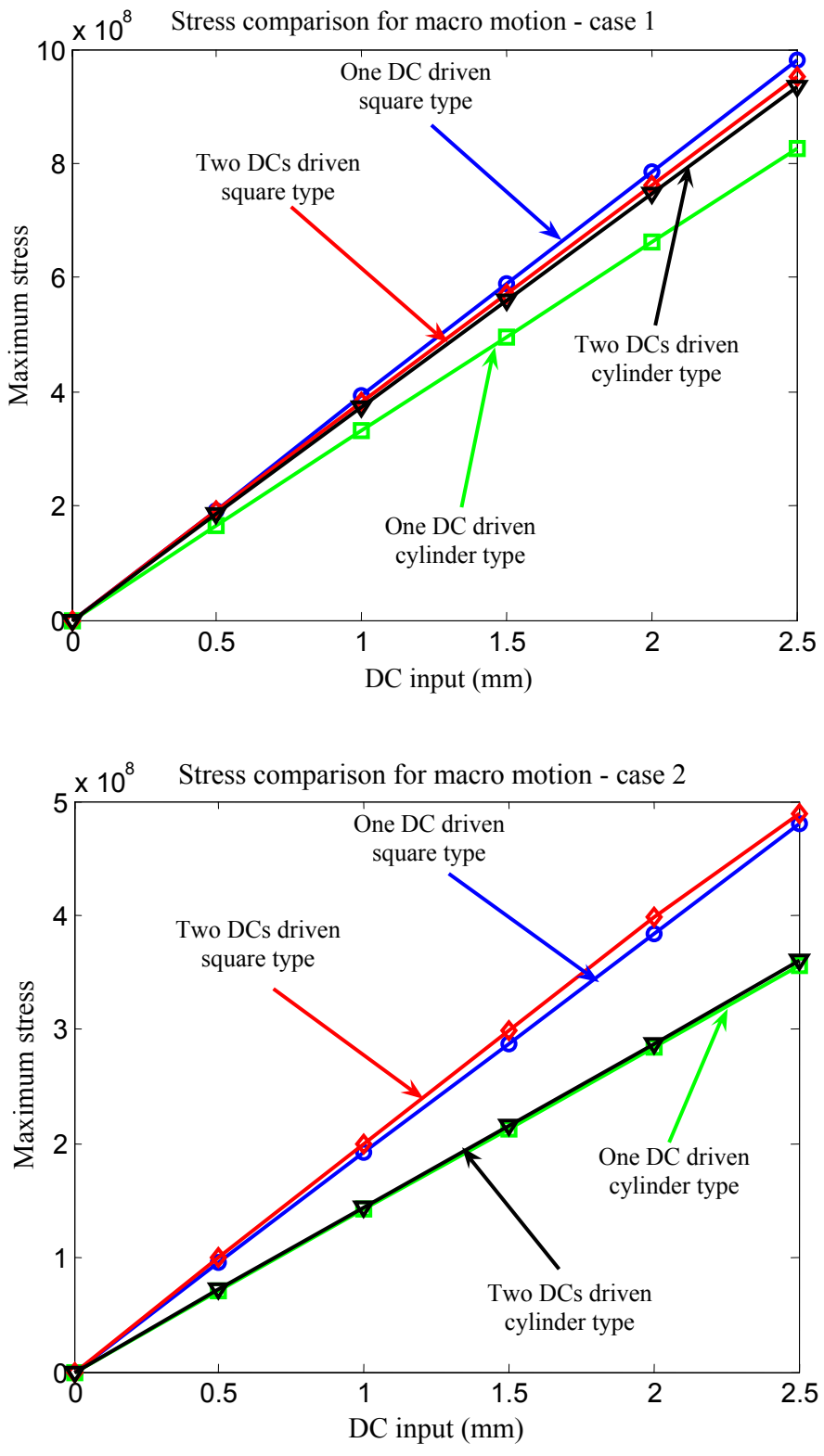

Figure 4.30 Stress comparisons for the macro motion of the HMMs.

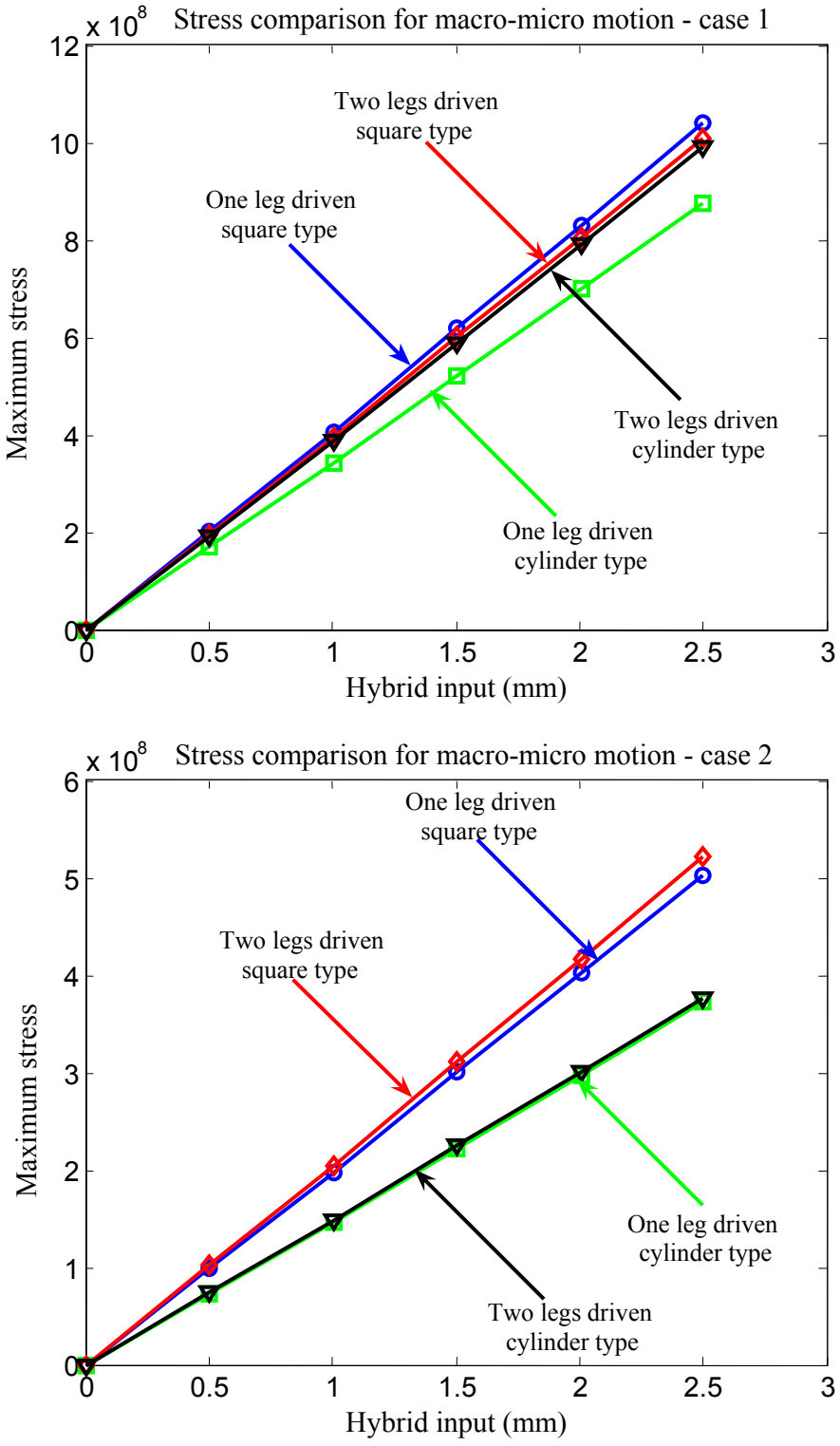

Figure 4.31 Stress comparisons for the macro-micro motion of the HMMs.

4.4.3.3 Dynamic Analysis of the HMM

Modal analysis is used to determine the natural frequencies and mode shapes of a structure. The natural frequencies and mode shapes are important parameters in the design of a structure for the dynamic loading conditions. The dynamic analysis is also performed on the HMMs for two cases. Figure 4.32 and Figure 4.33 show the schematics of the first four mode shapes of the designed HMM. From these two figures, one can see that the first two modes are associated with the spherical flexural hinges, while the last two modes are associated with the flexural hinge of the CMA. This means the stiffness of the CMA is larger than that of the spherical flexural hinge.

Table 4.11 lists the first four modes of the natural frequencies for the two types of HMMs under two different configurations. From this table, it can be seen that the designed HMMs have relatively good dynamic behaviours (The first natural frequency is above 500 Hz) that can satisfy the dynamic requirement of the HMM. Also, one can see that the increase of the section size of the HMM will increase the natural frequency of the system. This is because the size of the spatial flexural hinge dominates the stiffness of the flexural hinge, and further determines the natural frequency.

Table 4.11 Calculated natural frequencies of the HMMs.

Natural frequencies	Case 1		Case 2	
	Square type	Cylinder type	Square type	Cylinder type
f_1 (Hz)	709.81	687.17	568.6	501.7
f_2 (Hz)	730.18	704.37	576.4	520.65
f_3 (Hz)	906.08	903.5	941.5	833.02
f_4 (Hz)	1186.9	1164.2	968.4	928.91

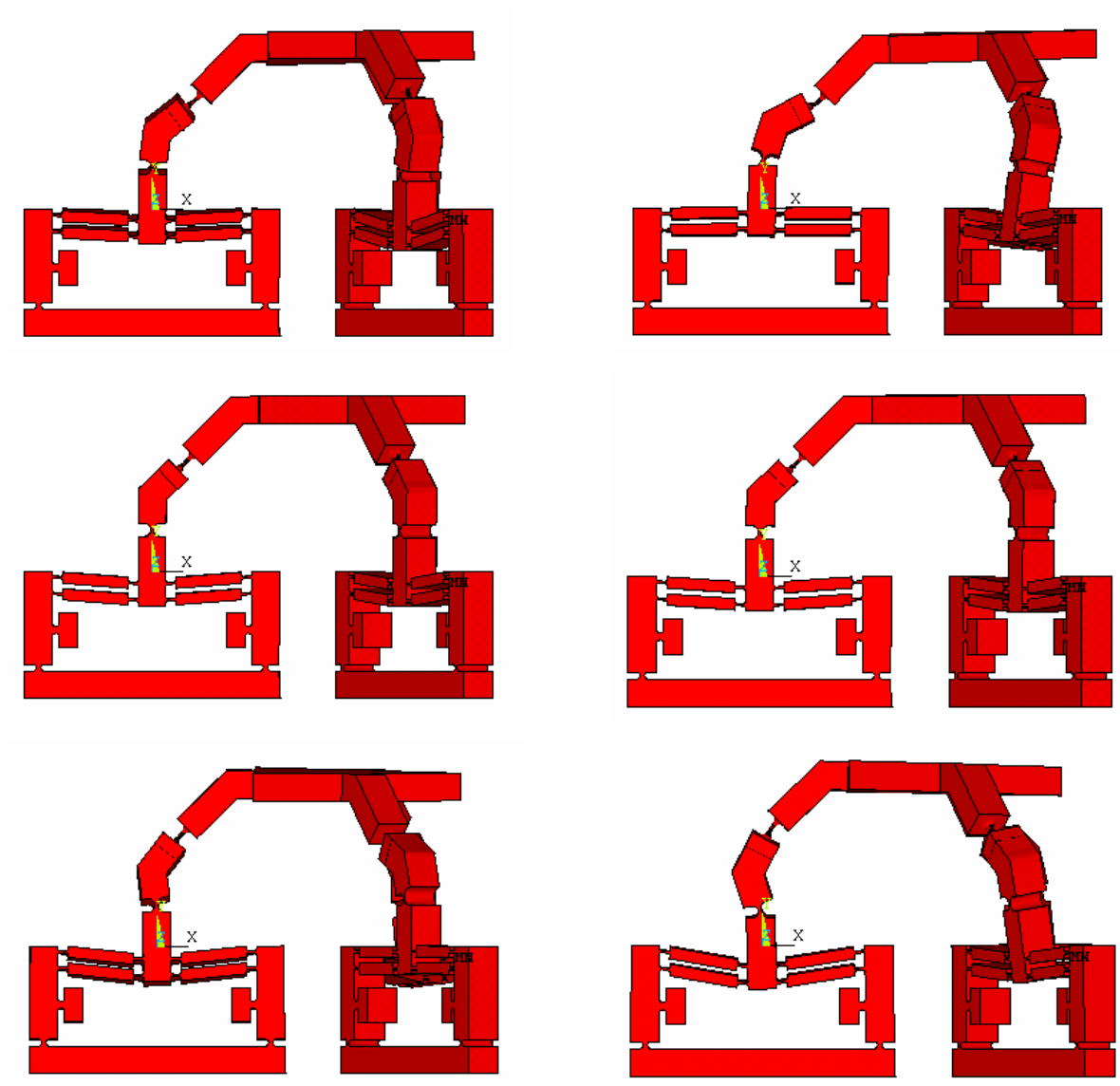

(a) First mode (b) Second mode

Figure 4.32 Schematic of the first and the second mode shapes of the HMM.

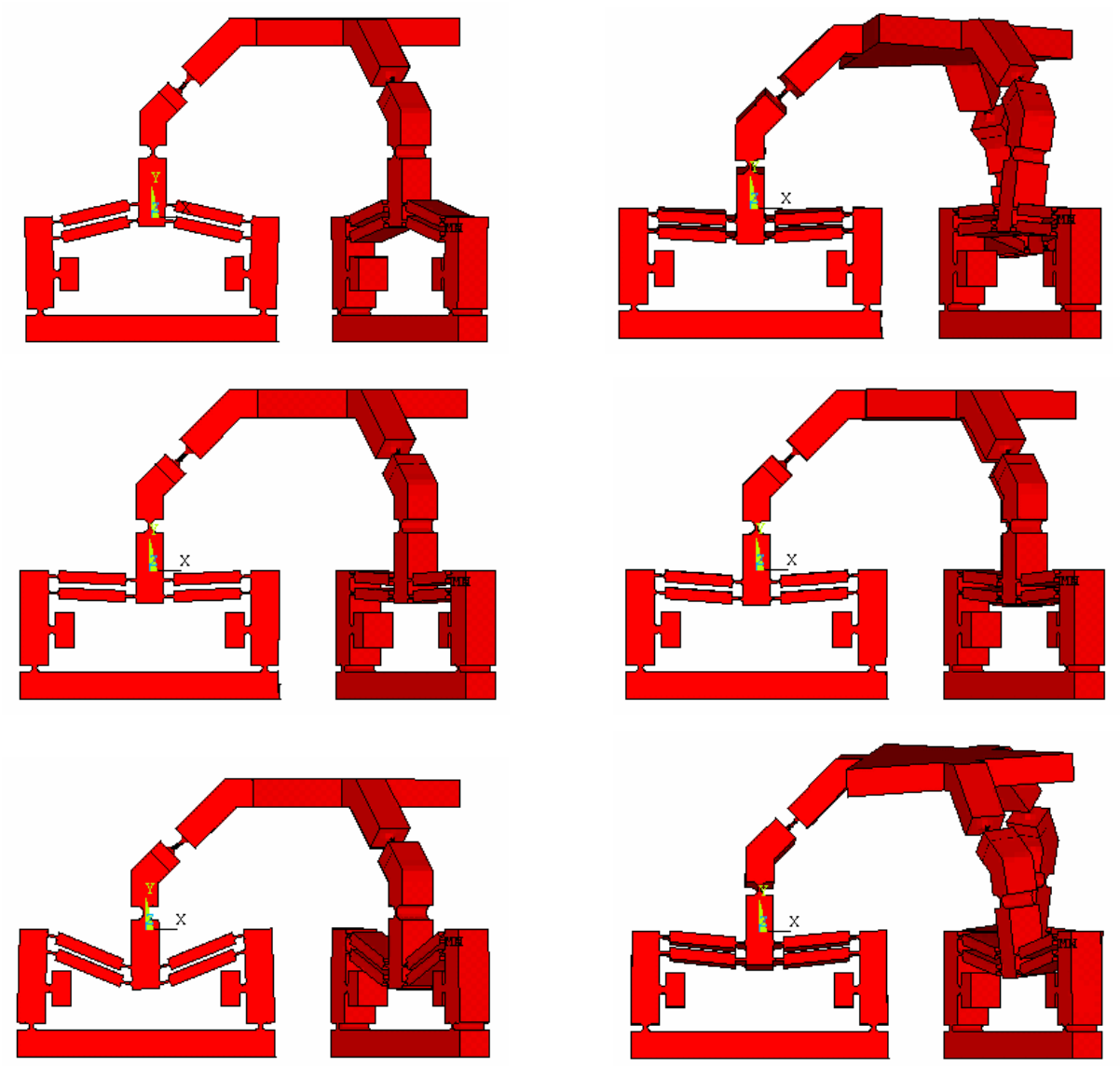

(a) Third mode (b) Fourth mode

Figure 4.33 Schematic of the third and the fourth mode shapes of the HMM.

After the static and dynamic analysis of two types of HMMs under two different design configurations, it can be seen that the cylinder type HMM can not only achieve a large and high accurate movement (orientation and translation) but also has a good dynamic behaviour. In the next section, the design optimization of the HMM will be carried out using the Taguchi method.

4.5 Optimal Design of the Spatial Hybrid Motion Mechanism

In the previous section, two types of spatial flexural hinges were used to build the HMM and some primary conclusions were obtained. The optimization is to obtain the optimal design parameters associated with the HMM in order to achieve the goal of the maximum orientation while taking into account the maximum stress of the HMM occurred at the flexural hinges. The Taguchi method for quality engineering provides the capability of solving the optimal design problem of the HMM.

4.5.1 Introduction of the Taguchi Method

The Taguchi method was first introduced in the 1980s and used for quality control and process improvements. There are several features with this method. *First*, the goal of design is the robustness in system performance; that is the ability of a system in rejecting the disturbance. *Second*, the value domain of a design parameter is simplified into a few levels (usually 2 or 3). *Third*, the variation of design parameters is performed such that different combinations of values or levels of design parameters are arranged according to the orthogonal array concept. *Fourth*, the quantitative definition of the robustness is based on the concept of signal-to-noise ratio. *Finally*, the evaluation of the robustness is based on the run of experiments (i.e., different combinations of the levels of design parameters). Later, this method is successfully applied to various fields. For instance, the method is widely applied to engineering design. Compared with other experimental design methods, such as full factorial designs, fractional factorial designs, the Taguchi method is more efficient due to a smaller number of experiments needed. The Taguchi method consists of a set of experiments using the orthogonal array (OA) where settings of design parameters are changed at different levels.

Lee et al. (2003) proposed a design procedure in a certain iteration to carry out the structure optimization in the discrete design space. In their approach, the orthogonal array method was used to the design of the experiment, and the analysis of means (ANOM) was used to find the optimal levels of the design variables. Chen et al. (1996)

discussed the use of the Taguchi method of experimental design in optimizing process parameters for laser microengraving of photomasks where the L16 OA was used to accommodate the experiments, and the analysis of variance (ANOVA) was used to calculate the statistical confidence associated with the conclusion drawn. Chen and Lin (2000) discussed the determination of the optimal design space for topology optimization. The Taguchi method and the genetic algorithm were used to determine the design space boundary. Chen et al. (2002) studied the optimal dimension problem for an electrothermal microactuator using the Taguchi method. In their study, the ANSYS finite element analysis program was used to calculate the deflection of the actuator, and the Taguchi method was used to analyze the effects of the dimensional variation on the performance of the actuator. Zang et al. (2005) gave a review of the robust optimal design where the Taguchi method was used to improve the performance of the system. Also, a simple dynamic structure was used as an application example to demonstrate the robust optimal design method. Wu et al. (2003) presented a method for the robust design of quartz crystals microbalance using the Taguchi method. The effects of the resonant frequency influenced by the variation of the deposited mass were studied by using the FEA software. Hyder et al. (2004) studied the effect of design variables on the dynamic response of a composite smart structure where the Taguchi method was applied as a robust design technique. Some parameters were identified that had significant contribution to the performance of the system. Bai and Lu (2004) discussed the optimal implementation of miniature piezoelectric panel speakers where the genetic algorithm and the Taguchi method were employed to achieve optimal design with low fundamental frequency and high acoustic output. Tsai et al. (2004) proposed a hybrid Taguchi-genetic algorithm to solve the global numerical optimization problems with continuous variables where the Taguchi method was applied to generate the optimal offspring used in the genetic algorithm.

Some other applications of the Taguchi method can be found in the literature, see Dar et al. (2002), Li and Hong (2005), Mertol (2000), Hwang et al. (2001), Unal et al. (1993), Chen et al. (2000), Sunar et al. (2001), Hwang et al. (203), Chen et al. (2000), Kunjur

and Krishnamurty (1997), Ren et al. (2001), Chang and Du (1998), Taguchi (1993), and Taguchi et al. (2000).

4.5.2 Design of the Experiment Using the Orthogonal Array

4.5.2.1 Signal to noise ratio

In the field of communication engineering, a quantity called the signal to noise ratio (SNR) has been used as the quality characteristic of the choice. Taguchi introduced this concept into the design of experiments. He suggested the SNR, $-10\log_{10}(\text{MSD})$, as a measure of the mean squared deviation (MSD) in the performance. The use of SNR in system analysis provides a quantitative value for response variation comparison. Maximizing the SNR results in the minimization of the response variation and more robust system performance. Three SNRs are often used depending on the types of characteristics: normal-the-best, smaller-the-better, and larger-the-better; see Taguchi (1993), and Taguchi et al. (2000), Wu and Wu (2000), and Taguchi et al (2005). The larger-the-better SNR can be defined as

$$\begin{aligned} SNR &= -10\log_{10}(\text{MSD}) \\ &= -10\log_{10}\left(\frac{1}{\text{n}}\sum_{i=1}^{n}\frac{1}{y_i^2}\right) \end{aligned} \tag{4.22}$$

where n is the number of tests in a trial, and y_i is the value of system performance for the i-th test in the trial. High SNRs are pursued in the Taguchi experiment.

4.5.2.2 Procedure of the Taguchi method

The objective of the optimal design is to determine the major design factors that contribute mostly to the orientation of the HMM and the best level for each design parameter so that the maximal orientation can be obtained. The Taguchi experiments are carried out by the simulation using the FEA software.

The steps of the Taguchi method for the design optimization of the HMM can be briefly stated as follows.

1. Decide the optimal function and the characteristics of the SNR.
2. Identify the design parameters and their levels based on the system physics.
3. Construct the OA table according to the number of design parameters and their levels.
4. Perform the FEA simulation and obtain the objective function for each experiment.
5. Calculate the SNR according to the characteristics.
6. Analyze the mean of the SNR using ANOM.
7. Obtain the optimal design parameters based on the maximum SNR principle.
8. Confirm the optimal design experiment if the optimization is achieved. Otherwise, select new design parameters and their proper levels.

4.5.2.3 Experiment design of the HMM

Previous analysis (Table 4.7) has shown that 11 design parameters appear to be major contributors to the performance of the HMM. In the optimal design process, these 11 parameters or factors called in the Taguchi experiments are set to be three levels and are listed in Table 4.12. For the present study, the L_{27} OA with 11 factors is chosen. Table 4.13 shows the selected parameter levels in each experiment in the OA table. The 27 rows represent 27 experiments (FEA simulations). Please note that in this table, 1, 2, and 3 means three different levels of the specific parameter, respectively, and the values for the three levels of each design parameter can be found in Table 4.12.

Table 4.12 Design parameters and their levels (unit: mm)

Parameter	h	l	t	d	R_b	R_i	L_3	L_4	L_s	F_s	R_s
Level 1	1.0	1.5	0.3	0.8	0.3	0.5	6	10	1.0	0.5	1.0
Level 2	1.1	2.0	0.4	1.0	0.4	0.6	8	12	2.0	0.6	1.25
Level 3	1.2	2.5	0.5	1.2	0.5	0.7	10	14	3.0	0.7	1.50

Table 4.13. L_{27} Orthogonal Array experiments

Trail No.	h	l	t	d	R_b	R_i	L_3	L_4	L_s	F_s	R_s
1	1	1	1	1	1	1	1	1	1	1	1
2	1	1	1	1	2	2	2	2	2	2	2
3	1	1	1	1	3	3	3	3	3	3	3
4	1	2	2	2	1	1	2	2	2	3	3
5	1	2	2	2	2	2	3	3	3	1	1
6	1	2	2	2	3	3	1	1	1	2	2
7	1	3	3	3	1	1	3	3	3	2	2
8	1	3	3	3	2	2	1	1	1	3	3
9	1	3	3	3	3	3	2	2	2	1	1
10	2	1	2	3	1	2	1	2	3	2	3
11	2	1	2	3	2	3	2	3	1	3	1
12	2	1	2	3	3	1	3	1	2	1	2
13	2	2	3	1	1	2	2	3	1	1	2
14	2	2	3	1	2	3	3	1	2	2	3
15	2	2	3	1	3	1	1	2	3	3	1
16	2	3	1	2	1	2	3	1	2	3	1
17	2	3	1	2	2	3	1	2	3	1	2
18	2	3	1	2	3	1	2	3	1	2	3
19	3	1	3	2	1	3	1	3	2	3	2
20	3	1	3	2	2	1	2	1	3	1	3
21	3	1	3	2	3	2	3	2	1	2	1
22	3	2	1	3	1	3	2	1	3	2	1
23	3	2	1	3	2	1	3	2	1	3	2
24	3	2	1	3	3	2	1	3	2	1	3
25	3	3	2	1	1	3	3	2	1	1	3
26	3	3	2	1	2	1	1	3	2	2	1
27	3	3	2	1	3	2	2	1	3	3	2

The FEA simulation is performed by each combination of the design parameters according to Table 4.13. In the optimal design of the HMM, the objective function can be chosen as the maximum orientation under the micro motion condition and macro motion condition, and a combination of the maximum orientation and the minimum stress under the macro-micro motion condition. In each experiment study, the PZT displacement is set 5 μm for the micro motion, and the DC motor is assumed to provide 1 mm movement for the macro motion. The macro-micro motion is the combination of the PZT displacement and the movement of the DC motor. After the finite element analysis, the characteristics of each combination of the design parameters are transformed into SNR according to Eq. (4.22). The following section will show the analysis results.

4.5.3 Data Analysis for Determining Optimal Setting

According to the combination of the design parameters in the selected OA Table 4.13, 27 different finite element models of the cylinder type HMM are built and the static and dynamic analysis by ANSYS are performed to obtain the orientation movement, the PZT forces, the maximum stress and the natural frequencies for each experiment. Table 4.14 lists the orientation angle and the PZT driving force for the micro motion. Table 4.15 and 4.16 show the prediction results for the macro motion and hybrid motion, respectively. In the optimal process, three objective functions are defined. They are (1) the maximum micro orientation driven by the PZTs, (2) the maximum macro motion with the minimum stress driven by the DC motors, and (3) the maximum macro-micro orientation with the minimum stress under the hybrid motion.

Table 4.14 Micro orientation of the cylinder type HMM.

Trial No.	Driven by one PZT		Driven by two PZTs	
	Angle β (°)	PZT force (N)	Angle β (°)	PZT force (N)
1	-9.10E-02	62.13	9.14E-02	61.77
2	-8.52E-02	65.46	8.51E-02	65.51
3	-7.73E-02	68.23	7.72E-02	71.95
4	-6.76E-02	78.52	6.71E-02	75.71
5	-6.27E-02	83.82	6.44E-02	82.09
6	-7.50E-02	86.02	7.22E-02	87.97
7	-5.08E-02	89.87	4.99E-02	89.99
8	-5.95E-02	94.95	5.89E-02	95.00
9	-5.67E-02	100.04	5.83E-02	98.86
10	-6.00E-02	81.03	6.17E-02	83.02
11	-5.86E-02	86.59	5.82E-02	88.23
12	-6.55E-02	86.75	6.65E-02	84.87
13	-4.79E-02	96.16	4.72E-02	97.64
14	-5.21E-02	101.94	5.32E-02	99.51
15	-5.01E-02	98.21	4.99E-02	98.93
16	-9.00E-02	50.40	9.15E-02	51.05
17	-8.83E-02	52.15	8.94E-02	51.90
18	-8.30E-02	51.93	8.53E-02	50.49
19	-4.42E-02	96.94	4.49E-02	95.47
20	-5.09E-02	95.72	5.00E-02	94.22
21	-4.95E-02	97.87	4.92E-02	98.88
22	-8.50E-02	51.64	8.57E-02	50.21
23	-8.28E-02	46.73	7.94E-02	49.83
24	-7.70E-02	52.59	7.66E-02	54.57
25	-7.06E-02	65.15	7.26E-02	61.50
26	-6.70E-02	63.99	6.75E-02	63.62
27	-7.21E-02	69.09	7.42E-02	65.69

Table 4.15 Macro orientation of the cylinder type HMM.

Trial No.	Driven by one DC motor		Driven by two DC motors	
	Angle β (°)	Stress (Pa)	Angle β (°)	Stress (Pa)
1	-1.21	3.31E+08	1.21	3.74E+08
2	-1.10	2.32E+08	1.10	2.49E+08
3	-1.01	1.74E+08	1.01	1.81E+08
4	-1.08	2.39E+08	1.08	2.70E+08
5	-1.04	1.42E+08	-1.04	1.42E+08
6	-1.19	3.52E+08	1.19	3.87E+08
7	-1.03	1.72E+08	1.03	1.66E+08
8	-1.17	3.88E+08	1.17	3.56E+08
9	-1.12	2.11E+08	1.12	2.09E+08
10	-1.09	1.69E+08	1.09	1.63E+08
11	-1.05	3.81E+08	1.05	4.18E+08
12	-1.19	2.21E+08	1.19	2.12E+08
13	-1.06	3.17E+08	1.06	3.22E+08
14	-1.17	2.34E+08	1.17	2.57E+08
15	-1.10	1.97E+08	1.10	1.99E+08
16	-1.15	2.91E+08	1.15	2.98E+08
17	-1.10	1.46E+08	1.10	1.58E+08
18	-1.04	2.83E+08	1.04	3.10E+08
19	-1.04	2.55E+08	1.04	2.75E+08
20	-1.16	1.49E+08	1.16	1.69E+08
21	-1.12	3.77E+08	1.12	3.76E+08
22	-1.17	1.87E+08	1.17	1.96E+08
23	-1.08	3.60E+08	1.08	3.75E+08
24	-1.04	1.93E+08	1.04	1.87E+08
25	-1.11	3.25E+08	1.11	3.12E+08
26	-1.05	2.30E+08	1.05	2.40E+08
27	-1.15	2.09E+08	1.15	2.26E+08

Table 4.16 Macro-micro motion of the cylinder type HMM.

Trial No.	Driven by one leg			Driven by two legs		
	Angle β (°)	PZT force (N)	Stress (Pa)	Angle β (°)	PZT force (N)	Stress (Pa)
1	-1.30	66.34	3.55E+08	1.30	63.86	4.02E+08
2	-1.19	69.75	2.50E+08	1.19	67.70	2.69E+08
3	-1.09	73.02	1.87E+08	1.09	73.96	1.95E+08
4	-1.15	84.36	2.54E+08	1.15	78.77	2.86E+08
5	-1.10	84.88	1.51E+08	1.11	82.68	1.53E+08
6	-1.27	92.43	3.70E+08	1.26	91.09	4.10E+08
7	-1.08	91.60	1.80E+08	1.08	90.86	1.74E+08
8	-1.23	103.04	4.08E+08	1.23	99.00	3.74E+08
9	-1.18	101.62	2.22E+08	1.18	99.60	2.20E+08
10	-1.15	83.15	1.78E+08	1.15	84.14	1.72E+08
11	-1.11	94.48	4.03E+08	1.11	92.30	4.41E+08
12	-1.25	88.60	2.33E+08	1.25	85.78	2.23E+08
13	-1.11	98.13	3.31E+08	1.11	98.67	3.37E+08
14	-1.22	104.86	2.45E+08	1.22	100.96	2.69E+08
15	-1.15	101.80	2.06E+08	1.15	100.71	2.08E+08
16	-1.24	58.73	3.14E+08	1.24	55.01	3.22E+08
17	-1.19	53.55	1.57E+08	1.19	52.62	1.71E+08
18	-1.12	57.20	3.06E+08	1.12	53.07	3.36E+08
19	-1.08	101.45	2.66E+08	1.08	97.70	2.87E+08
20	-1.21	96.74	1.55E+08	1.21	94.72	1.76E+08
21	-1.17	102.57	3.93E+08	1.17	101.23	3.92E+08
22	-1.25	54.84	2.01E+08	1.25	51.96	2.11E+08
23	-1.16	57.45	3.87E+08	1.16	54.72	4.02E+08
24	-1.12	54.34	2.07E+08	1.12	55.45	2.00E+08
25	-1.18	67.80	3.46E+08	1.19	62.90	3.32E+08
26	-1.12	66.99	2.45E+08	1.12	65.31	2.55E+08
27	-1.22	73.90	2.22E+08	1.22	68.29	2.41E+08

For the optimal design of the micro orientation, the predicted data of the orientation angles β in Table 4.14 are used to find the optimal design parameters using ANOM based on the SNR information. Figure 4.34 shows the effect of each design parameter on the SNR. From this figure, it can be seen that, for the micro motion, parameter t (the thickness of the flexural hinge on the CMA) is the most important design parameter contributing to the micro orientation. The smaller the parameter the bigger the orientation angle. Also, the parameters h, l, and L_4 are important design parameters. On the other hand, the parameters R_b, R_i (that are associated with the input flexural hinge of the CMA), L_3, Fs and Rs (that are associated with the spatial flexural hinge) have little effect on the micro orientation.

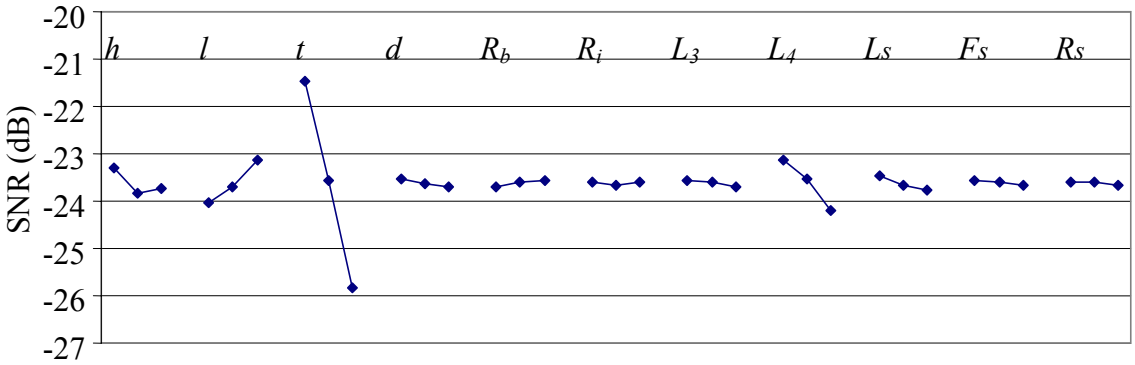

Figure 4.34 Effect of design parameters on the micro orientation of the HMM.

For the macro motion and the hybrid motion optimization, the system performance y is defined as

$$y = \frac{\beta}{\sigma} \tag{4.23}$$

where β (deg.) is the orientation angle of the platform, and σ (MP) is the first maximum stress of the HMM for the macro motion or the hybrid motion, respectively. The definition of this performance reflects the ideal goal, that is the HMM with a large orientation angle yet a small stress. Note that the SNR in this case can be found from Eq. (4.22).

Figures 4.35 and 4.36 show the effects of the design parameters on the SNRs for the macro motion and hybrid motion, respectively. It can be seen that the patterns shown in these two figures are very similar. This is because of the dominance of the macro motion over the micro motion in the hybrid motion. From these two figures, one can see that the most significant design parameter on the system performance is the parameter *L*s (the length of the spatial flexural hinge). The longer the spatial flexural hinge the better the system performance. Other two design parameters, *F*s and *R*s (that are associated with the spatial flexural hinge), are important to the system performance, as well.

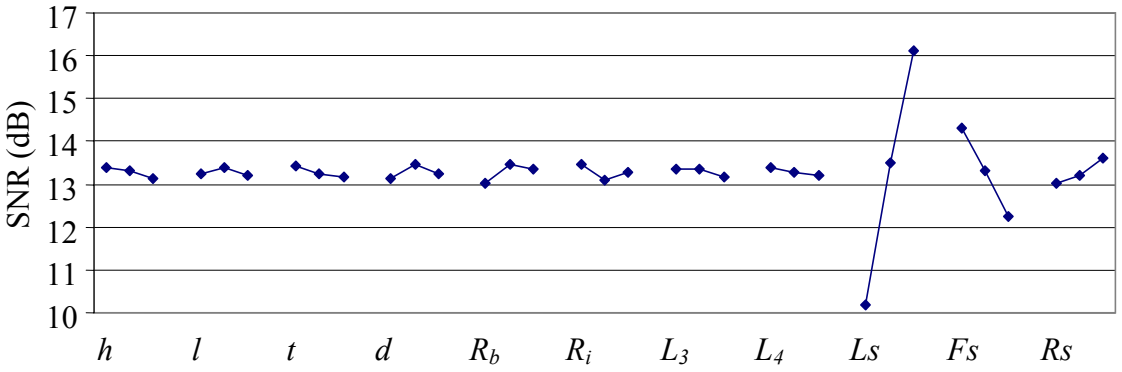

Figure 4.35 Effect of design parameters on the macro orientation of the HMM.

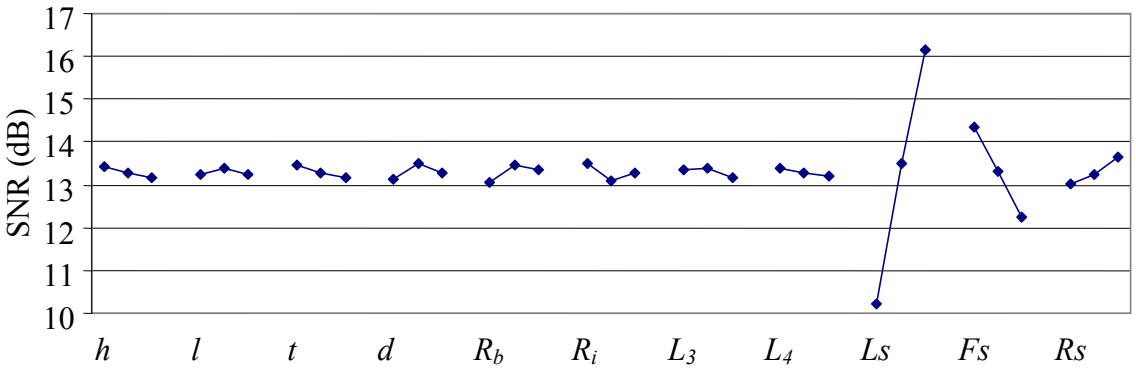

Figure 4.36 Effect of design parameters on the angle/stress for the hybrid motion.

From Figures 4.34 to 4.36, the optimal levels of the design parameters for each optimal function can be found according to the largest SNR principle, and they are listed in Table 4.17.

Table 4.17 Optimum design parameter levels identified by the L_{27} study.

Parameter		h	l	t	d	R_b	R_i	L_3	L_4	L_s	F_s	R_s
Optimum level	**Micro**	1	3	1	1	3	1	1	1	1	1	1
	Macro	1	2	1	2	2	1	2	1	3	1	3
	Hybrid	1	2	1	2	2	1	2	1	3	1	3

4.5.4 Confirmation Experiments

Running the confirmation experiment is necessary to compare the optimal result with the experimental results in order to demonstrate the effectiveness of the optimization. Figures 4.37 to 4.39 show the optimal results and the experimental results for all three objective functions, respectively. From these figures, it can be seen that the optimal values are higher than that of every experimental result.

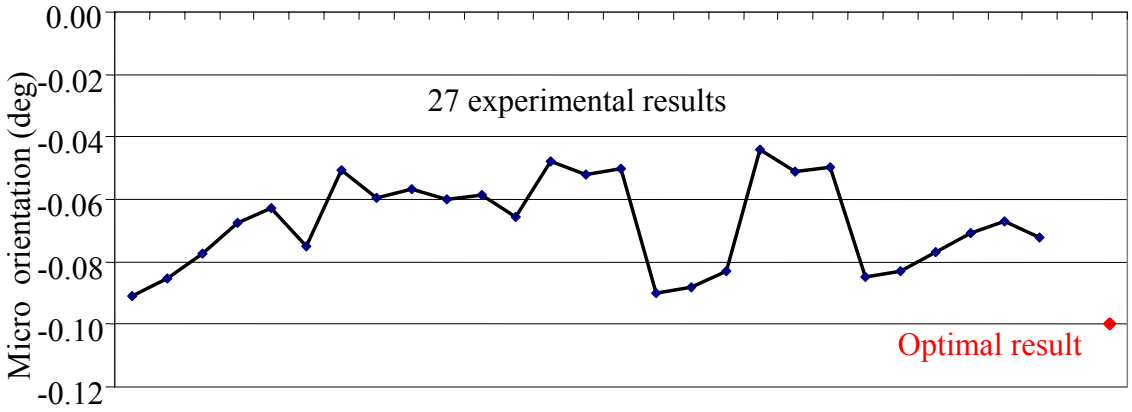

Figure 4.37 Experimental and optimal results for the micro motion.

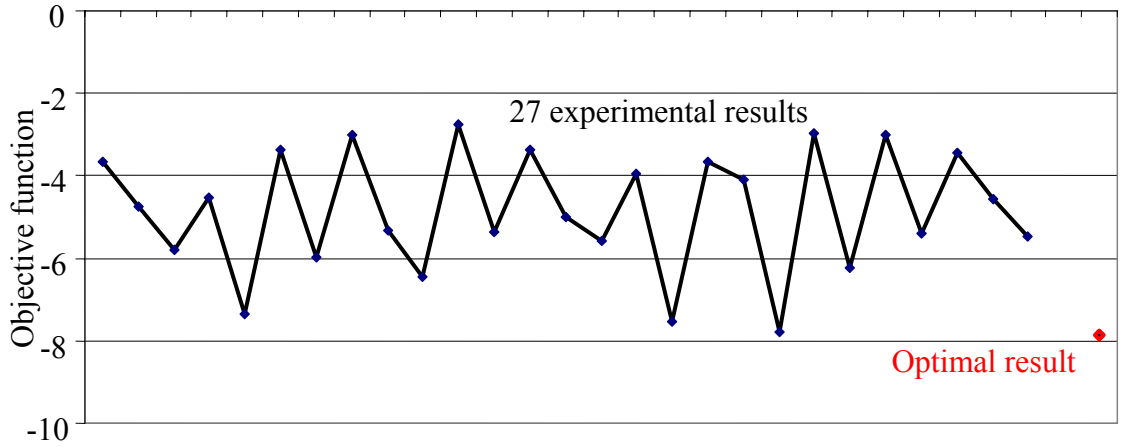

Figure 4.38 Experimental and optimal results for the macro motion.

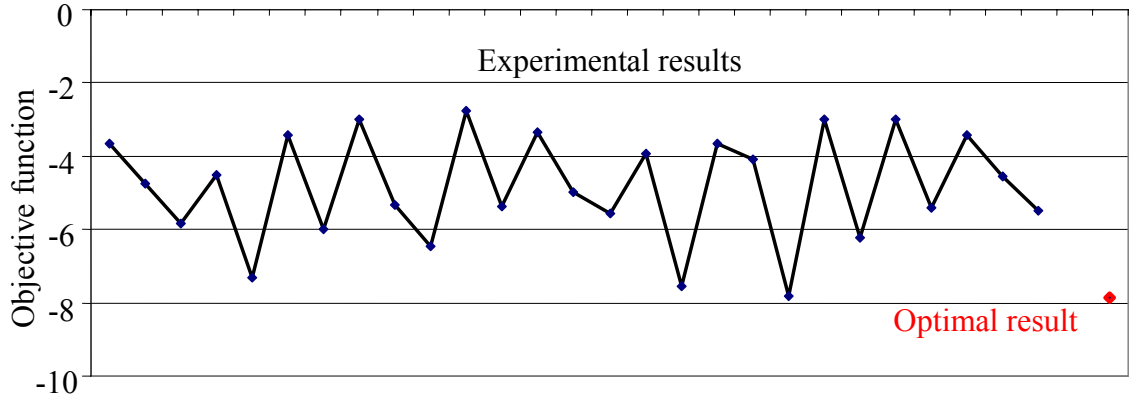

Figure 4.39 Experimental and optimal results for the hybrid motion.

4.6 Concluding remarks

In this chapter, the design, modeling and optimization of a HMM with 3 DOFs were performed. For the micro motion of the HMM, a new topology of the mechanical amplifier was proposed that has the potential of high amplifier ratio and high natural frequencies. Based on the proposed topology, a new type of CMA was developed and it was used in the HMM as the micro motion part. Then, the HMM was discussed in detail in the aspects of design principle, kinematics design and analysis, the prediction of the

orientation movement based on two types of spatial flexural hinges. It was shown that the cylinder type HMM is promising in terms of a large orientation of the HMM and small stress on the flexural hinge. After that, the optimization of the HMM was performed for three objective functions using the Taguchi method. Some important design parameters have been identified, and the optimal levels for the design parameters have been obtained as well. It is concluded that, for the optimal design, the design parameters associated with the beam flexural hinge have great impact to the orientation in the micro motion while the design parameters related to the spherical flexural hinge have significant effect on the orientation and the maximum stress of the HMM for the macro motion and the hybrid motion as well. Verification tests are fulfilled to confirm the effectiveness of the optimal design parameters.

In conclusion, the five bar topology concept for developing the mechanical amplifier appears to be an excellent idea. The design concept for a parallel architecture for the macro-micro system can certainly achieve a better performance with the HMM. The Taguchi method is suitable to the optimization of the design for the HMM.

5. HYBRID CONTROL SYSTEMS

5.1 Introduction

Following the definition of the hybrid system presented in Chapter 1, a hybrid control system is a control system where two or more control laws (the elements in the hybrid system) are included that contribute to the tracking performance (the behaviour in the hybrid system) of the controlled system. Obviously, a control system with discrete event modes and with continuous equations govern the behaviour of the system is a hybrid control system that was studied extensively in the literature. Also, the control system developed in Chapter 3 is a hybrid control system as it includes three different control methods. It should be noted that, in the above two hybrid control systems, the control laws are applied in the time domain.

In this chapter, the hybrid control systems will be extended to the iteration domain using the iteration learning strategy. This is the unique feature of the hybrid control systems discussed in this chapter. Specifically, three different PD type learning control laws, which integrate different control laws for the purpose of improving the control performance, are developed to deal with the tracking problem of different controlled systems.

The reminder of this chapter is organized as follows. Section 5.2 discusses the PD type online learning control (PD-OLC) system for a nonlinear time-varying system with uncertainty and disturbance. The PD-OLC can be viewed as a hybrid control system that combines the feedback and feedforward control in the iteration domain. The convergence analysis of the PD-OLC is presented based on the λ-norm of the bound of the output tracking error. Section 5.3 presents an adaptive NPD learning control for the trajectory tracking of robotic manipulators. The adaptive NPD learning control can also

be viewed as a hybrid control in which the nonlinear control gains are constructed in the error domain and the feedback and feedforward control in the iteration domain. Section 5.4 describes the adaptive switching learning PD control (ASL-PD). The ASL-PD control is a hybrid control that combines three control methods together. The three control methods are: (1) feedback control, (2) feedforward control, and (3) switching control. The switching control rule is used not in the time domain but in the iteration domain. Section 5.5 gives a conclusion.

5.2 PD type Online Learning Control with Uncertainty and Disturbance

Motivated by the wide application of the PD control in the industrial automatic control system, a PD –type online learning control called PD-OLC is proposed for the tracking problem of a class of nonlinear time-varying systems with uncertainties and disturbances. The PD-OLC method can be summarized as follows: (1) the control model consists of two parts: a PD feedback part and a feedforward part using the input profile obtained from the previous iteration; (2) the control is a kind of evolutionary one through several generations of changes – a feature borrowed from ILC. The robustness of the PD-OLC algorithm is analyzed. The boundedness of the final tracking error is verified through the convergence analysis.

5.2.1 PD-type Online Learning Control Design

Consider a repetitive nonlinear time-varying system with uncertainties and disturbances as follows:

$$\begin{aligned} \dot{x}_k(t) &= f(x_k(t),t) + B(t)u_k(t) + \eta_k(t) \\ y_k(t) &= C(t)x_k(t) + \xi_k(t) \end{aligned} \tag{5.1}$$

where k denotes the iterative index. $x \in \Re^n$, $u \in \Re^r$, and $y \in \Re^m$ are the state, control input and output of the system, respectively. The function $\eta_k(t) \in \Re^n$ represents both the deterministic and random disturbances of the system, and function $\xi_k(t) \in \Re^m$ is the measurement noise of the system. From the above assumption, one can see that $f(x(t),t) \in \Re^n$, $B(t) \in \Re^{n \times r}$ and $C(t) \in \Re^{m \times n}$.

For the convergence analysis of the PD-OLC, the following norms are introduced:

$$\|f\| = \max_{1 \le i \le n} |f_i|$$

$$\|h(t)\|_\lambda = \sup_{t \in [0,T]} e^{-\lambda t} \|h(t)\|, \quad \lambda > 0$$

$$\|M(t)\| = \max_{1 \le i \le m} \left(\sum_{j=1}^{n} |m_{i,j}| \right)$$

where $f = [f_1, \ ..., \ f_n]^T$ is a vector, $M = [m_{i,j}] \in \Re^{m \times n}$ is a matrix, and $h(t)$ $(t \in [0,T])$ is a real number function.

To facilitate the discussion, the following assumptions are also made.

A1) The desired trajectory $y_d(t)$ is derivative for $t \in [0,T]$.

A2) The function $f(x(t),t)$ is globally uniformly Lipschitz in x for $t \in [0,T]$. That means $\|f(x_{k+1}(t),t) - f(x_k(t),t)\| \le c_f \|x_{k+1}(t) - x_k(t)\|$ where k is the iteration number and $c_f > 0$ is the Lipschitz constant.

A3) The uncertainty and disturbance terms $\eta_k(t)$ and $\xi_k(t)$ are bounded as follows, $\forall\, t \in [0,T]$ and $\forall\, k$: $\|\eta_{k+1}(t) - \eta_k(t)\| \le b_\eta$, $\|\xi_{k+1}(t) - \xi_k(t)\| \le b_\xi$.

A4) The control input matrix $B(t)$ is of the first-order continuity for $t \in [0,T]$.

Remark 1: Assumption A1 is for the purpose that the high order of the plant output y(t) can be used for feedback signal. A2 is a basic requirement for the system (5.1). In fact, the function $f(x,t)$ may be structurally unknown or uncertain. A3 restricts the disturbance and noise to be bounded, but they may be discontinuous. A4 is a reasonable assumption for the purpose of the continuity of the controlled system.

For clarification of the remaining discussion, the following notations are introduced.

$$B_d = \max_{t\in[0,T]} \|B(t)K_d\|,\ B_{pd} = \max_{t\in[0,T]} \left\| B(t)K_p - \frac{dB(t)}{dt}K_d \right\|,\ \alpha = 1 - {c_f}/{\lambda}$$

$$K_{x\lambda} = \frac{1}{\alpha}\left(B_d + {B_{pd}}/{\lambda} \right),\ \rho_0 = \max_{t\in[0,T]} \left\| \left(I_m + C(t)B(t)K_d \right)^{-1} \right\| < 1$$

$$\rho = \frac{\rho_0}{1 - \frac{\rho_0}{\lambda}\left(c_f K_{x\lambda} + B_{pd} \right) \max_{t\in[0,T]} \|C(t)\|},\ \beta_0 = \max_{t\in[0,T]} \|C(t)\| \rho$$

$$\beta_1 = \beta_0 \left(\frac{c_f}{\alpha\lambda} + 1 \right) \left(2 + \|B(0)K_d\| \|C(0)\| \right)$$

The following PD-type OLC law is proposed for the control of the system described in Eq. (5.1).

$$u_k(t) = u_{k-1}(t) + K_p e_k(t) + K_d \dot{e}_k(t) \tag{5.2}$$

where $e_k(t) = y_d(t) - y_k(t)$ and $\dot{e}_k(t) = \dot{y}_d(t) - \dot{y}_k(t)$ are the position error and the velocity error of the output vector, respectively. $K_p \in \Re^{m\times r}$ and $K_d \in \Re^{m\times r}$ are the constant proportional and derivative gain matrices, respectively.

From Eq. (5.2), one can see that the control law is a simple combination of a feedback control using the traditional PD control and a feedforward control using the input profile of the previous iteration. As the new control law has the feedback control component, one can call the control based on Eq. (5.2) the on-line learning control.

For the first iteration, one just simply sets $u_0(t) = 0$, so only the traditional PD feedback control is presented in the first iteration. For subsequent iterations, the controlled input profile of the previous iteration is recorded and used for the current iteration as feedforward. Therefore, the learning process can also be called the direct learning.

For all *k*, the repeatability of the initial setting is satisfied within an admissible deviation level, i.e.,

$$\|x_k(0) - x_0(0)\| \le \varepsilon_x \qquad \text{for} \quad k = 1, 2, ... \tag{5.3}$$

where ε_x is a small positive constant that represents the acceptable accuracy of the designed state vector, and $x_0(0)$ represents the desired initial state value and $y_d(0) = C(0)x_0(0)$.

Remark 2: Constraint (5.3) represents the uncertainty of the initial state. It should be noted that constraint (5.3) is more relaxing and robust than the requirement of the zero initialization error in most ILC control methods, as the zero initialization error is only a special case of the study presented in this thesis.

From Eq. (5.1), if the uncertainty and disturbance were ignorable, then the following holds:

$$\|y_d(0) - y_k(0)\| \le \|C(0)\| \varepsilon_x \qquad \text{for} \quad k = 1, 2, ... \tag{5.4}$$

Remark 3: The initial output error is the consequence of the initial state error; see Eq. (5.3). If the initial state error is zero, then the initial output error will become zero too.

After the above preparation, the following theorem is presented.

Theorem 5.1: To the nonlinear time-varying system Eq. (5.1) with uncertainty and disturbance, for a given desired output trajectory $y_d(t)$, if the PD-type online learning control law Eq. (5.2) is used and the initial state in each iteration is bounded as in Eq. (5.3), then the finial output tracking error is bounded provided that the control gain K_d is selected in such a way so that $I_m + C(t)B(t)K_d$ is non-singular and

$$\rho_0 = \max_{t\in[0,T]} \left\| \left(I_m + C(t)B(t)K_d \right)^{-1} \right\| < 1 \tag{5.5}$$

For a sufficiently large λ, the bound of the tracking error is given by

$$\lim_{k\to\infty} \left\| e_k(t) \right\|_\lambda \le \frac{\varepsilon}{1-\rho} \quad \text{for } t \in [0,T] \tag{5.6}$$

where
$$\rho = \frac{\rho_0}{1 - \frac{\rho_0}{\lambda}\left(c_f K_{x\lambda} + B_{pd} \right) B_C} \tag{5.7}$$

$$\varepsilon = \beta_0 \left(\frac{c_f}{\lambda} b_\eta T + b_\xi \right) + \beta_1 \varepsilon_x \tag{5.8}$$

with $\beta_0 = B_C \rho$, $\beta_1 = \beta_0 \left(\frac{c_f}{\alpha\lambda} + 1 \right) \left(2 + \left\| B(0)K_d \right\| \left\| C(0) \right\| \right)$.

From Eq. (5.5), one can see that with the increase of the control gain K_d, the value of ρ_0 will decrease, and the value of ρ will decrease as well according to Eq. (5.7). Furthermore, the tracking error will decrease according to Eq. (5.6). This feature will be demonstrated in the simulation study to be presented in Chapter 6. In the next section, the convergence of the proposed PD-OLC will be proved.

5.2.2 Convergence Analysis of the PD Online Learning Control

First, a relation between norm and λ–norm is represented by Lemma 5.1.

Lemma 5.1: Suppose that $x(t)=[x_1(t),x_2(t),\cdots,x_n(t)]^T$ is defined in $t\in[0,T]$. Then

$$\left(\int_0^t \|x(\tau)\|d\tau\right)e^{-\lambda t} \le \frac{1}{\lambda}\|x(t)\|_\lambda$$

Proof:

$$\left(\int_0^t \|x(\tau)\|d\tau\right)e^{-\lambda t} = \int_0^t \|x(\tau)\|e^{-\lambda\tau}e^{-\lambda(t-\tau)}d\tau$$

$$\le \sup_{t\in[0,T]}\left\{\|x(t)\|e^{-\lambda t}\right\}\int_0^t e^{-\lambda(t-\tau)}d\tau$$

$$\le \sup_{t\in[0,T]}\left\{\|x(t)\|e^{-\lambda t}\right\}\frac{1-e^{-\lambda t}}{\lambda}$$

$$\le \frac{1}{\lambda}\|x(t)\|_\lambda$$

[End of proof].

Proof of the Theorem 5.1.

For the k^{th} iteration, from Eq. (5.1) one obtains

$$x_k(t) = x_k(0) + \int_0^t \left(f\left(x_k(\tau),\tau\right) + B(\tau)u_k(\tau)\right)d\tau + \int_0^t \eta_k(t)d\tau \tag{5.9}$$

For the $k+1^{th}$ iteration, from Eq. (5.1) one obtains

$$x_{k+1}(t) = x_{k+1}(0) + \int_0^t \left(f\left(x_{k+1}(\tau), \tau\right) + B(\tau) u_{k+1}(\tau) \right) d\tau + \int_0^t \eta_{k+1}(t) d\tau \tag{5.10}$$

Submitting Eq. (5.2) into Eq. (5.10) yields

$$\begin{aligned} x_{k+1}(t) = x_{k+1}(0) &+ \int_0^t f\left(x_{k+1}(\tau), \tau\right) d\tau + \int_0^t B(\tau) u_k(\tau) d\tau + \int_0^t \eta_{k+1}(\tau) d\tau \\ &+ \int_0^t B(\tau) K_p e_{k+1}(\tau) d\tau + \int_0^t B(\tau) K_d \dot{e}_{k+1}(\tau) d\tau \end{aligned} \tag{5.11}$$

Using the partial integration equation, one obtains

$$\int_0^t B(\tau) K_d \dot{e}_{k+1}(\tau) d\tau = B(t) K_d e_{k+1}(t) - B(0) K_d e_{k+1}(0) - \int_0^t \frac{d\left(B(\tau)\right)}{d\tau} K_d e_{k+1}(\tau) d\tau \tag{5.12}$$

Submitting Eqs. (5.12) and (5.9) into Eq. (5.11) yields

$$\begin{aligned} x_{k+1}(t) - x_k(t) = x_{k+1}(0) - x_k(0) &- B(0) K_d e_{k+1}(0) + B(t) K_d e_{k+1}(t) \\ &+ \int_0^t \left(f\left(x_{k+1}(\tau), \tau\right) - f\left(x_k(\tau), \tau\right) \right) d\tau + \int_0^t \left(\eta_{k+1}(\tau) - \eta_k(\tau) \right) d\tau \\ &+ K_p \int_0^t B(\tau) e_{k+1}(\tau) d\tau - K_d \int_0^t \frac{d\left(B(\tau)\right)}{d\tau} e_{k+1}(\tau) d\tau \end{aligned} \tag{5.13}$$

From Eq. (5.3), one obtains

$$\left\| x_{k+1}(0) - x_k(0) \right\| \leq 2\varepsilon_x \tag{5.14}$$

According to A2 and A3, submitting Eq. (5.4) into Eq. (5.13) yields

$$\begin{aligned}\left\|x_{k+1}(t)-x_k(t)\right\| &\le b_\eta T+\left(2+\left\|B(0)K_d\right\|\left\|C(0)\right\|\right)\varepsilon_x+\left\|B(t)K_d\right\|\left\|e_{k+1}(t)\right\| \\ &+\int_0^t\left\|\left(B(\tau)K_p-\frac{d\left(B(\tau)\right)}{d\tau}K_d\right)\right\|\left\|e_{k+1}(\tau)\right\|d\tau \\ &+c_f\int_0^t\left\|x_{k+1}(\tau)-x_k(\tau)\right\|d\tau\end{aligned} \tag{5.15}$$

Multiplying Eq. (5.15) by $e^{-\lambda t}$ where $\lambda>1$ and $\lambda>c_f$, one obtains

$$\begin{aligned}\left\|x_{k+1}(t)-x_k(t)\right\|_\lambda &\le b_\eta T+\left(2+\left\|B(0)K_d\right\|\left\|C(0)\right\|\right)\varepsilon_x+B_{pd}e^{-\lambda t}\int_0^t\left\|e_{k+1}(\tau)\right\|d\tau \\ &+c_f e^{-\lambda t}\int_0^t\left\|x_{k+1}(\tau)-x_k(\tau)\right\|d\tau+B_d\left\|e_{k+1}(t)\right\|_\lambda\end{aligned} \tag{5.16}$$

Applying Lemma 5.11 to Eq. (5.16), one can get the following inequality

$$\left\|x_{k+1}(t)-x_k(t)\right\|_\lambda \le K_{x\lambda}\left\|e_{k+1}(t)\right\|_\lambda+\left(b_\eta T+\left(2+\left\|B(0)K_d\right\|\left\|C(0)\right\|\right)\varepsilon_x\right)/\alpha \tag{5.17}$$

The formula for the tracking error at the k+1th iteration is

$$\begin{aligned}e_{k+1}(t) &= y_d(t)-y_{k+1}(t) \\ &= e_k(t)-\left(y_{k+1}(t)-y_k(t)\right) \\ &= e_k(t)-C(t)\left(x_{k+1}(t)-x_k(t)\right)-\left(\xi_{k+1}(t)-\xi_k(t)\right)\end{aligned} \tag{5.18}$$

Multiplying $C(t)$ to the both sides of Eq. (5.13), one obtains

$$e_{k+1}(t) = e_k(t) - C(t)\int_0^t \left(f\left(x_{k+1}(\tau),\tau\right) - f\left(x_k(\tau),\tau\right)\right)d\tau - C(t)B(t)K_d e_{k+1}(t)$$

$$- C(t)\int_0^t \left(B(\tau)K_p - \frac{d\left(B(\tau)K_d\right)}{d\tau}\right)e_{k+1}(\tau)d\tau - \left(\xi_{k+1}(t) - \xi_k(t)\right) \tag{5.19}$$

$$+ C(t)\left(x_{k+1}(0) - x_k(0)\right) - C(t)B(0)K_d e_{k+1}(0)$$

Rearranging Eq. (5.19) leads to

$$\left(I_m + C(t)B(t)K_d\right)e_{k+1}(t) = e_k(t) - C(t)\int_0^t \left(f\left(x_{k+1}(\tau),\tau\right) - f\left(x_k(\tau),\tau\right)\right)d\tau$$

$$- C(t)\int_0^t \left(B(\tau)K_p - \frac{d\left(B(\tau)K_d\right)}{d\tau}\right)e_{k+1}(\tau)d\tau - \left(\xi_{k+1}(t) - \xi_k(t)\right)$$

$$+ C(t)\left(x_{k+1}(0) - x_k(0)\right) - C(t)B(0)K_d e_{k+1}(0) \tag{5.20}$$

Submitting assumption Eq. (5.5) into Eq. (5.20), one obtains

$$\left\|e_{k+1}(t)\right\| \le \rho_0 \left\{c_f \max_{t\in[0,T]}\left\|C(t)\right\|\int_0^t \left\|x_{k+1}(\tau) - x_k(\tau)\right\|d\tau\right.$$

$$+ \left\|e_k(t)\right\| + \max_{t\in[0,T]}\left\|C(t)\right\| B_{pd}\int_0^t \left\|e_{k+1}(\tau)\right\|d\tau \tag{5.21}$$

$$\left. + \max_{t\in[0,T]}\left\|C(t)\right\|\left(2 + \left\|B(0)K_d\right\|\left\|C(0)\right\|\right)\varepsilon_x + b_\xi\right\}$$

Multiplying Eq. (5.21) by $e^{-\lambda t}$ where $\lambda > c_f$, and using Lemma 5.1, one obtains

$$\left\|e_{k+1}(t)\right\|_\lambda \le \rho_0 \left\{ \left\|e_k(t)\right\|_\lambda + \frac{c_f}{\lambda} \max_{t\in[0,T]} \left\|C(t)\right\| \left\|x_{k+1}(t) - x_k(t)\right\|_\lambda \right.$$

$$\left. + \frac{1}{\lambda} \max_{t\in[0,T]} \left\|C(t)\right\| B_{pd} \left\|e_{k+1}(t)\right\|_\lambda + \max_{t\in[0,T]} \left\|C(t)\right\| \left(b_\xi + \left(2 + \left\|B(0)K_d\right\| \left\|C(0)\right\|\right) \varepsilon_x \right) \right\} \tag{5.22}$$

Submitting Eq. (5.17) into Eq. (5.22) and doing some simplification, one can get

$$\left\|e_{k+1}(t)\right\|_\lambda \le \rho \left\|e_k(t)\right\|_\lambda + \beta_0 \left(\frac{c_f}{\lambda} b_\eta + b_\xi \right) + \beta_1 \varepsilon_x \tag{5.23}$$

If λ is set to be large enough so that the following relationship holds:

$$\lambda > \frac{\rho_0}{1-\rho_0} \left(c_f K_{x\lambda} + B_{pd} \right) \max_{t\in[0,T]} \left\|C(t)\right\| \tag{5.24}$$

then from Eq. (5.7), one can prove

$$\rho < 1 \tag{5.25}$$

From Eqs. (5.23) and (5.25), one can guarantee that the final tracking error is bounded as

$$\lim_{k\to\infty} \left\|e_k(t)\right\|_\lambda \le \frac{\beta_0 \left(\frac{c_f}{\lambda} b_\eta T + b_\xi \right) + \beta_1 \varepsilon_x}{1-\rho} \quad \text{for all } t \in [0,T] \tag{5.26}$$

[End of proof].

From Eq. (5.26), one can see that the PD-OLC is robust with respect to the uncertainties and disturbances on the controlled system.

Remark 4: The convergence rate depends on the selection of control gains. From Eq. (5.5), one can see that ρ_0 will decrease if the control gain K_d increases. On the other hand, the properly selected control gain K_p can compensate the change of K_d so that the parameters $K_{x\lambda}$ and B_{pd} vary little with the increase of K_d. This means that K_p offers more flexibility for the resultant output tracking. Therefore, the convergence rate will increase if high control gains are used. It should also be noted that the use of a high control gain may saturate the system. Therefore, a trade-off may exist between the convergence rate and the saturation protection of the system.

Remark 5: There is no upper boundary but only a lower boundary with the control gain for the on-line learning control. The lower boundary can be obtained from Eq. (5.5), so the choice of the control gains is very easy. It should be noted that, for the ILC schemes, the learning gains are restricted in a bounded area; this means the learning gain in ILC has an upper limit; also, the learning gain has a lower limit, that is, zero. For example, for P-type or D-type ILC schemes, to make the tracking error converge to a bounded area, the following norm should be satisfied: $\|I - ML\| < 1$, where L is the learning gain and M is a system related matrix. Here, one can see that the selection of the learning gain depends on the system characteristics. Therefore, a model of the system is a priori in order to select a proper learning gain in the ILC.

***Remark 6*:** Following the similar idea discussed by Chen et al. (1999) and Yan et al. (2001), if the initial state updating law is used

$$x_{k+1}(0) = \left(I_n + B(0)K_d C(0)\right)^{-1}\left(x_k(0) + B(0)K_d y_d(0)\right) \tag{5.27}$$

then

$$x_{k+1}(0) = x_k(0) + B(0)K_d e_{k+1}(0) \tag{5.28}$$

In such a way, one can set $\varepsilon_x = 0$ in Eq. (5.26). It should be noted that Eqs. (5.27) and (5.28) provide initial state learning schemes where the initial condition can be assessed, but some system parameters are required to be known.

Remark 7: From a practical point of view, it is difficult to know exactly the model of the controlled system. Only a predicted model can be used. Therefore, the updating law for the initial condition may not be accurate.

Remark 8: If the uncertainties and disturbances are repeatable at each iteration, i.e., they are the same at every iteration, then one gets $b_\eta = b_\xi = 0$. In this case, the final tracking error bound becomes $\beta_1 \varepsilon_x / (1-\rho)$.

Remark 9: If the initial state updating law Eq. (5.27) is applied, and the uncertainty and disturbance are repeatable, then the final tracking error bound will be zero; this can be derived directly from ***Remark 6*** and ***Remark 8***.

In summary, in this section, a PD type online learning control for the tracking task of a class of nonlinear time-varying system with uncertainty and disturbance was developed. The PD-OLC is attractive for its simple structure, easy implementation, and fast convergence rate. It was proved that the PD-OLC was robust and the tracking error was bounded in the presence of the initial state error and the disturbance.

5.3 Adaptive Nonlinear PD Learning Control

Many researches have demonstrated that the nonlinear PD (NPD) control is better than PD control in terms of the increased damping, reduced rise time, and improved tracking accuracy. This is because the control gains in the NPD control can be adjusted online as a function of the tracking errors. It is natural to apply the learning strategy to NPD control in an iterative mode, resulting in a new control, namely, adaptive NPD learning control (NPD-LC).

5.3.1 Dynamic Model of a Robotic Manipulator

For a robot manipulator with *n* active joints driven by *n* actuators, where each joint consists of a prismatic or rotational joint, it is known (Craig, 1986) that the dynamic equation can be expressed as

$$D(q(t))\ddot{q}(t) + C(q(t), \dot{q}(t))\dot{q}(t) + G(q(t)) = T(t) \tag{5.29}$$

where $q(t) = [q_1(t) \quad q_2(t) \quad \dots \quad q_n(t)]^T \in \Re^n$ is the joint position vector, $\dot{q}(t) \in \Re^n$ is the joint velocity vector, and $\ddot{q}(t) \in \Re^n$ is the joint acceleration vector. $D(q(t)) \in \Re^{nxn}$ is the inertia matrix, $C(q(t), \dot{q}(t))\dot{q}(t) \in \Re^n$ denotes a vector containing the Coriolis, centrifugal and other coupling terms, $G(q(t)) \in \Re^n$ is the gravitational and other disturbance vector, and $T(t) \in \Re^n$ is the input torque vector.

It is common knowledge that robot manipulators have the following properties (Craig, 1986):

P1) $D(q^j(t))$ is a symmetric, bounded, and positive definite matrix;

P2) The matrix $\dot{D}(q^j(t)) - 2C(q^j(t), \dot{q}^j(t))$ is skew symmetric. Therefore,

$$x^T \left(\dot{D}(q^j(t)) - 2C(q^j(t), \dot{q}^j(t)) \right) x = 0, \ \forall \quad x \in \Re^n$$

Assume that all parameters of the robot are unknown and that the following properties hold.

A1) The desired trajectory $q_d(t)$ is of the third-order continuity *for* $t \in [0, t_f]$.

A2) For each iteration, the same initial conditions are satisfied, that is,

$q_d(0) - q^j(0) = 0$, $\dot{q}_d(0) - \dot{q}^j(0) = 0$, $\forall\ j \in \mathbb{N}$.

Define $e(t) = q_d(t) - q(t)$. According to A1, equation (5.29) can be linearized along the desired trajectory ($q_d(t), \dot{q}_d(t), \ddot{q}_d(t)$) in the following way, i.e.,

$$D(t)\ddot{e}(t) + \left[C(t) + C_1(t)\right]\dot{e}(t) + F(t)e(t) + n(\ddot{e}, \dot{e}, e, t) = T_d(t) - T(t) \tag{5.30}$$

with $D(t) = D\left(q_d(t)\right)$, $C(t) = C\left(q_d(t), \dot{q}_d(t)\right)$, $C_1(t) = \left.\frac{\partial C}{\partial \dot{q}}\right|_{q_d(t), \dot{q}_d(t)} \dot{q}_d(t)$

$$F(t) = \left.\frac{\partial D}{\partial q}\right|_{q_d(t)} \ddot{q}_d(t) + \left.\frac{\partial C}{\partial q}\right|_{q_d(t)\dot{q}_d(t)} \dot{q}_d(t) + \left.\frac{\partial G}{\partial q}\right|_{q_d(t)}$$

$$T_d(t) = D\left(q_d(t)\right)\ddot{q}_d(t) + C\left(q_d(t), \dot{q}_d(t)\right)\dot{q}_d(t) + G\left(q_d(t)\right)$$

The term of $n(\ddot{e}, \dot{e}, e, t)$ is the higher order term of $\ddot{e}(t)$, $\dot{e}(t)$, and $e(t)$ and may be negligible.

5.3.2 Nonlinear PD Control

An NPD control law may be any control structure of the following form

$$T(t) = K_p(t)e(t) + K_d(t)\dot{e}(t) \tag{5.31}$$

where $K_p(t)$ and $K_d(t)$ are the time-varying diagonal proportional and derivative gain matrices. The nonlinear gain function for the NPD control in Eq. (5.31) is not unique; see Xu et al. (1995), Armstrong and Wade (2000), and Ouyang et al. (2002).

5.3.3 Adaptive NPD Learning Control

For the adaptive NPD-LC method, the controlled torque of the second iteration is a combination of current NPD control (feedback) with the torque produced in the first

iteration (feedforward) for the same tracking task at the same initial condition. This procedure will continue until a satisfied tracking performance is obtained. Therefore, the adaptive NPD-LC law can be expressed by

$$T^{j+1}(t) = \underbrace{K_p^{j+1}(t)e^{j+1}(t) + K_d^{j+1}(t)\dot{e}^{j+1}(t)}_{feedback} + \underbrace{T^j(t)}_{feedforward} \tag{5.32}$$

or in a more general form

$$T^{j+1}(t) = T^j(t) + \Delta T^{j+1}(e^{j+1}(t), \dot{e}^{j+1}(t))$$

In Eq. (5.32), the nonlinear control gains are selected as

$$\begin{cases} K_p^j(t) = K_{p0} * K^j(t) \\ \\ K_d^j(t) = K_{d0} * K^j(t) \end{cases} \tag{5.33}$$

For simplicity, K_{p0} and K_{d0} are set to be initial diagonal gain matrices, and $K^p(t)$ and $K^d(t)$ are the varying diagonal gain matrices with

$$K_i^j(t) = \mathrm{K}_{\max} - \mathrm{K}_{\min} \sec h(\alpha_i * e_i^j(t)), \quad i=1,..,n \tag{5.34}$$

where $\mathrm{K}_{\max}$, $\mathrm{K}_{\min}$, and α_i are user-defined positive constants. Also, $\mathrm{K}_{\max} - \mathrm{K}_{\min} \geq 1$. It should be noted that if α_i is set to zero, then $K_i^j(t)$ becomes constant. In such a case, NPD control becomes fixed gain PD control. Therefore, the PD control method is a special case of the NPD control method.

The major difference between the adaptive NPD-LC and the classical ILC is that the adaptive NPD-LC is feedback plus feedforward control, while the classical ILC is only feedforward control. Hence, the adaptive NPD-LC is an on-line learning control, while the classical ILC is an off-line learning control. So the adaptive NPD-LC method is expected to have a faster convergent speed.

Furthermore, the adaptive NPD-LC algorithm is adaptive. This is due to the property of nonlinear control. The feedback part in the control law Eq. (5.32) enables the controller to adjust its response by changing the gains in accordance with the errors. When the error between the desired and actual values of the controlled variables is large, the control gain increases, which amplifies the error substantially to generate a large corrective action to rapidly drive the system approaching to its goal. As the error diminishes, the gain is automatically reduced to avoid excessive oscillations and large overshoots in the response.

The adaptive NPD-LC method is also a learning process because it repeats the processes of the same tracking task, much the same way as humans learn a desired motion pattern through training. In the proposed control law, the action of the iterative learning is to memorize the torque profiles generated by previous iteration that includes some information about the dynamics of the system. The main difference between the ILC method and the adaptive NPD-LC method is that the ILC method does not use the information of the system dynamics in the current iteration, while the adaptive NPD-LC method uses that information and further inherits the information from NPD control.

5.3.4 Convergence Analysis of Adaptive Nonlinear PD Learning Control

In a repetitive operation mode, for the *j*th iteration, according A1, the initial conditions are as follows.

$$\begin{cases} e^j(0) = q_d(0) - q^j(0) = 0 \\ \\ \dot{e}^j(0) = \dot{q}_d(0) - \dot{q}^j(0) = 0 \end{cases} \qquad j=1,2,\ldots,m \tag{5.35}$$

In the jth iteration, Equation (5.30) can be rewritten as

$$D(t)\ddot{e}^j(t) + [C(t) + C_1(t)]\dot{e}^j(t) + F(t)e^j(t) = T_d(t) - T^j(t) \tag{5.36}$$

Similarly, in the j+1th iteration, one obtains

$$D(t)\ddot{e}^{j+1}(t) + [C(t) + C_1(t)]\dot{e}^{j+1}(t) + F(t)e^{j+1}(t) = T_d(t) - T^{j+1}(t) \tag{5.37}$$

Assume $K_p(t) = \Lambda K_d(t)$, where Λ is a positive constant. Define the following parameter

$$y^j(t) = \dot{e}^j(t) + \Lambda e^j(t) \tag{5.38}$$

After the above preparation, the following theorem for trajectory control of robot manipulators is proposed.

***Theorem* 5.2**: Considering a robot manipulator that performs repetitive tasks under the adaptive NPD-LC law Eq. (5.32) with the nonlinear gain rule Eq. (5.33), the following relationships hold for all $t \in [0, t_f]$.

$$q^j(t) \xrightarrow{j\to\infty} q_d(t)$$

$$\dot{q}^j(t) \xrightarrow{j\to\infty} \dot{q}_d(t)$$

If the control gains are selected such that

$$l_p = \lambda_{\min}(K_{d0} + 2C_1 - 2\Lambda D) > 0 \tag{5.39}$$

$$l_r = \lambda_{\min}(K_{d0} + 2C + 2F/\Lambda - 2\dot{C}_1/\Lambda) > 0 \tag{5.40}$$

$$l_p l_r \geq \left\| F/\Lambda - (C + C_1 - \Lambda D) \right\|_{\max}^2 \tag{5.41}$$

where $\lambda_{\min}(A)$ is the minimum eigenvalue of matrix A, and $\|M\|_{\max} = \max\|M(t)\|$ for $0 \le t \le t_f$. Here, $\| M \|$ represents the Euclidean norm of M.

Proof of theorem 5.2.

For simplicity, let K_d represent $K_d(t)$. Define a Lyapunov function candidate as

$$V^j = \int_0^t e^{-\rho\tau} y^{jT} K_d y^j d\tau \ge 0 \tag{5.42}$$

where K_d is positive definite and ρ is a positive constant.

From Eqs. (5.32, 5.36-5.38), one can obtain the following equation

$$D\delta\dot{y}^j + (C + C_1 - \Lambda D + K_d)\delta y^j + (F - \Lambda(C + C_1 - \Lambda D))\delta e^j = -K_d y^j \tag{5.43}$$

From the definition of V^j, for the $j+1$th iteration, one obtains

$$V^{j+1} = \int_0^t e^{-\rho\tau} y^{j+1^T} K_d y^{j+1} d\tau$$

Define $\Delta V^j = V^{j+1} - V^j$, and $\delta y = y^{j+1} - y^j$. From Eqs. (15) and (16), one can obtain

$$\Delta V^j = \int_0^t e^{-\rho\tau} (\delta y^{jT} K_d \delta y^j + 2\delta y^{jT} K_d y^j) d\tau$$

$$= \int_0^t e^{-\rho\tau} \delta y^{jT} K_d \delta y^j d\tau - 2\int_0^t e^{-\rho\tau} \delta y^{jT} D\delta\dot{y}^j d\tau - 2\int_0^t e^{-\rho\tau} \delta y^{jT} (C + C_1 - \Lambda D + K_d)\delta y^j d\tau$$

$$-2\int_0^t e^{-\rho\tau} \delta y^{jT} (F - \Lambda(C + C_1 - \Lambda D))\delta e^j d\tau$$

Applying the partial integration and the initial condition Eq. (5.35), one can get

$$\int_0^t e^{-\rho\tau}\delta y^{jT} D\delta\dot{y}^j d\tau = e^{-\rho\tau}\delta y^{jT} D\delta y^j\Big|_0^t - \int_0^t (e^{-\rho\tau}\delta y^{jT} D)'\delta y^j d\tau$$

$$= e^{-\rho\tau}\delta y^{jT}(t)D(t)\delta y^j(t) + \rho\int_0^t e^{-\rho\tau}\delta y^{jT} D\delta y^j d\tau$$

$$-\int_0^t e^{-\rho\tau}\delta y^{jT} D\delta\dot{y}^j d\tau - \int_0^t e^{-\rho\tau}\delta y^{jT}\dot{D}\delta y^j d\tau$$

According to P2, the following equation holds.

$$\int_0^t \delta y^{jT}\dot{D}\delta y^j d\tau = 2\int_0^t \delta y^{jT} C\delta y^j d\tau$$

Hence,

$$\Delta V^j = -e^{-\rho t}\delta y^{jT}(t)D(t)\delta y^j(t) - \rho\int_0^t e^{-\rho\tau}\delta y^{jT} D\delta y^j d\tau$$

$$-\int_0^t e^{-\rho\tau}\delta y^{jT}(K_d + 2C_1 - 2\Lambda D)\delta y^j d\tau - 2\int_0^t e^{-\rho\tau}\delta y^{jT}(F - \Lambda(C + C_1 - \Lambda D))\delta e^j d\tau \tag{5.44}$$

Here, the matrix K_d is not a constant matrix but a time-varying matrix. From Eq. (5.33), the following relationship holds

$$K_{d0}(K_{\max} - K_{\min}) \le K_d \le K_{d0}K_{\max} \tag{5.45}$$

where K_{d0} is a constant matrix, and K_d and K_{d0} are positive definite matrices. From Eq. (5.45), one obtains

$$\int_0^t e^{-\rho\tau}\delta y^{jT}K_d\delta y^j d\tau \geq \int_0^t e^{-\rho\tau}\delta y^{jT}K_{d0}(K_{\max}-K_{\min})\delta y^j d\tau$$

$$= (K_{\max}-K_{\min})\int_0^t e^{-\rho\tau}\delta y^{jT}K_{d0}\delta y^j d\tau$$

$$> \int_0^t e^{-\rho\tau}\delta y^{jT}K_{d0}\delta y^j d\tau$$

Substituting $\delta y^j = \delta\dot{e}^j + \Lambda\delta e^j$ into Eq. (5.44) yields

$$\Delta V^j < -e^{-\rho t}\delta y^{jT}(t)D(t)\delta y^j(t) - \rho\int_0^t e^{-\rho\tau}\delta y^{jT}D\delta y^j d\tau$$

$$-\int_0^t e^{-\rho\tau}\delta\dot{e}^{jT}(K_{d0}+2C_1-2\Lambda D)\delta\dot{e}^j d\tau$$

$$-2\Lambda\int_0^t e^{-\rho\tau}\delta e^{jT}(K_{d0}+2C_1-2\Lambda D)\delta\dot{e}^j d\tau$$
$$-2\int_0^t e^{-\rho\tau}\delta\dot{e}^{jT}(F-\Lambda(C+C_1-\Lambda D))\delta e^j d\tau$$

$$-\Lambda^2\int_0^t e^{-\rho\tau}\delta e^{jT}(K_{d0}+2C_1-2\Lambda D)\delta e^j d\tau$$
$$-2\Lambda\int_0^t e^{-\rho\tau}\delta e^{jT}(F-\Lambda(C+C_1-\Lambda D))\delta e^j d\tau$$

Applying partial integration again, one can get

$$\int_0^t e^{-\rho\tau}\delta e^{jT}(K_{d0}+2C_1-2\Lambda D)\delta\dot{e}^j d\tau$$

$$= e^{-\rho\tau}\delta e^{jT}(K_{d0}+2C_1-2\Lambda D)\delta e^j\Big|_0^t + \rho\int_0^t e^{-\rho\tau}\delta e^{jT}(K_{d0}+2C_1-2\Lambda D)\delta e^j d\tau$$

$$-\int_0^t e^{-\rho\tau}\delta\dot{e}^{jT}(K_{d0}+2C_1-2\Lambda D)\delta e^j d\tau + 2\int_0^t e^{-\rho\tau}\delta e^{jT}(\Lambda\dot{D}-\dot{C}_1)\delta e^j d\tau$$

Therefore, from Eq. (5.39), one obtains

$$\Delta V^j < -e^{-\rho t}\delta y^{jT} D\delta y^j - \Lambda e^{-\rho t}\delta e^{jT} l_p \delta e^j - \rho\int_0^t e^{-\rho\tau}\delta y^{jT} D\delta y^j d\tau$$
$$-\rho\int_0^t e^{-\rho\tau}\delta e^{jT} l_p \delta e^j d\tau - \int_0^t e^{-\rho\tau} w d\tau \tag{5.46}$$

where $w = \delta\dot{e}^{jT}(K_{d0} + 2C_1 - 2\Lambda D)\delta\dot{e}^j + 2\Lambda\delta\dot{e}^{jT}(F/\Lambda - (C + C_1 - \Lambda D)\delta e^j$

$$+\Lambda^2\delta e^{jT}(K_{d0} + 2C + 2F/\Lambda - 2\dot{C}_1/\Lambda)\delta e^j$$

Let $Q = F/\Lambda - (C + C_1 - \Lambda D)$. From Eqs. (5.39 – 5.40), one obtains

$$w \geq l_p \left\|\delta\dot{e}\right\|^2 + 2\Lambda\delta\dot{e}^T Q\delta e + \Lambda^2 l_r \left\|\delta e\right\|^2$$

Apply the Cauchy-Schwartz inequality, $\delta\dot{e}^T Q\delta e \geq -\left\|\delta\dot{e}\right\| \left\|Q\right\|_{\max} \left\|\delta e\right\|$. From Eqs. (5.39 – 5.41), one can get

$$w \geq l_p \left\|\delta\dot{e}\right\|^2 - 2\Lambda\left\|\delta\dot{e}\right\|\left\|Q\right\|_{\max}\left\|\delta e\right\| + \Lambda^2 l_r \left\|\delta e\right\|^2$$

$$= l_p(\left\|\delta\dot{e}\right\| - \frac{\Lambda}{l_p}\left\|Q\right\|_{\max}\left\|\delta e\right\|)^2 + \Lambda^2(l_p - \frac{1}{l_r}\left\|Q\right\|_{\max}^2)\left\|\delta e\right\|^2 \geq 0$$

Noticing D is a positive definite matrix and $w \geq 0$, and considering the assumption Eq. (5.39), one can guarantee $\Delta V^j \leq 0$. Therefore,

$$V^{j+1} \leq V^j \tag{5.47}$$

As K_d is a positive definite matrix, from the definition Eq. (5.42), one obtians $V^j \geq 0$. As a result, $y^j(t) \to 0$ when $j \to \infty$. Because $e^j(t)$ and $\dot{e}^j(t)$ are two independent variables, and Λ is a positive constant, from Eq. (5.38), one can conclude:

$$\text{If } j \to \infty \text{ then } e^j(t) \to 0 \text{ and } \dot{e}^j(t) \to 0$$

Finally, the following conclusions hold.

$$\begin{aligned} q^j(t) &\xrightarrow{j\to\infty} q_d(t) \\ & \qquad\qquad \text{for } t \in [0, t_f] \\ \dot{q}^j(t) &\xrightarrow{j\to\infty} \dot{q}_d(t) \end{aligned}$$

[End of proof].

Note that the verification examples to demonstrate the effectiveness of the adaptive NPD-LC law will be presented in Chapter 6.

The nonlinear control gains are functions of the tracking errors. For the adaptive NPD learning control, the more iteration cycles result in the smaller tracking errors. Therefore, from Eq. (5.34), one can see that the nonlinear control gains will tend to be fixed control gains with the increase of iteration. This means that the characteristics of the NPD control will disappear. An improvement of the adaptive NPD-LC will be discussed in the next section.

5.4 Adaptive Switching Learning PD (ASL-PD) Control

The adaptive control can cope with parameter uncertainties, such as the link length, mass, inertia, and frictional nonlinearity, with a self-organizing capability. Having such a capability requires extensive computation and thus compromises its application for real-time control problems (especially in high-speed operations). In addition, since the adaptive control generally does not guarantee that the estimated parameters of the

manipulators converge to their true values (Sun and Mills, 1999), the tracking errors would repeatedly be brought into the system as the manipulators repeat their tasks.

Currently, one of the most active areas of research in control theory is the switching control technique. More detailed information can be found in Section 2.6. For this technique, the control of a given plant can be switched among several controllers, and each controller is designed for a specific "nominal model" of the plant. A switching control scheme usually consists of an inner loop, where a candidate controller is connected in closed-loop with the system, and an outer loop, where a supervisor decides which controller to be used and when to switch to a different one. As such, the switching of controllers is taken place in the time domain. However, this underlying philosophy has the possibility of being applied to other control structures in the domains other than the time domain, such as the iteration domain.

In this section, a new control method is proposed for the trajectory tracking of robotic manipulators. The basic concept of this new control method is to combine several control methods by taking advantage of each of them into a hybrid one. The architecture of this hybrid control system is as follows: (1) the control is a learning process through several iterations of the operations of a robotic manipulator, (2) the control structure consists of two parts: a PD feedback part and a feedforward learning part using the torque profile obtained from the previous iteration, and (3) the gains in the PD feedback control law are adapted according to the gain switching strategy. This new control method is called the adaptive switching learning PD (ASL-PD) control method.

5.4.1 ASL-PD Controller Design

Following the above discussion, one can see that the ASL-PD control method has two operational modes: the single operational mode and the iterative operational mode. In the single operational mode, the PD control feedback with the gain switching is used, where the information from the present operation is utilized. In the iterative operational mode, a simple iterative learning control is applied as feedforward where information

from previous operations is used. Together with these two operational modes, the information from both the current and previous operations is utilized.

The ASL-PD control method can be described as follows:

Consider the *j*th iterative operation for the robotic manipulator described by Eq. (5.30) with properties (P1 and P2) and assumptions (A1 and A2) under the following control law

$$T^j(t) = \underbrace{K_p^j e^j(t) + K_d^j \dot{e}^j(t)}_{feedback} + \underbrace{T^{j-1}(t)}_{feedforward} \qquad j = 0,1,\cdots,N \tag{5.48}$$

with the following gain switching rule

$$\begin{cases} K_p^j = \beta(j) K_p^0 \\ K_d^j = \beta(j) K_d^0 \qquad j = 1,2,\cdots,N \\ \beta(j+1) > \beta(j) \end{cases} \tag{5.49}$$

where $T^{-1}(t) = 0$, $e^j(t) = q_d(t) - q^j(t)$, $\dot{e}^j(t) = \dot{q}_d(t) - \dot{q}^j(t)$, and K_p^0 and K_d^0 are diagonal positive definite matrices. The matrices K_p^0 and K_d^0 are called the initial proportional and derivative control gains, respectively, while matrices K_p^j and K_d^j are the control gains of the *j*th iteration. $\beta(j)$ is the gain switching factor where $\beta(j) > 1 \quad for\ j = 1,2,\cdots,N$, and it is a function of the iteration number.

The gain switching law in Eq. (5.49) is used to adjust the PD gains from iteration to iteration. Such a switching in the ASL-PD control method acts not in the time domain but in the iteration domain. This is the main difference between the ASL-PD control method and the traditional switching control method, where switching occurs in the time

domain. Therefore, the transient process of the switched system, which must be carefully treated to maintain the stability of the system in the case of using the traditional switching control method, does not occur in the ASL-PD control method.

From Eqs. (5.48) and (5.49), it can be seen that the ASL-PD control law is a combination of feedback (with switching gains in each iteration) and feedforward (with learning strategy). Therefore, the ASL-PD is a hybrid control system. The ASL-PD control method possesses the adaptive ability, which is demonstrated by different control gains in different iterations; see Eq. (5.49). Such a switching takes place at the beginning of each iteration. Therefore, a rapid convergence rate for the trajectory tracking can be expected.

Furthermore, in the ASL-PD control law, the learning occurs due to the memorization of the torque profiles generated by the previous iterations that include information about the dynamics of a controlled system. It should be noted that such learning is direct in the sense that it generates the controlled torque profile directly from the existing torque profile in the previous iterations without any modification. Because of the introduction of the learning strategy in the iteration, the state of the controlled object changes from iteration to iteration. This requires an adaptive control to deal with those changes, and the ASL-PD has such an adaptive capability.

Following the similar process discussed in Section 5.3, the proof of the asymptotic convergence of the ASL-PD control method for both position tracking and velocity tracking will be demonstrated.

5.4.2 Asymptotic Convergence with the ASL-PD Method

For the simplicity of analysis, let $K_p^0 = \Lambda K_d^0$ for the initial iteration, and define the following parameter

$$y^j(t) = \dot{e}^j(t) + \Lambda e^j(t) \tag{5.50}$$

The following theorem can be proved.

Theorem 5.3. Suppose a robot system described in Eq. (5.29) satisfies properties (P1, P2) and assumptions (A1, A2). Consider that the robot manipulator performs repetitive tasks under the ASL-PD control method Eq. (5.48) with the gain switching rule Eq. (5.49). The following should hold for all $t \in [0, t_f]$

$$q^j(t) \xrightarrow{j\to\infty} q_d(t)$$

$$\dot{q}^j(t) \xrightarrow{j\to\infty} \dot{q}_d(t)$$

Provided that the control gains are selected such that the following relationships hold

$$l_p = \lambda_{\min}(K_d^0 + 2C_1 - 2\Lambda D) > 0 \tag{5.51}$$

$$l_r = \lambda_{\min}(K_d^0 + 2C + 2F/\Lambda - 2\dot{C}_1/\Lambda) > 0 \tag{5.52}$$

$$l_p l_r \geq \left\| F/\Lambda - (C + C_1 - \Lambda D) \right\|_{\max}^2 \tag{5.53}$$

where $\lambda_{\min}(A)$ is the minimum eigenvalue of matrix A, and $\|M\|_{\max} = \max\|M(t)\|$ for $0 \leq t \leq t_f$. Here, $\| M \|$ represents the Euclidean norm of M.

Proof of theorem 5.3.

Define a Lyapunov function candidate as

$$V^j = \int_0^t e^{-\rho\tau} y^{jT} K_d^0 y^j d\tau \geq 0 \tag{5.54}$$

where $K_d^0 > 0$ is the initial derivative gain of PD control, and ρ is a positive constant.

Also, define $\delta y^j = y^{j+1} - y^j$ and $\delta e^j = e^{j+1} - e^j$. Then, from Eq. (5.50)

$$\delta y^j = \delta \dot{e}^j + \Lambda \delta e^j \tag{5.55}$$

and from Eq. (5.48)

$$T^{j+1}(t) = K_p^{j+1} e^{j+1}(t) + K_d^{j+1} \dot{e}^{j+1}(t) + T^j(t) \tag{5.56}$$

One can obtain the following equation

$$D\delta \dot{y}^j + (C + C_1 - \Lambda D + K_d^{j+1})\delta y^j + (F - \Lambda(C + C_1 - \Lambda D))\delta e^j = -K_d^{j+1} y^j \tag{5.57}$$

From the definition of V^j, for the j+1th iteration

$$V^{j+1} = \int_0^t e^{-\rho\tau} y^{j+1^T} K_d^0 y^{j+1} d\tau$$

Define $\Delta V^j = V^{j+1} - V^j$, then from Eqs. (5.54-5.55,) and (5.57), one obtains

$$\begin{aligned}
\Delta V^j &= \int_0^t e^{-\rho\tau} (\delta y^{jT} K_d^0 \delta y^j + 2\delta y^{jT} K_d^0 y^j) d\tau \\
&= \frac{1}{\beta(j+1)} \int_0^t e^{-\rho\tau} (\delta y^{jT} K_d^{j+1} \delta y^j + 2\delta y^{jT} K_d^{j+1} y^j) d\tau \\
&= \frac{1}{\beta(j+1)} \left\{ \int_0^t e^{-\rho\tau} \delta y^{jT} K_d^{j+1} \delta y^j d\tau - 2\int_0^t e^{-\rho\tau} \delta y^{jT} D\dot{\delta} y^j d\tau \right. \\
&\quad \left. -2\int_0^t e^{-\rho\tau} \delta y^{jT} ((C + C_1 - \Lambda D + K_d^{j+1})\delta y^j + (F - \Lambda(C + C_1 - \Lambda D))\delta y^j) d\tau \right\}
\end{aligned}$$

Finally, the following relationship holds.

$$\Delta V^j \le \frac{1}{\beta(j+1)}\left\{-e^{-\rho t}\delta y^{jT} D\delta y^j - \rho\int_0^t e^{-\rho\tau}\delta y^{jT} D\delta y^j d\tau - \Lambda e^{-\rho t}\delta e^{jT}(K_d^0 + 2C_1 - 2\Lambda D)\delta e^j \right.$$

$$\left. - \rho\Lambda\int_0^t e^{-\rho\tau}\delta e^{jT}(K_d^0 + 2C_1 - 2\Lambda D)\delta e^j d\tau - \int_0^t e^{-\rho\tau} w d\tau\right\}$$

$$\le \frac{1}{\beta(j+1)}\left\{-e^{-\rho t}\delta y^{jT} D\delta y^j - \Lambda e^{-\rho t}\delta e^{jT} l_p \delta e^j - \rho\int_0^t e^{-\rho\tau}\delta y^{jT} D\delta y^j d\tau \right.$$

$$\left. - \rho\Lambda\int_0^t e^{-\rho\tau}\delta e^{jT} l_p \delta e^j d\tau - \int_0^t e^{-\rho\tau} w d\tau\right\} \tag{5.58}$$

where $w = \delta\dot{e}^{jT}(K_d^0 + 2C_1 - 2\Lambda D)\delta\dot{e}^j + 2\Lambda\delta\dot{e}^{jT}(F/\Lambda - (C + C_1 - \Lambda D)\delta e^j$

$$+ \Lambda^2\delta e^{jT}(K_d^0 + 2C + 2F/\Lambda - 2\dot{C}_1/\Lambda)\delta e^j$$

Let $Q = F/\Lambda - (C + C_1 - \Lambda D)$. Then from Eqs. (5.51 – 5.52), one can get

$$w \ge l_p \left\|\delta\dot{e}\right\|^2 + 2\Lambda\delta\dot{e}^T Q\delta e + \Lambda^2 l_r \left\|\delta e\right\|^2$$

According to Eqs. (5.51 – 5.53), one can get

$$w \ge l_p \left\|\delta\dot{e}\right\|^2 - 2\Lambda\left\|\delta\dot{e}\right\|\left\|Q\right\|_{\max}\left\|\delta e\right\| + \Lambda^2 l_r \left\|\delta e\right\|^2$$

$$= l_p(\left\|\delta\dot{e}\right\| - \frac{\Lambda}{l_p}\left\|Q\right\|_{\max}\left\|\delta e\right\|)^2 + \Lambda^2(l_p - \frac{1}{l_r}\left\|Q\right\|_{\max}^2)\left\|\delta e\right\|^2 \ge 0 \tag{5.59}$$

From (P1) and Eq. (5.51), based on Eq. (5.58), it can be ensured that $\Delta V^j \le 0$. Therefore,

$$V^{j+1} \le V^j \tag{5.60}$$

From the definition, K_d^0 is a positive definite matrix. From the definition of V^j, $V^j > 0$, and V^j is bounded. As a result, $y^j(t) \to 0$ when $j \to \infty$. Because $e^j(t)$ and $\dot{e}^j(t)$ are two independent variables, and Λ is a positive constant. Thus, if $j \to \infty$, then $e^j(t) \to 0$ and $\dot{e}^j(t) \to 0$ for $t \in [0, t_f]$.

Finally, the following conclusions hold

$$\begin{cases} q^j(t) \xrightarrow{j\to\infty} q_d(t) \\ \dot{q}^j(t) \xrightarrow{j\to\infty} \dot{q}_d(t) \end{cases} \quad \text{for } t \in [0, t_f] \tag{5.61}$$

[End of Proof].

From the above analysis it can be seen that the ASL-PD control method can guarantee that the tracking errors converge arbitrarily close to zero as the number of iterations increases. The case studies based on both simulation and experiments will be presented in Chapter 6 to demonstrate this conclusion.

5.5 Concluding Remarks

In this chapter, three PD type learning control laws were developed and their convergence analyses were performed. First, the PD-OLC was proposed for the tracking control of the nonlinear time-varying system. The PD-OLC is robust and the tracking errors are uniformly bounded in the presence of the initial state errors and the uncertainties and disturbances. The convergence analysis was conducted based on the λ-norm of the bound of the output tracking error. Then, the adaptive NPD-LC was proposed for the trajectory tracking of robotic manipulators. The adaptive NPD-LC possesses the adaptive property by means of its designed NPD controller to change the control gains based on the tracking errors during the trajectory tracking process, and the learning ability through its iterations. The asymptotic convergence for both tracking

positions and tracking velocities was theoretically proved using the Lyapunov's method. Finally, the ASL-PD control method was developed to further improve the convergence rate in the learning process. This control method is a simple combination of a traditional PD control with a gain switching strategy as feedback and an iterative learning control using the input torque profile obtained from the previous iterations as feedforward. The ASL-PD control incorporates both adaptive and learning capabilities; therefore, it can provide an incrementally improved tracking performance with the increase of the iteration number. The ASL-PD control method achieves the asymptotic convergence based on the Lyapunov's method.

It should be noted that the dynamic model of a robotic manipulator described by Eq. (5.29) can be represented by a state space equation with properly selecting the state variables. Also, one can see that a state space equation is a special case of Eq. (5.1). Therefore, the convergences of the adaptive NPD learning control and the ASL-PD control can also be analyzed following the similar procedure described in Section 5.2 based on the λ-norm of the bound of the output tracking errors.

6. SIMULATION AND EXPERIMENT RESULTS

6.1 Introduction

In Chapter 5, a family of PD-type hybrid control systems with learning capability were developed. The convergences of all these hybrid control systems were theoretically proved based on the Lyapunov method and in the sense of λ-norm, respectively.

The purpose of this chapter is to verify the proposed hybrid control systems developed in Chapter 5 through simulation and experiments. This chapter is organized as follows. Section 6.2 presents the simulation study of the PD-OLC algorithm using a nonlinear time-varying system taken from literature to show the effectiveness of the PD-OLC by comparing them. In Section 6.3, the adaptive NPD-LC is tested for the trajectory tracking of both the serial and parallel robotic manipulators. Different control laws are compared to show the advantage of the adaptive NPD-LC. Section 6.4 discusses the simulation study of the ASL-PD control using the examples in the literature. Section 6.5 discusses the experiment setup for the real applications of the proposed control algorithms, followed by some test results using the adaptive NPD-LC and the ASL-PD control. In Section 6.6, a prototype CMA is built and the static and dynamic experiments are performed to verify the analysis model of the CMA discussed in Chapter 4. Section 6.7 gives the conclusions.

6.2 Simulation of the PD type Online Learning Control for Nonlinear System

In this section, the simulation study is carried out for the tracking control of a nonlinear time-varying system using the PD-OLC proposed in Section 5.2. The purpose is to demonstrate the effectiveness of the proposed PD-OLC method.

The following nonlinear time-varying system taken from Chen et al. (1999) with uncertainty and disturbance is used to demonstrate the effectiveness of the PD-OLC.

$$\begin{bmatrix} \dot{x}_{1_k} \\ \dot{x}_{2_k} \end{bmatrix} = \begin{bmatrix} a_1 \sin(x_{2_k}) & 1 + a_1 \sin(x_{1_k}) \\ -2 - 5t & -3 - 2t \end{bmatrix} \begin{bmatrix} x_{1_k} \\ x_{2_k} \end{bmatrix} + \begin{bmatrix} 1 & 0 \\ 0 & 2 \end{bmatrix} \begin{bmatrix} u_{1_k} \\ u_{2_k} \end{bmatrix} + \begin{bmatrix} \eta_{1_k} \\ \eta_{2_k} \end{bmatrix} \tag{6.1}$$

$$\begin{bmatrix} y_{1_k} \\ y_{2_k} \end{bmatrix} = \begin{bmatrix} 4 & 0 \\ 0 & 1 \end{bmatrix} \begin{bmatrix} x_{1_k} \\ x_{2_k} \end{bmatrix} + \begin{bmatrix} \xi_{1_k} \\ \xi_{2_k} \end{bmatrix} \tag{6.2}$$

where k is the iteration number and time $t \in [0, 1]$. The uncertainties and disturbances are introduced as follows:

$$\begin{bmatrix} \eta_{1_k} \\ \eta_{2_k} \end{bmatrix} = a_2 \begin{bmatrix} \cos(2\pi ft) \\ 2\cos(4\pi ft) \end{bmatrix}, \quad \begin{bmatrix} \xi_{1_k} \\ \xi_{2_k} \end{bmatrix} = a_2 \begin{bmatrix} \sin(2\pi ft) \\ 2\sin(4\pi ft) \end{bmatrix}$$

with $f = 5$ Hz. The desired tracking trajectories are

$$y_{1_d} = y_{2_d} = 12t^2(1-t) \tag{6.3}$$

The initial state at the first iteration is set as

$$\begin{cases} x_1(0) = a_3 \\ x_2(0) = -a_3 \end{cases} \tag{6.4}$$

To examine the robustness of the PD-OLC, four cases are considered and the parameters are listed as follows.

Case 1: $a_1 = 1, a_2 = 0$, and $a_3 = 0$. This is the ideal case without any initial state error, uncertainty and disturbance.

Case 2: $a_1 = 1, a_2 = 1$, and $a_3 = 0$. This is the case where the system model has some uncertainty but without any initial state error.

Case 3: $a_1 = 1, a_2 = 1$, and $a_3 = 0.5$. This means that the system parameters are known but there are some disturbances in the state and the output. Also, the initial state error is updated using the initial state updating law Eq. (5.27).

Case 4: $a_1 = 1, a_2 = 1$, and $a_3 = 0.01 rand(j)$ where j is the iteration number. This is the worst case where the system has some uncertainties and disturbances, and some random initial states from iteration to iteration. In this case, no initial state updating law is used.

For each case, the following three sets of control gains are selected to examine the convergence rate of the PD-OLC.

- Low control gains: $K_p = diag\{1,5\}, \quad K_d = diag\{0.5, 2.5\}$
- Middle control gains: $K_p = diag\{2,10\}, \quad K_d = diag\{1,5\}$
- High control gains: $K_p = diag\{5,25\}, \quad K_d = diag\{2.5,12.5\}$

The maximum tracking position errors in each iteration for all four cases are shown in the following three figures where Figures 6.1, 6.2 and 6.3 represent the results under low control gains, middle control gains, and high control gains, respectively. Also, the maximum tracking velocity errors in each iteration are shown in Figures 6.4, 6.5 and 6.6, respectively. In all these figures, the dashed line represents the maximum error of y_{1_k} or $\dot{y}_{1_k}$, while the solid line represents the maximum error of y_{2_k} or $\dot{y}_{2_k}$.

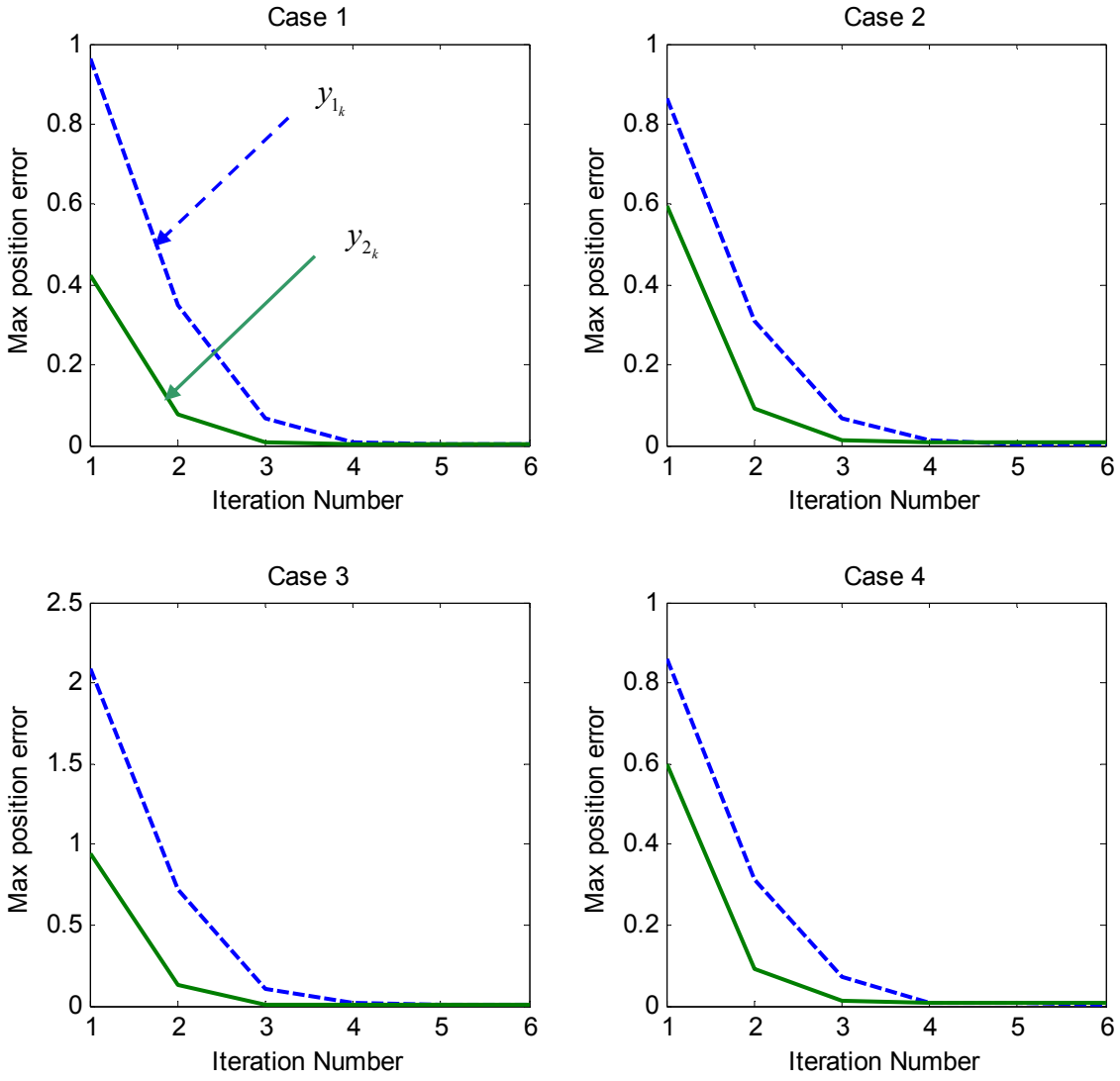

Figure 6.1 The maximum position tracking error vs. the iteration number for four cases with the low control gains.

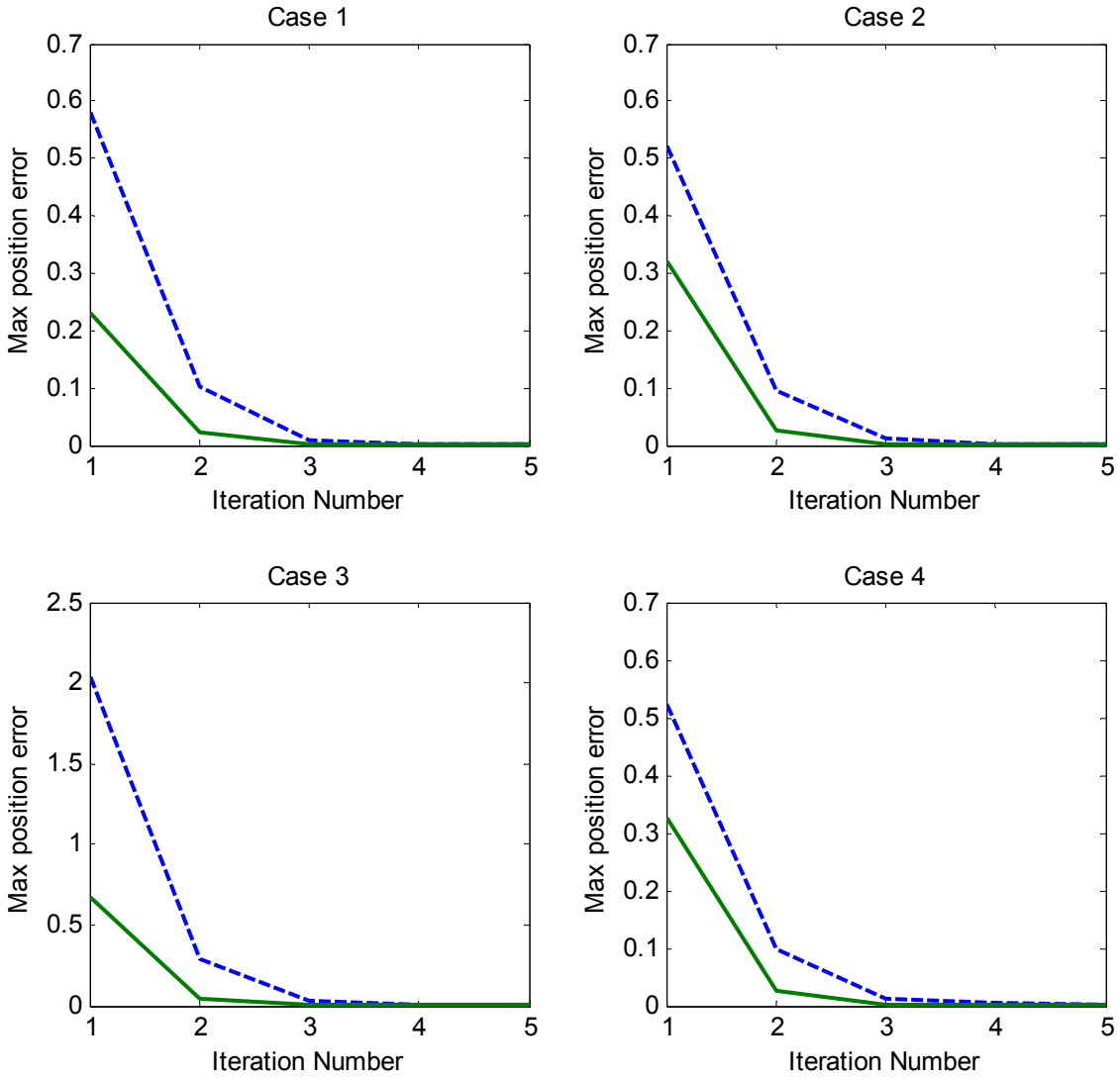

Figure 6.2 The maximum position tracking error vs. the iteration number for four cases with the middle control gains.

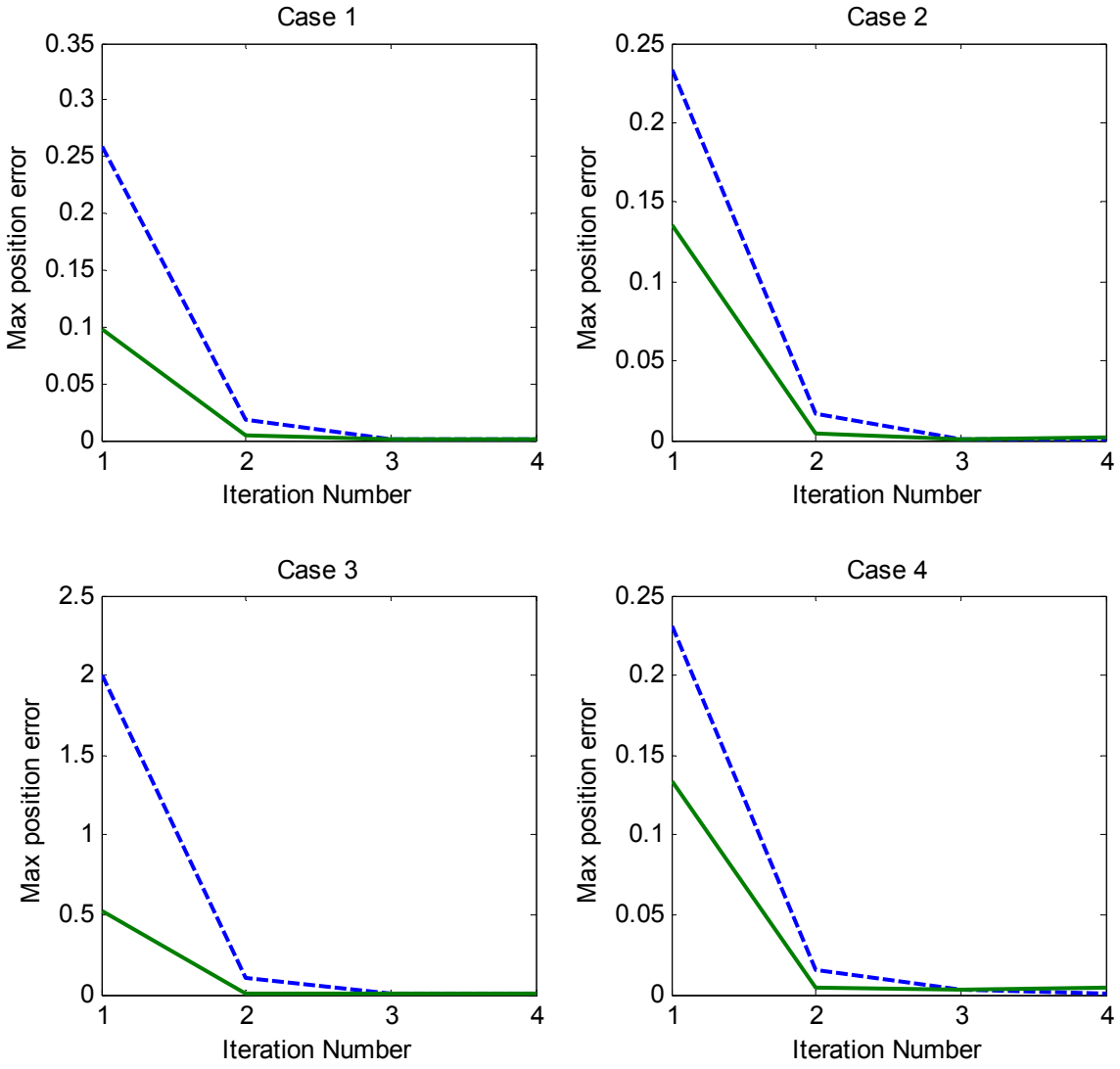

Figure 6.3 The maximum position tracking error vs. the iteration number for four cases with the high control gains.

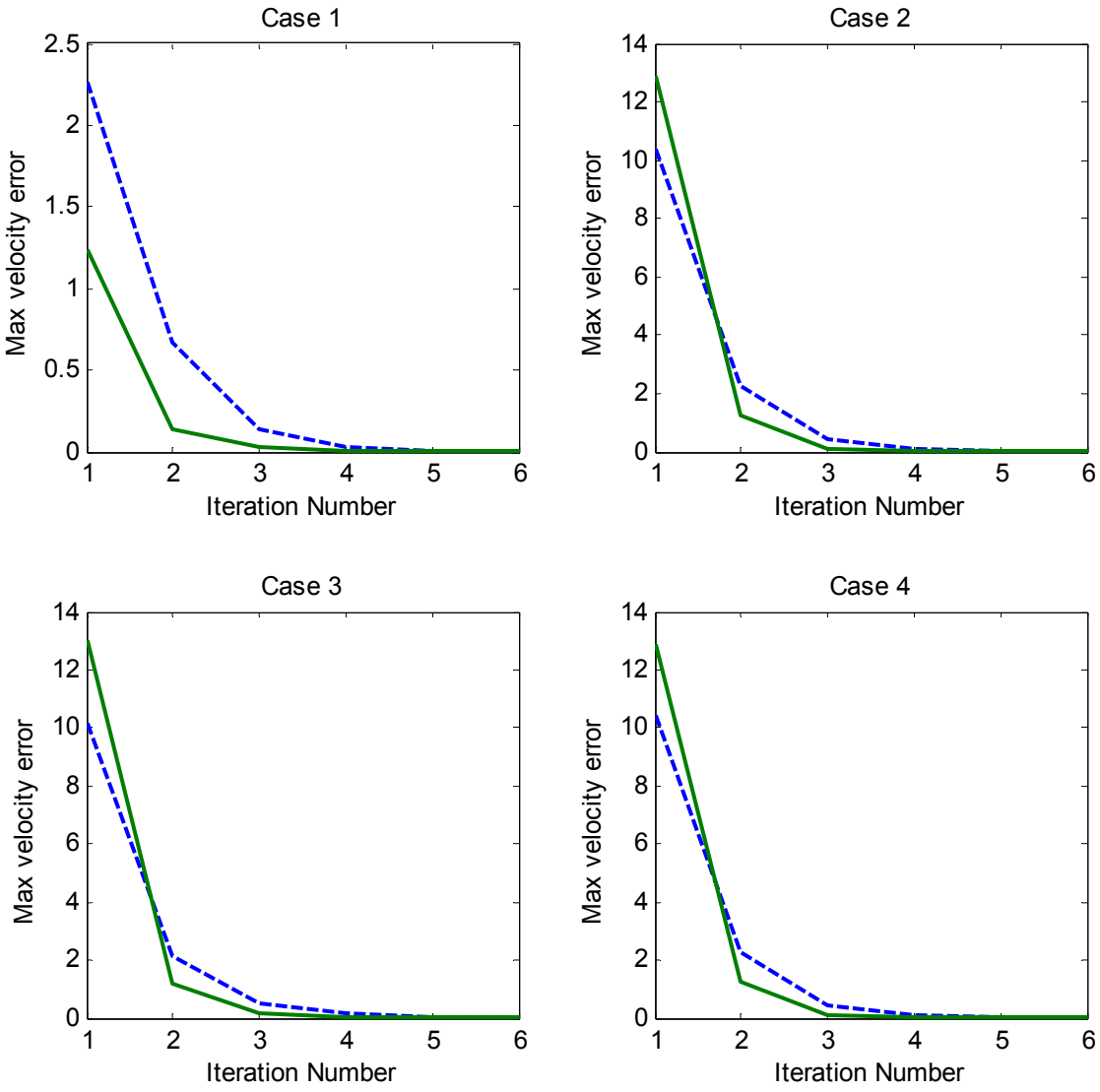

Figure 6.4 The maximum velocity tracking error vs. the iteration number for four cases with the low control gains.

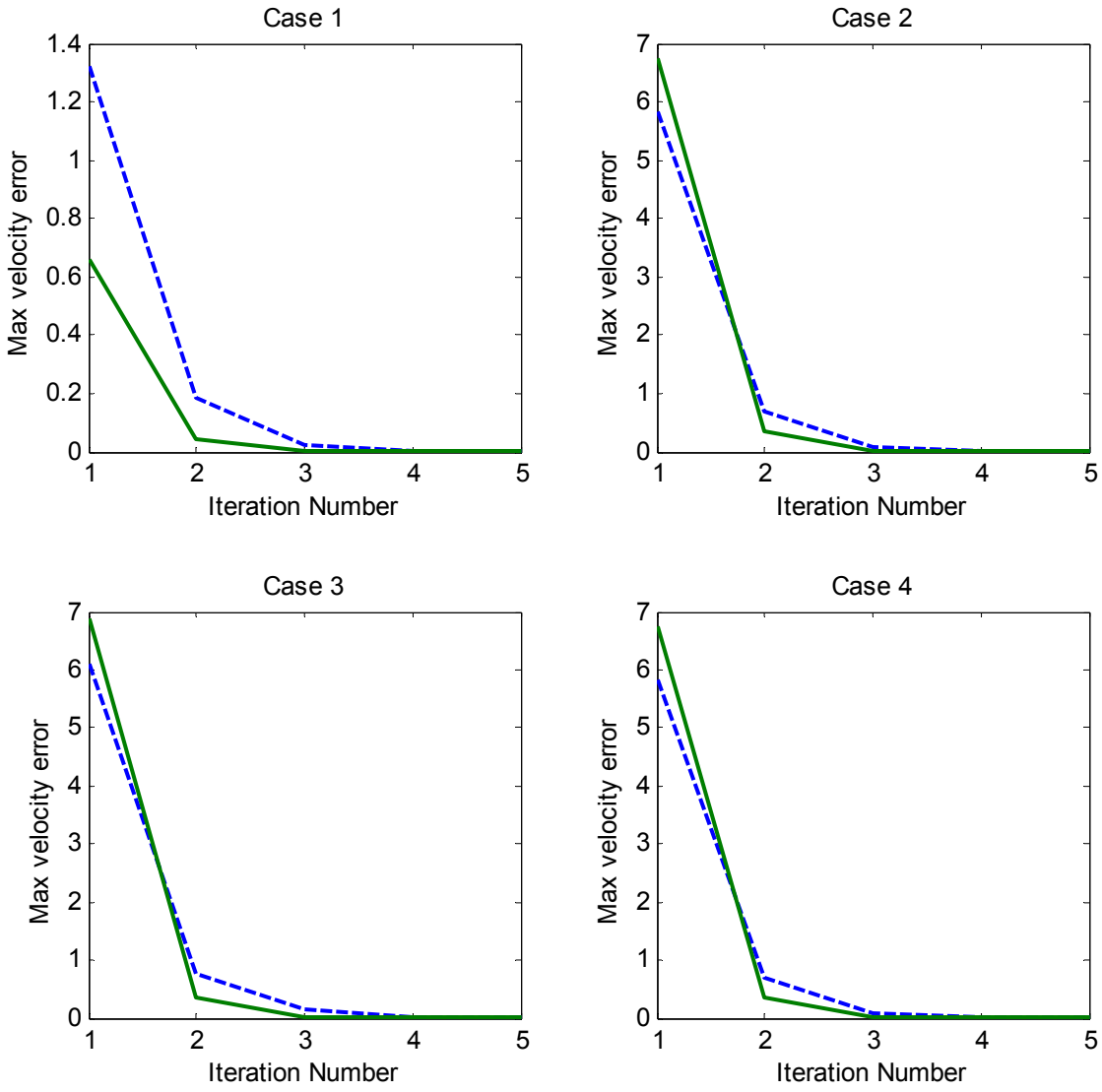

Figure 6.5 The maximum velocity tracking error vs. the iteration number for four cases with the middle control gains.

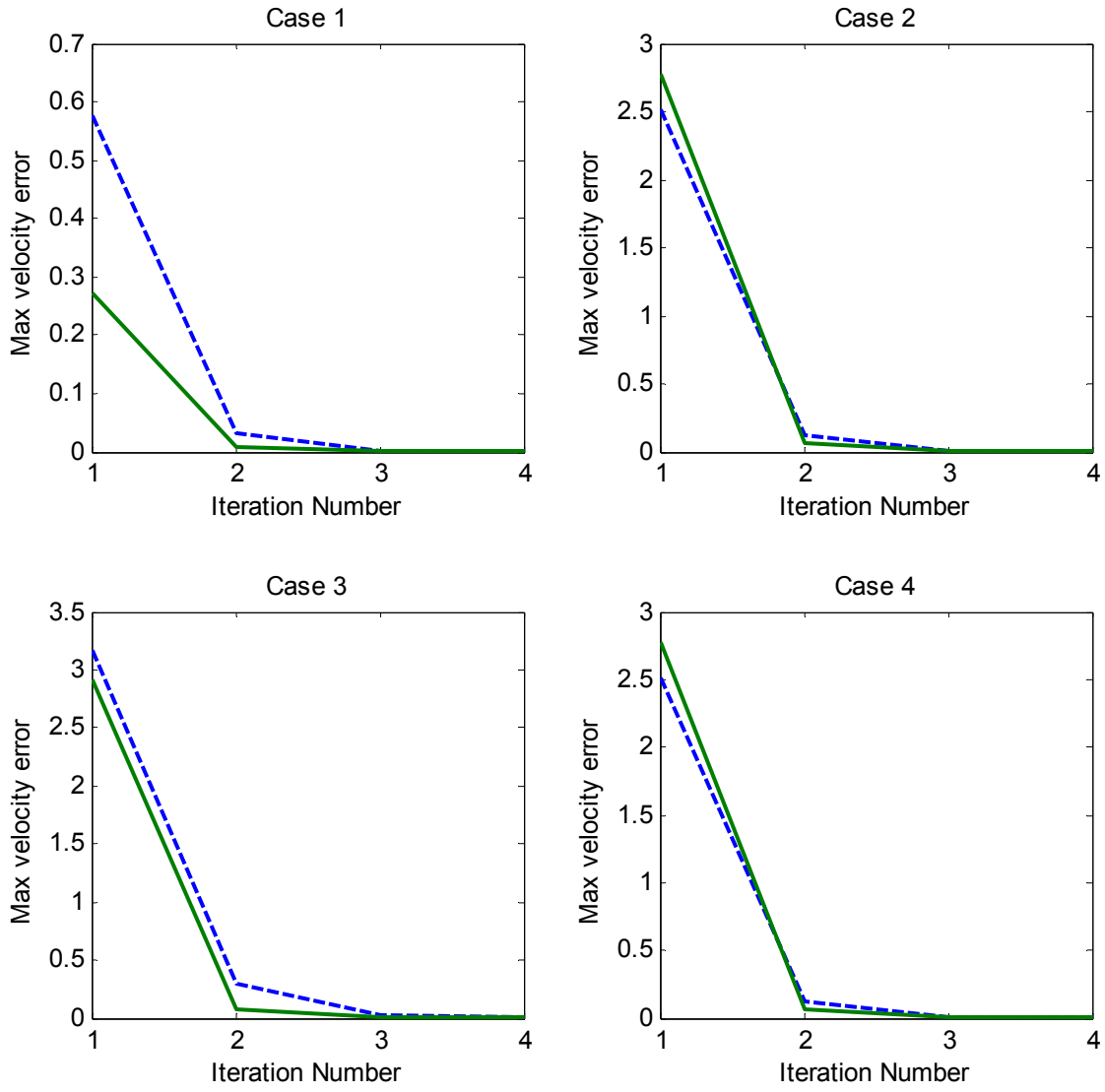

Figure 6.6 The maximum velocity tracking error vs. the iteration number for four cases with the high control gains.

From the above six figures, one can observe that with the increase of the control gains, the tracking performances both for the tracking position and the tracking velocity improve and the convergence rate increases too. It should be noted that all iteration processes were stopped if the maximum error was less than 0.01. If small control gains were used, after 6 iterations, the maximum error was less than 0.01, while when the high control gains were used, only after 4 iterations, the maximum error was less than 0.001.

Table 6.1 Final tracking errors for four cases with different control gains

Cases	Maximum error	Low gains	Mid. gains	High gains
Case 1	Iteration No.	7	6	5
	e_{y_1}	0.0009	0.0006	0.0004
	e_{y_2}	0.0005	0.0005	0.0004
	$\dot{e}_{y_1}$	0.0006	0.0003	0.0002
	$\dot{e}_{y_2}$	0.0003	0.0003	0.0002
Case 2	Iteration No.	10	7	5
	e_{y_1}	0.0036	0.002	0.0009
	e_{y_2}	0.0055	0.0029	0.0013
	$\dot{e}_{y_1}$	0.0024	0.0013	0.0005
	$\dot{e}_{y_2}$	0.003	0.0015	0.0007
Case 3	Iteration No.	8	6	5
	e_{y_1}	0.0036	0.0021	0.0009
	e_{y_2}	0.0054	0.0029	0.0012
	$\dot{e}_{y_1}$	0.0025	0.0014	0.0005
	$\dot{e}_{y_2}$	0.0028	0.0015	0.0006
Case 4	Iteration No.	6	5	4
	e_{y_1}	0.003	0.0031	0.0012
	e_{y_2}	0.0073	0.0033	0.0027
	$\dot{e}_{y_1}$	0.0071	0.0028	0.0014
	$\dot{e}_{y_2}$	0.0043	0.0024	0.0025

Table 6.1 lists the final maximum tracking errors for all four cases. One interesting phenomenon is that although there are some uncertainties and disturbances in the control model for Case 2 compared with Case 1, the final tracking error did not vary so much; see Table 6.1. This demonstrated the robustness of the PD-OLC for the model uncertainty. From case 3, one can observe that the initial state learning scheme is effective. For case 4, although the initial state at each iteration was set as a random function, the final tracking errors were still bounded and acceptable. This example demonstrates the robustness of the PD-OLC.

The same example was tested by Chen et al. (1997) where a D-type OLC was used. It was shown that 9 iterations were needed to make the final tracking error less than 0.01 using the best learning gains. But only after 6 iterations, the PD-OLC can get much better results. Therefore, the PD-OLC considerably improved the convergence rate.

6.3 Simulation of the Adaptive Nonlinear PD Learning Control

To demonstrate the effectiveness of the adaptive NPD-LC algorithm, simulation studies were carried out using examples from the literature.

6.3.1 Case study 1: Random Disturbance

The robotic manipulator example in Tayebi (2003) was used in this study to examine the effectiveness of the proposed control scheme. A two DOF planar robotic manipulator with revolute joints has the following dynamic equation where random disturbance is included.

$$\begin{bmatrix} m_{11} & m_{12} \\ m_{21} & m_{22} \end{bmatrix} \begin{bmatrix} \ddot{q}_1 \\ \ddot{q}_2 \end{bmatrix} + \begin{bmatrix} c_{11} & c_{12} \\ c_{21} & c_{22} \end{bmatrix} \begin{bmatrix} \dot{q}_1 \\ \dot{q}_2 \end{bmatrix} + \begin{bmatrix} G_1 \\ G_2 \end{bmatrix} + \begin{bmatrix} d_1 \\ d_2 \end{bmatrix} = T \tag{6.5}$$

with

$$m_{11} = m_1 l_{c1}^2 + m_2 (l_1^2 + l_{c2}^2 + 2 l_1 l_{c2} \cos q_2) + I_1 + I_2$$

$$m_{12} = m_{21} = m_2 (l_{c2}^2 + l_1 l_{c2} \cos q_2) + I_2, \quad m_{22} = m_2 l_{c2}^2 + I_2$$

$$c_{11} = h\dot{q}_2, \quad c_{12} = h(\dot{q}_1 + \dot{q}_2), \quad c_{21} = -h\dot{q}_1, \quad c_{22} = 0, \quad h = -m_2 l_1 l_{c2} \sin q_2$$

$$G_1 = (m_1 l_{c1} + m_2 l_1) g \cos q_1 + m_2 l_{c2} g \cos(q_1 + q_2), \quad G_2 = m_2 l_{c2} g \cos(q_1 + q_2)$$

Here, the physical parameters were selected as the same as in Tayebi (2003). They are: $m_1 = m_2 = 1\text{kg}$, $l_1 = l_2 = 0.5\text{m}$, $l_{c1} = l_{c2} = 0.25\text{m}$, $I_1 = I_2 = 0.1\text{kgm}^2$, $\text{g} = 9.81\text{m/s}^2$. Also all the disturbances were assumed to be time-varying and random as follows, $d_1 = d_2 = rand(j)\sin(t)$, where $rand(j)$ was a random function taking the values between 0 and 1.

The desired trajectories for the two joints were chosen as

$$\begin{cases} q_1 = \sin(2\pi t) \\ \\ q_2 = \cos(2\pi t) \end{cases} \quad \text{for } t \in [0 \quad 1] \tag{6.6}$$

The same control gains in Tayebi (2003) were selected as follows

For PD control: $K_p = K_d = \text{diag}\{10,10\}$

For NPD and adaptive NPD-LC:

$K_{p0} = K_{d0} = \text{diag}\{10,10\}$, $\text{K}_{\max} = 4$, $\text{K}_{\min} = 3$, $\alpha_1 = \alpha_2 = 50$.

Figure 6.7 shows the tracking performance where the result for the adaptive NPD-LC case was obtained only after 5 iterations. It should be noted that, although NPD control was used in the first iteration for the adaptive NPD-LC and it had very large tracking errors for both positions and velocities, the adaptive NPD-LC dramatically improved the tracking performance from iteration to iteration. The fixed-gain PD control and NPD control were not suitable for this example when small control gains were used, but adaptive NPD-LC was very suitable for the same problem using the same control gains. The reason is that the adaptive NPD-LC could inherit and adapt the dynamics of the robotic system from the previous trials. The more iterations that the adaptive NPD-LC employed, the more accurate was the dynamic model that the adaptive NPD-LC

obtained, and the more accurate tracking performance that the adaptive NPD-LC achieved.

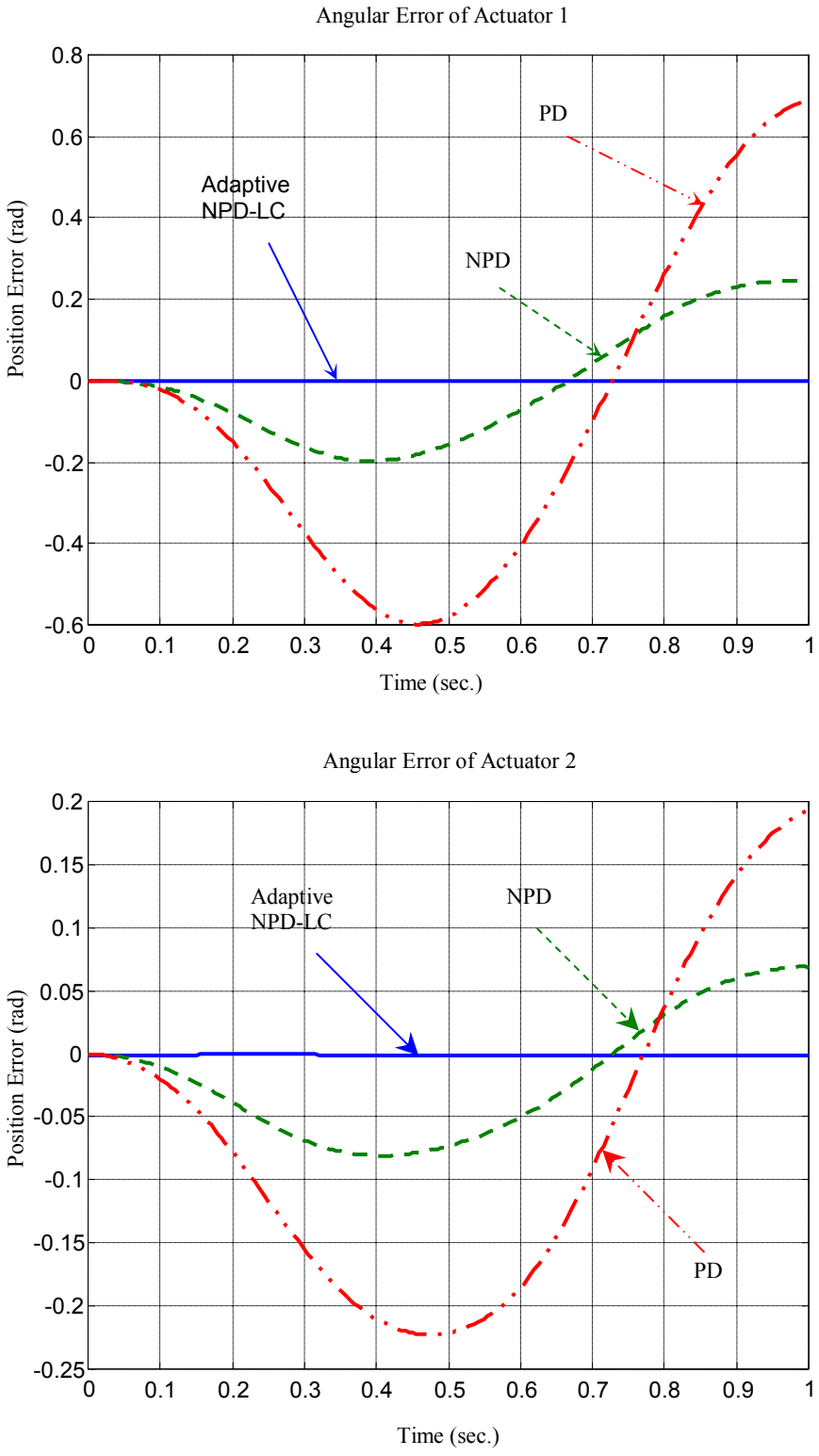

(a) Position errors

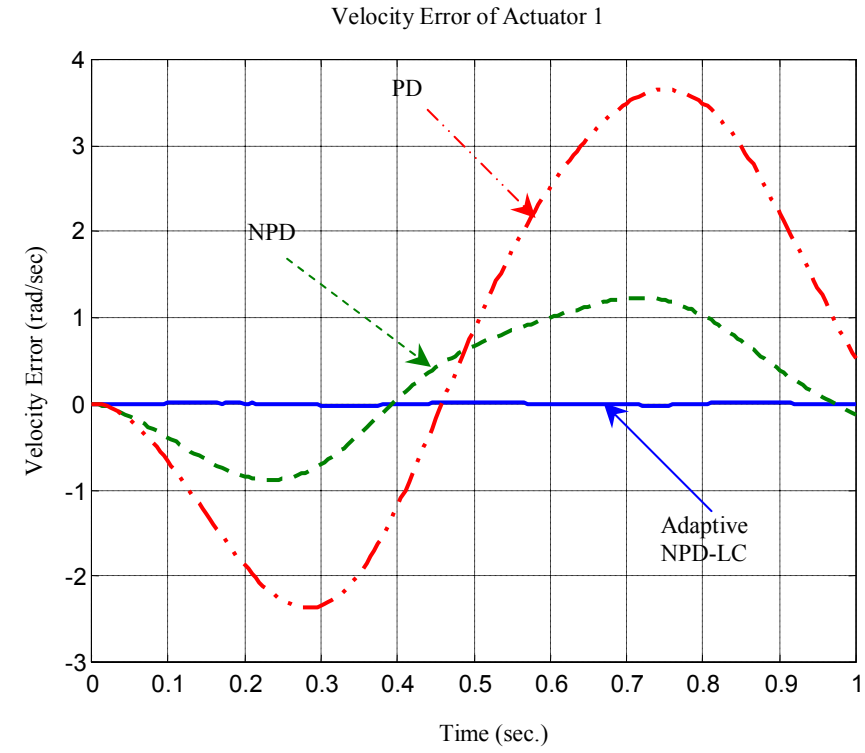

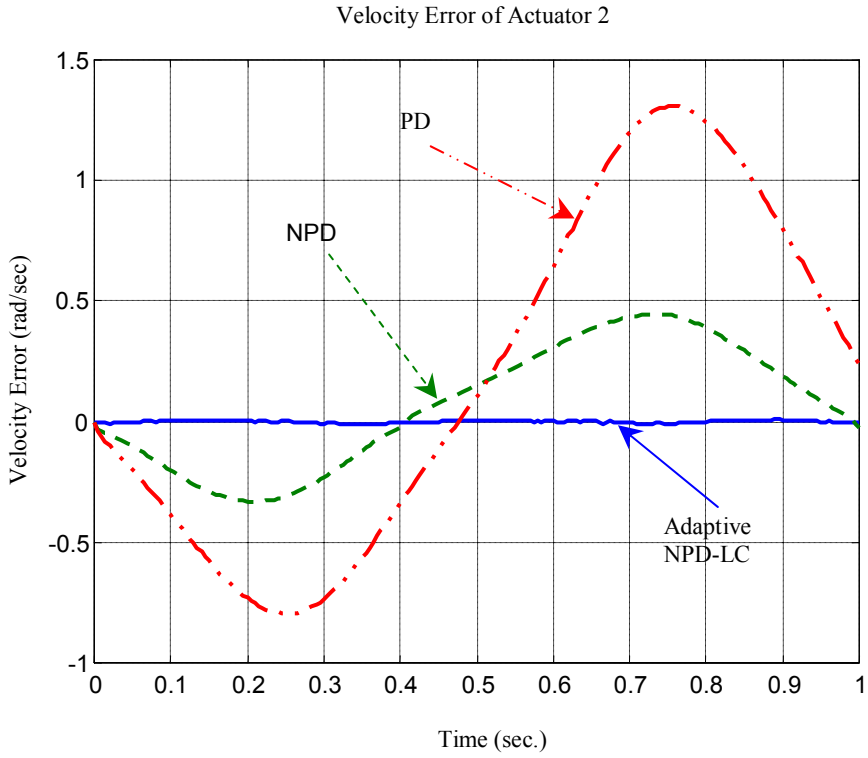

(b) Velocity errors

Figure 6.7 Position and velocity errors using PD, NPD, and adaptive NPD-LC.

To illustrate performance improvement, Figure 6.8 shows the tracking errors from the first iteration to the 5th iteration. It clearly shows that adaptive NPD-LC is a simple but promising control method when subjected to external random disturbances. Comparing these results with those in Tayebi (2003), it can be seen that the proposed adaptive NPD-LC has a faster convergence speed for trajectory tracking.

It should also be noted that, although the tracking performance improved from iteration to iteration, the torques required to drive the two actuators were nearly the same as can be seen from Figure 6.9. This means that the performance improvement is not produced by supplying more energy, but by the designed control strategy.

To examine further the effect of the user-defined coefficients on the tracking performance, different α_i (50, 100, and 250) was used in simulation. Figure 6.10 shows some results for tracking performance from iteration to iteration under different user-defined coefficient α_i. From Figure 6.10, one can see that as α_i increases, the tracking errors decreases. This result is coincident with that of NPD control.

6.4.2 Case study 2: Repetitive Disturbance

In this case, the example in Choi and Lee (2000) was used to validate the effectiveness of the proposed adaptive NPD-LC. All the parameters were selected to be the same as in Choi and Lee (2000). In this example, the repetitive disturbances were included in simulation.

The physical parameters and desired trajectories are the same as in Choi and Lee (2000) and are listed as follows.

Physical parameters: $m_1 = 10\text{kg}$, $m_2 = 5\text{kg}$, $l_1 = 1\text{m}$, $l_2 = 0.5\text{m}$, $l_{c_1} = 0.5\text{m}$, $l_{c_2} = 0.25\text{m}$, $I_1 = 0.83\text{kgm}^2$ and $I_2 = 0.3\text{kgm}^2$.

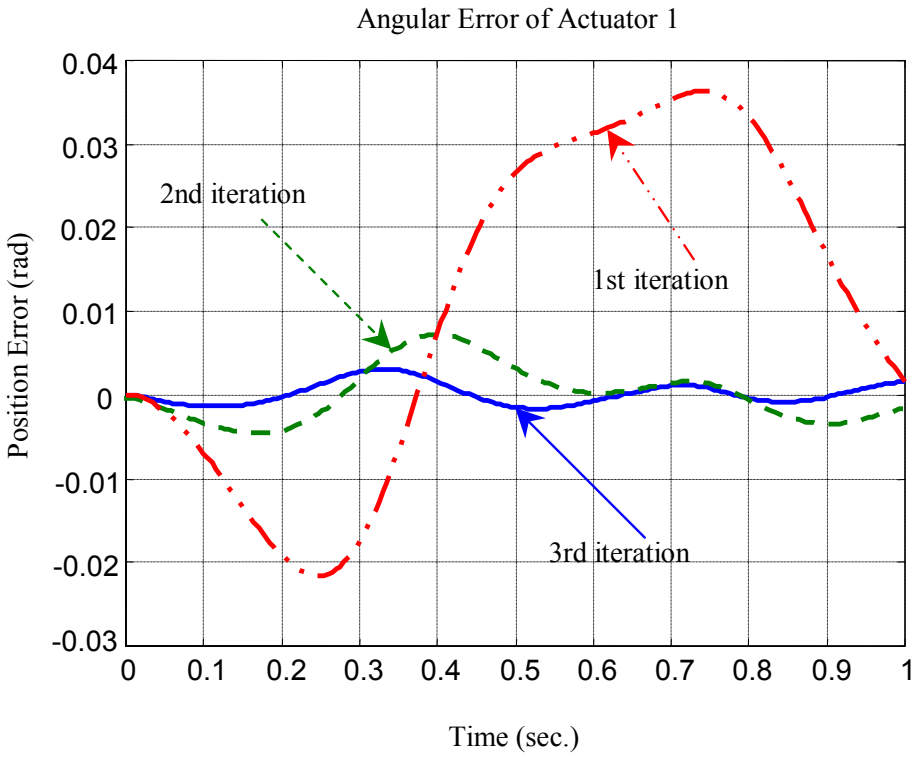

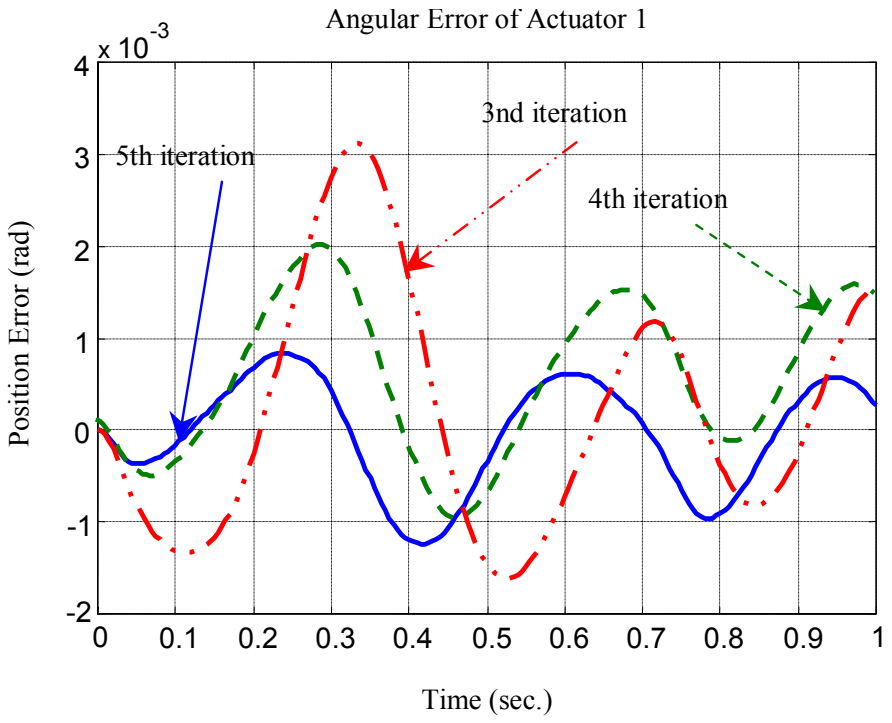

Figure 6.8 Position performance improvements for actuator 1 for iteration j=1,2,3,4,5.

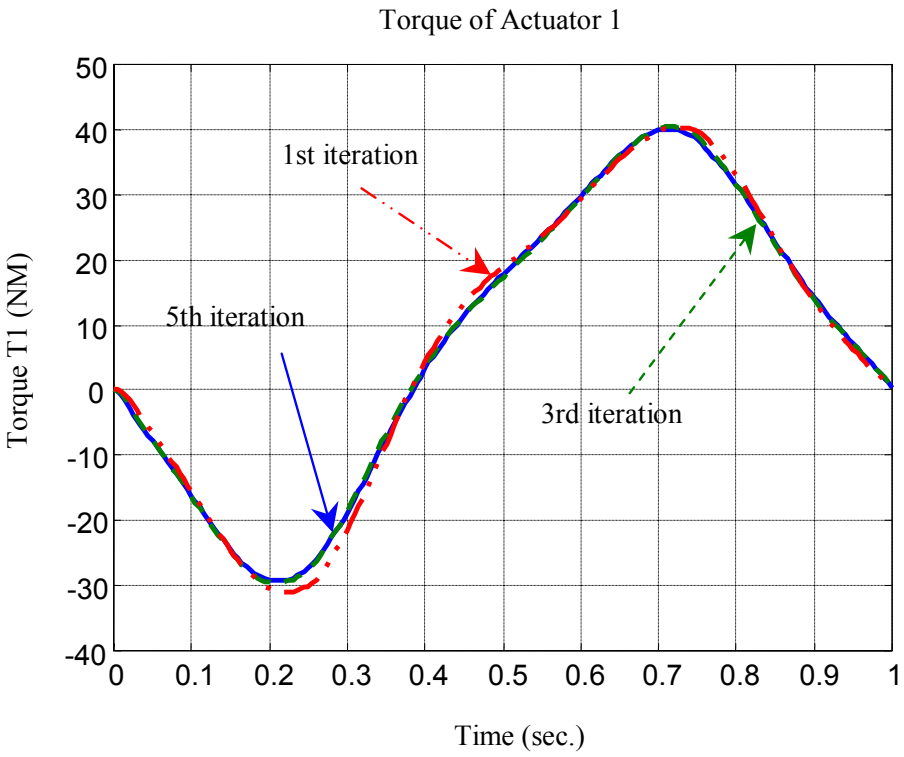

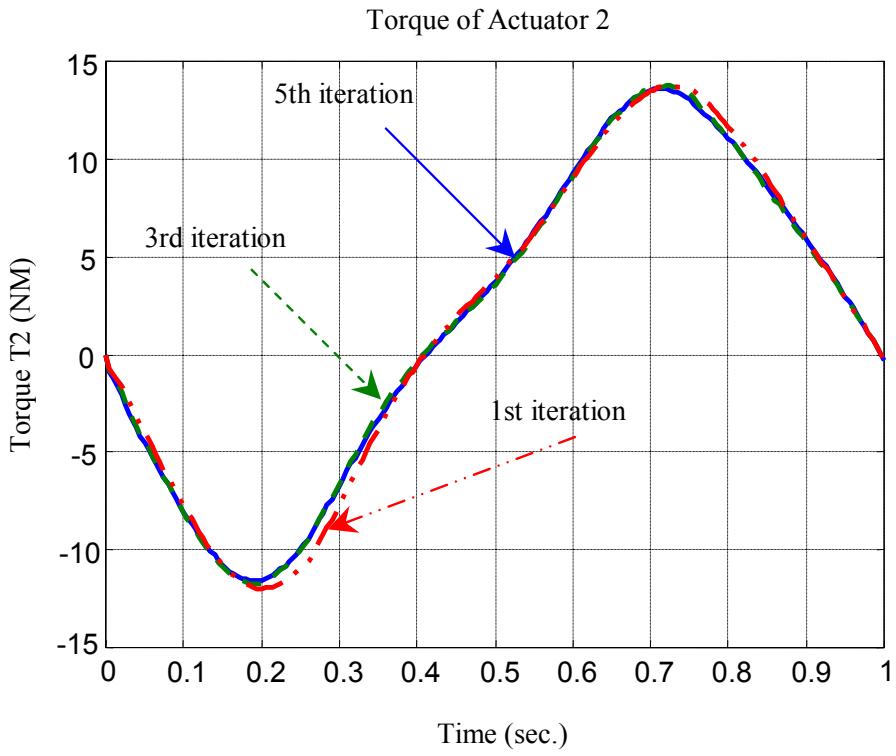

Figure 6.9 Torques profiles for actuators 1 and 2 for iterations j=1,3,5.

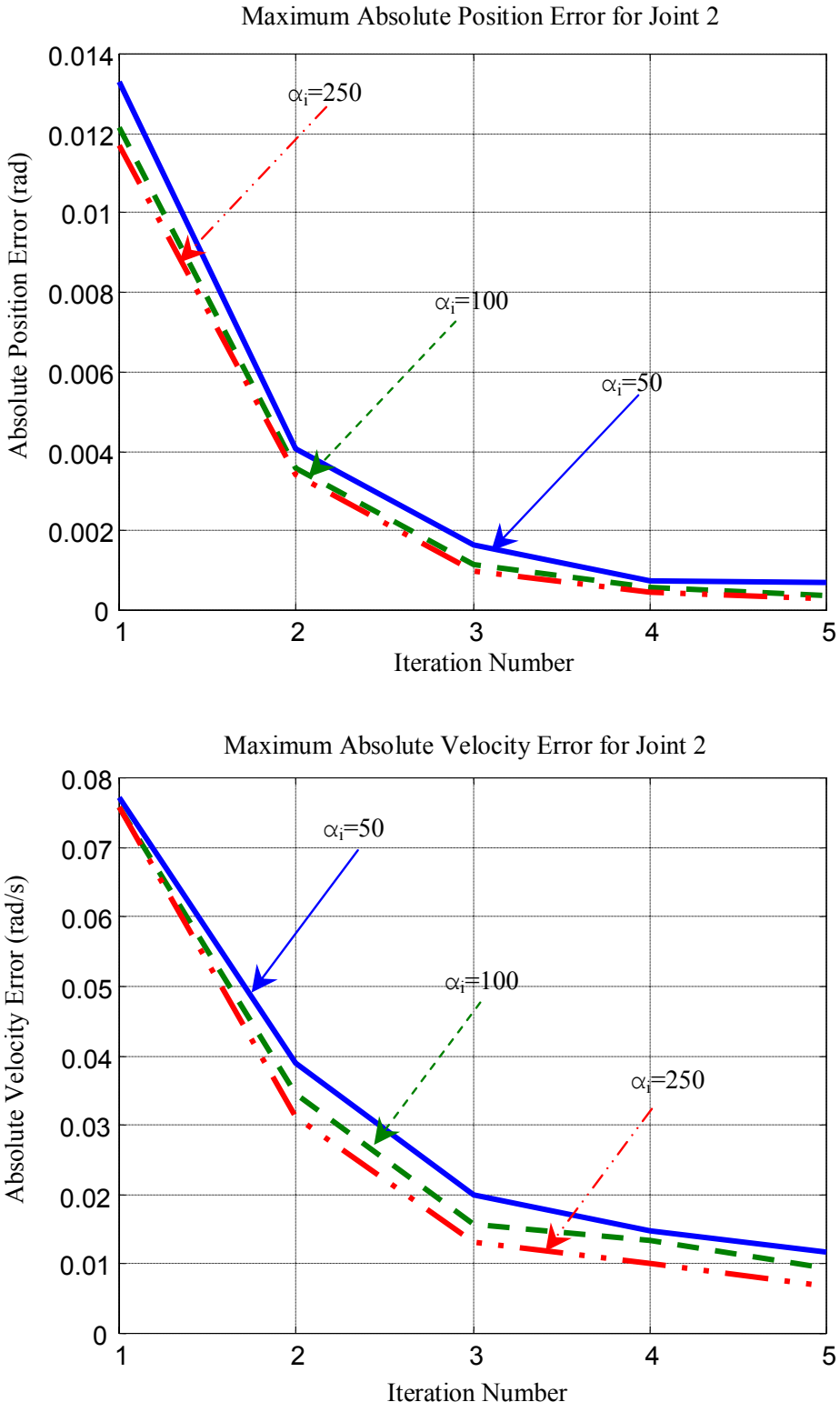

Figure 6.10 Position and velocity tracking errors under different control parameters.

The desired trajectories and the repeatable disturbances:

$$\begin{cases} q_1 = \sin 3t \\ \\ q_2 = \cos 3t \end{cases} \quad \text{for} \quad t \in [0,5] \tag{6.7}$$

$$\begin{cases} d_1(t) = 0.3\sin t \\ \\ d_2(t) = 0.1(1-e^{-t}) \end{cases} \quad \text{for} \quad t \in [0,5] \tag{6.8}$$

The control nonlinear gain matrices were as follows

$$K_p = K_d = \text{diag}\{20,10\}\,, \mathrm{K}_{\max} = 4\,,\ \mathrm{K}_{\min}=3,\ \alpha_i = 1000$$

Table 6.2 The tracking errors versus the iteration number (example 1)

Iteration	0	5	10	15	20
$\max\left\|e_1^j\right\|$ (rad)	0.8355	0.0313	0.0073	0.0027	0.0017
$\max\left\|e_2^j\right\|$ (rad)	0.2214	0.0123	0.0025	9.4E-4	5.5E-4
$\max\left\|\dot{e}_1^j\right\|$ (rad/s)	1.1291	0.2055	0.0804	0.0581	0.0462
$\max\left\|\dot{e}_2^j\right\|$ (rad/s)	0.4412	0.0475	0.0238	0.0166	0.0135

The simulation results from the first to the 20$^{\text{th}}$ iteration are listed in Table 6.2. Comparing the results using the proposed control scheme with those in Choi and Lee (2000), it was found that the adaptive NPD-LC achieved the better tracking performance with a fewer iteration number than the method developed by Choi and Lee (2000). Only after 15 iterations, the adaptive NPD-LC obtained more accurate trajectory tracking performance than the Adaptive-ILC in Choi and Lee (2000) with 30 iterations (the

maximum position errors for joint 1 and 2 were 0.0041 rad and 0.0046 rad at the 30th iteration, and 0.0149 rad and 0.0155 rad at the 20th iteration, respectively).

Table 6.3 shows another simulation result with the following control gains and user-defined constants.

$$K_p = K_d = \text{diag}\{20,10\}\,, \mathrm{K}_{\max} = 5, \quad \mathrm{K}_{\min} = 4\,, \ \alpha_i = 100$$

Table 6.3 The tracking errors versus the iteration number (example 2)

Iteration	0	4	8	12	16
$\max\left\|e_1^j\right\|$ (rad)	0.7400	0.0360	0.0056	0.0026	0.0018
$\max\left\|e_2^j\right\|$ (rad)	0.1907	0.0152	0.0029	0.0016	8.9E-4
$\max\left\|\dot{e}_1^j\right\|$ (rad/s)	0.9480	0.1232	0.0705	0.0518	0.0140
$\max\left\|\dot{e}_2^j\right\|$ (rad/s)	0.3595	0.0404	0.0254	0.0206	0.0175

From the results shown above, one can see that adaptive NPD-LC is a very promising control method in terms of good tracking performance, the simplification of the realization, and rejection of the random or repetitive disturbances for repetitive tracking tasks. Furthermore, the adaptive NPD-LC method has a faster convergence rate than other control methods reported in the literature (Choi and Lee, 2000; Tayebi, 2003).

6.4 Simulation of the Adaptive Switching Learning PD Control

In order to have some ideas about the effectiveness of the ASL-PD, a simulation study was conducted. Specifically two robotic manipulators were used. The first one was the same as in Section 6.3.2 for the purpose of comparing the ASL-PD method with the adaptive NPD-LC method discussed in previous section and the adaptive ILC proposed

in Choi and Lee (2000). Shown in section 6.3.2, the first one is a serial robotic manipulator. It is noted that the result for the serial robotic manipulator may not be applicable to the parallel manipulator. The second one is a parallel robotic manipulator, for which the effectiveness of the ASL-PD control method both in the trajectory tracking errors and the required torque in the motor were examined.

6.4.1 Trajectory Tracking of a Serial Robot Manipulator

For the purpose of comparison, the same example discussed in Section 6.3.2 was used. The physical parameters and desired trajectories can be found in Section 6.3.2. In the ASL-PD control method, the initial control gains are selected the same as the example in Section 6.3.2 and listed below:

$$K_p^0 = K_d^0 = \text{diag}\{20,10\}$$

The control gains are switched from iteration to iteration based on the following switching rule:

$$\begin{cases} K_p^j = 2jK_p^0 \\ \\ K_d^j = 2jK_d^0 \end{cases} \qquad j = 1,2,\cdots,N \tag{6.9}$$

Figure 6.11(a) shows the tracking performance for the initial iteration, where only the PD control with small control gains was used, and no feedforward was used. It can be seen that the tracking performance is not acceptable because the errors were too large for both joints. However, at the sixth iteration where the ASL-PD control method was applied, the tracking performance was improved dramatically as shown in Figure 6.11(b). At the eighth iteration, the performance was very good (Figure 6.11(c)). It is further noted here that there were repeatable disturbances at each iteration. This implies that the ASL-PD control method can provide a good rejection capability for repeatable disturbances.

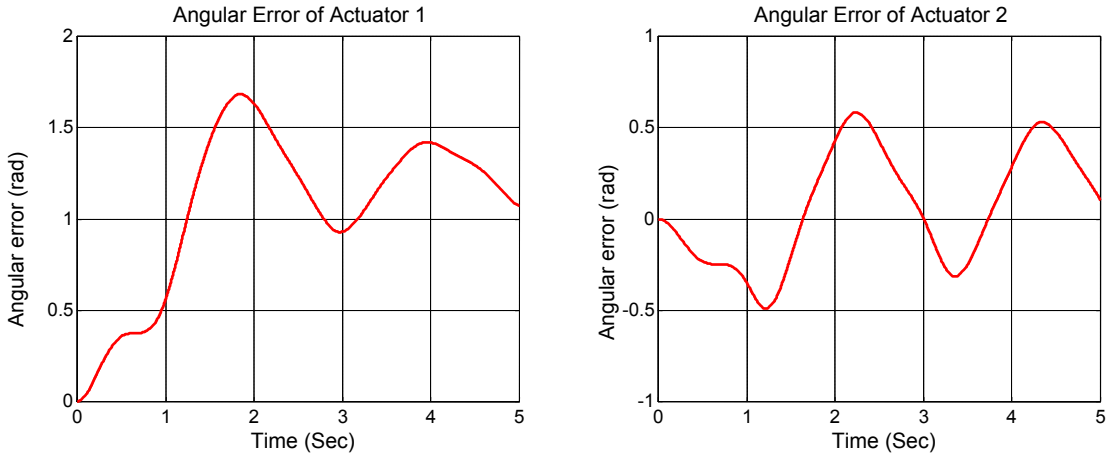

(a) Angular errors for two joints in the initial iteration

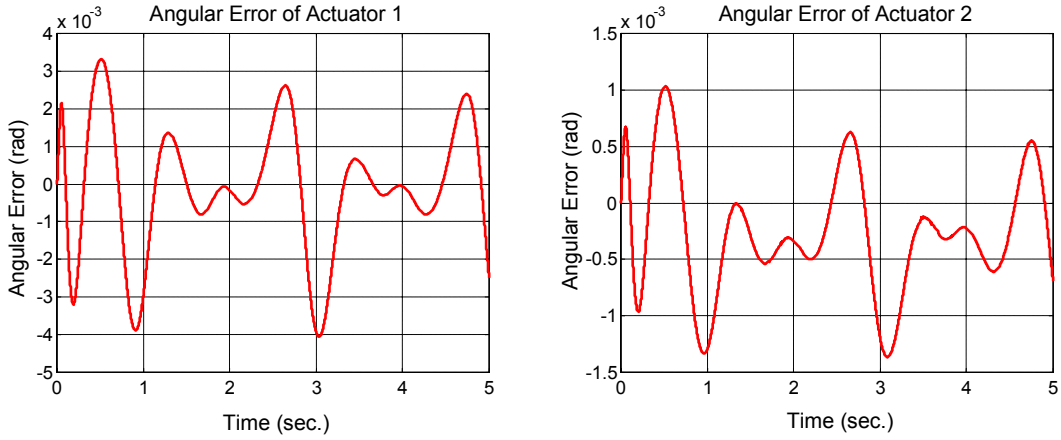

(b) Angular errors for two joints at the 6th iteration

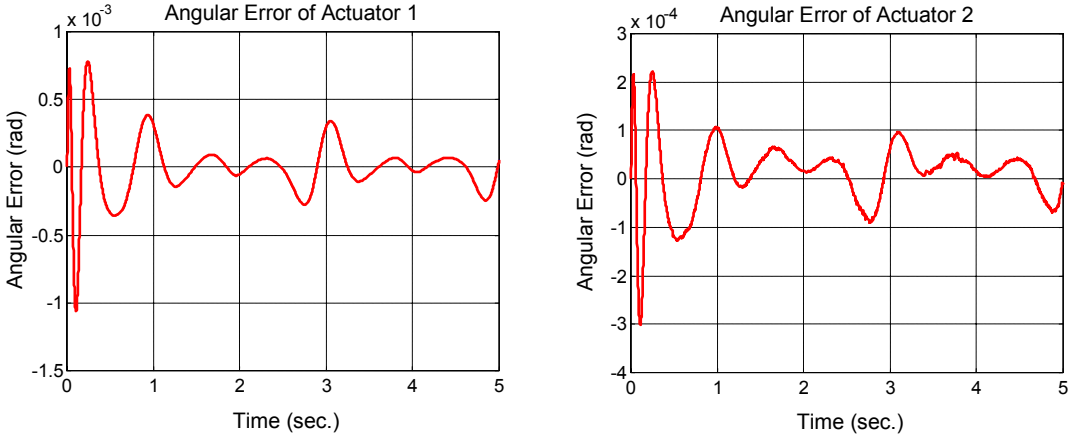

(c) Angular errors for two joints at the 8th iteration

Figure 6.11 Position tracking performance for different iterations.

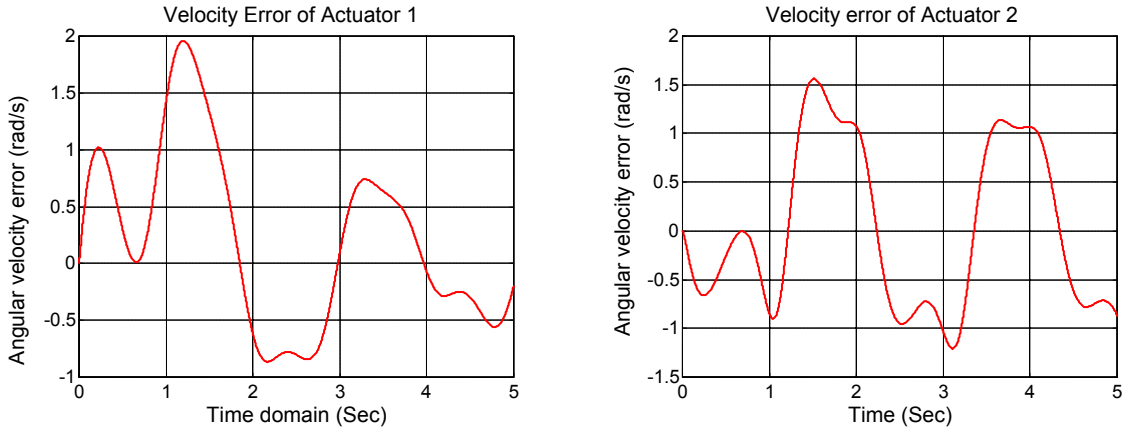

(a) Velocity errors for two joints in the initial iteration

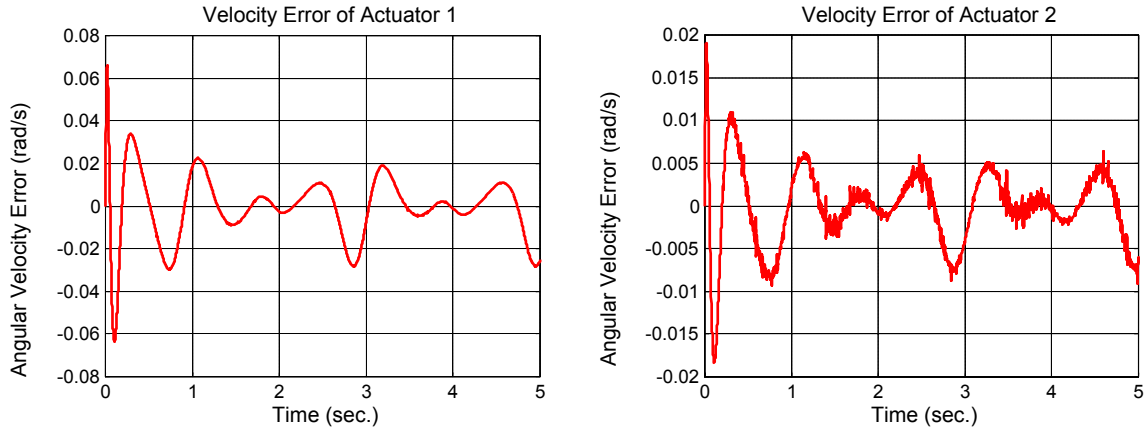

(b) Velocity errors for two joints at the 6th iteration

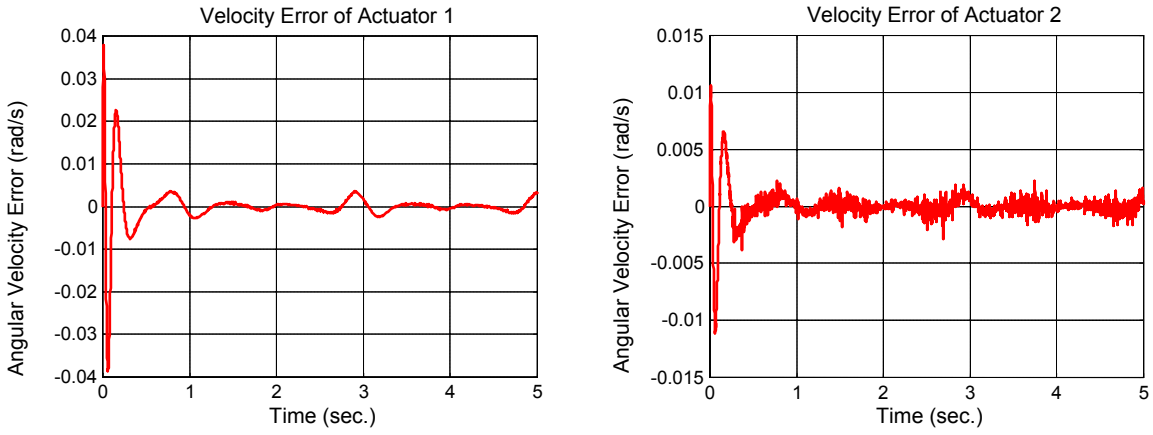

(c) Velocity errors for two joints at the 8th iteration

Figure 6.12 Velocity tracking performance for different iterations.

The velocity tracking performance was shown in Figure 6.12. From it one can see that the velocity errors reduced from 1.96 (rad/s) at the initial iteration to 0.0657 (rad/s) at the sixth iteration, and further to 0.0385 (rad/s) at the eighth iteration for joint 1. The similar decreasing trend can be found in joint 2. From Figures 6.11 and 6.12 it can be seen that the tracking performances were improved incrementally with the increase of the iteration number.

As the gain switching rule in Eq. (6.9) was introduced at each iteration, the convergence rate increased greatly compared with the control method used in Choi and Lee (2000). Table 6.4 shows the trajectory tracking errors from the initial iteration to the eighth iteration. From Table 6.3 it can be seen that the tracking performance is considerably improved at the sixth iteration. The maximum position errors for joints 1 and 2 are 0.0041 rads and 0.0014 rads, respectively, while the similar results were achieved after thirty iterations using the adaptive ILC in Choi and Lee (2000) (The maximum position errors for joints 1 and 2 were 0.0041 and 0.0046 (rad), respectively). Therefore, the comparison of their method and our method demonstrated a fast convergence rate with the ASL-PD control method. It should be noted that the comparison of the velocity errors is not done as such information was not presented in Choi and Lee (2000).

Table 6.4 Trajectory tracking errors from iteration to iteration

Iteration	0	2	4	6	8
$\max\left\|e_1^j\right\|$ (rad)	1.6837	0.4493	0.0433	0.0041	0.0011
$\max\left\|e_2^j\right\|$ (rad)	0.5833	0.1075	0.0122	0.0014	3.01E-4
$\max\left\|\dot{e}_1^j\right\|$ (rad/s)	1.9596	0.7835	0.1902	0.0657	0.0385
$\max\left\|\dot{e}_2^j\right\|$ (rad/s)	1.5646	0.2534	0.0523	0.0191	0.0111

Comparing Table 6.4 with Tables 6.2 and 6.3, the following observations can be made. In the initial iteration, there is no feedforward control for both control laws. So the

adaptive NPD-LC became a NPD control and the ASL-PD control became a PD control. As the NPD control used larger control gains than the PD control in the simulations. Therefore, the tracking errors for the NPD control are smaller than that for the PD control; see Tables 6.2 – 6.4 for iteration 0. For the adaptive NPD-LC law, when the iteration cycle continues, the tracking errors become smaller and smaller, the nonlinear control gains trend to be constant ones. Therefore, the convergence speed slowed down compared with the first few iteration cycles. On the other hand, for the ASL-PD control, the control gains increased from iteration to iteration, which accelerated the convergence speed. The tracking errors (after 8 iteration cycles using the ASL-PD control) were the same as those using the adaptive NPD-LC (after 16 or 20 iteration cycles). It means that the ASL-PD control has a faster convergence speed than the adaptive NPD-LC.

6.4.2 Trajectory Tracking of a Parallel Robot Manipulator

A two DOF parallel robotic manipulator shown in Figure 3.1 is used as an example; the physical parameters used in the simulation are listed in Table 6.5. The details for the dynamics of the parallel robot manipulator were discussed in Chapter 3.

Table 6.5 Physical parameters of the parallel robotic manipulator

link	m_i (kg)	l_i (m)	r_i (m)	I_i (kgm^2)	θ_i (rad)
1	1	0.4	0.2	0.5	0
2	1.25	0.6	0.3	1	0
3	1.5	0.8	0.3	1	0
4	1	0.6	0.2	0.5	0
5	-	0.6	-	-	-

The end-effector of the manipulator is required to move from point A(0.7, 0.3), to point B(0.6, 0.4), and to point C(0.5,0.5). The time duration between two nearby points is 0.25 seconds. The control was carried out at the joint level where the inverse kinematics is used to calculate the joint position and velocity associated with the specific path of the end-effector. The path was designed to pass through these three points with the objective of meeting the positions, velocities, and accelerations at these three points using the motion planning method in Ouyang (2002).

In this example, the control gains are selected as follows

$$K_p^0 = \text{diag}\{20, 20\}\,, \quad K_d^0 = \text{diag}\{12, 12\}$$

The gain switching rule is set to be

$$K_p^j = 2\,jK_p^0\,, \quad K_d^j = 2\,j\,K_d^0 \quad \text{for } j = 1, 2, ..., N$$

Figure 6.13 shows the position tracking performance improvement for the two actuators from iteration to iteration. From it one can see that, at the initial iteration, the maximum position errors were about 0.11 and 0.38 rad, respectively; only after four iterations, the maximum position errors were reduced to 0.08 and 0.05 rad, respectively; Finally, after eight iterations, the maximum errors were reduced to 0.0003 and 0.0008 rad, respectively.

Figure 6.14 shows the velocity tracking performance improvement for the two actuators. At the initial iteration, the maximum velocity errors were about 1.17 and 2.68 rad/s in the two actuators, respectively. But after four iterations, the maximum values were reduced to 0.15 and 0.14 rad/s. After eight iterations, the maximum errors in the two actuators became 0.0046 and 0.0102 rad/s for velocity, respectively.

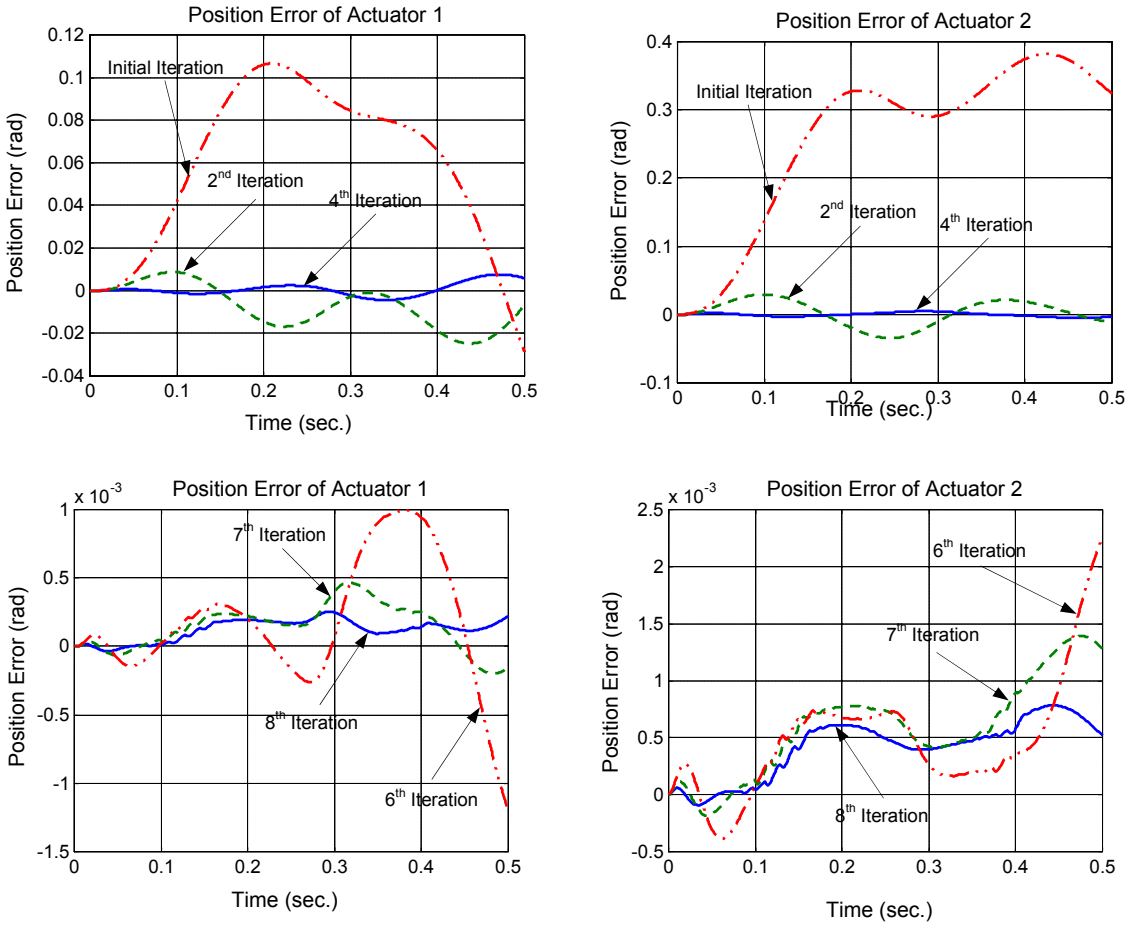

Figure 6.13 Position error tracking improvement from iteration to iteration.

It should be noted that, while the tracking performance improved from iteration to iteration, the torques required to drive the two actuators were nearly the same from iteration to iteration after a few iterations. This can be seen from Figure 6.15, especially for actuator 2 from the fifth iteration to the eighth iteration. It can be seen also from Figure 6.15 that the profiles of the required torques are very smooth even as the control gains became larger when the iteration number increased. Such a property is very useful for the safe use of the actuators and the attenuation of vibration of the controlled plant. It is noted that this property was missed in the switching technique used in the time domain.

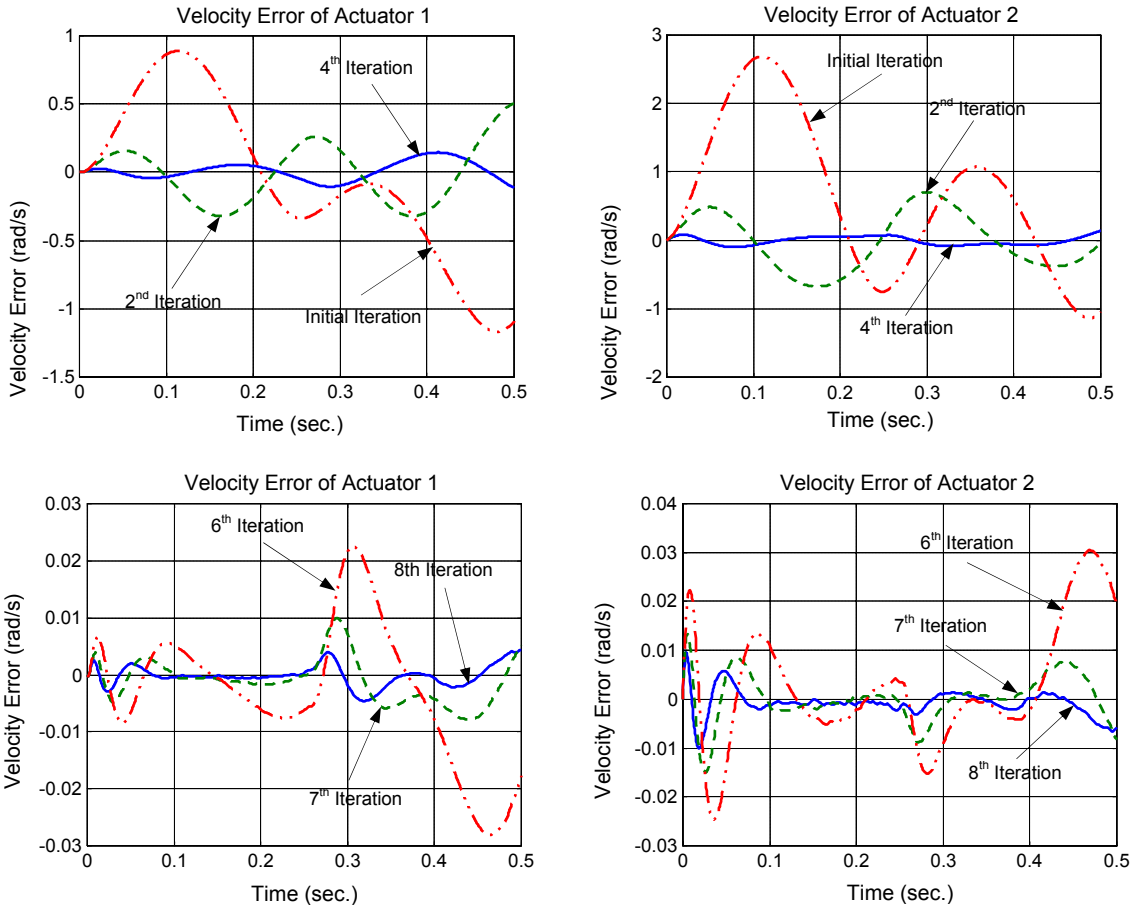

Figure 6.14 Velocity error tracking improvement from iteration to iteration.

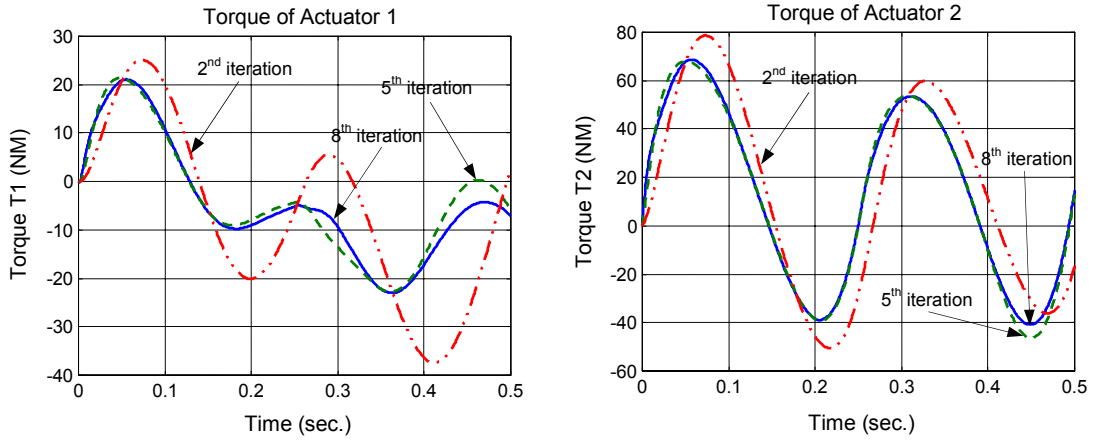

Figure 6.15 Required torque profiles from iteration and iteration.

6.5 Experiments for the Hybrid Control Systems

In this section, some experiments are conducted to verify the effectiveness of the proposed adaptive PD-type learning control laws for the trajectory tracking control of a parallel robotic manipulator.

6.5.1 Experiment Setup

A 2 DOF parallel manipulator shown in Figure 6.16 was used for the trajectory tracking where two servomotors drive the two input links directly. The desired trajectories for the two servomotors are defined as follows:

$$q_1(t) = 2\pi * (6\frac{t^5}{t_f^5} - 15\frac{t^4}{t_f^4} + 10\frac{t^3}{t_f^3}) \text{ with } t_f = 4 \text{ sec.}$$

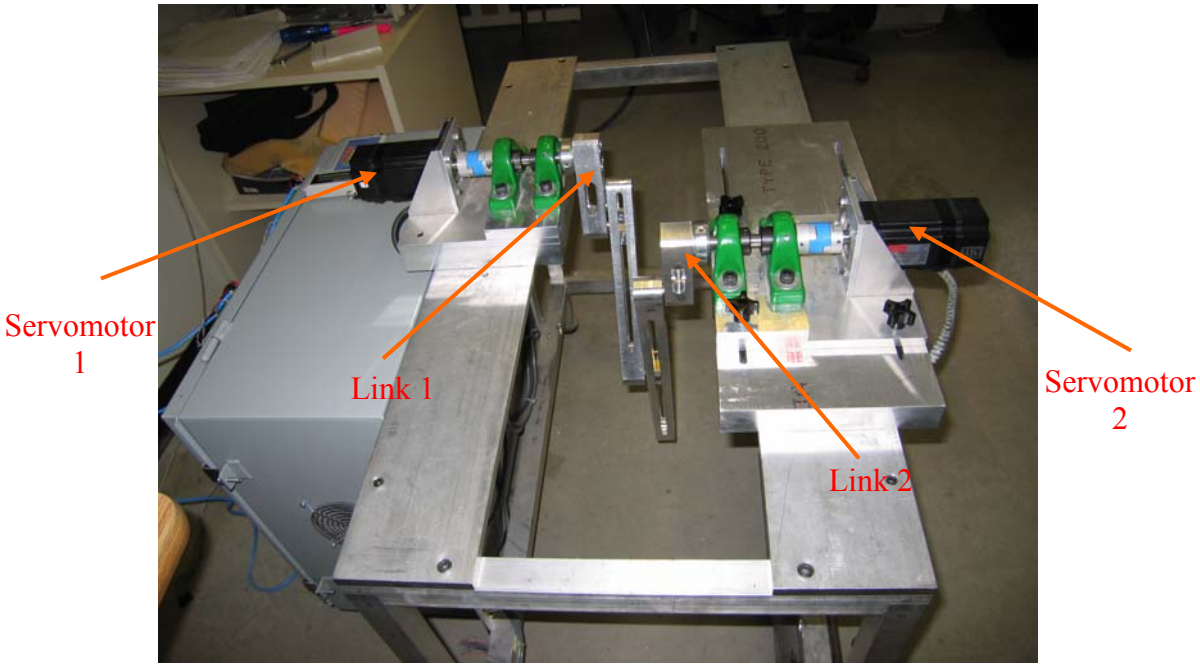

Figure 6.16 Experiment setup for the hybrid control system.

6.5.2 Experimental Results Using the Adaptive NPD-LC Law

In this experiment, four tests were carried out under different control parameters. For all four cases, the PD control gains are selected the same as follows.

$$K_p = diag\{0.00002,\ 0.00002\},\ K_d = diag\{0.000002,\ 0.000002\}.$$

The nonlinear parameters are selected differently for each case as follows.

Case 1: $K_{\max} = 2.12$, $K_{\min} = 1$, and $\alpha = 0.5$

Case 2: $K_{\max} = 2.3$, $K_{\min} = 1$, and $\alpha = 0.9$

Case 3: $K_{\max} = 2.6$, $K_{\min} = 1$, and $\alpha = 1.2$

Case 4: $K_{\max} = 2.9$, $K_{\min} = 1$, and $\alpha = 1.5$

For each test, the experiments were performed from iteration to iteration at nearly the same initial condition. As the encoder used in the experiment was a relative one, one can not make sure that the initial position of each experiment was exactly the same from experiment to experiment. For case 2, Figures 6.17 and 6.18 show the adaptive NPD-LC results from iteration to iteration for joint 1 and joint 2, respectively. In the first iteration, the maximum tracking errors were about 0.25 rad for two joints. After 7 iterations, the maximum tracking error was about 0.03 rad for joint 1 and 0.02 rad for joint 2, respectively. From these two figures, one can see the trajectory performance improvement from iteration to iteration. The other three tests also demonstrated the similar conclusion.

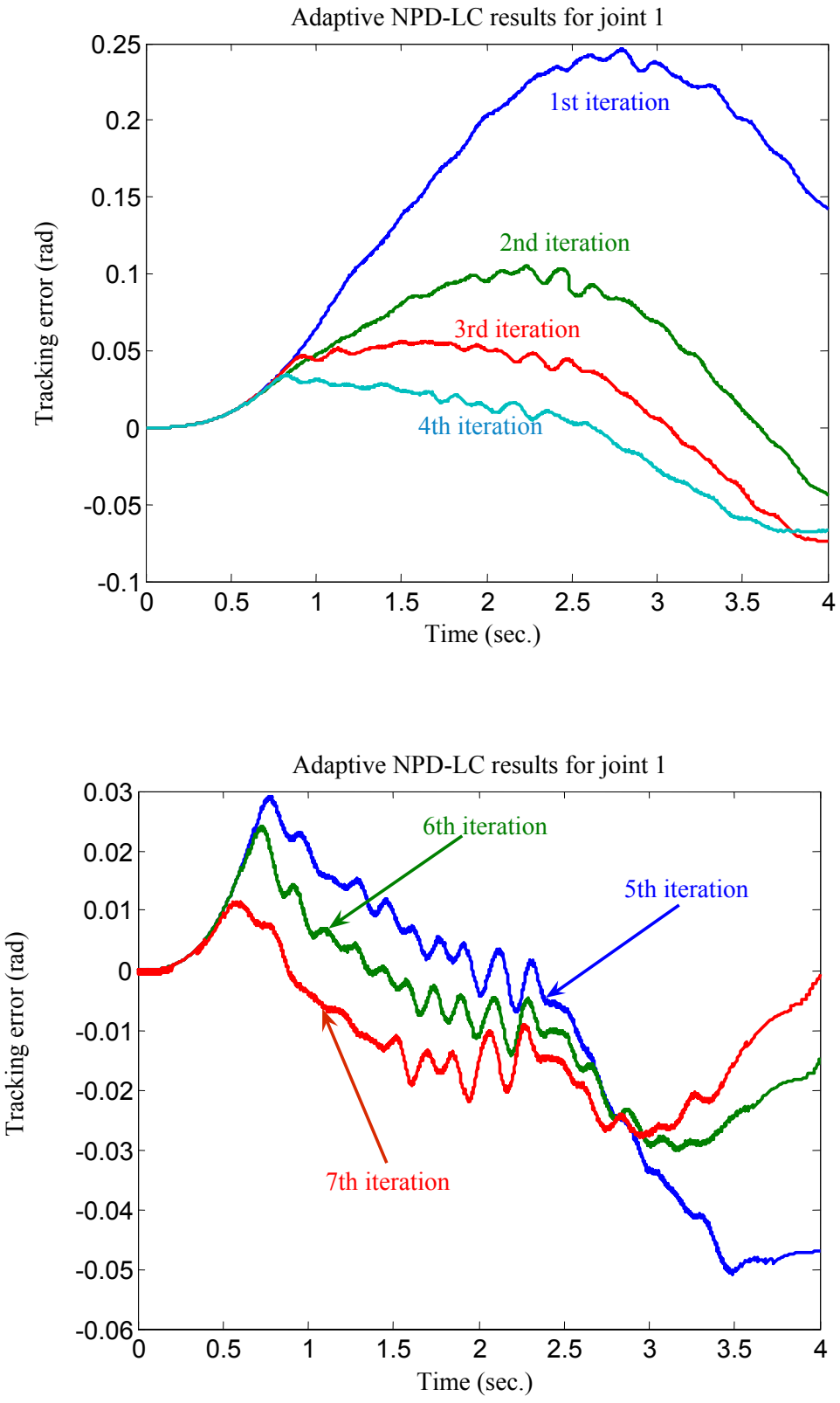

Figure 6.17 Adaptive NPD-LC control results from iteration to iteration for joint 1.

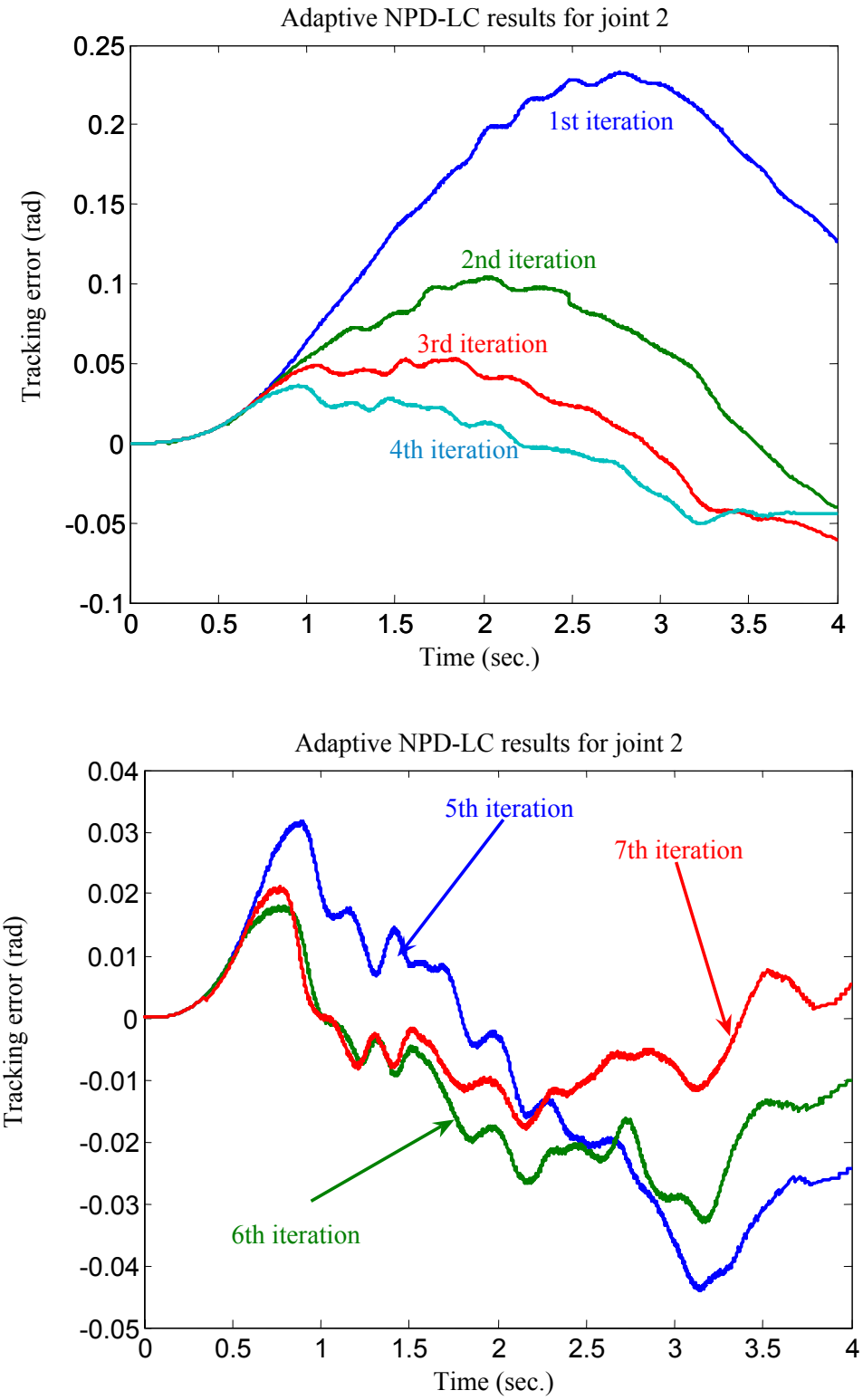

Figure 6.18 Adaptive NPD-LC control results from iteration to iteration for joint 2.

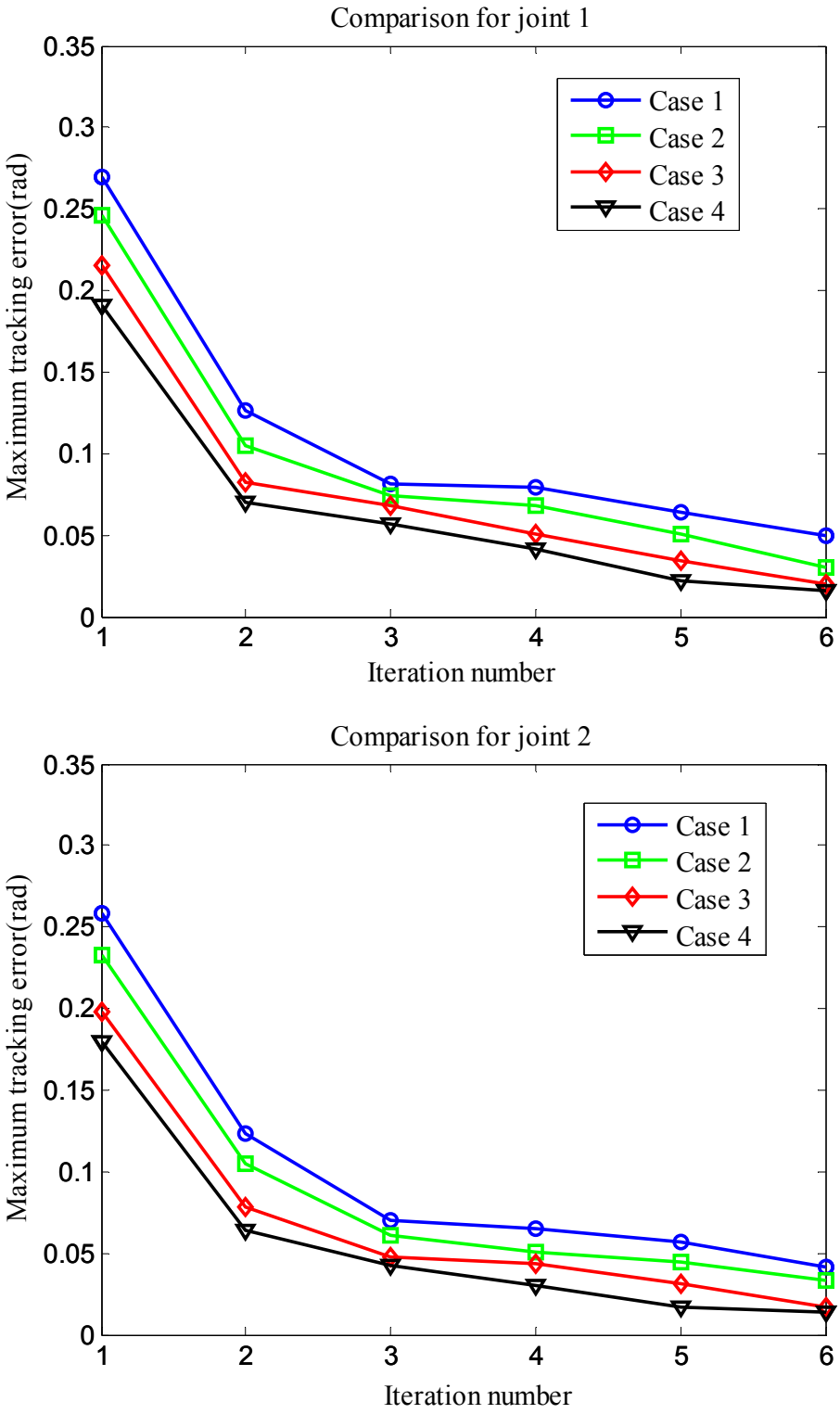

Figure 6.19 Adaptive NPD-LC control results under different control parameters.

To examine the effect of the nonlinear parameters on the tracking performance using the adaptive NPD-LC method, Figure 6.19 shows the maximum tracking errors for the four cases from iteration to iteration. From this figure, one can see that, with the increase of the nonlinear parameters, the tracking performance can be improved. This conclusion coincides with that obtained from the simulation study and the theoretical analysis as presented previously.

6.5.3 Experimental Results Using the ASL-PD Control Law

In the experiments, for the ASL-PD control, the initial PD control gains are selected as: $K_p = diag\{0.00002,\ 0.00002\}$, $K_d = diag\{0.000002,\ 0.000002\}$, and the switching gain factor is set $\beta = 2$. It can be seen that the PD control gains of the ASL-PD control are selected the same as that of the adaptive NPD-LC. Figure 6.20 shows the experimental result from iteration to iteration. From this figure, one can see that the tracking performance improved clearly from iteration to iteration.

To demonstrate the effectiveness of the ASL-PD control, the ASL-PD control results were compared with the PD control results. For the PD control, the control gains were selected as: $K_p = diag\{0.00022,\ 0.00022\}$, and $K_d = diag\{0.00055,\ 0.00055\}$. It should be noted that the control gains obtained are almost the optimal ones for the PD control after the trial and error experiments.

Comparing the control gains in the PD control and the ASL-PD control, one can see that the proportional gains of the PD control only is ten times larger than that of the ASL-PD control, while the derivative gains of the PD control is 25 times larger than that of the ASL-PD control. The tracking errors using the PD control and the ASL-PD control are depicted in Figure 6.21. From this figure, it can be seen that the ASL-PD control obtained much better tracking performance for both of the joints than the PD control did where large control gains were used.

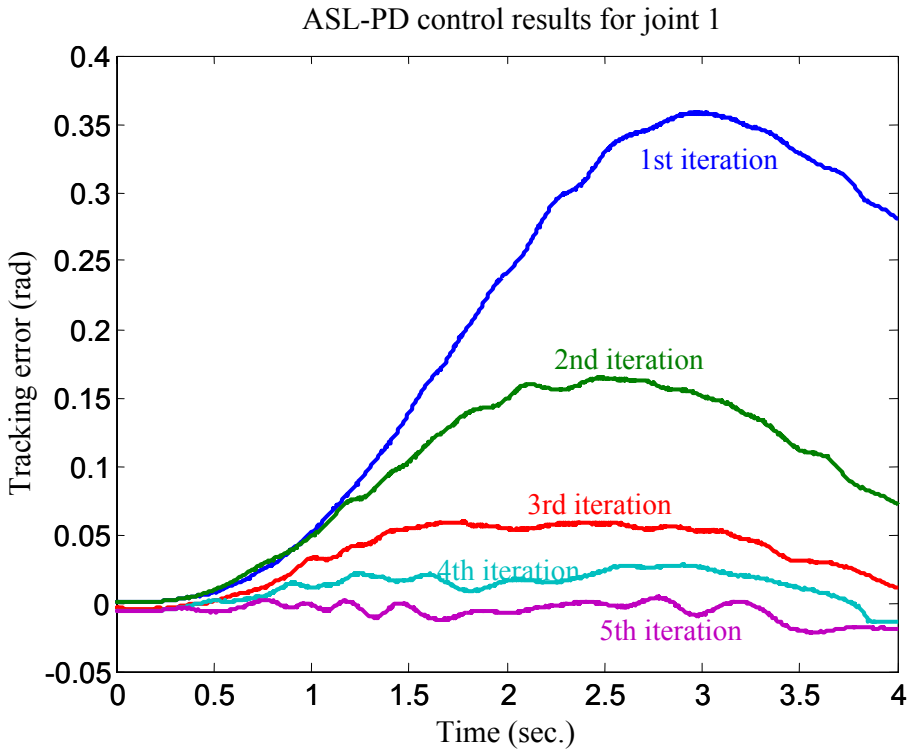

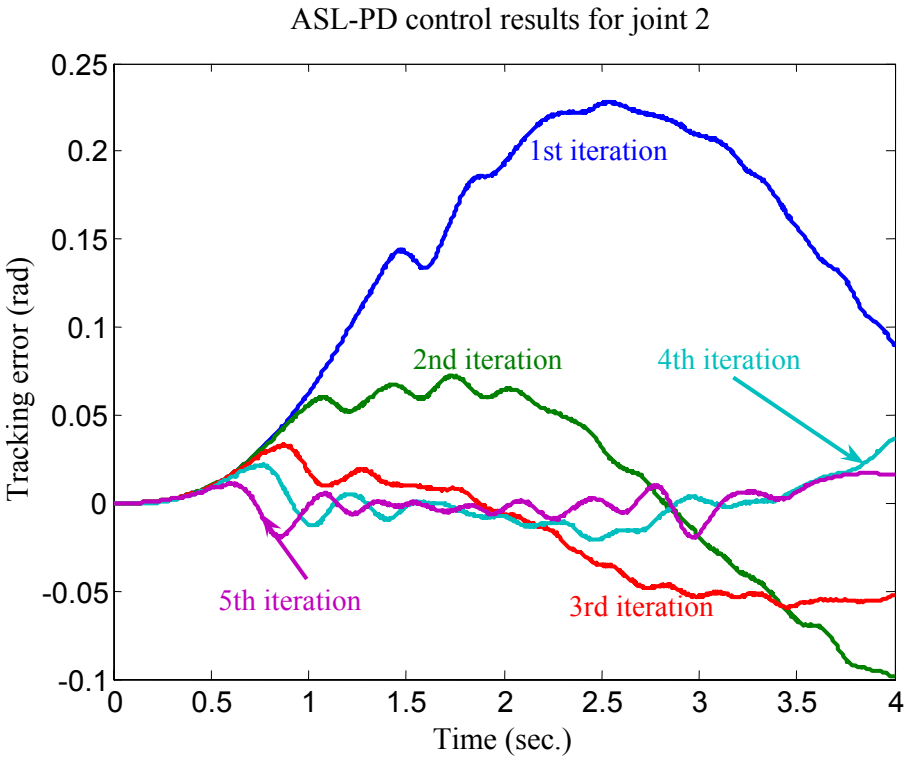

Figure 6.20 ASL-PD control results from iteration to iteration.

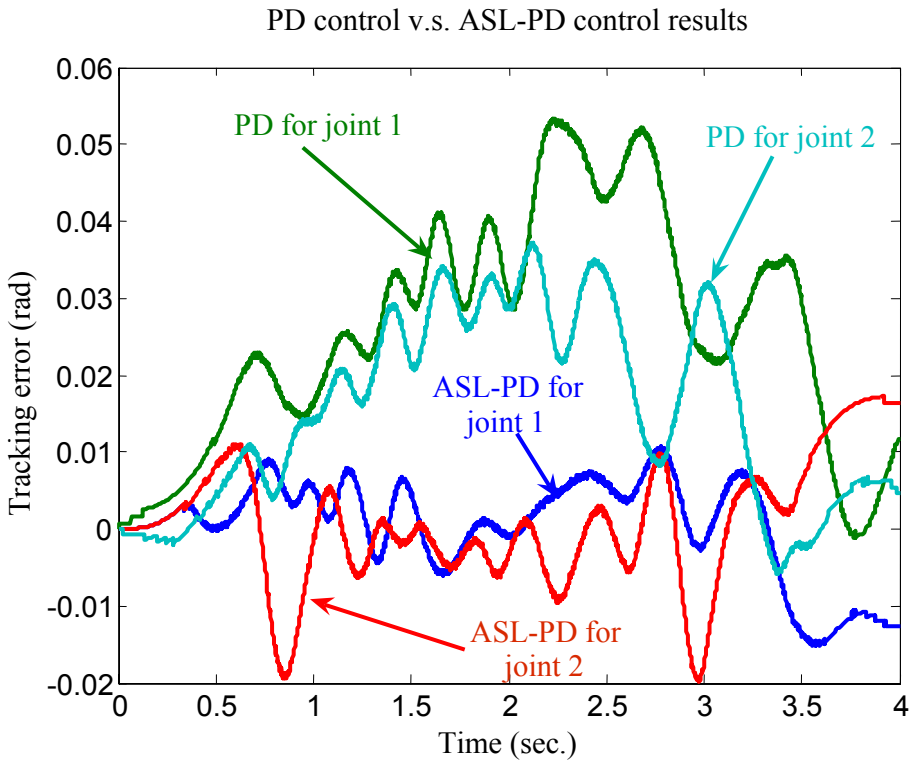

Figure 6.21 Comparison of the PD control and the ASL-PD control.

6.5.4 Comparison of the ASL-PD and the Adaptive NPD-LC

As shown in the previous two sections, the adaptive NPD-LC and the ASL-PD control could be used to improve the tracking performance of the parallel robotic manipulator. It should be noted that the convergence rate was different. Generally speaking, the ASL-PD control has a faster convergence rate than the adaptive NPD-LC. Figure 6.22 shows the comparison results obtained from the experiments. From this figure, one can see that the tracking errors after 5 iterations using the ASL-PD control were better than the tracking errors after 7 iterations using the adaptive NPD-LC. Such a conclusion agrees with the theoretical analysis and the simulation results as presented before.

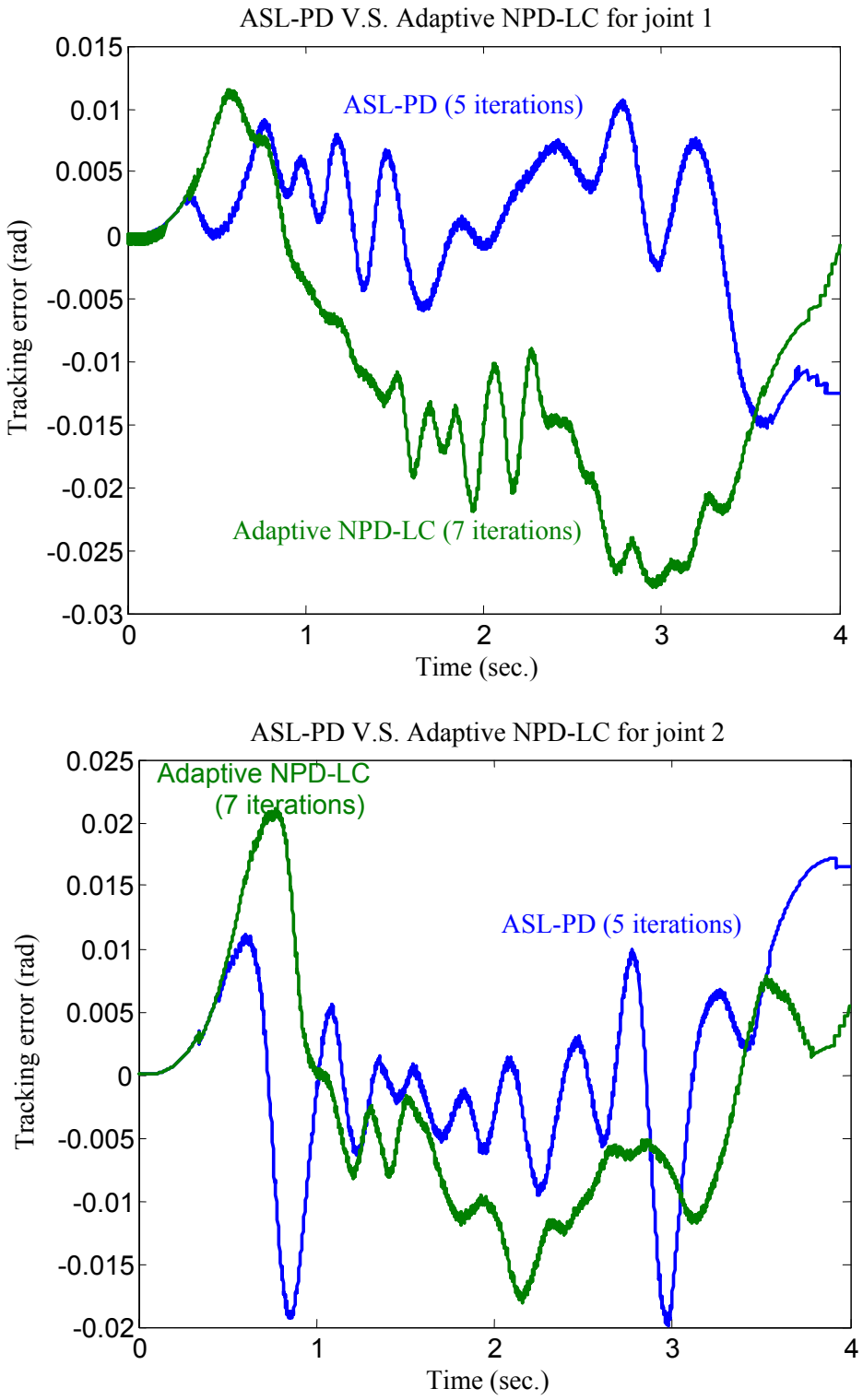

Figure 6.22 Comparing results of the adaptive NPD-LC and the ASL-PD.

6.5.5 Comments about the Experiments

The experiments performed in this section are based on some simplifications. The results are acceptable for the purpose of demonstrating the effectiveness of the proposed control algorithms, but they are not good enough for the accurate tracking of the system. The following problems have significant effects on the final tracking performance and need to be addressed in the real applications.

6.5.5.1 The initial position error problem.

The servomotor has only a relative position encoder. In the iteration running mode, one cannot ensure that the initial position is the same from iteration to iteration. This means that there are some initial position errors when the adaptive NPD-LC and the ASL-PD control are used in the experiments. The initial position error will affect the trajectory tracking performance of the control system. One solution for this problem is the use of an absolute position encoder.

6.5.5.2 The sampling timer problem

The second problem in the experiments is the inaccuracy of the sampling timer. In the learning control algorithms, the equation $T_{j+1}(t) = T_j(t) + T_{j+1,fb}(t)$ requires that the sampling timer be very accurate and be the same from iteration to iteration. Based on the experimental observation, it was very difficult to get the same sampling timer even when the high resolution timer in the Windows XP was used. The reason can be explained as follows. The Windows XP is a multiply task operating system, and there are a lot of system programs running at the same time. Because a timer's accuracy depends on the system clock rate and how often the application retrieves messages from the message queue, the time-out value is only approximate. The minimum value of the sampling timer is about 2 ms, or the sampling frequency is about 500 Hz. Such a sampling timer is not small enough for the purpose of trajectory tracking control. In addition, experiments showed that the sampling timer varied from 2 ms to 4 ms in a random pattern. In the

implementation of the experiment, the assumption of the equal sampling timer was applied to the control algorithms. Such an assumption was not always true. Therefore, the inaccuracy of the sampling timer directly affected the tracking performance. The solution to this problem is the use of a hardware device such as dSPACE which can provide the accurate and small sampling timer.

6.5.5.3 The velocity error problem

For the PD type learning control methods, not only the position information but also the velocity information is needed to form the PD feedback control. In the present experiments, only the position information was obtained from the relative position encoder. The actual velocity was estimated based on the current sampling position value and the previous one. In such a way, only the average velocity was obtained by calculation. Therefore, a smaller sampling timer yields a more accurate calculated velocity, one that is closer to the true instantaneous velocity. However, if the sampling timer of the encoder was large and inaccurate, the calculated velocity could become inaccurate too. The inaccuracy of the actual velocity affects the control torque and further affects the tracking performance of the control system. A possible solution to avoid the estimated velocity is to use a speed sensor such as a Tachometer.

6.5.5.4 The control gain tuning problem

The selection of the control gain is very important in the experiment. Small control gains will result in the large tracking errors, while big control gains may cause saturation of the system. In practice, the selection of the control gain depends on the desired trajectory and the configuration of the system and is based on the trial and error method. The purpose of the experiments conducted in this section was to demonstrate the effectiveness of the proposed PD type learning control algorithms, so little attention was paid to the selection of the control gain. A systematic procedure could be developed using the gain tuning method in the literature (Ellis, 2004).

6.6 Experiments of the Compliant Mechanical Amplifier

Based on the structure design discussed in Section 4.3, a prototype CMA was built from stainless steel using the wire EDM. In this section, the static experiments are conducted first followed by the dynamic experiments.

6.6.1 Experiment Setup

Several experiments were performed on the CMA to characterize its behaviour under various prestress conditions. The experiment setup is shown in Figure 6.23. In this setup, two PZT actuators (AE0505D16, size 20 x 5 x 5, Tokin) were installed between the two driving links and a mechanism was used to adjust the prestress of the PZT actuators. A high voltage amplifier (ENV 400, Piezosystem Jena) was used to supply high voltages about 150 V. To measure the displacement of the PZTs, the strain gauges were glued to two sides of PZT actuators and acted as a pair. The strain gauges were calibrated using the Kaman measuring device (SMU-9000). An eddy current sensor (15N-001, Kaman SMU-9000) with high resolution (10 *nm*) and precision (0.1% of the full range) was used to measure the output displacement of the compliant mechanical amplifier.

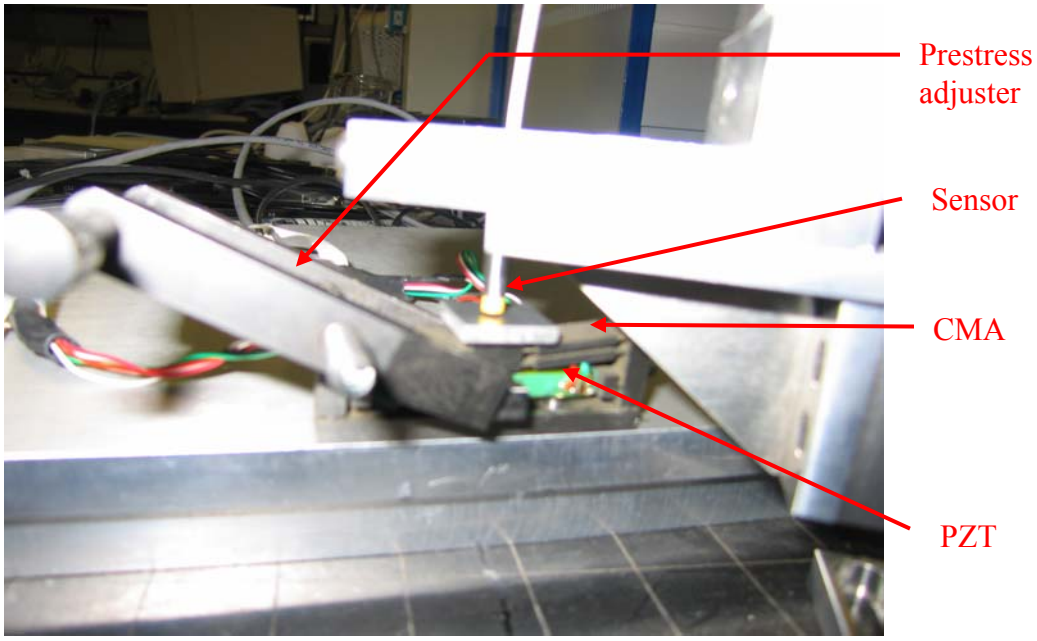

Figure 6.23 Experiment setup of the CMA.

6.6.2 Experiment procedure

For the static experiments, the dSPACE hardware was used as the controller. The PZT actuators were driven by the PZT amplifiers through the control of the input voltage. The stroke of the PZT actuators was measured using the strain gauge attached to the PZTs and then obtained by the controller through the ADCs of the dSPACE. The output of the CMA was captured using the eddy current sensor and recorded by a voltmeter. Figure 6.24 shows the schematic of the experiment setup.

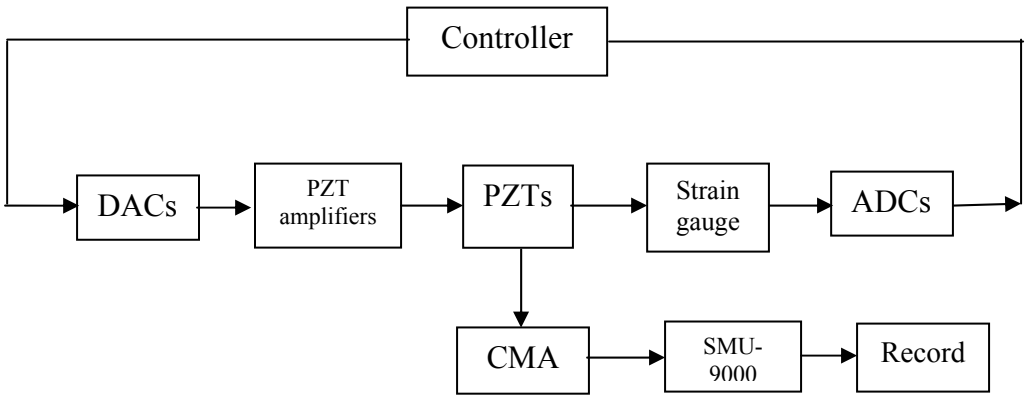

Figure 6.24 Schematic of the CMA experiment setup.

For the dynamic experiments, the PZT amplifiers were directly connected with the signal generator of the dynamic analyzer where a pseudo random signal was produced, and the output of the CMA measured by the sensor was sent to the dynamic analyzer also. In such a way, the dynamic analysis was completed by the dynamic analyzer and the results were recorded.

6.6.3 Experiment Results and Discussions

6.6.3.1 Static experiment

The purpose of the static experiments was to examine the amplification ratio of the designed CMA and the repeatability of the experiments. Three different prestress conditions (low, middle, and high prestress) were performed. In each prestress condition,

three tests were completed. Figures 6.25 to 6.27 show the experiment results for these three cases. In the experiments, the PZT actuator was given a voltage increase of 16V for each step test. The PZT displacement was measured through the calibrated strain gauge. From these three figures, one can see that the CMA can produce about 200 μm displacement when the PZT actuator applied a voltage of 112V. The repeatability of the experiments was very good for all three cases. Also one can see that with the increase of the prestress, the amplification ratio increases as well. The experiment results are quite agreeable with the FEA results.

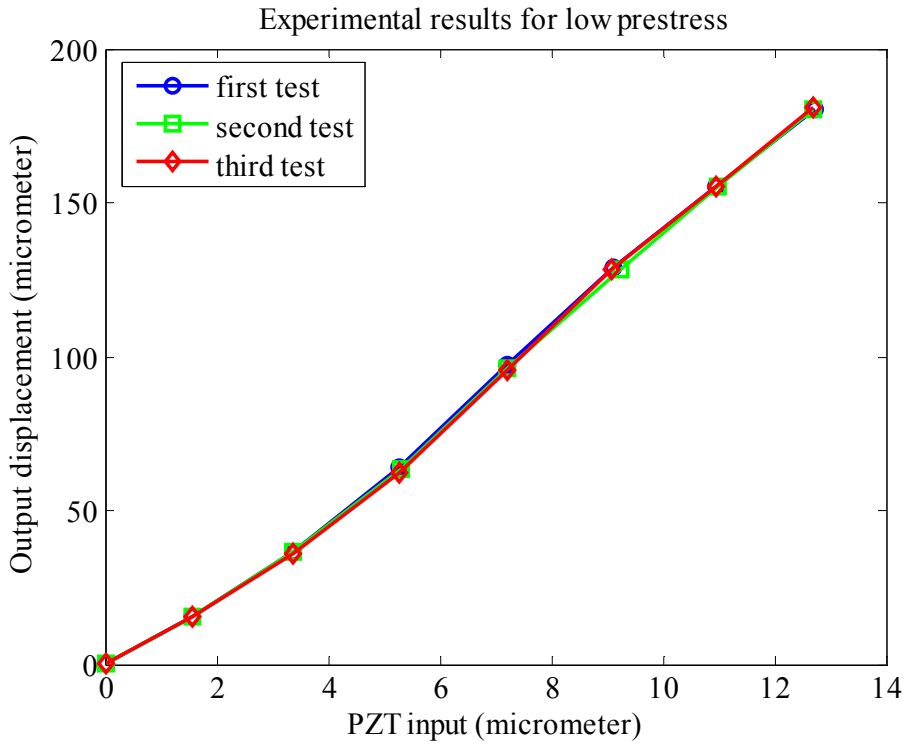

Figure 6.25 Static experiment of the CMA – Case 1.

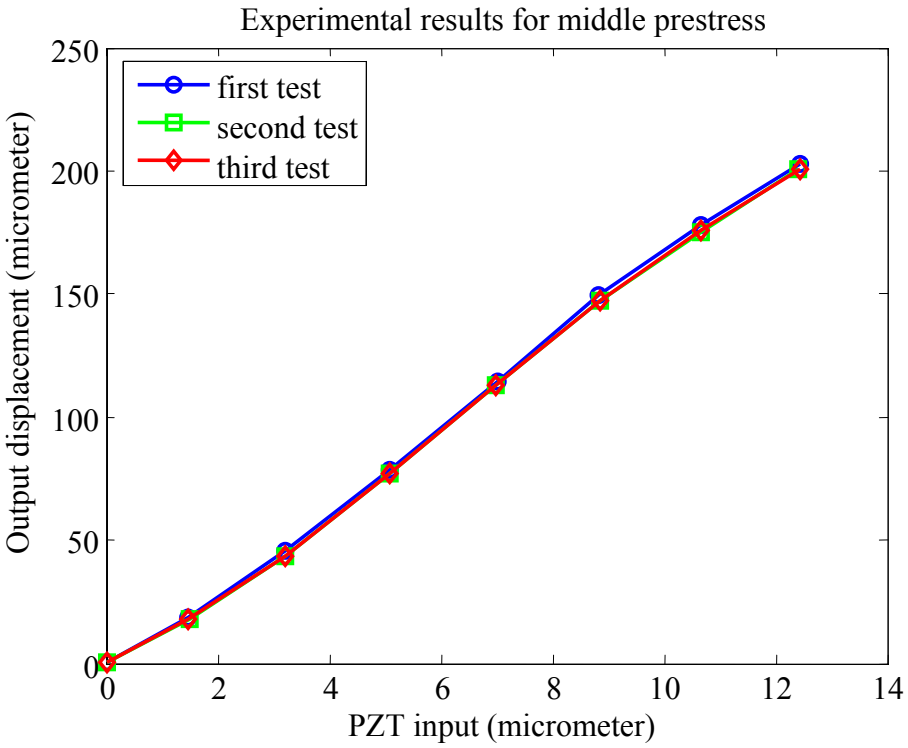

Figure 6.26 Static experiment of the CMA – Case 2.

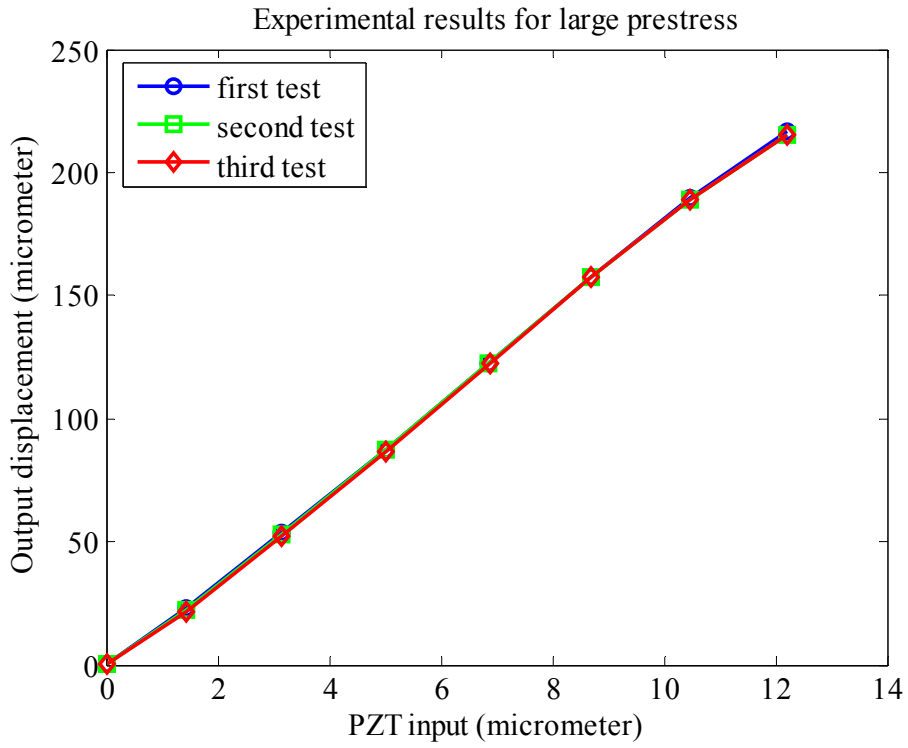

Figure 6.27 Static experiment of the CMA – Case 3.

6.6.3.2 Prestress effects

To hold the PZT actuator in the CMA and to help prevent separation, the CMA is preloaded by manipulating the prestress adjuster. In this circumstance, the prestress exists in the system, and it will affect the amplification ratio of the CMA. Figure 6.28 shows the experiment results under different prestress conditions.

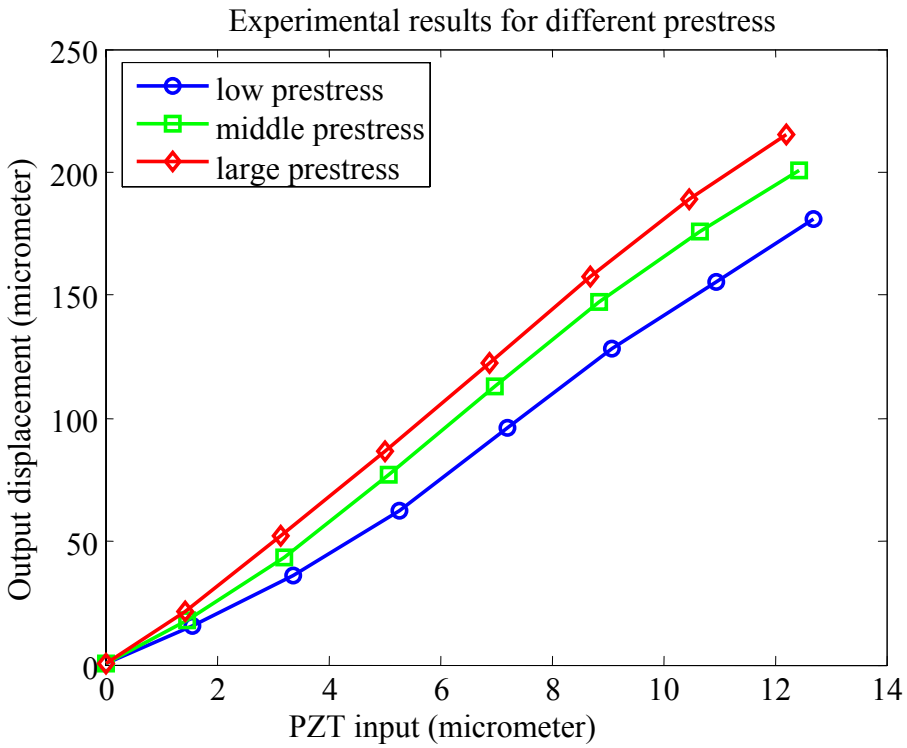

Figure 6.28 Prestress effects on amplification of the CMA.

From this figure, one can see that with the increase of the prestress acted on the PZT actuator, the amplification ratio will increase as well. Such a phenomenon can be explained as follows. Different prestress will produce different initial height h of the CMA. The larger the prestress the smaller the initial height h. According to the discussion in Section 4.3, a small initial height h will produce a big amplification ratio. Therefore, the experiment results coincide with the theoretical analysis. From this figure, one can also see that the prestress affected the displacement of the PZT actuator driven by the same voltage. A large prestress acted on the PZT actuator made the PZT actuator

more difficult to extend. From Figure 6.28, one can see that the amplification ratio is about 14 ~ 19 for different prestress conditions.

6.6.3.3 Dynamic experiment

For a precision mechanical amplifier, a wide dynamic operating range is needed. The purpose of the dynamic experiment was to obtain the characteristics of the designed CMA. The HP dynamic analyzer was used to perform the frequency response measurement and analysis for the output displacement of the CMA using the SMU-9000 instrument as a sensor. In the dynamic experiments, the pseudo random signal excitation produced by the analyzer was used as the input signal. Figures 6.29 and 6.30 show the frequency responses of the CMA system that includes the PZT actuator and the prestress adjustment mechanism for two different prestress conditions. From these two figures, it can be seen that the prestress has no effect on the first natural frequency (about 620 Hz). This result coincides with the theoretical analysis result.

In summary, the static and dynamic experiments demonstrated that the CMA has a large amplification ratio and a high natural frequency that are the essential requirements in the building of the hybrid motion mechanism developed in this thesis.

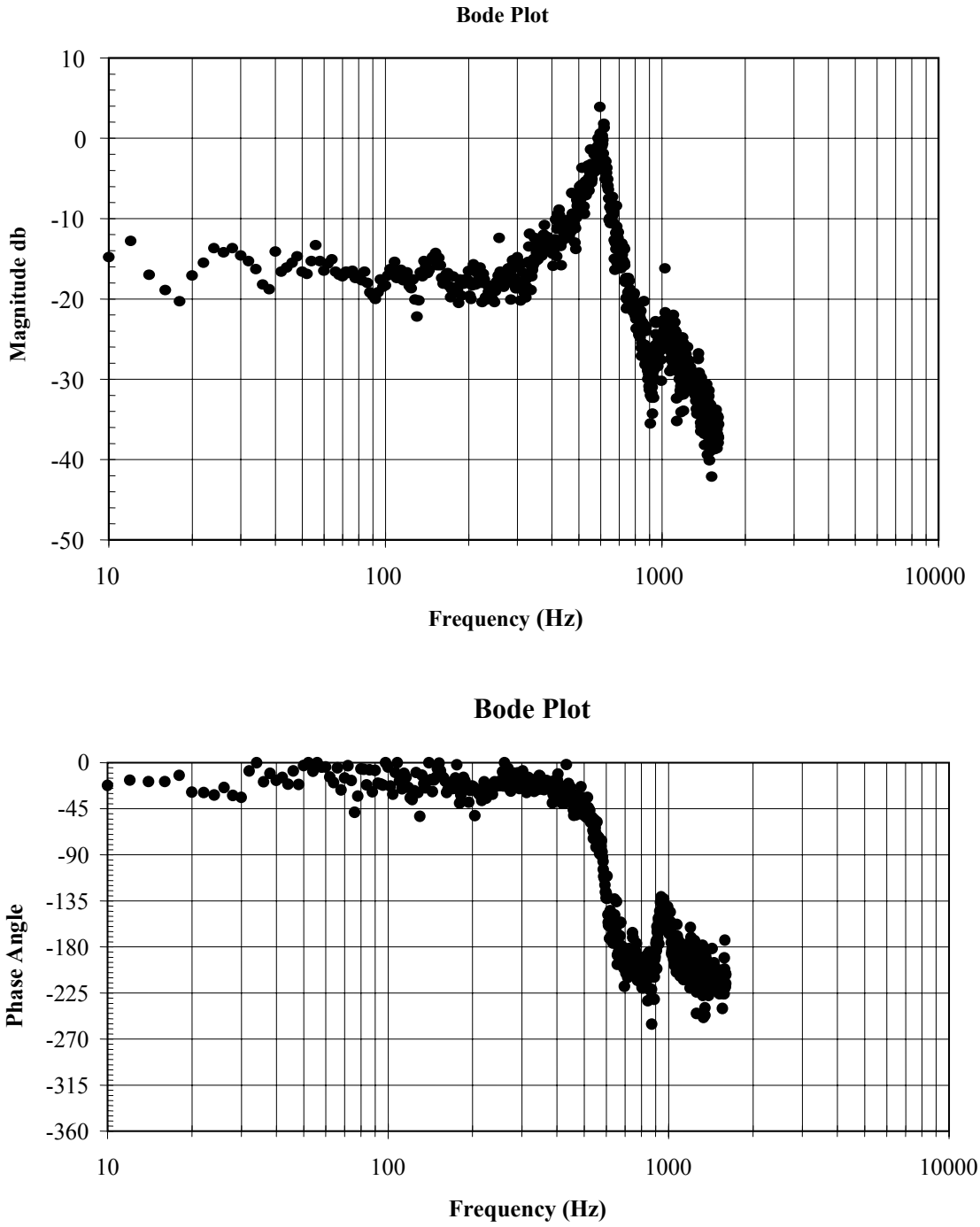

Figure 6.29 Dynamic response of the CMA – Case 1.

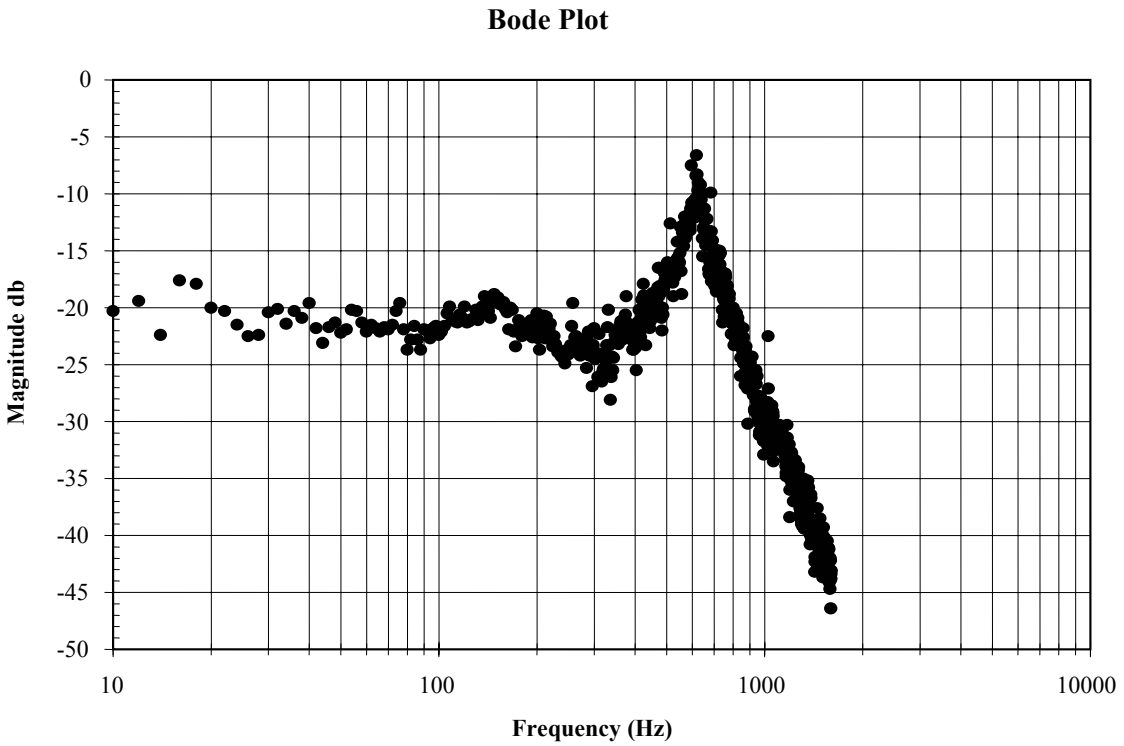

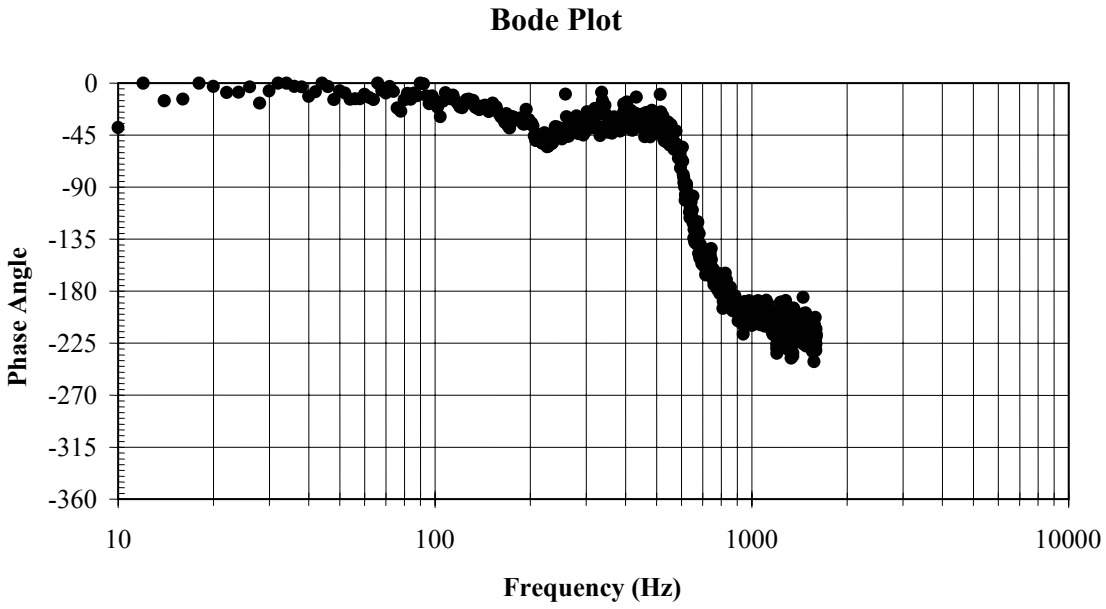

Figure 6.30 Dynamic response of the CMA – Case 2.

6.7 Conclusions

In this chapter, simulations and experiments were presented to demonstrate the effectiveness of the hybrid control systems developed in this thesis. Specifically, Several examples were used in simulation to test the effect of the PD type learning control laws and to demonstrate the unique features of wide ranges in choosing control gains and the improvement of convergence rate for the PD-OLC, the adaptive NPD-LC, and the ASL-PD control. Experiments were also carried out for a parallel robotic manipulator using the developed hybrid control systems. All the experiment results have shown the effectiveness of the adaptive NPD-LC and the ASL-PD control systems. Further, the ASL-PD was shown to have a faster convergence rate than the adaptive NPD-LC. In addition, the static and dynamic experiments for the CMA prototype were performed. Experiment results have shown that the amplification ratio is about 14 ~ 19 and the natural frequency is about 620 Hz for the CMA; such a performance with the mechanical amplifier is superior to all those existing mechanical amplifiers to the author's best knowledge.

7. CONCLUSIONS AND FUTURE WORK

7.1 Overview and Conclusions

This thesis study was aimed to develop theories and methodologies for the hybrid systems. Specifically, three hybrid systems were studied in this thesis, and they are: (1) the hybrid actuation system, (2) the hybrid motion system (mechanism), and (3) the hybrid control system.

This thesis study was started with an extensive review of the state-of-the-art of the hybrid systems. The problems associated with the three types of hybrid systems were identified. The motivation of the research described in this thesis was to overcome those problems. The thesis first presented a general architecture of the hybrid system based on the function-behaviour-structure model (Lin and Zhang, 2003; Zhang et al., 2005). This architecture is useful to bring in three kinds of hybrid systems to a common ground. In fact, with this architecture, more types of hybridization could be developed.

Next, a hybrid actuation system was discussed where its drive system integrates a servomotor and a CV motor. A general strategy for controlling the hybrid actuation system was developed which incorporated the speed fluctuation in the CV motor into the controller designed for the servomotor. Both the theoretical analysis and experiment demonstrated the effectiveness and robustness of the controller for the servo motor in the hybrid actuation system.

After that, a design strategy was proposed the hybrid motion mechanism where the micro motion and the macro motion are combined into one compliant mechanism. In this design, the main feature of the hybrid motion mechanism different from the

traditional macro-micro motion mechanism is that a compliant mechanism serves as a framework where the DC motor (for a macro motion) and the PZT actuator (for a micro motion) were integrated. Further, this compliant mechanism follows a parallel robot architecture, in which a new type of compliant mechanical amplifier was developed. The design, modeling, and optimization of the hybrid motion mechanism were discussed in detail.

In this thesis, the hybrid control systems were applied to the iteration domain through different learning strategies. Specifically, three different PD type learning control laws were developed to deal with the tracking control problem with different systems. The PD type online learning control system was developed for a nonlinear time-varying system with uncertainties and disturbances where the hybrid control occurs in the iteration domain. The adaptive NPD learning control was proposed for the trajectory tacking of robotic manipulators. The ASL-PD control system was developed to further improve the convergence rate in the learning process in which the control gains were switched from iteration to iteration.

Validation of the developed theories and methodologies for the hybrid systems was performed through both simulation and experiments. Simulation studies were presented for the hybrid actuation system and the hybrid control systems. Experiment tests for the trajectory tracking of a parallel robotic manipulator were carried out using the hybrid control systems. In addition, the static and dynamic experiments were presented for the proposed CMA.

The general conclusion of this study is that hybridization of physical entities is very promising to enhance the intelligent behaviours, and in the hybridization process, the FCBS architecture is useful to providing a framework within which hybridization of physical entities can be carried out in a systematic way. For instance, one could consider a hybrid end-effector system, and a hybrid sensor system.

Specific conclusions include:

(1) The control method for the hybrid actuation system in the literature, in which the CV motor is substituted by the servomotor with a constant velocity profile when designing a controller, is inadequate; a more sophisticated control strategy as well as method can be developed to effectively control the hybrid actuation system.

(2) The symmetric five-bar structure using the compliant mechanism concept is the most promising structure for mechanical amplification.

(3) It is possible to design a so-called parallel hybrid motion system, especially the macro-micro motion system, which conceptually eliminates the interaction problems in the serial macro-micro motion system.

(4) The hybrid control system, especially the one which combines the iteration domain and the time domain, is very promising in terms of its convergence rate and trajectory tracking error.

7.2 Major Contributions of the Thesis

The following contributions have been made through this thesis study.

First, in this study a new control algorithm for the hybrid actuation system was developed, and its stability was proved. This control algorithm could achieve excellent performance for the hybrid actuation system where CV motor was truly used. The existing hybrid actuation system uses a servomotor to simulate the CV motor, which departs from the real situation. In other words, the existing hybrid actuation systems can not be practical.

Second, a new topology for mechanical amplifier was developed, which is based on the symmetric five bar structure. Based on this new topology, a CMA was designed. The unique features of the CMA are the large amplification ratio and high natural frequency. Note that the mechanical amplification mechanism is very important in the micro-

motion technology, in particular in the need of having the motion with a long range yet high accuracy.

Third, a hybrid motion mechanism was designed where micro motion and macro motion are integrated into one compliant mechanism. The micro motion is provided by the PZT actuators installed in the CMA and the macro motion is supplied by the DC servomotors connected to the base of the CMA. The unique feature of this hybrid motion mechanism is the elimination of the interface between the micro motion and the macro motion. Note that such an interface is a source of position errors.

Fourth, Two types of hybrid control systems were developed that can be viewed as the extension of the switching control and the sliding control. The first type of hybrid control systems was a combination of switching control and compensation control, and it was applied to the control of the hybrid actuation system. The second type of hybrid control systems is PD type iterative learning control systems where the PD feedback control and feedforward control based on the direct learning strategy are combined together in the iteration domain. The PD type iterative learning control system is the online learning control and can be used to control the hybrid motion system and the generic robotic systems. Specifically, the PD type online learning control, adaptive NPD learning control, and the adaptive switching learning PD control were developed, and their convergence behaviours were verified. The developed hybrid control systems possess the adaptive property by means of their designed NPD controller or the gain switching strategy.

Finally, the verification of the developed hybrid systems was fulfilled through simulation and experiments. For the hybrid actuation system, the interaction problem between the servomotor and the CV motor was resolved very well using the developed hybrid control algorithm, and good tracking performance for the servomotor was demonstrated by simulation study. For the hybrid motion mechanism, the large amplification ratio and high natural frequencies with the proposed CMA were experimentally verified. The optimization of the hybrid motion mechanism was achieved

through the finite element analysis and the Taguchi method. For the hybrid control systems, both simulation and experiments demonstrated that the proposed hybrid control systems had a fast convergence rate and good trajectory tracking performance.

7.3 Future Research Work

There are a couple of limitations with the present study, which derive suggestions of future research work.

First, in the present study, only the simulation study for the hybrid actuation system was performed to verify the effectiveness of the developed control system. A more detailed experimental study is needed in the future, including the measurement of speed fluctuation in the CV motor, how flywheel affects some other dynamics of the system such as vibration of the whole machine system. Furthermore, it is worth to investigate whether the hybrid control system developed in Chapter 5 could be applied to the hybrid actuation system.

Second, the present study has not provided rationale for determining the level of the design variables when using the Taguchi method for the optimization of the hybrid motion mechanism. The future study is directed to determine the optimal level of variables in a continuous domain. This is because the fuzzy set and fuzzy logics could model such imprecise information during the discretization of continuous domain variable. It is expected that, by doing so, the hybrid system can be further optimized. Moreover, for design optimization using the Taguchi method, the current approach considered only two objectives, namely the maximum orientation and the minimum stress. When there are more than two objectives whether the Taguchi method can still be applied with some modifications is worthy of study.

There are some other perspectives leading to suggestions for future work. *First*, in the hybrid motion system, the resource allocation between the DC motor (for macro motion)

and the PZT actuator (for micro motion) is an interesting issue. This issue also makes sense to the hybrid actuation system, namely what should be an "optimal" resource allocation between the actuators (a CV motor and a servomotor). The gateway to tackle this issue is to understand tasks. *Second*, in general, there is a scalability issue here, i.e., whether the design methodologies developed in the present study can be applied to a "large" hybrid system. By large, it is meant that a hybrid system could be built with hybridization at more than one level, e.g., hybrid actuation, hybrid motion, and hybrid control. Another situation which makes a hybrid system grow is that the number of physical entities brought into a hybridization process increases, e.g., two CV motors and one servomotor for the hybrid actuation system as defined in this thesis. For this particular case, the question is, for example, how the resource of the servomotor should be allocated to the two corresponding CV motors.

REFERENCES

Ahn, H., Choi, C., and Kim, K., 1993. "Iterative learning control for a class of nonlinear systems," *Automatica*, Vol. 29, No. 6, pp. 1575-1578.

Allamehzadeh, H., and Cheung, J. Y., 2002. "Chattering-free sliding mode fuzzy control with continuous inherent boundary layer,", *IEEE International Conference on Plasma Science*, Honolulu, HI, USA, Vol. 2, pp. 1393-1398.

Angeles, J., Morozov, A., Slutski, L., Navarro, O., and Jabre, L., 2000. "The modular design of a long-reach, 11-axis manipulator," Proceedings of 2000 CISM-IFToMM Symposium on Robots and Manipulators, Zakopane, Poland, July 3-6, pp. 225-233.

Antsaklis, P. J., Koutsoukos, X., and Zaytoon, J., 1998, "On hybrid control of complex systems: a survey," European Journal of Automation, Vol .32, No.9-10, pp. 1023-1045.

Antsaklis, P. J., and Nerode, A., 1998. "Hybrid control systems: an introductory discussion to the special issue," IEEE Trans. on Automatic Control, Vol. 43, No. 4, pp. 457-460.

Antsaklis, P. J., and Koutsoukos, X. D., 2003. "Hybrid systems: review and recent progress," in Software-enabled Control : Information Technology for Dynamical Systems edited by Samad, T., and Balas, G., IEEE Press : Wiley-Interscience.

Arai, T., Yuasa, K, Mae, Y., Inoue, K., Miyawaki, K., and Koyachi, N., 2002. "A hybrid drive parallel arm for heavy material handling," IEEE Robotics and Automation Magazine, Vol. 9, No. 1, pp. 45-54.

Arimoto, S., Kawamura, S., and Miyasaki, F., 1984. "Bettering operation of robots by learning," Journal of Robotic Systems, Vol.1, No.2, pp. 123-140.

Arimoto, S., Kawamura, S., and Miyazaki, F., 1986. "Convergence, stability and robustness of learning control schemes for robot manipulators," in *Recent Trends in Robotics: Modeling, Control, and Education*, pp. 307-316, Elsvier, New York

Arimoto, S., 1990. "Robustness of learning control for robot manipulators," *Proceedings of IEEE International Conference on Robotics and Automations*, pp.1528-1533.

Armstrong, B., and Wade, B. A., 2000. "Nonlinear PID Control with Partial State Knowledge: Damping without Derivatives," *The International Journal of Robotics Research*, Vol.19, No. 8, pp. 715-731.

Bai, M., and Lu, Y., 2004. "Optimal implementation of miniature piezoelectric panel speakers using the Taguchi method and genetic algorithm," *Transactions of the ASME, Journal of Vibration and Acoustics*, Vol. 126, No. 3, pp. 359-369.

Bharti, S., and Frecker, M., 2004. "Optimal design and experimental characterization of a compliant mechanism piezoelectric actuator for inertially stabilized rifle," *Journal of Intelligent Material Systems and Structures*, Vol. 15, No. 2, pp. 93-106.

Branicky, M. S., Borkar, . S., and Mitter, K., 1998. "A unified framework for hybrid control: model and optimal control theory," *IEEE Trans. on Automatic Control*, Vol. 43, No. 1, pp. 31-45.

Cervantes-Sanchez, J. J., and Rendon-Sanchen, J. G., 1999. "A simplified approach for obtaining the workspace of a class of 2-dof planar parallel manipulators," *Mechanism and Machine Theory*, Vol. 34, No. 11, pp. 1057–1073.

Chandraseharan, P. C., 1996, *Robust Control of Linear Dynamical Systems*, Academic Press, San Diego, CA.

Chang, J. L., Li, K. T., and Chen, Y. P., 2002. "Sliding control with genetic algorithm for mismatched disturbance," *Asian Journal of Control*, Vol. 4, No. 2, pp. 186-192.

Chang, S. H., and Du, B. C., 1998. "A precision piezodriven micropositioner mechanism with large travel range," *Review of Scientific Instruments*, Vol. 69, No. 4, pp. 1785-1791.

Chen, M. S., Hwang, Y. R., and Tomizuka, M., 2002. "A state-dependent boundary layer design for sliding mode control," *IEEE Trans. on Automatic Control*, Vol. 47, No. 10, pp. 1677-1681.

Chen, Q. J., Chen, H. T., Wang, Y. J., and Woo, P. Y., 2001. "Global stability analysis for some trajectory tracking control schemes of robotic manipulators," *Journal of Robotic Systems*, Vol. 18, No. 2, pp. 69-75.

Chen, R. S., Lin, H. C., and Kung, C., 2000. "Optimal dimension of PQFP by using Taguchi method," *Composite Structures*, Vol. 49, No. 1, pp. 1-8.

Chen, R. S., Kung, C., and Lee, G. B., 2002. "Analysis of the optimal dimension on the electrothermal microactuator," *Journal of Micromechanics and Microengineering*, Vol. 12, No. 3, pp. 291-296.

Chen, S. X., and Moskwa, J. J., 1997. "Application of nonlinear sliding-mode observers for cylinder pressure reconstruction," *Control Engineering Practice*, Vol. 5, No. 8, pp. 1115-1121.

Chen, T. Y., and Lin, C. Y., 2000. "Determination of optimum design spaces for topology optimization," *Finite Elements in Analysis and Design*, Vol. 36, No. 1, pp. 1-16.

Chen, Y. H., Tam, S. C., Chen, W. L., and Zheng, H. Y., 1996. "Application of Taguchi method in the optimization of laser micro-engraving of photomasks," *International of Materials and Product Technology*, Vol. 11, No. 3-4, pp. 333-344.

Chen, Y. Q., Wen, C. Y., and Sun, M. X., 1997. "A robust high-order P-type iterative learning controller using current iteration tracking error," *International Journal of Control*, Vol. 68, No. 2, pp. 331-342.

Chen, Y. Q., Wen, C. Y., Gong, Z., and Sun, M. X., 1999. "An iterative learning controller with initial state learning," *IEEE Trans. on Automatic Control,* Vol. 44, No. 2, pp. 371-376.

Chen, Y. Q., and Moore, K. L., 2002. "An optimal design of PD-type iterative learning control with monotonic convergence," *Proceedings of the 2002 IEEE International symposium on Intelligent Control*, pp. 55-60.

Choi, J.Y., and Lee, J.S., 2000. "Adaptive iterative learning control of uncertain robotic systems," *IEE Proc. – Control Theory Application*, Vol. 147, No. 2, pp. 217-223.

Chou, W.-D., Lin, F.-J., and Shyu, K.-K., 2003. "Incremental motion control of an induction motor servo drive via a genetic-algorithm-based sliding mode controller," *IEE Proceedings: Control Theory and Applications*, Vol. 150, No. 3, pp. 209-220.

Chung, G. B., et al., 2001. "Design and analysis of a spatial 3-DOF micromanipulator for tele-operation," *Proceedings of the 2001 IEEE/RSJ Internaitonal Conference on Intelligent Robots and Systems*, pp. 337-342.

Conway, N. J. and Kim, S. G., 2004. "Large-strain, piezoelectric, in-plane micro-actuator," *Proceedings of the IEEE International Conference on Micro Electro Mechanical Systems (MEMS): Maastricht MEMS 2004 Technical Digest*, pp. 454-457.

Craig, J. J., 1986, *Introduction to robotics: mechanics and control*. Reading, Addison-Wesley, MA.

Craig, J.J., 1988, *Adaptive control of mechanical manipulators*, Addison-Wesley.

Dar, F. H., Meakin, J. R., and Aspden, R. M., 2002. "Statistical methods in finite element analysis," *Journal of Biomechanics*, Vol. 35, No. 9, pp. 1155-1161.

Derderian, J. M., Howell, L. L., Murphy, M. D., Lyon, S. M., and Pack, S. D., 1996. "Compliant parallel-guiding mechanisms," *Proceedings of the 1996 ASME Design Engineering Technical conferences and Computers in Engineering Conference*, August, 18-22, pp.1-12.

Dou, H. F., Tan, K. K., Lee, T. H., and Zhou, Z. Y., 1999. "Iterative feedback control of human limbs via functional electrical stimulation," *Control Engineering Practice*, Vol. 7, No. 3, pp. 315-325.

Du, H. J., Lau, G. K., Lim, M. K., and Qui, J. H., 2000. "Topological optimization of mechanical amplifiers for piezoelectric actuators under dynamic motion," *Smart Materials and Structures*, Vol. 9, No. 6, pp. 788-800.

Du, R., and Guo, W. Z., 2003. "The design of a new metal forming press with controllable mechanism," *ASME Journal of Mechanical Design*, Vol. 125, No. 3, pp. 582-592.

Dulger, L. C., Kirecci, A., and Topalbekiroglu, M., 2003. "Modeling and simulation of a hybrid actuator," *Mechanism and Machine Theory*, Vol. 38, No. 5, pp. 395-407.

Edwards, C. and Spurgeon, S. K., 1998, *Sliding Mode Control Theory and Application*, Taylor & Francis Ltd, Padstow, UK.

Ellis, G., 2004, *Control System Design Guide*, third edition, Elsevier Academic Press,

Emelyanov, S. V., 1967, *Variable Structure Control systems*, Nauka, Moscow.

Feng, G.. et al., 1996. "A physical model of the solution space and the atlas of the reachable workspace for 2-DOF parallel planar manipulators," *Mechanism and Machine Theory*, Vol. 31, No. 2, pp. 173–184.

Ferrara, A., Magnani, L., and Scattolini, R., 2001. "A switching scheme for mixed PZT-based/jet thrusters control of a large flexible structure," *ASME Journal of Dynamic Systems, Measurement, and Control*, Vol. 123, No. 4, pp. 722-727.

Fu, M., and Barmish, B. R., 1986. "Adaptive stabilization of linear systems via switching control," *IEEE Trans. on Automatic Control*, Vol. 31, No. 6, pp. 1097-1103.

Furukawa, E. and Mizuno, M., 1992. "Piezo-driven translation mechanisms utilizing linkages", *Int. J. Japan Soc. Proc. Eng.*, Vol. 26, No.1, pp.54-59.

Gao, P., Swei, S. M., and Yuan, Z. J., 1999. "A new piezodriven precision micropositioning stage utilizing flexure hinges," *Nanotechnology,* Vo. 10, No.4, pp. 394-398.

Ghorbel, F., and Gunawardana, R., 1997. "A validation study of PD control of a closed-chain mechanical system," *Proceeding of the 36th Conference on Decision & Control*, San Diego, California, USA, Dec., 1997, pp. 1998-2004.

Ghorbel, F., 1995. "Modelling and PD control of a closed-chain mechanical system," *Proceeding of the 34th Conference on Decision & Control*, New Orleans, LA, USA, Dec., 1995, pp. 540-542.

Gilsinn, J. D. et al., 2002. "A macro micro motion system for a scanning tunneling microscope," *Proceedings of the World Automation Congress (WAC) 2002 as Part of the International Symposium on Robotics & Applications (ISORA),* Orlando, FL.

Go, S. J., Lee, M. C., and Park, M. Y., 2001. "Fuzzy-sliding mode control of automatic polishing robot system with the self tuning fuzzy inference based on genetic algorithm," *Proceedings of IEEE International Conference on Robotics and Automation*, Vol. 3, pp. 2962-2967.

Gosselin, C., and Guillot, M., 1991. "Synthesis of manipulators with prescribed workspace," *ASME Journal of Mechanical Design*, Vol. 113, No. 4 , pp. 451-455.

Greenough, J. D., Bradshaw, W. K., and Gilmartin, M. J., 1995. "Design of hybrid machines," *Proceedings of the 9th World Congress on the Theory of Machines and Mechanisms*, pp. 2501-2505.

Hara, A. and sugimoto, K., 1989. "Synthesis of parallel micromanipulators", ASME Trans. *Journal of Mechanisms, Transmissions, and Automation in Design*, Vol. 111. pp.34-39.

Hatonen, J. J., Owens, D. H., and Moore, K.L., 2004. "An algebraic approach to iterative learning control," *International Journal of Control*, Vol. 10, No. 1, pp.45-54.

Heinzinger, G., Fenwick, D., Paden, B., and Miyazaki, F., 1992 "Stability of learning control with disturbances and uncertain initial conditions," *IEEE Trans. on Automatic Control*, Vol. 37, No. 1, pp. 110-114.

Her, I. And Chang, J. C., 1994. "A linear scheme for the displacement analysis of micropositioning stages with flexure hinges", *ASME Trans. Journal of Mechanical Design*, Vol. 116, No. 4, pp.770-776.

Hodac A., Siegwart R., 1999. "A decoupled macro/micro-manipulator for fast and precise assembly operations: design and experiment," *Proceedings of SPIE's International Symposium on Intelligent Systems and Advanced Manufacturing*, Boston, Massachusetts, USA, Vol. 3834-16.

Howell, L. L., 2001, *Compliant Mechanisms*, John Wiley and Sons, New York, NY.

Howell, L. L. and Midha, A., 1994. "A method for the design of compliant mechanisms with small-length flexural pivots," *ASME Trans. Journal of Mechanical Design*, Vol. 116, No.1, pp. 280-290.

Hwang, C. L., 2002. "A trajectory tracking of biped robots using fuzzy-model-based sliding-mode control," *Proceedings of the IEEE Conference on Decision and Control*, Las Vegas, NV, USA, Vol. 1, pp. 203-208.

Hwang, K. H., Lee, K. W., and Park, G. J., 2001. "Robust optimization of an automobile rearview mirror for vibration reduction," *Structural and Multidisciplinary Optimization*, Vol. 21, No. 4, pp. 300-308.

Hwang, K. H., Lee, K. H., et al., 2003. "Robust design of a vibratory gyroscope with an unbalanced inner torsion gimbal using axiomatic design," *Journal of Micromechanics and Microengineering*, Vol. 13, No. 1, pp. 8-17.

Hyder, S. J., Sunar, M., and Mahmood, F., 2004. "Piezoelectromagnetic smart structures," *Proceedings of the Institution of Mechanical Engineers. Part I: Journal of Systems and Control Engineering*, Vol. 218, No. 1, pp. 27-37.

Jang, T. J., Choi, C. H., and Ahn, H. S., 1995. "Iterative learning control in feedback systems," *Automatica*, Vol. 31, No. 2, pp. 243-248.

Jensen, B. D., Howell, L. L., and Salmon, L. G., 1999. " Design of two-link, in-plane, bistable compliant micro mechanisms," *ASME Trans. Journal of Mechanical Design*, Vol.121. No.3, pp.416-423.

Jiang, J. and Mockensturm, E. M., 2003. "A novel motion amplifier using axially driven buckling beam," *Proceedings of 2003 ASME International Mechanical Engineering Congress & Exposition*, Washington, D.C., IMECE2003-42317.

Jiang, Z. H., and Goldenberg, A. A., 1998. "Dynamic end-effector trajectory control for flexible micro-macro manipulators using an ideal manifold," *JSME International Journal, Series C,* Vol.41, No.2, pp.269-277.

Jouaneh, M., and Yang, R. Y., 2003. "Modeling of flexure-hinge type lever mechanisms," *Precision Engineering*, Vol. 27, No. 4, pp. 407-418.

Kachroo, P., 1999. "Existence of solutions to a class of nonlinear convergent chattering-free sliding mode control systems," *IEEE Trans. on Automatic Control*, Vol. 44, No. 8, pp. 1620-624.

Katic, D., and Vukobratovic, M, 2003. *Intelligent Control of Robotic Systems*, Kluwer Academic Publishers, Dordrecht, Boston, USA.

Kawamura, W., Miyazaki, F., and Arimoto, S., 1988. "Realization of robot motion based on a learning method," *IEEE Trans. on Systems, Man and Cybernetics*, Vol. 18, No. 1, pp. 126-134.

Kim, J. H., Kim, S. H., and Kwak, Y. K., 2003. "Development of a piezoelectric actuator using a three-dimensional bridge-type hinge mechanism," *Review of Scientific Instruments*, Vol, 74, No. 5, pp. 2918-2924.

Kerry, R., 1997. "PD control with desired gravity compensation of robotic manipulators: a review," *The International Journal of Robotics Research*, Vol.16, No. 5, pp. 660-672.

King, T. and Xu, W., 1996. "The design and characteristics of piezomotors using flexure-hinged displacement amplifiers," *Robotics and Autonomous Systems*, Vol. 19, No.2, pp. 189-197.

Kirecci, A., and Dulger, L. C., 2000. "A study on a hybrid actuator," *Mechanism and Machine Theory*, Vol. 35, No. 8, pp. 1141-1149.

Kota, S., et. al., 1999. "Tailoring unconventional actuators using compliant transmissions: design methods and applications," *IEEE/ASME Trans. on Mechatronics*, Vol.4, No.4, pp.396-408.

Kuc, T. Y., and Han, W. G., 2000. "An adaptive PID learning control of robot manipulators," *Automatica*, Vol. 36, pp. 717-725.

Kuc, T. Y., Nam, K., and Lee, J. S., 1991. "An iterative learning control of robot manipulators," *IEEE Trans. on Robotics and Automation*, Vol. 7, No. 6, pp. 835-842.

Kuc, T. Y., Lee, J. S., and Nam, K., 1992. "An iterative learning control theory for a class of nonlinear dynamic systems," *Automatica*, Vol. 28, No. 6, pp. 1215-1221.

Kunjur A., and Krishnamurty, S., 1997. "A robust multi-criteria optimization approach," *Mechanisms & Machine Theory*, Vol. 32, No. 7, pp. 797-810.

Kwon, S., Chung, W. K., and Youm, Y., 2001. "On the coarse/fine dual-stage manipulators with robust perturbation," *Proceedings of the 2001 IEEE International Conference on Robotics & Automation*, Seoul, Korea, pp. 121-126.

Lee, H. S., and Bien, Z., 1997. "A note on convergence property of iterative learning controller with respect to sup norm," *Automatica*, Vol. 33, No. 8, pp.1591-1593.

Lee, K. M. and Arjunan, S., 1991. "A three-degrees-of-freedom micromotion in-parallel actuated manipulator", *IEEE Trans. on Robots and Automation*, Vol.7, No.5, pp.634-641.

Lew, J. Y., 1997. "Contact control of flexible micro/macro-manipulators," *Proceedings of the 1997 IEEE International Conference on Robotics & Automation, Albuquerque*, New Mexico, pp.2850-2855.

Lew, J. Y. and Trudnowski, D. J., 1996. "Vibration control of a micro/macro-manipulator system," *IEEE Control System Magazine*, Vol.16, No. 1, pp. 26–31.

Lee, K. H, Yi, J. W., Park, J. S., and Park, G. J., 2003. "An optimization algorithm using orthogonal arrays in discrete design space for structures," *Finite Elements in Analysis and Design*, Vol. 40, No. 1, pp. 121-135.

Lee, K. H., and Park, G. J., 2002. "Robust optimization in discrete design space for constrained problems," *AIAA Journal*, Vol. 40, No. 4, pp. 774-780.

Li., M. C., and Hong, S. M., 2005. "Optimal parameter design for chip-on-film technology using the Taguchi method," *International Journal of Advanced Manufacturing Technology*, Vol. 25, No. 1-2, pp. 145-153.

Li, Q, Poo, A. N., Teo, C. L., and Lim, C. M., 1996. "Developing a neuro-compensator for the adaptive control of robots," *IEE Proc. Control Theory and Applications*, Vol. 142, No. 6, pp. 562-568.

Li, Q., Poo, A. N., and Teo, C. L., 1996. "A multi-rate sampling structure for adaptive robot control using a neuro-compensator," *Artificial Intelligence in Engineering*, Vol. 10, No. 1, pp. 85-94.

Li, Q., Tso, S. K., and Zhang, W. J., 1998. "Trajectory tracking control of robot manipulators using a neural-network-based torque-compensator," *Proceedings of Institute Mechanical Engineering, Part I, Journal of System and Control,* Vol. 212, No. 5, pp. 361-372.

Li, Q., Zhang, W. J., and Chen, L., 2001. "Design for control (DFC): a concurrent engineering approach for mechatronic system design," *IEEE/ASME Trans. on Mechatronics*, Vol. 6, No. 2, pp. 161-169.

Li, Y. et al., 1996. "Genetic algorithm automated approach to design of sliding mode control systems," *International Journal of Control*, Vol. 63, No. 4, pp. 721-739.

Lin, C. S., and Lee, T., 2003. "A classification method for input joints of planar five-bar mechanisms," *Mechanism and Machine Theory*, Vol. 38, No. 11, pp. 1307-1322.

Lin, Y., and Zhang, W. J., 2003. "Towards a novel interface design framework: function-behavior-state paradigm," *International Journal of Human Computer Studies*, Vol. 61, No. 3, pp. 259-297.

Lobontiu, N., Paine, J. S. N., Garcia, E., and Goldfarb, M., 2001. "Corner-filleted flexure hinges," *ASME Trans. Journal of Mechanical Design*, Vol. 123, No. 3, pp. 346-352.

Lobontiu, N., and Garcia, E., 2003. "Analytical model of displacement amplification and stiffness optimization for a class of flexure-based compliant mechanisms," *Computers and Structures*, Vol. 81, No. 32, pp. 2797-2810.

Man, Z., and Palaniswami, M., 1994. "Robust tracking control for rigid robotic manipulators," *IEEE Trans. on Automatic Control*, Vol. 39, No. 1, pp. 154-159.

Martensson, B., 1985. "The order of any stabilizing regulator is sufficient a priori information for adaptive stabilizing," *Systems & Control Letters*, Vol. 6, No. 2, pp. 87-91.

Mermoud, O., 2000. "Dynamics of a planar parallel mechanism: the equilateral five bar linkage," *Dynamics and Stability of Systems*, Vol. 15, No. 4, pp. 387-399.

Mertol, A., 2000. "Application of the Taguchi method to chip scale package (CSP) design," *IEEE Trans. on Advanced Packaging*, Vol. 23, No. 2, pp. 266-276.

Middleton, R. H., Goodwin, G. C., Hill, D. J., and Mayne, D. Q., 1988. "Design issues in adaptive control," *IEEE Trans. on Automatic Control*, Vol. 33, No. 1, pp. 50-58.

Millar, A. J., Howell, L. L., and Leonard, J. N., 1996. "Design and evaluation of compliant constant-force mechanism," *Proceedings of the 1996 ASME Design Engineering Technical conferences and Computers in Engineering Conference*, 96-DETC/MECH-1209.

Moore, K. L., 1992. *Iterative Learning Control for Deterministic System*, Springer, London, UK.

Moore, K. L, and Chen, Y. Q., 2003. "A separative high-order framework for monotonic convergent iterative learning controller design," *Proceedings of the American Control Conference*, pp. 3644-3649.

Morrell, J. B. and Salisbury, J. K., 1998. "Parallel-coupled micro-macro actuators," *International Journal of Robotics Research*, Vol.17, No. 7, pp. 773-791.

Nakamura, Y. et al., 2002. "Development of a uni-axial hybrid actuator using the combination of an air actuator and a giant-magnetostrictive actuator," *Smart Materials and Structures*, Vol. 11, No. 3, pp. 361-369.

Nasar, S. A., and Unnewehr, L. E., 1979. *Electromechanics and Electric Machines*, John Wiley & Sons, New York.

Niezrecki, C., Brei, D., Balakrishnan, S., and Moskalik, A. 2001. "Piezoelectric actuation: State of the art," *Shock and Vibration Digest*, Vol. 33, No. 4, pp. 269-280.

Niku, S. B., 2001. *Introduction to Robotics: Analysis, Systems, Applications*, Prentice Hall, NJ, USA.

Norrlof, M., and Gunnarsson, S., 2002. "Experimental comparison of some classical iterative learning control algorithms, *IEEE Trans. on robotics and Automation*, Vol. 18, No. 4, pp. 636-641.

Nussbaum, R. D., 1983. "Some remarks on a conjecture in parameter adaptive control," *Systems & Control Letters*, Vol. 3, No. 2, pp. 243-246.

Ouyang, P. R., 2002, *Force Balancing Design and Trajectory Tracking Control of Real-time Controllable Mechanisms*, Master Thesis, University of Saskatchewan.

Ouyang, .P. R, Zhang, W. J., and Wu, F. X., 2002. "Nonlinear PD Control for Trajectory Tracking with Consideration of the Design for Control Methodology," *Proceedings of 2002 IEEE ICRA*, May 9-11, Washington, USA, pp. 4126-4131.

Ouyang, P. R., Li, Q., Zhang, W. J., and Guo, L. S., 2004. "Design, modeling and control of a hybrid machine system," *Mechatronics*, Vol. 14, No. 10, pp. 1197-1217.

Ouyang, P. R., and Zhang, W. J., 2004. "Comparison of PD-based Controllers for Robotic Manipulators," *Proceedings of the ASME Design Engineering Technical Conference*, Vol. 2, pp. 23-31.

Ouyang, P. R., Zhang, W. J., and Gupta, M. M., 2004. "A Robust PD-type Evolutionary Learning Control for Nonlinear Time-varying systems," *the 2004 IEEE International Symposium on Intelligent Control*, September 1 - 4, Taipei, Taiwan, pp. 90-95.

Ouyang, P. R., Zhang, W. J., and Gupta, M. M., 2004. "Adaptive Nonlinear PD Learning Control for Robot Manipulators," *Proceedings of the ASME Design Engineering Technical Conference*, Vol. 2, pp. 357-365.

Ouyang, P. R., Zhang, W. J., and Gupta, M. M., 2005. "An Adaptive Switching Learning Control Method for Trajectory Tracking of Robot Manipulators," Accepted by *Mechatronics* in Feb. 2005.

Ouyang, P. R., Zhang, W. J., and Gupta, M. M., 2005. "Design of a new compliant mechanical amplifier," Accepted by *the ASME 2005 International Design Engineering Technical Conference*, DETC2005-84371.

Owens, J. E., Amann, N., and Rogers, E., 1995. "Iterative learning control – an overview of recent algorithms," *Applied Mathematics & Computational Sciences*, Vol. 5, No. 3, pp. 425-438.

Park, B. H., Kuc, T. Y., and Lee, J. S., 1996. "Adaptive learning control of uncertain robotic system," *International Journal of Control*, Vol. 65, No.5, pp. 725-744.

Paros, J. M., and Weisbord, L., 1965. "How to design flexure hinges," *Machine Design*, Vol. 27, pp. 151-156.

Pillay, P., and Krishnam, R., 1989. "Modelling, simulation and analysis of permanent-magnet motor drives. Part I: the permanent-magnet synchronous motor drive," *IEEE Trans. on Industrial Applications*, Vol. 25, No. 2, pp.265-273.

Pokines, B. J., and Garcia, E., 1998. "A smart material microamplification mechanism fabricated using LIGA," *Smart Materials and Structures*, Vol. 7, No. 1, pp. 105-112.

Prechtl, E. F. and Hall, S. R., 1999. "Design of a high efficiency, large stroke, electromechanical actuator," *Smart Materials and Structures*, Vol. 8, No. 1, pp. 13-30.

Qu, Z. H., 1995. "Global stability of trajectory tracking of robot under PD control," *Dynamics and Control,* Vol. 5, No. 1, pp. 59-71.

Qu, Z. H., Dorsey, J., Dawson, D. M., and Johnson, R.W., 1993. "Linear learning control of robot motion," *Journal of Robotic systems*, Vol. 10, No.1, pp. 123-140.

Ren, H., Jog, A., and Fair, R. B., 2001. "Statistical optimal design of microelectromechanical system (MEMS)," *2001 International Conference on Modeling and Simulation of Microsystems*, pp. 169-172.

Rue, J. W., and Gweon, D. G., 1997. "Error analysis of a flexure hinge mechanism induced by machining imperfection," *Precision Engineering*, Vol. 21, No. 1, pp. 83-89.

Rugh, W. J., 1987. "Design of nonlinear PID controllers," *AIChE Journal*, Vol. 33, No. 10, pp. 1738-1742.

Ryu, W., Gweon, D. G., and Moon, K. S., 1997. "optimal design of a flexure hinge based xyθ wafer stage", *Precision Engineering*, Vol.21, pp.18-28.

Saab, S. S., 1994. "On the P-type learning control," *IEEE Trans. on Automatic Control*, Vol. 39, No. 11, pp. 2298-2302.

Saif, M. T. A. and MacDonald, N. C., 1998. "Measurement of forces and spring constants of microinstruments," *Review of Scientific Instruments*, Vol. 69, No. 3, pp. 1410- 1422.

Schaft, A. J. and Schumacher, J. M., 1998. "Complementary modeling of hybrid systems," *IEEE Trans. on Automatic Control*, Vol. 43, No. 4, pp. 483-490.

Sciavicco, L. and Siciliano, B., 1995. *Modelling and Control of Robot Manipulators*, The McGraw-Hill Companies, Inc., New York.

Scire, F. E., and Teague, E. C., 1978. "Piezodriven 50-μm range stage with subnanometer resolution," *Review of Scientific Instruments*, Vol. 49, No. 12, pp. 1735-1740.

Seraji, H., 1998. "Nonlinear and adaptive control of force and compliance in manipulators," *International Journal of Robotics Research*, Vol. 17, No. 5, pp. 467-484.

Seth, B., and Vaddi, S. S., 2003. "Programmable function generators – I: bas five-bar mechanism," *Mechanism and Machine Theory*, Vol. 38, No. 4, pp. 321-330.

Sharon, A., Hogan, N., and Hardt, D. E., 1993. "The macro/micro manipulator: An improved architecture for robot control," *Robotics and Computer Integrated Manufacturing*, Vol.10, No. 3, pp. 209-222.

Shahruz, S. M., and Schwartz, A. L., 1994. "Design and optimal tuning of nonlinear PI compensators," *Journal of Optimization Theory and Applications*, Vol. 83, No. 1, pp. 181-198.

Slotine, J. E., and Sastry, S. S., 1983. "Tracking control of nonlinear systems using sliding surfaces with application to robot manipulator," *International Journal of Control*, Vol. 38, No. 2, pp. 465-492.
Slotine, J. E., and Li, W. P., 1991. *Applied Nonlinear Control*, Prentice Hall, Eaglewood Cliffs, N. J.

Straete, H. J. V. and Schutter, J. D., 1996. "Hybrid cam mechanisms," *IEEE/ASME Trans. on Mechatronics*, Vol. 1, No. 4, pp. 284-289.

Su, X. P. S., and Yang, H. S., 2001. "Design of compliant microleverage mechanisms," *Sensors and Actuators*, Vol. 87, No. 3, pp.146-156.

Sun, D., and Mills, J. K., 1999. "Performance improvement of industrial robot trajectory tracking using adaptive-learning scheme," *ASME Trans. Journal of Dynamic Systems, Measurement and Control*, Vol. 121, No. 2, pp. 285-292.

Sun, M.X., and Wang, D.W., 2002. "Iterative learning control with initial rectifying action," *Automatica*, Vol. 38, pp. 1177-1182.

Sunar, M., Hyder, S. J., and Yilbas, B. S., 2001. "Robust design of piezoelectric actuators for structural control," *Computer Methods in Applied Mechanics and Engineering*, Vol. 190, No. 46-47, pp. 6257-6270.

Taguchi, G., 1993. *Taguchi on Robust Technology Development*, ASME Press, New York.

Taguchi, G., Chowdhury, S., and Taguchi S., 2000. *Robust Engineering*, McGraw-Hill, New York.

Taguchi, G., Chowdhury, S., and Wu, Y., 2005. *Taguchi's Quality Engineering Handbook*, John Wiley, Livonia, Mich.

Tayebi, A., 2003. "Adaptive iterative learning control for robot manipulators," *Proceedings of the American Control Conference*, pp.4518-4523.

Tenzer, P. E., and Mrad, R. B., 2004. "On amplification in inchworm precision positioners," *Mechatronics*, Vol. 14, (No. 5, pp. 515-531.

Timoshenko, S. P. and Gere, J. M., 1961, *Theory of Elastic Stability*, McGraw-Hill, New York.

Ting, K. L. and Liu, Y., 1991. "Rotatability laws for N-bar kinematic chains and their proof," *ASME Trans. Journal of Mechanical Design*, Vol. 113, No. 1, 32-39.

Ting, K. L., 1991. "Mobility criteria of single-loop N-bar linkage," *ASME Trans. Journal of Mechanical Design*, Vol. 111, No. 4, 504-507.

Tokuz, L.C. and Jones, J.R., 1991. "Programmable modulation of motion using hybrid machines," *Proceedings of ImechE*, C414/071, pp.85-91.

Tokuz, L.C., 1992. *Hybrid machine modelling and control*, Ph.D. dissertation, Liverpool Polytechnic, U.K..

Tol, U. A., Clerc, J. P., and Wiens, G. J., 2002. "Micro/macro approach for dexterity enhancement of PKM's," *Proceedings of the Workshop on Fundamental Issues and Future Research Directions for Parallel Mechanisms and Manipulators*, Quebec City, Quebec, Canada, pp. 34-39.

Tomei, P., 1991. "Adaptive PD controller for robot manipulators," *IEEE. Trans. on Robot and Automation*, Vol. 7, No. 4, pp. 565-570.

Tsai, J. T., Liu, T. K., and Chou, J. H., 2004. "Hybrid Taguchi-genetic algorithm for global numerical optimization," *IEEE Trans. on Evolutionary Computation*, Vol. 8, No. 4, pp. 365-377.

Unal, R., Stanley, D. O., and Joyner, C. R., 1993. "Propulsion system design optimization using Taguchi methods," *IEEE Trans. on Engineering Management*, Vol. 40, No. 3, pp. 315-322.

Utkin, V. I., 1977. "Variable structure systems with sliding modes," *IEEE Trans. on Automatic Control*, Vol. 22, No. 2, pp. 212-222

Utkin, V. I., 1992. *Sliding Modes in control and Optimization*, Springer-Verlag.

Varma, V. K., and Dixon, W. E., 2002. "Design of a piezoelectric meso-scale mobile robot: a compliant amplification approach," *Proceedings of IEEE International Conference on Robotics and Automation*, Vol. 2, pp. 1137-1142.

Vliet, J. V. and Sharf,I., 1998, "Development of a planar macro-micro manipulator facility: from design through model validation," *CASI Journal*, Vol. 44, pp. 40-50.

Wai, R. J., Lin, c. M., and Hsu, C. F., 2004. "Adaptive fuzzy sliding-mode control for electrical servo drive," *Fuzzy Sets and systems*, Vol. 143, No. 2, pp. 295-303.

White, D. A., and Sofge, D. A., 1992. *Handbook of Intelligent Control*, Van Nostrand Reinhold, NY.

Wu, D. H., Tsai, Y. J., and Yen, Y. T., 2003. "Robust design of quartz microbalance using finite element and Taguchi method," *Sensors and Actuators B: Chemical*, Vol. 92, No. 3, pp. 337-344.

Wu, F. X., Zhang, W. J., Li, Q., **Ouyang, P.R.**, and Zhou, Z. X., 2005. "Control of Hybrid Machines with 2-DOF for Trajectory Tracking Problems," *IEEE Transactions on Control Systems Technology*, Vol. 13, No. 2, pp. 338-342.

Wu, Y. and Wu, A., 2000. *Taguchi Methods for Robust Design*, ASME Press, New York.

Xu, J. X., and Tan, Y., 2002. "On the P-type and Newton-type ILC schemes for dynamic systems with non-affine-in-input factors," *Automatica*, Vol. 38, No. 7, pp. 1237-1242.

Xu, W. and King, T., 1996. "Flexure hinges for piezoactuator displacement amplifiers: flexibility, accuracy, and stress considerations," *Precision Engineering*, Vol. 19, No. 1, pp. 4-10.

Xu, W. L., Yang, T. W., and Tso, S. K., 2000. "Dynamic control of a flexible macro-micro manipulator based on rigid dynamics with flexible state sensing," *Mechanism and Machine Theory*, Vol.35, pp.41-53.

Xu, Y. M., Hollerbach, J. M., and Ma, D. H., 1995. "A Nonlinear PD Controller for Force and Contact transient control," *IEEE Control Systems Magazine*, Vol. 15, No. 1, pp. 15-21.

X.G. Yan, X. G., Chen, I. M., and Lam, J., 2001. "D-type learning control for nonlinear time-varying systems with unknown initial states and inputs," *Transactions of the Institute of Measurement and Control*, Vol. 23, No. 2, pp. 69-82.

Yan, X.G., Chen, I.M., and Lam, J., 2001. "D-type learning control for nonlinear time-varying systems with unknown initial states and inputs," *Transactions of the Institute of Measurement and Control*, Vol. 23, No. 2, pp. 69-82.

Yang, R. Y., Jouaneh, M., and Scheweizer, R., 1996. "Design and characterization of a low-profile micropositioning stage," *Precision Engineering*, Vol. 18, No. 1, pp. 20-29.

Yang, G., Gaines, J. A., and Nelson, B. J., 2003. "A supervisory wafer-level 3D microassembly system for hybrid MEMS fabrication," *Journal of Intelligent and Robotic Systems*, Vol. 37, No. 1, pp. 43-68.

Young, K.D., Kokotovic, P. V., Utkin, V. I., 1977. "A singular perturbation analysis of high-gain feedback systems," *IEEE Trans. on Automatic Control*, Vol. AC- 22, pp. 931-938.

Young, K. D., Utkin, V. I., and Ozguner, U., 1999. "A control engineer's guide to sliding mode control," *IEEE Trans. on Control Systems Technology*, Vol. 7, No. 3, pp. 328-342.

Yoshikawa, T., Harada, K., Matsumoto, A., 1996. "Hybrid position/force control of flexible-macro/rigid-micro manipulator systems," *IEEE Trans. on Robotics and Automation*, Vol. 12, No. 4, pp. 633-640.

Yuan, Z. F., Gilmartin, M. J., and Douglas, S. S., 2004. "Optimal mechanism design for path generation and motions with reduced harmonic content," *ASME Trans. Journal of Mechanical Design,* Vol. 126, No. 1, pp.191-196.

Zang, C., Friswell, M. I., and Mottershead, J. E., 2005. "A review of robust optimal design and its application in dynamics," *Computers and Structures*, Vol. 83, No. 4-5, pp. 315-326.

Zhang, W. J., Li, Q., and Guo, L. S., 1999. "Integrated design of mechanical structure and control algorithm for a programmable four-bar linkage," *IEEE/ASME Trans. on Mechatronics*, December, Vol. 4, No. 4, pp. 354-362.

Zhang, W. J., Zou, J., Watson, G., Zhao, W., Zong, G. H. and Bi, S. S., 2002. "Constant-jacobian method for kinematics of a 3-DOF planar micro-motion stage," Journal of Robotic Systems, Vol. 19, No. 2, pp. 63-79.

Zhang, W. J., Lin, Y., and Sinha, N., 2005. "On the Function-Behavior-Structure Framework for Design," *The 2nd CDEN Annual Conference*, July 16-20, Alberta, Canada.

Zong, G. H., Zhang, W. J., et al., 1997. "A hybrid serial-parallel mechanism for micro-manipulation," *The 5th Applied Mechanisms and Robotics Conference*, USA, October, AMR97-050.